Investigating the role of *HOTTIP, HOXA13* and PSIP1 in cancer

Fionnuala McKenna, B.Sc. (Hons)

University of Essex

A thesis submitted for the degree of Doctor of Philosophy.

School of Life Sciences

University of Essex

May 2020

Statement of originality

I clarify that the content of this thesis is the result of my own work. All sources and previously published material used are acknowledged accordingly in the text. I further confirm that this work has not been previously used for the award of any degree.

Acknowledgements

Summary

Worldwide, colorectal cancer (CRC) is the third most prevalent cancer and prostate cancer (PCa) is the second most prominent cancer in men. Treatments for both CRC and PCa have greatly improved over the last 10-20 years; however, there is still a high mortality rate for both cancers. There is therefore a great need to better understand the factors that drive disease development and progression, and therapy resistance.

Long non-coding RNAs (lncRNAs) have gained attention in recent years as potential therapeutic targets for cancer. *HOTTIP* is one such lncRNA that has previously been implicated in CRC and PCa. *HOTTIP* is located on the 5' end of the *HOXA* locus and regulates nearby *HOXA* genes including *HOXA13* in *cis.* It has previously been shown that *HOTTIP* and *HOXA* genes are regulated by the oncogenic PSIP1 protein. Using both siRNA mediated knockdown and CRISPR-Cas9 mediated genetic knockout approaches, the role of *HOTTIP, HOXA13* and PSIP1 were investigated in both CRC and PCa.

Through loss of function studies, depletion of *HOTTIP, HOXA13* and PSIP1 led to increased sensitivity to chemotherapeutic drugs. This has not previously been observed for *HOXA13* in PCa, or *HOTTIP, HOXA13* and PSIP1 in CRC. These observations suggest that further study of these genes may help with understanding therapy resistance in CRC and PCa. More in-depth characterisation of how these genes are regulated may identify methods to enhance therapy response or re-sensitise tumours to chemotherapy.

Abbreviations

5FU = Fluorouracil

AR = Androgen receptor

Bcl-2 = B-cell lymphoma 2

BMI = Body mass index

bp = Base pairs

BPH = Benign prostatic hyperplasia

C. difficile = Clostridium difficile

CASC15 = Cancer susceptibility candidate 15

CD = Crohn's disease

cDNA = Complementary DNA

CIMP = CpG island methylation

CIN = chromosomal instability

CR = Charged region

CRC = Colorectal cancer

CRISPRa = CRISPR activation

CRPC = Castrate resistant prostate cancer

DOC = Docetaxel

DSB = Double strand break

EMT = Epithelial-to-mesenchymal transition

ESCC = Esophageal squamous cell carcinoma

FDA = Food and Drug Administration

FOBT = Fecal occult blood test

gRNA = Guide RNA

h = Hours

H3K27me3 = Histone H3 lysine 27 trimethylation

H3K4me3 = Histone H3 lysine 4 trimethylation

HCC = Hepatocellular carcinoma

HIV = Human immunodeficiency virus

HNPCC = Hereditary non-polyposis colorectal cancer

HOTAIRM1 = HOXA transcript antisense RNA, myeloid-specific 1

HOTTIP = HOXA transcript at the distal tip

HOX = HOMEOBOX

IBD = Inflammatory bowel disease

IBD = Integrase binding domain

IBS = Irritable bowel syndrome

KD = Knock down

kDa = Kilodaltons

K-M plot = Kaplan Meier plot

KO = Knock out

L19 = 60S ribosomal protein L19

LEDGF = Lens epithelium-derived growth factor

lncRNA = Long non-coding RNA

MLL1 = Mixed Lineage Leukaemia 1

MMR = Mismatch repair

mRNA = Messenger RNA

ncRNA = Non-coding RNA

NLS = Nuclear localisation signal

nm = Nanometre

NTC = Non-targeting control

OD = Optical density

OX = Oxaliplatin

PC4 = Positive Cofactor 4

PCa = Prostate cancer

PCA3 = Prostate Cancer Antigen 3

PCDHA-PC = Protocadherin-PC

PcG = Polycomb group

PCNA = Proliferating cell nuclear antigen

PI = Propidium iodide

PIA = Proliferative inflammatory atrophy

PIN = Prostatic intraepithelial neoplasia

PRC1 = Polycomb repressive complex 1

PRC2 = Polycomb repressive complex 2

PRE = Polycomb response elements

PSIP1 = PC4- and SF-interacting protein 1

PWWP = Proline Tryptophan Tryptophan Proline

RALP = Robot-assisted laparoscopic radical prostatectomy

RIN = RNA integrity number

RNA Pol II = RNA Polymerase II

RPKM = Reads per kilobase of transcript per million mapped reads

RT-qPCR = Quantitative reverse transcription PCR

SDS-PAGE = Sodium dodecyl sulfate-polyacrylamide gel electrophoresis

siRNA = Short interfering RNA

SMA = Superior mesenteric artery

SP-RALP = Single port robot-assisted laparoscopic radical prostatectomy

TFs = Transcription factors

Trx = Trithorax

TS = Thymidylate synthase

TSS = Transcriptional start site

TUG1 = Taurine UpRegulated 1

UC = Ulcerative colitis

WDR5 = WD repeat-containing protein 5

Table of contents

List of figures

List of Tables

1   General Introduction

1.1 Colorectal cancer

1.1.1   Diseases of the bowel and colon

The human colon forms part of the gastrointestinal tract (Wolpin and Mayer, 2008) and is often referred to as the large intestine. The colon is home to the largest part of the human microbiota and as a result has a crucial role in maintaining a balance between the host (human) and the microbiome at the mucosal barrier; a balance that is important for maintaining a healthy immune system (Longley, Harkin and Johnston, 2003). When this balance is interrupted, certain diseases of the bowel and colon can arise. These can include inflammatory bowel diseases (IBD), the most common being Crohn's disease (CD) and ulcerative colitis (UC) (Zhang *et al.*, 2008; Wyatt and Wilson, 2009). CD affects both the small and large intestine, whereas UC only affects the colon (Longley, Harkin and Johnston, 2003). Other diseases that affect the bowel and colon include celiac disease, irritable bowel syndrome (IBS) and infections with pathogens such as *Clostridium difficile* (*C. difficile*) (Peters *et al.*, 2002) or *Helicobacter pylori* (*H. pylori*). Some of these inflammatory diseases can result in a predisposition to developing colorectal cancer (CRC) (Rose, Farrell and Schmitz, 2002).

1.1.2   Colorectal cancer statistics

Worldwide, CRC is the third most prevalent cancer (Peters *et al.*, 2002) and is responsible for at least 600,000 deaths every year (Chu and Allegra, 1996). CRC is a term given to cancerous tumours or tissues that occur in both the colon and rectum.

It also includes some other less common cancers such as carcinoid tumours, gastrointestinal stromal tumours, as well as some forms of lymphoma and sarcoma that develop in the colorectal region (Van Triest *et al.*, 1999). It is a frequently occurring cancer with 1 in 20 people developing the disease in their lifetime (Longley, Harkin and Johnston, 2003). It is a highly metastatic cancer, with only 40 % of cases being diagnosed at the primary site (Arango *et al.*, 2004). Remaining cases are diagnosed at secondary or further metastatic sites.

The most common secondary site is the liver, with up to 70 % of patients presenting with liver metastasis (Gonçalves-Ribeiro *et al.*, 2016; McQuade *et al.*, 2017; García-Alfonso *et al.*, 2019), followed by lung metastasis, with approximately 5-15 % of CRC cases (Almeida *et al.*, 2006). As with any cancer, the stage at which CRC is diagnosed is an important indicator of survival rate (Oppelt *et al.*, 2019). For example, in the USA the 5-year survival rate of CRC between 2001 and 2007 was 90.1 % for patients with localised disease, 69.2 % for patients with regional spread, and only 11.7 % for patients with distant tumour spread (Brenner, Kloor and Pox, 2014).

1.1.2.1 Epidemiology of colorectal cancer

The increasing incidence of CRC has been associated with changes in risk factors such as a more Westernised diet in some developing countries (Kolligs, 2016), with the highest incidence rates found in the most Westernised countries such as Australia and Central and Eastern Europe, and the lowest incidence rates found in Central Africa (Gandomani *et al.*, 2017). However, mortality rates have dropped in

more economically-developed countries as a result of better screening and earlier detection methods, as well as prevention and reduction of risk factors, such as improving diets (Gandomani *et al.*, 2017).

1.1.2.2 Symptoms and diagnosis of colorectal cancer

A diagnosis of CRC is usually a result of a patient presenting with a particular set of symptoms, or after a routine screen for the disease (Schroder *et al.*, 2004). Symptoms can include blood in the stool, a change in bowel habits, abdominal pain, fatigue, sudden weight loss and anaemia-related symptoms (Teo, Rathkopf and Kantoff, 2019). Genetic material originating from primary and/or secondary metastatic lesions can be used as non-invasive, blood-based biomarkers to diagnose and personalise treatment options for a patient with CRC (Tabaczar *et al.*, 2010; Nader, El Amm and Aragon-Ching, 2018). The faecal occult blood test (FOBT) (Nader, El Amm and Aragon-Ching, 2018) is the gold standard for identifying blood in the stool. This can indicate the presence of pre-cancerous polyps or early stage cancer. In the UK, persons between the ages of 60 and 74 are provided with an at-home screening kit biannually to complete (Masoodi *et al.*, 2017). If results are positive, patients are invited for a colonoscopy. This type of screening has resulted in a 15 % reduction in colorectal cancer mortality (Nader, El Amm and Aragon-Ching, 2018) as CRC is detected at an earlier stage and better treatment options are available to the patient.

1.1.2.3 Histology and grading of colorectal cancer

The majority (60 %) of CRC cases are diagnosed at secondary or metastatic sites (Placzek *et al.*, 2010). CRC is generally a slow developing cancer that begins as an abnormal growth, called a polyp that starts to grow on the wall of the rectum or colon (Lin *et al.*, 2007). As CRC develops, the polyp progresses from an adenomatous polyp, to a pre-cancerous polyp; it is then defined as an adenocarcinoma before fully progressing to a tumour (Figure 1.1). It can take over ten years for the disease to develop fully (Nguyen and Duong, 2018). As the cancer progresses, the polyp proliferates and starts to grow into blood or lymph vessels increasing the risk of metastasis, allowing the cancer to spread to other regions of the body, mainly to the liver and lungs (Nguyen and Duong, 2018). CRC cases are classified according to the following three stages: T stage, which represents local invasion depth; N stage, if lymph node involvement has occurred; and M stage, whether distant metastases are present (Table 1.1). Together, these stages are combined to produce one overall definition which is used when deciding on therapeutic options (Nguyen and Duong, 2018).
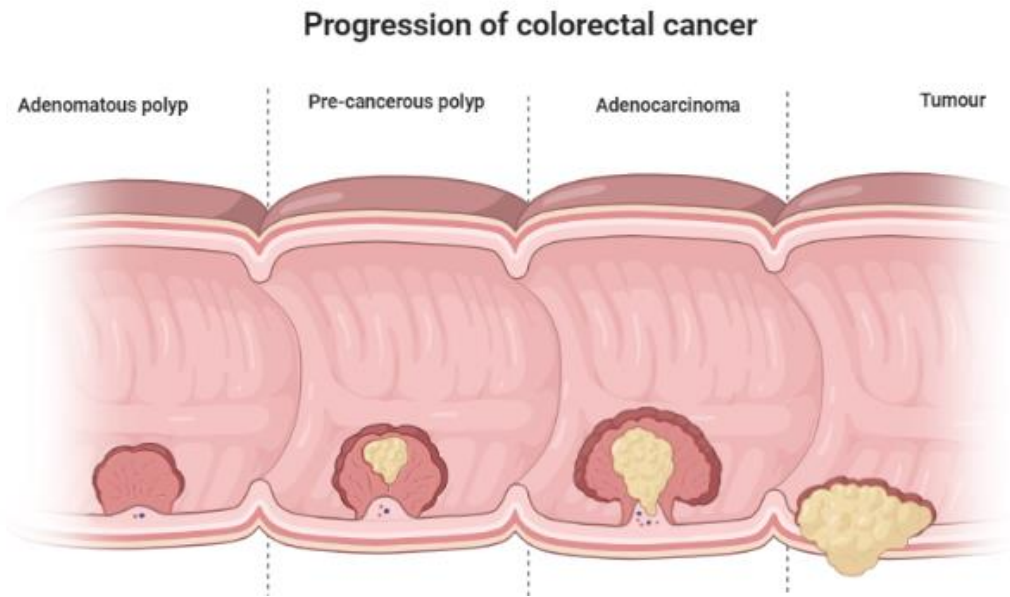
Figure 1.1 Schematic showing the progression of colorectal cancer: from a non-cancerous polyp to a cancerous tumour.

Adapted from (Nguyen and Duong, 2018). Created with BioRender.com

Table 1.1: Classification of CRC according to T, N and M stage (Brenner, Kloor and Pox, 2014)

Stage	Definition
Tx	No information about local tumour infiltration available
Tis	Tumour restricted to mucosa, no infiltration of lamina muscularis mucosae
T1	Infiltration through lamina muscularis mucosae into submucosa, no infiltration of lamina muscularis propria
T2	Infiltration into, but not beyond, lamina muscularis propia
T3	Infiltration into subserosa or non-peritonealised pericolic or perirectal tissue, or both; no infiltration of serosa or neighbouring organs
T4a	Infiltration of the serosa
T4b	Infiltration of neighbouring tissues or organs
Nx	No information about lymph node involvement available
N0	No lymph node involvement
N1a	Cancer cells detectable in 1 regional lymph node
N1b	Cancer cells detectable in 2-3 regional lymph nodes
N1c	Tumour satellites in subserosa or pericolicor periectal fat tissue, regional lymph nodes not involved
N2a	Cancer cells detectable in 4-6 regional lymph nodes
N2b	Cancer cells detectable in 7 or greater regional lymph nodes
Mx	No information about distant metastases available
M0	No distant metastases detectable
M1a	Metastasis to 1 distant organ or distant lymph nodes
M1b	Metastasis to more than 1 distant organ or set of distant lymph nodes or peritoneal metastasis

1.1.2.4 Colorectal cancer risk factors

Many risk factors have been linked to an increased risk of developing CRC. CRC is increasing in individuals over the age of 50 (Nguyen and Duong, 2018), however the mean age of CRC diagnosis is 72 years (female) and 75 years (male) (Nguyen and Duong, 2018). It is estimated that lifestyle plays a role in up to 71 % cases of CRC in the Western world (Testa, Pelosi and Castelli, 2018). This 'Western lifestyle' can include many factors such as obesity, sedentary behaviour, smoking, alcohol consumption and a diet high in calories, fat and low in fibre (Nguyen and Duong, 2018).

A 2-3 % increased risk of CRC has been described with every unit increase of the body mass index (BMI) (Fearon and Vogelstein, 1990). Those with type 2 diabetes are also at an increased risk of developing CRC (Nguyen and Duong, 2018). Infection with some types of bacteria such as *H. pylori* has also been shown to increase CRC risk (Testa, Pelosi and Castelli, 2018). A family history of CRC can also increase a person's risk of developing the disease, with the risk being strongest for those with a first-degree relative with CRC (Testa, Pelosi and Castelli, 2018). There are several forms of hereditary CRC, including familial adenomatous polyposis and hereditary non-polyposis colon cancer (HNPCC) (also known as Lynch syndrome) (Testa, Pelosi and Castelli, 2018).

Lynch syndrome is the most common genetic syndrome that can lead to CRC and is responsible for up to 6 % of CRC cases (Woenckhaus and Fenic, 2008; Sharifi *et al.*, 2016). It is caused by a germline mutation in the *MutL* homolog 1 (*MLH1*) gene

(Knudsen and Vasioukhin, 2010; Koh *et al.*, 2010); a DNA mismatch repair (MMR) gene that is involved in the detection and repair of DNA mismatches, many of which occur during cell replication (Knudsen and Vasioukhin, 2010). However, familial risk of CRC is less than that of the other lifestyle risk factors listed above (Knudsen and Vasioukhin, 2010). Other genetic factors that are not related to a familial history of the disease can also increase a person's risk of developing CRC. Mutations of the Adenomatous polyposis coli (*APC*) tumour suppressor gene can occur early on in the development of CRC, and occur in over 70 % of all colorectal adenomas (Knudsen and Vasioukhin, 2010; Koh *et al.*, 2010).

As CRC develops, further genetic mutations occur including mutations of Kirsten rat sarcoma 2 viral oncogene homolog (KRAS) and TP53 (p53) (Kim and Shiekhattar, 2016). KRAS is an oncogene that drives progression of the diseases, whereas p53 is a tumour suppressor. Mutations in both KRAS and p53 are usually accompanied by other genetic aberrations, including chromosomal instability (CIN) and CpG island methylation (CIMP) (Li *et al.*, 2011; Cheng *et al.*, 2015). Individuals with a germline mutation of DNA MMR genes such as *MLH1* have an increased risk of developing many types of cancer, including CRC (Pradeepa *et al.*, 2017). Preventative factors to reduce a person's risk of developing CRC include engaging in regular physical activity, use of aspirin or hormone replacement therapy, and a diet rich in fruit, vegetables, fibre, whole grains, dairy products and fish (Wen *et al.*, 2018).

There are three main pathways that lead to CRC. These include the classic pathway where colorectal adenoma progresses to colorectal carcinoma mainly

through CIN mechanisms (Wang *et al.*, 2011). CIN mutations are found in 85% of adenoma-carcinoma transitions and include mutations of *KRAS* and *BRAF* as well as in tumour suppressor genes *APC* and *TP53* (Wang *et al.*, 2011). According to the multistep genetic model of colorectal carcinogenesis (Wang *et al.*, 2011), inactivation of the tumour suppressor *APC* occurs first, followed by mutations in the *KRAS* oncogene which usually occur during the adenomatous stage of CRC disease progression. Eventually at the later stages of carcinogenesis, deletion of chromosome 18q and *TP53* inactivation occurs, continuing the transition to malignancy (Kingston and Tamkun, 2014). The second pathway of colon carcinogenesis is the germline mutation pathway (Kingston and Tamkun, 2014), which involves mutation of MMR genes as is seen in Lynch Syndrome (previously described). The final pathway of CRC progression is the serrated-sessile-methylation pathway (Kingston and Tamkun, 2014). Mutations involved in this third pathway also include tumours with *KRAS* and *BRAF* mutations and hypermethylation of genes such as *MGMT, p16* and *MLH1* (Smith, Zyoud and Allegrucci, 2019).

1.1.2.5   Screening and treating colorectal cancer

The main preventative precaution available for CRC is to screen regularly to catch the disease at an earlier, more treatable stage. There are several types of screening tests used to diagnose CRC. This includes the FOBT, colonoscopies, and stool DNA testing (Kingston and Tamkun, 2014). However, these screening methods lack sensitivity and hence there is a need for updated, more vigorous screening methods for the detection of CRC (Kingston and Tamkun, 2014). Once detected, colectomy surgery is often performed on patients with CRC (Milne *et al.*, 2002; Smith, Zyoud

and Allegrucci, 2019), although this is dependent on disease stage (Mármol *et al.*, 2017). In some cases, surgery may be followed by chemotherapy treatment.

Fluorouracil (5FU) treatment is one chemotherapeutic drug commonly administered to CRC patients (Lian, Y; Cai, Z; Gong, 2016). It is an antimetabolite drug (Quagliata *et al.*, 2015; Chang *et al.*, 2016; Zhang *et al.*, 2016) that attacks cancerous cells by promoting DNA damage, interfering with the metabolism of nucleotides, leading to cytotoxicity and apoptosis (Li *et al.*, 2015; Li, Zhao and Wang, 2016; H. Jiang *et al.*, 2019). This mechanism of cytotoxicity is a result of the incorporation of fluoronucleotides into DNA and RNA inhibiting their function (Wang *et al.*, 2011; Pradeepa *et al.*, 2017) by targeting the nucleotide synthetic enzyme thymidylate synthase (TS) (Peters *et al.*, 2002) during both S and G1 phase of the cell cycle (Li *et al.*, 2011; Sun, Hu, *et al.*, 2018). TS is an essential enzyme required for the synthesis of DNA and is often a target of chemotherapeutic drugs (Carethers *et al.*, 2004). 5FU can be administered on its own, or in conjunction with other chemotherapeutic drugs.

Oxaliplatin (OX) is another commonly administered chemotherapy treatment for CRC. It is often used clinically when cancerous cells have become resistant to 5FU (Comella *et al.*, 2009), or in combination with 5FU (Ito *et al.*, 2018). It is a platinum-based chemotherapeutic drug (T. Liu *et al.*, 2018) and its mechanisms of action include promoting DNA damage, causing G2/M arrest, and preventing DNA/RNA synthesis (Zhuang, Li and Ma, 2019). One way in which oxaliplatin can lead to apoptosis in cells is by forming crosslinks (both DNA-DNA and DNA-protein) that can induce DNA lesions, resulting in DNA damage (Li *et al.*, 2011; Sun, Hu, *et al.*, 2018).

Similarly, to the mechanisms of action of 5FU, oxaliplatin can also arrest DNA synthesis by inhibiting thymidylate synthase, which prevents the incorporation of thymidine in nucleic acid synthesis. This results in arrest during the G2/M phase of the cell cycle (Wang *et al.*, 2011; Pradeepa *et al.*, 2017), however some delay in S phase has also been observed in cells treated with OX (William-Faltaos *et al.*, 2007). Inhibition of RNA synthesis, through disrupting transcription, particularly during initiation and elongation, is also one of the mechanisms of action of oxaliplatin (Iman *et al.*, 2016; Huang *et al.*, 2017; Ying *et al.*, 2020). It has also been reported that after exposure to oxaliplatin, colon cancer cells can emit immunogenic signals on their surface before they undergo apoptosis (Ding *et al.*, 2017). This helps trigger the production of interferon γ by T cells, which can stimulate macrophages, natural killer cells and neutrophils, resulting in removal of cancer cells from the body (Funayama *et al.*, 2017; Chai *et al.*, 2019; Chang *et al.*, 2019).

Many of these treatment options are considered aggressive and are not always effective, therefore it is important to continue researching and developing new therapies to improve overall survival and the quality of life of patients with this disease (Cantarino *et al.*, 2016).

1.2   Prostate Cancer

1.2.1   The prostate gland

The prostate is the largest male accessory gland (Chen *et al.*, 2017) and is an essential part of the male reproductive system. It is located at the base of the bladder and surrounds the urethra (Cantarino *et al.*, 2016). It is composed of two

major compartments, the epithelium and the stroma. Epithelial cells exert the glands secretory functions (Funayama *et al.*, 2017), which are important to male fertility (Chai *et al.*, 2019; Chang *et al.*, 2019). The prostate gland is also associated with several prostatic diseases, including prostatitis, benign prostatic hyperplasia (BPH), and prostate cancer (Berx and van Roy, 2009).

1.2.2 Prostate cancer

Prostate cancer (PCa) is the second most prominent cancer in men (Rawla, 2019) and is the second most common cause of cancer-related death worldwide (Kumar and Lupold, 2016; Gamat and McNeel, 2017). It is thought that PCa arises from precancerous legions known as proliferative inflammatory atrophy (PIA) and/or prostatic intraepithelial neoplasia (PIN) (Kumar and Lupold, 2016). There have been some genetic markers associated with PIA/PIN, including the oncogene HER-2, the antiapoptotic protein BCL-2 and the loss of tumour suppressor genes such as CDK1, NKX3-1 and GSTP1 (Peek, Mah and Weiner, 2017).

PCa can develop from PIA/PIN to a low-grade carcinoma which is often characterised with increased expression of MYC, SPINK1 and members of the ETS family, as well as loss of p27 and FOXP3 (Chang *et al.*, 2016; Qin *et al.*, 2019). Further progression of PCa to a high-grade carcinoma is associated with loss of tumour suppressors PTEN and p53 (Li *et al.*, 2015). Once PCa has become metastatic, tumours have been found to overexpress EZH2 which promotes proliferation, invasion and tumorigenicity, the antiapoptotic *BCL2* gene, PIM1 which has been

shown to regulate androgen-dependent survival signalling and the androgen

receptor (AR) (Quagliata *et al.*, 2018), as well as loss of Mir-101 (Zhang *et al.*, 2016).

As PCa is a hormone cancer, the male sex hormone androgen also plays a

role in its pathogenesis (Grozescu and Popa, 2017). The AR is expressed in all stages

of prostate carcinogenesis, from primary sites to metastatic tumours (Culig and

Santer, 2014; Grozescu and Popa, 2017). It is involved in the regulation of

proliferation, apoptosis, migration, invasion, and differentiation (Culig and Santer,

2014). PCa tumour growth is known to be dependent on AR signalling (Brooke et al.,

2014) and as a result many therapies target this pathway.

1.2.2.1   Symptoms and diagnosis of prostate cancer

PCa is an age associated disease with incidence rates associated with age (Bhatlekar,

Fields and Boman, 2018; Tatangelo *et al.*, 2018). The mean age of PCa diagnosis is 66

years (Li *et al.*, 2015; Zhang *et al.*, 2016). Early stages of PCa are hard to diagnose as

they are usually symptomless (Wang *et al.*, 2011; Pradeepa *et al.*, 2017). It is a slow

developing cancer and sometimes minimal or no treatment is required (Li *et al.*,

2011). When symptoms do start to present, these may include an increased urgency

and frequency to urinate or poor urinary stream and leakage, as well as erectile

dysfunction (Chang *et al.*, 2016; Qin *et al.*, 2019). These are collectively known as

lower urinary track symptoms (LUTS) (Shen and Chen, 2011).

PCa can be diagnosed through several tests: a digital rectal examination

(DRE), a trans-rectal ultrasound (TRUS), biomarkers and finally as a result of biopsy

confirmation (Zhang *et al.*, 2016; Dong *et al.*, 2017a). A higher rate of detection is

reached if these tests are used in combination (Chang *et al.*, 2016).The Prostate

Specific Antigen (PSA) is a 34 kDa glycoprotein produced in the prostate (Xie *et al.*,

2019). It is detectable in the blood and quantification of this antigen aims to detect

PCa at an early stage, to aid treatment and reduce mortality (Mansour and Senga,

2017). Serum PSA levels can also indicate the stage of PCa with higher PSA levels

indicating a later disease stage and can be used to measure therapy response (Dong

et al., 2017a). Biomarker analysis allows more precise diagnosis of the cancer staging

and aids with treatment decisions (Falaschi, Abdurashidova and Biamonti, 2010).

1.2.2.2 Histology and grading of prostate cancer

The Gleason score is currently the most commonly used system to establish the

degree of a prostate tumour. A Gleason score is given by adding the grades of the

two most prevalent neoplastic legions together, taken from biopsy samples, with a

higher score indicating a more advanced disease state (Duan *et al.*, 2015). The

Gleason system was originally defined in the 1960s-1970s (Schatoff, Leach and Dow,

2017) but has now been updated to include five histological grades (Figure 1.2, Table

1.2), with Grade 1 being the least aggressive and Grade 5 being the most aggressive

and correlated with poorer prognosis (Yeh *et al.*, 2019).

Figure 1.2 Schematic of the Gleason grading system.

Schematic of the modified Gleason diagram updated by the World Health Organisation (WHO) and David Grignon, that was globally accepted in 2016 (Shi *et al.*, 2018).

Table 1.2 : Prostate cancer grading system (Epstein, 2018):

Grade	Definition
Grade 1 (3+3=6)	Only individual discrete well-formed glands
Grade 2 (3+4=7)	Predominantly well-formed glands with lesser component of poorly formed/fused/cribriform glands
Grade 3 (4+3=7)	Predominantly poorly formed/fused/cribriform glands with lesser component of well-formed glands
Grade 4 (Gleason score 8)	Only poorly formed/fused/cribriform glands Predominantly well-formed glands and lesser component lacking glands Predominantly lacking glands and lesser component of well-formed gland
Grade 5 (Gleason scores 9/10)	Lack gland formation (or with necrosis) with or w/o poorly formed/fused/cribriform glands

1.2.2.3 Epidemiology of prostate cancer

Geographical, racial and ethnic differences have been reported in PCa incidence (Han *et al.*, 2018). Worldwide, men of African descent have a higher risk of developing PCa and tend to have poorer prognosis and higher mortality rates (Li *et al.*, 2015). This has been found to be true for African-American, Caribbean, and Black European men, indicating a shared genetic trait could be contributing to an increased risk of PCa (Han *et al.*, 2018). Although, part of the disparity in this increased risk of PCa and poorer prognosis may also be the result of differences in accessibility to screening programmes and treatment (Boyd *et al.*, 1988; Arango *et al.*, 2004). High incidence rates have also been observed in the 'Western' world that are thought to largely be a result of lifestyle factors (Yokoyama and Cleary, 2008).

1.2.2.3   Prostate cancer risk factors

Only a small number of PCa risk factors have been identified as the initial onset of the disease is still relatively unknown (Grozescu and Popa, 2017). In most cases, a combination of several risk factors likely contributes to PCa development. Ageing is positively correlated with developing PCa (Kimura and Egawa, 2018) and is thought to be the largest risk factor, with 50 % of men age 50 and 80 % of men ages 80 presenting with PCa (French *et al.*, 2016). Environmental or lifestyle risk factors that have been attributed to PCa include a 'Western' diet that is high in saturated fat, red meat and dairy products, as well as being obese or having type 2 diabetes (Pradeepa *et al.*, 2017). Obesity has also been associated with increased risk of PCa mortality and recurrence (Pernar *et al.*, 2018). Ensuring healthy lifestyle habits including

exercising regularly, not smoking and maintaining a healthy weight can lower the

risk of developing PCa (Pernar *et al.*, 2018).

Having a family history of prostate cancer is a significant genetic risk factor

for PCa, particularly if a close relative has been diagnosed with the disease (Aarons,

Shanmugan and Bleier, 2014; Delavari *et al.*, 2014). Having a first-degree relative

diagnosed with the disease increases PCa risk by 2-3 fold (Giri and Beebe-Dimmer,

2016). Two types of inherited PCa have been identified: hereditary and familial

(Grozescu and Popa, 2017). As previously mentioned, men of African descent also

have an increased risk of developing PCa which could be due to shared genetic traits

(Rawla, 2019). Genetic mutations may also contribute to PCa development or

progression (Ríos-Colón *et al.*, 2017). These can include genes involved in DNA

damage and repair, inflammation, carcinogen metabolism and steroid hormone

metabolism (French *et al.*, 2016). There has been a rise in reports of some inherited

gene mutations such as in *BRCA1* and *BRCA2* that may correlate with PCa metastasis

and increase the risk of PCa specific death (Guo *et al.*, 2008; Focaccetti *et al.*, 2015).

1.2.2.4   Screening and treating prostate cancer

Due to the increased risk of developing PCa if a close relative, such as a father or

brother has been diagnosed with the disease, there is a strong need for screening

and early diagnosis in men who fall into this risk category. . Biomarkers can be an

effective form of screening for disease as they are often non-invasive and relatively

cheap tests to perform. One of the most specific PCa biomarkers is Prostate Cancer

Antigen 3 (*PCA3*)*,* a long non-coding RNA (lncRNA) (William-Faltaos *et al.*, 2007;

Todd and Lippard, 2009; T. Alcindor and Beauger, 2011). Many lncRNAs can often be

detected in body fluids (Tabaczar *et al.*, 2010; Nader, El Amm and Aragon-Ching, 2018) making them attractive biomarker targets. *PCA3* expression has been found to be 60-100 fold higher in more than 95 % PCa tumours compared to nearby non-cancerous tissue (Misawa, K.-I. Takayama and Inoue, 2017). It is detectable in the urine (Misawa, K.-I. Takayama and Inoue, 2017) making screening tests for this gene very simple to perform.

After diagnosis, there are several treatment options for PCa including: radical prostatectomy (Triantafillidis, Nasioulas and Kosmidid, 2009), radical radiotherapy (Wlodarska, Kostic and Xavier, 2015), chemotherapy, hormone therapy (Wlodarska, Kostic and Xavier, 2015) and conservative management (Grozescu and Popa, 2017). Radical prostatectomy involves removing the prostate gland and surrounding tissue or lymph nodes (Z. Li *et al.*, 2017; Garrett, 2019). With the development of robot-assisted laparoscopic radical prostatectomy (RALP) systems such as the da Vinci SP Surgical System, promising surgical results are being observed (Kolligs, 2016) compared to older techniques that were associated with many high-risk side-effects including urinary problems and sexual incontinence (Marley and Nan, 2016).

For non-organ confined PCa, radiotherapy, chemotherapy and hormone therapy are common treatment options; both individually and as a combined course of action. Docetaxel (DOC) was the first chemotherapy agent to show an overall improvement in survival in metastatic CRPC (Zellweger *et al.*, 2018). It is a taxane derivative and its mechanisms of action include inhibiting microtubule depolymerisation in cancer cells, a process crucial to cell mitosis; DOC specifically targets the S, M and G2 cell cycle phases (Tao *et al.*, 2019). In order to inhibit

microtubule depolymerisation, DOC binds to the microtubules, preventing androgen receptor nuclear translocation, which is a key regulatory step of the AR (Valderrama-Treviño *et al.*, 2017). Targeting this nuclear localisation through chemotherapy can prevent uncontrolled cell growth (Zellweger *et al.*, 2018). DOC can also initiate apoptosis through B-cell lymphoma (Bcl-2) phosphorylation (Oppelt *et al.*, 2019). Bcl-2 is an anti-apoptotic protein and can be up-regulated in cancer (Brenner, Kloor and Pox, 2014). In PCa, Bcl-2 is essential for the progression of cells from an androgen-dependent state to an androgen-independent state (Kolligs, 2016); therefore it is an important target for PCa chemotherapy to induce apoptosis in cancerous cells.

However, as with any chemotherapeutic agent, there is a risk of PCa tumours becoming chemoresistant to DOC. Androgen deprivation therapy (ADT) is often used in advanced PCa cases to slow tumour progression and ease symptoms (Gandomani *et al.*, 2017). Here, the AR can be targeted via chemical castration (reduced androgen production in the testes) and through use of antiandrogens, drugs that bind to the AR and hold it in an inactive state (Gandomani *et al.*, 2017). ADT is designed to target prostate tumour cells directly, but there are concerns about the effects of androgen depletion on the immune system (Kuipers *et al.*, 2015). Androgen deprivation can result in an increase in naïve T cells, antigen-specific T cells and IFNy production (Kuipers *et al.*, 2015). An infiltration of T-cells into the prostate can also occur as a result of androgen deprivation, which could trigger a local inflammatory response (Zarour *et al.*, 2017). ADT is initially successful

in many cases, but eventually tumour cells become resistant to hormone therapy and PCa can become castrate resistant (CRPC) (Kolligs, 2016).

Conservative management is also referred to as active surveillance; it involves monitoring the disease and only treating the symptoms that present in a patient (Koo *et al.*, 2017). It has become the preferred option for men with a less aggressive cancer (Koo *et al.*, 2017) and helps to avoid overtreatment which may improve long-term quality of life in patients (Zellweger *et al.*, 2018). Gene therapy is a promising treatment option for PCa to increase specificity and reduce side effects that are associated with current therapies (Marley and Nan, 2016). Continuing to understand the genetics of this disease will increase the possibility of precision medicine and tumour-specific treatment as well as assisting with overcoming chemoresistance in this disease (Brenner, Kloor and Pox, 2014).

As therapy resistance is common in PCa, a number of groups are developing novel strategies to target the disease that will overcome this barrier. This includes cell therapy with mesenchymal stem cells (MSCs) that can deliver therapeutic genes to tumours (Tao *et al.*, 2019). An example of a therapeutic gene targets for MSCs in PCa includes the death ligand Tumour necrosis factor related apoptosis-inducing ligand (TRAIL) that can specifically induce apoptosis in cancerous cells without targeting normal, non-cancerous cells (Brenner, Kloor and Pox, 2014). Oncolytic virotherapy is an example of using genetically engineered viruses to treat tumour cells (Thrymurthy, 2016). Once integrated into a tumour cell, an oncolytic virus can replicate and induce tumour cell death; it also has the added benefit of having the ability to specifically target tumour cells without harming normal tissue (Garrett,

2019). Many types of naturally occurring viruses can be manipulated for therapeutic use, however adenoviruses are among the most studied as they have low levels of pathogenicity and are relatively easy to manipulate (Kolligs, 2016). Oncolytic adenoviruses have been engineered to target many pathways in PCa tumours including deregulated cell cycle and apoptosis pathways induced by chemotherapy (Valderrama-Treviño *et al.*, 2017). As a result, several clinical trials have been carried out using adenovirus as a method of gene therapy delivery to treat PCa (Kolligs, 2016; Marley and Nan, 2016). One such adenovirus is Ad-p53, a viral vector expressing the tumour suppressor p53, which attempts to counteract the p53 alternations associated with metastatic PCa (Kuipers *et al.*, 2015).

1.3   Long non-coding RNAs

The human genome can be categorised into two regions: coding and non-coding. For many years, research efforts had focused on understanding protein-coding genes and their regulation. Upon completion of the human genome project in 2003 it was discovered that DNA with protein coding potential only accounted for around 2 % of the entire genome (Kuipers *et al.*, 2015). The remaining 98 % of the genome is comprised of non-coding DNA that had previously been discounted as the 'noise' of the genome (Brenner, Kloor and Pox, 2014). Since such a large proportion of the genome turned out to be this 'junk' non-coding DNA, a new field of research was born as scientists attempted to understand the relevance of non-coding DNA. In recent years, it has become known that non-coding DNA can be further characterised into various genetic elements with different roles and regulatory responsibilities. One major group are non-coding RNAs (ncRNAs); regulatory

transcripts that are transcribed from DNA but do not have the ability to be translated into protein (Brenner, Kloor and Pox, 2014). NcRNAs can be classified further based on each transcript's size or function. One such group are long non-coding RNAs (lncRNAs) which are defined as being greater than 200 nucleotides in length with little or no protein coding ability (Brenner, Kloor and Pox, 2014).

The field of lncRNA biology has grown drastically in the last decade (Jasperson and Burt, 2015). Mammalian genomes are now known to encode thousands of lncRNAs (Dowty *et al.*, 2013) and there are many more lncRNAs that occur in the genome compared to protein-coding messenger RNA (mRNA) (Dowty *et al.*, 2013). It is known that lncRNAs have a wide range of functions in the cell (Marley and Nan, 2016), and although they do not directly encode proteins, they are key regulators of gene expression (Brenner, Kloor and Pox, 2014). Key lncRNA functions include: involvement in epigenetic control through chromatin modifications (Brenner, Kloor and Pox, 2014); acting as enhancer RNAs (eRNAs) to promote gene expression (Brenner, Kloor and Pox, 2014); regulation of the cell cycle, apoptosis (Dowty *et al.*, 2013), as well as roles in pattern formation and differentiation during embryonic development (Brenner, Kloor and Pox, 2014). However, many of the mechanisms by which lncRNAs carry out these functions are still under investigation. In general, lncRNAs have a wide range of properties that vary between each individual transcript. They can be located in either the nucleus or the cytoplasm of a cell and are transcribed by RNA Polymerase II (RNA Pol II) from either the sense or anti-sense strand meaning that transcription can occur in any direction (3' or 5') (Testa, Pelosi and Castelli, 2018). They exhibit low conservation properties between

species (Nguyen and Duong, 2018) so evolve quicker than other protein-coding genes. LncRNAs can be preferentially expressed in specific tissues, and the location of a particular lncRNA may indicate its functional role (Fearon and Vogelstein, 1990). LncRNAs have the ability to function either in *cis* (close proximity, usually on the same chromosome) or in *trans* (distally transcribed, often from a different chromosome) in order to regulate gene expression (Nguyen and Duong, 2018). This highlights the wide variety of ways in which lncRNAs regulate gene expression.

1.3.1 LncRNAs and gene regulation

Some studies have attempted to group the ways in which lncRNAs influence gene regulation into four categories, those acting as decoys, guides, signals, or as scaffolds (Testa, Pelosi and Castelli, 2018). Many lncRNAs can be placed into more than one of these categories. LncRNAs that are classified as 'guides' are able to control target genes and influence their expression in an allele-specific manner (Testa, Pelosi and Castelli, 2018). They bind to proteins and direct complexes to specific genomic targets. This can occur in either a *cis* or *trans* manner (Testa, Pelosi and Castelli, 2018). *HOTTIP* is one such lncRNA that regulates gene expression through working as a guide. It binds to the WDR5/MLL complex, enabling the transcription of nearby *HOXA* genes through chromosomal looping, hence 'guiding' the genome to activate gene expression (Qi, Zhou and Du, 2016).

1.3.2 LncRNAs in disease

Due to their key roles in the regulation of gene expression and important cellular processes, the dysregulation of lncRNAs can lead to the development of many

diseases (Hadjipetrou *et al.*, 2017). Aberrant lncRNA expression has been described in neurological disorders such as Alzheimer's disease and Huntington's disease (Mike and Kano, 2015), Cardiovascular disease (Mármol *et al.*, 2017), autoimmune diseases (Wolpin and Mayer, 2008), as well as a variety of cancers (Longley, Harkin and Johnston, 2003).

1.3.2.1   LncRNAs in cancer

In cancer, the dysregulation of lncRNAs can exhibit either oncogenic or tumour suppressor like functions (Zhang *et al.*, 2008; Wyatt and Wilson, 2009) that affect important processes including oncogenesis, cell growth, cell proliferation, and apoptosis (Longley, Harkin and Johnston, 2003). Overexpression of lncRNAs has been linked to tumour cell proliferation and metastasis (Peters *et al.*, 2002), leading to the progression of cancer. Some lncRNAs are detectable in serum, plasma and other bodily fluids such as the urine. Therefore, oncogenic lncRNAs could serve as potential prognostic biomarker targets (Guo *et al.*, 2008; Focaccetti *et al.*, 2015). As described previously, one such example is PCA3, a lncRNA that has been found to be overexpressed in 95% of PCa sites. It was the first urine-based diagnostic test to be approved by the Food and Drug Administration (FDA), in the U.S. (Rose, Farrell and Schmitz, 2002). This type of test is inexpensive to run, enables many patients to be screened quickly, and is non-invasive, something which many other cancer screening formats lack. This highlights the ever-increasing potential for lncRNAs to be used as biomarkers and/or therapeutic targets in the future for a multitude of diseases and syndromes.

1.4 HOX genes

HOMEOBOX (HOX) genes are an important set of developmental genes that were first discovered in *Drosophila* (Arango *et al.*, 2004), and since then have been reported in every animal genome that has been sequenced so far (Gonçalves-Ribeiro *et al.*, 2016; McQuade *et al.*, 2017; García-Alfonso *et al.*, 2019). As a result, *HOX* genes are extremely important when studying animal development. They are an extremely conserved set of genes (Almeida *et al.*, 2006) and are involved in gene regulation during embryonic development (Wang *et al.*, 2016) and are found on every chromosome, organised into clusters. In mammals, there are four *Hox* clusters: *Hoxa, Hoxb, Hoxc,* and *Hoxd* that consist of 39 *Hox* transcription factors and multiple transcripts (Wang *et al.*, 2016). Each *HOX* cluster is arranged from the 3' to 5' end with its *HOX* genes are named from 1 to 13. (Joo, Park and Chun, 2016). These *Hox* clusters are important for specifying the position of cells and defining how crucial structures within the body are formed by regulating gene transcription (William-Faltaos *et al.*, 2007). *HOX* genes located at the 3' end are expressed early in development, while *HOX* genes expressed from the 5' end are expressed later in the developmental process (Joo, Park and Chun, 2016). They are an extremely conserved set of genes (De Kumar and Krumlauf, 2016); again highlighting their importance to animal development.

The expression of *Hox* and other developmental genes is regulated by the MLL/Trithorax (Trx) and Polycomb group (PcG) proteins, which influence the activation of genes through trimethylation of histone H3 lysine 4 (H3K4me3) and the repression of genes through trimethylation of histone H3 lysine 27 (Schroder *et al.*,

2004). Trx group proteins regulate the 'ON' state of *Hox* genes, whereas the PcG proteins control their 'OFF' state (Mármol *et al.*, 2017). Most PcG genes encode the subunits of Polycomb repressive complex (PRC)1 and PRC2; both of which are involved in transcriptional repression (Zhang *et al.*, 2018). Through *cis*-regulatory elements called Polycomb-response elements (PREs), PRC1 and PRC2 target the promoters of *Hox* genes (Motrich *et al.*, 2018). This is achieved through methylation of Histone H3 residues which results in transcriptional repression (Wang *et al.*, 2018). On the other hand, MLL (human ortholog of *Trx)* (Hoover and Naz, 2012) proteins are responsible for maintaining cell fates during embryonic development (Verze, Cai and Lorenzetti, 2016) through positively regulating the *Hox* genes via the active H3K4me3 histone mark (Woenckhaus and Fenic, 2008; Sharifi *et al.*, 2016).

Hox clusters show transcriptional activity from both coding and non-coding regions of the genome during the developmental stages (Knudsen and Vasioukhin, 2010; Koh *et al.*, 2010). The *Hoxa* cluster is the most studied (Knudsen and Vasioukhin, 2010) and as a result more research has been carried out into its surrounding lncRNAs over the other three clusters. LncRNAs are often located in close proximity to these *Hox* clusters (Knudsen and Vasioukhin, 2010). The presence of lncRNAs within the *HOX* clusters suggests a different way in which *HOX* genes are involved in gene regulation (Knudsen and Vasioukhin, 2010; Koh *et al.*, 2010). Recent advances in genomic research has uncovered many lncRNA transcripts embedded within the *Hox* clusters and surrounding regions including: *Hotair* and *Hottip* (Grozescu and Popa, 2017)*.*

The expression of *Hox* and other developmental genes is regulated by the MLL/Trithorax (Trx) and Polycomb group (PcG) proteins, which influence the activation of genes through trimethylation of histone H3 lysine 4 (H3K4me3) and the repression of genes through trimethylation of histone H3 lysine 27 (Rawla, 2019). Trx group proteins regulate the 'ON' state of *Hox* genes, whereas the PcG proteins control their 'OFF' (Pentyala *et al.*, 2016). These two groups of regulatory proteins play essential roles maintaining cell fates during embryonic development Two lncRNA loci are found on either end of the *HOXA* cluster; the 3' end is home to HOXA transcript antisense RNA, myeloid-specific 1 (*HOTAIRM1),* a lncRNA with roles in neuronal differentiation as well as being implicated in actute myeloid leukemia (Rawla, 2019). On the opposite, 5' end of the cluster, HOXA transcript at the distal tip (*HOTTIP*) is located, a lncRNA involved in embryonic development (Pentyala *et al.*, 2016) (Figure 1.3).
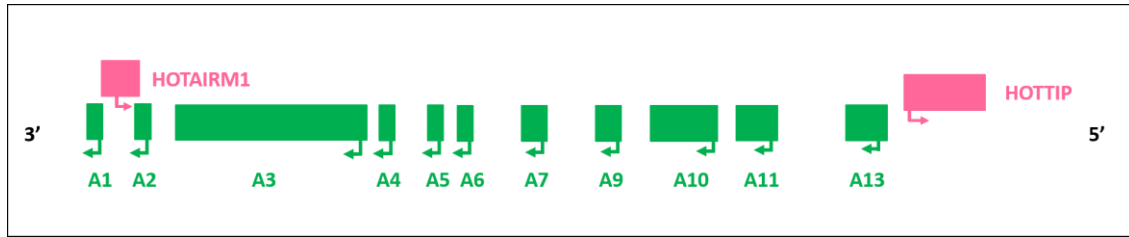
Figure 1.3 Schematic of the HOXA cluster and flanking lncRNAs

Schematic of the human HOXA cluster with HOXA 1-13 genes. The lncRNAs HOTAIRM1 and HOTTIP are located on the 3' and 5' ends of the cluster (respectively). Adapted from (Wang et al. 2011).

1.4.1 *HOX* genes in cancer

As well as having key roles in development, *HOX* genes are also involved in regulating many cellular process such as apoptosis, receptor signalling, differentiation, motility and angiogenesis (Young *et al.*, 2015). Therefore any mutations or changes in expression of these genes has the potential to develop and progress into many forms of cancer (Grozescu and Popa, 2017). One such *HOX* gene is Homeobox (HOX) A13 (*HOXA13*), the most distally located of the *HOXA* genes (Grozescu and Popa, 2017). Aberrant *HOXA13* expression has been associated with some cancers, including gastric (Grozescu and Popa, 2017), pancreatic (Ilic *et al.*, 2018), liver (Pentyala *et al.*, 2016) and prostate (Litwin and Tan, 2017). HOXA13 expression has been associated with cancer progression (Grozescu and Popa, 2017; Litwin and Tan, 2017) through promoting proliferation and metastasis (Rawla, 2019), and interacting with factors that regulate the cell cycle progression (Gordetsky and Epstein, 2016; Epstein, 2018). It has also been described as having some chemoresistant properties, protecting cancer cells from apoptosis after exposure to chemotherapy (Epstein, 2018).

1.4.1.1 HOXA13 in colorectal cancer

Despite being documented in other cancer types, the role of *HOXA13* in CRC has yet to be discussed in the literature. *HOXA9*, closely located to *HOXA13* on the *HOXA* cluster, has been reported to be overexpressed in CRC and correlated with lymph node metastasis (Grozescu and Popa, 2017; Kimura and Egawa, 2018), suggesting a role for *HOXA* genes in CRC. *HOXA13* has however been described in GI cancers

30

(Rebbeck, 2017; Taitt, 2018), which is a closely related cancer. In GI cancers, *HOXA13*

overexpression has been associated with cancer cell invasion, assisting with

epithelial-to-mesenchymal transition (EMT), and overall contributing to

tumourigenesis (Rawla, 2019).

1.4.1.2 HOXA13 in prostate cancer

The role of *HOXA13* in PCa has been studied in more detail than in CRC. *HOXA13*

expression is upregulated in PCa, and this has been documented in both cell lines

and patient tumour samples (Rawla, 2019). High *HOXA13* expression has also been

correlated with poorer overall survival in PCa (Giri and Beebe-Dimmer, 2016). It has

been found to promote proliferation, migration and invasion, and inhibit apoptosis

of PCa cells both individually and in combination with the lncRNA *HOTTIP* (Rebbeck,

2017).

1.5 HOTTIP

HOXA transcript at the distal tip (*HOTTIP*) is a lncRNA located at the 5' end of the

HOXA cluster (Kimura and Egawa, 2018). It is located near chromosome 7p15.2

(Grozescu and Popa, 2017) and is transcribed in an antisense direction (Grozescu

and Popa, 2017). *HOTTIP* is expressed in both posterior and distal sites in developing

embryos (Kimura and Egawa, 2018) and in limb bud cells (Grozescu and Popa, 2017).

It is involved in embryonic development, coordinating the expression of *HOXA* genes

in fibroblasts (Grozescu and Popa, 2017; Kimura and Egawa, 2018). *HOTTIP* activates

nearby 5' *HOXA* genes in a *cis* fashion, including *HOXA13*, the most proximal *HOXA* gene*,* located ~330bp upstream of *HOTTIP* (Pernar *et al.*, 2018)*.*

This activation of *HOXA13* occurs as a result of *HOTTIP* interacting with DNA through chromosomal looping (Pernar *et al.*, 2018). This chromosomal looping allows *HOTTIP* to be brought into close proximity to the chromatin modifying WD repeat containing protein 5 (WDR5)/mixed lineage leukaemia 1 (MLL1) complex across the *HOXA* cluster and targets its binding to the WDR5 protein (Grozescu and Popa, 2017; Kimura and Egawa, 2018), regulated by the Psip1 protein (Giri and Beebe-Dimmer, 2016). *HOTTIP* expression is associated with an increase in the histone modification H3K4me3, which in turn leads to the activation of nearby 5' *HOXA* genes (Figure 1.4). This tri-methylation marker indicates an active chromatin state, ensuring gene expression. *MLL* is recruited to the promoters of *HOX* genes to maintain their activation sites and subsequent gene expression; *HOTTIP* is critical for maintaining this occupancy (Grozescu and Popa, 2017).
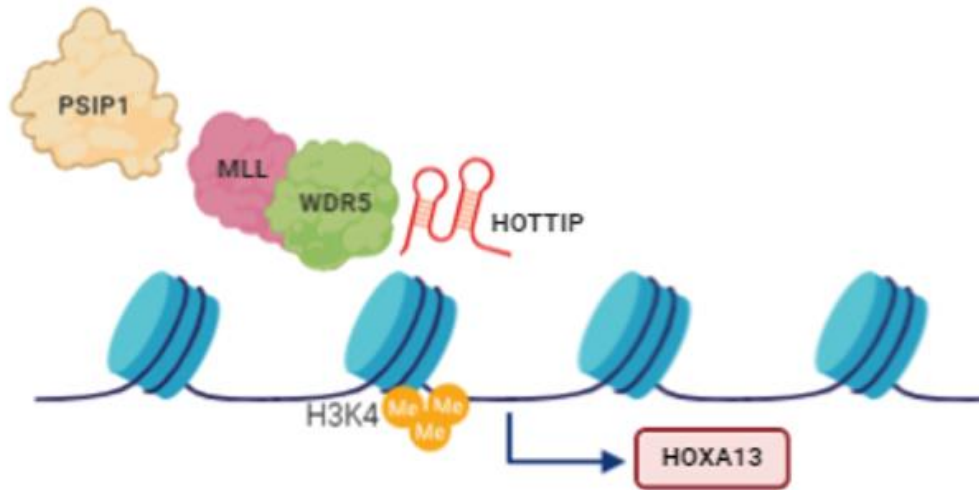
Figure 1.4 Schematic of the interactions between the lncRNA HOTTIP and chromatin modifying complexes.

Schematic of the lncRNA *HOTTIP* (regulated by PSIP1) recruiting the MLL/WDR5 complex to induce *HOXA13* expression through H3K4me3 methylation (adapted from Schuettengruer *et al.* 2011). Created with BioRender.com.

1.5.1   *HOTTIP* in cancer

As their key regulatory roles have become more apparent in many cellular functions,

lncRNAs have been implicated in the pathogenesis of many diseases including cancer

(Giri and Beebe-Dimmer, 2016). As a result, lncRNAs such as *HOTTIP* have become

attractive therapeutic targets. *HOTTIP* expression has been found to be up-regulated

in many human cancers, including: colorectal (Misawa, K. I. Takayama and Inoue,

2017), pancreatic (Bolha, Ravnik-Glavač and Glavač, 2017), hepatocellular carcinoma

(HCC) (Misawa, K.-I. Takayama and Inoue, 2017), gastric, lung, prostate,

osteocarcinoma (Misawa, K.-I. Takayama and Inoue, 2017), and breast (Metcalfe *et*

al., 2017). *HOTTIP* has been described as having roles in metastasis, proliferation,

migration and invasion, and the expression of this lncRNA correlates with poor

patient prognosis (Caffo *et al.*, 1996). *HOTTIP* expression has also been associated

with tumour cell chemoresistance (Teo, Rathkopf and Kantoff, 2019). Together, this

indicates a need to understand the mechanisms of how *HOTTIP* contributes to

cancer progression and how it promotes chemotherapy resistance.

1.5.1.1   HOTTIP in colorectal cancer

HOTTIP expression is upregulated in CRC, in both cell lines and patient CRC tissue

samples (Grozescu and Popa, 2017). Previous studies have shown that

downregulation of *HOTTIP* in CRC resulted in reduced proliferation and increased

apoptosis as a result of p21-dependent cell cycle arrest (Metcalfe *et al.*, 2017). Other

studies have suggested that this also could be due to *HOTTIP* interacting with

Serum-and glucocorticoid-inducible kinase 1 (SGK1) (Pal and Koupparis, 2018). SGK1

has independently been implicated in CRC, through involvement in cellular stress response, and SGK1 inhibitors have shown to be promising CRC therapeutic targets (Pontes, Huben and Wolf, 1986). A role for *HOTTIP* in regulating CRC metastasis has also been suggested through downregulating the tumour suppressor Dickkopf-1 (DKK1) (Teo, Rathkopf and Kantoff, 2019), a key gene involved in the Wnt/β-catenin signalling pathway (Tabaczar *et al.*, 2010; Nader, El Amm and Aragon-Ching, 2018). *HOTTIP* has also suggested as a potential prognostic biomarker for CRC due its involvement in CRC progression and its ability to be detected in blood plasma (Nader, El Amm and Aragon-Ching, 2018). Despite being previously described as having chemoresistant properties in other cancers (Masoodi *et al.*, 2017), it is yet to be determined if this is case for *HOTTIP* in CRC.

1.5.1.2 HOTTIP in prostate cancer

HOTTIP is upregulated in PCa (Nader, El Amm and Aragon-Ching, 2018), where it has been described as having roles in cell proliferation, migration and metastasis (Placzek *et al.*, 2010). In some instances it has been shown that *HOTTIP* interacts with chromatin modifying complexes to upregulate the expression of nearby *HOXA9* (Lin *et al.*, 2007) and *HOXA13* (Evans, 2018)*.* Both *HOXA9* and *HOXA13* have been implicated in prostate development (Brooke *et al.*, 2015), and high expression of *HOXA13* has been correlated with PCa tumour proliferation (Gamat and McNeel, 2017).

A role for *HOTTIP* in promoting epithelial-mesenchymal transition (EMT) in PCa has also been described through regulating the *ZEB1-miR-101-1* axis (Gamat and

McNeel, 2017), which has a well-documented role in cancer EMT (Mercader *et al.*, 2001; Gamat and McNeel, 2017). Other studies have shown that *HOTTIP* depletion resulted in cell survival inhibition through reducing the expression of B-cell lymphoma 2 (BCL-2) and enhancing the expression of the apoptosis regulator Bcl-2 associated X (BAX) (Brooke *et al.*, 2015). *HOTTIP* knockdown has also been implicated in causing G0/G1 cell cycle arrest (Grozescu and Popa, 2017), which in one study was suggested to be a result of downregulation of the cell cycle regulator Cycle D1 (Litwin and Tan, 2017). A role of *HOTTIP* in contributing to chemoresistance in PCa through inhibition of the Wnt/β-catenin pathway has also been described (Romero-Otero *et al.*, 2016). However, this has only been documented once suggesting that there is scope to explore this mechanism further.

1.6   PSIP1

PC4- and SF-interacting protein 1 (PSIP1), also known as lens epithelium-derived growth factor (LEDGF) is a chromatin-adapter protein (Altwaijry, Somani and Dufès, 2018) that interacts with chromatin in order to regulate gene expression (Giri and Beebe-Dimmer, 2016). It has been described as an 'epigenetic reader' (Mohr *et al.*, 2019). In humans it is found on chromosome 9 (Mohr *et al.*, 2019) and has two protein isoforms: p52 and p75 which interact with the transcription factor PC4, where they act as transcriptional coactivators (Cockle and Scott, 2018).

The N-terminus of PSIP1 contains a PWWP domain which recognises methylation sites on histone tails (Cockle and Scott, 2018). The N-terminus also contains a nuclear localisation signal (NLS), two AT hook-like motifs and three

relatively charged regions (CR) (Baker *et al.*, 2018). The C-terminus of PSIP1 contains

an integrase binding domain (IBD) (Adam *et al.*, 2012) (Figure 1.5). Integrase (IN) is

the enzyme used by viruses such as HIV-1 to integrate host genomes (Tamura *et al.*,

2018), allowing replication of the disease to occur.
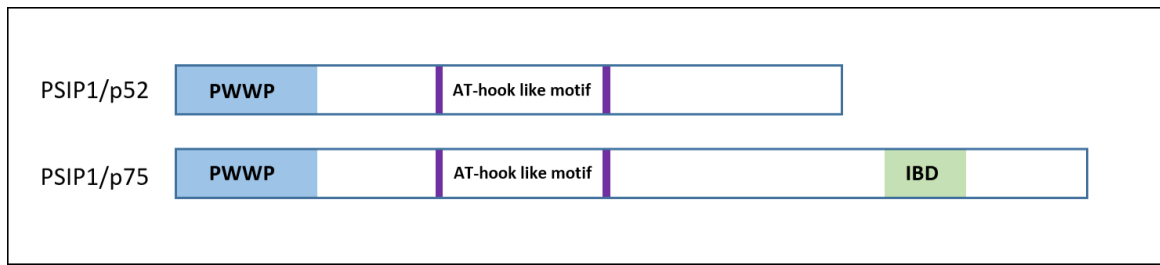
Figure 1.5 Schematic of PSIP1/p52 and PSIP1/p75 isoforms.

Schematic of the shorter PSIP1/p52 isoform that results from splice variation, and the longer PSIP1/p75 isoform. Both isoforms share a PWWP domain and AT-hook like motif, however the PSIP1/p52 isoform lacks the IBD domain that has been implicated in HIV replication. (Adapted from Pradeepa et al. 2012).

It has been established in mouse models that Psip1 is involved in transcriptional regulation of *Hox* genes, in particular the Psip1/p75 isoform regulates *Hoxa* and *Hoxd* expression (Tamura *et al.*, 2018). Psip1/p75 has roles in DNA repair through the homologous recombination (HR) pathways to promote the repair of DNA double-strand breaks (DSBs) (Alexander *et al.*, 2010). On the other hand, the shorter Psip1/p52 isoform which occurs as a result of alternative splicing (Alexander *et al.*, 2010), acts as a transcriptional coactivator to regulate lncRNA *Hottip* expression through binding to the Mixed Lineage Leukaemia 1 (MLL1) complex (Zhou *et al.*, 2016). The shorter Psip1/p52 isoform is also involved in alternative splicing through interacting with splicing factors such as Serine and Arginine Rich Splicing Factor 1 (Srsf1) (Zhou *et al.*, 2016).

1.6.1 The role of PSIP1 in HIV replication

PSIP1 is associated with the human immunodeficiency virus (HIV-1) (Ignarski *et al.*, 2019). Replication is an essential process of lentiviruses such as HIV to enable integration of their genomes into host cell DNA (Engreitz, Ollikainen and Guttman, 2016). The IBD of PSIP1 located on the C-terminus of the protein binds to HIV-1 integrase (IN), promoting transcription and therefore replication of the HIV virus (Zhu *et al.*, 2013). Therefore, the longer isoform PSIP1/p75 has been determined as contributing to HIV replication (Zhu *et al.*, 2013) as the shorter isoform lacks the IBD binding domain. A class of HIV inhibitors termed LEDGINS were developed to block PSIP1/p75/IN binding as a result of the discovery of this interaction (Hajjari and Salavaty, 2015).

1.6.2 PSIP1 in cancer

PSIP1 has been shown to reduce apoptosis when cells are exposed to stressful circumstances, e.g. in patients with inflammatory conditions such as dermatitis (Li *et al.*, 2011). The same could be true in a cancer cell, where a reduction in cell death can drive progression of the disease through cell proliferation. The presence of PSIP1 could promote cell survival in the event of further cell stress, such as from chemotherapy (Ignarski *et al.*, 2019). In support of this, some studies have shown that PSIP1 has the ability to protect cancer cells from cytotoxicity introduced by chemotherapeutic drugs (Zhu *et al.*, 2013). When PSIP1 is present, cancer cells appear to be protected against treatments that lead to lysosomal membrane permeabilisation and eventually cell death (Rinn *et al.*, 2007). Therefore, there is a need to understand the molecular workings of this protein in cancer models to increase the rate of efficacy of cancer therapies. Singh et al. describes PSIP1 as having roles in regulating key genes associated with cell-cycle progression, cell migration and invasion (Zhu *et al.*, 2013); all of which contribute to the development of cancer. Studies such as this has led to PSIP1 being termed an oncogenic protein.

Through its ability to interact with chromatin (Zhu *et al.*, 2013), PSIP1 has been shown to be important to the development of leukemia via the *MLL* complex (Zhu *et al.*, 2013). *MLL* is a target of chromosomal rearrangements found in many forms of aggressive leukaemia (Khalil *et al.*, 2009) that result after *MLL* forms a complex with MENIN, encoded by Multiple Endocrine Neoplasia I (*MEN1*), and PSIP1/p75 (Wang and Chang, 2011; Flynn and Chang, 2014; Quinn and Chang, 2016). Therefore, the role of PSIP1 is crucial for initiating *MLL* rearrangement in leukaemia

(Rinn and Chang, 2012). Inhibition of *MLL* may lead to new treatment options for leukaemia, among other cancers (Wang and Chang, 2011), highlighting the importance of understanding the role of PSIP1 in disease progression further.

1.6.2.1 PSIP1 in colorectal cancer

As well as its involvement in leukaemia, PSIP1 has been documented in several other cancers including breast (Wang and Chang, 2011), ovarian (Hajjari and Salavaty, 2015) and prostate (Dempsey and Cui, 2016). Overexpression of PSIP1 has been documented in CRC (Zhu *et al.*, 2013), however, it is not understood how this overexpression is involved in CRC. As previously described, PSIP1/p52 is involved in regulating the expression of the lncRNA *HOTTIP* which has been shown to be upregulated in CRC (Dempsey and Cui, 2016). It would be interesting to examine whether PSIP1 is also found to be implicated in CRC.

1.7 Aims of this study

Early diagnosis is important in both CRC and PCa to provide a patient with more treatment options and a better prognosis. Therefore, more diagnostic tools that can identify early-stage cancer are crucial to improving survival rates. Further, the identification of novel targeted therapies will also improve the survival and quality of life of patients with these cancers. This study aims to investigate the role of the lncRNA *HOTTIP* (Chapter 3)*,* its nearby *HOXA13* gene (Chapter 4) and the regulatory transcriptional co-activator PSIP1 protein (Chapter 5) to:

- Investigate the effect of depletion of *HOTTIP* in CRC and PCa.

- Investigate the effect of depletion of *HOXA13* in CRC and PCa.

- Investigate the effect of depletion of PSIP1 in CRC.

- Decipher the contribution of *HOTTIP, HOXA13* and PSIP1 to chemoresistance in CRC and PCa.

It is hypothesised that depletion of *HOTTIP, HOXA13* and PSIP1 promote CRC and PCa progression and therapy resistance. Downregulation of these factors will therefore inhibit proliferation, migration and motility, and promote cell death and chemosensitivity.

2   Materials and Methods

2.1   Reagents, buffers and solutions

2.1.1   Reagents and commercially available kits.

The details of all reagents and commercially available kits used in this work are

detailed below (Table 2.1), otherwise stated accordingly in the text.

Table 2.1 List of reagents and commercially available kits used in this study.

Reagent/Kit	Supplier
Acetate	Thermo Fisher
Acetic Acid	Thermo Fisher
Agarose	Thermo Fisher
Ampicillin	Thermo Fisher
ATP Solution	Thermo Fisher
Benzonase	EMD Millipore
Blasticidin S	Thermo Fisher
Bovine Serum Albumin	Sigma Aldrich
Clarity^{TM} Western ECL Substrate	Bio-Rad
Crystal Violet	Sigma Aldrich
DC^{TM} protein assay	Bio-Rad
Dimethyl sulfoxide	Sigma Aldrich
DMEM	SLS
Dimethyl sulfoxide (DMSO)	SIGMA
Docetaxel	Sigma Aldrich
DreamTaq green DNA Polymerase	Thermo Fisher
Dithiothreitol (DTT) 10X	NEB

Ethylenediaminetetraacetic acid (EDTA)	Sigma Aldrich
Ethanol	Thermo Fisher
FastDigest *Bbs*I	Thermo Fisher
Fetal Bovine Serum (FBS)	Hyclone
Fluorouracil (5-FU)	Sigma Aldrich
GeneJET Plasmid Midiprep Kit	Thermo Fisher
Igepal	Thermo Fisher
Kanamycin sulfate	Thermo Fisher
LB Agar	Sigma Aldrich
LB Broth, Miller (Granulated)	Thermo Fisher
Lipofectamine RNAiMAX Transfection Reagent	Thermo Fisher
Lipofectamine 3000	Thermo Fisher
LunaScript™ RT SuperMix Kit	NEB
Methanol	Thermo Fisher
Monarch® Plasmid Miniprep Kit	NEB
OptiMEM	Gibco
Oxaliplatin	Sigma Aldrich
PageRuler Plus Prestained Protein Ladder	Thermo Fisher
Penicillin/Streptomycin	Gibco
Phenymethylsulponyl fluoride (PMSF)	Sigma Aldrich
Phosphate buffered saline (PBS)	MELFORD
Polybrene	Sigma Aldrich
Proteinase K	Bioline
Protein inhibitor cocktail	MELFORD
Propidium iodide	Sigma Aldrich
Puromycin	Thermo Fisher
Purple Loading Dye	NEB

PVDF Western Blotting Membrane	Roche
RPMI	Gibco
RNase A	Thermo Fisher
RNeasy Mini Kit	Qiagen
SDS Gel Preparation Kit	Sigma Aldrich
SensiFAST™ SYBR No-ROX	Bioline
Sodium chloride	Sigma Aldrich
Sodium citrate	Thermo Fisher
Sodium deoxycholate	Thermo Fisher
Sodium dodecyl sulfate (SDS)	Thermo Fisher
Superscript II Reverse Transcriptase	Thermo Fisher Scientific
SYBR® Green Master mix	Bio-rad
SYBR™ Safe	Thermo Fisher
10X Tango Buffer	Thermo Fisher
Tetramethylethylenediamine (TEMED)	Sigma Aldrich
Tris	Thermo Fisher
Triton x100	Thermo Fisher
TRIzol Reagent	Thermo Fisher
Trypsin EDTA	Gibco
Tween 20	Thermo Fisher
T4 Ligation Buffer 10X	NEB
T4 Polynuleotide Kinase	NEB
T7 DNA Ligase	NEB
QuantiNova Reverse Transcription Kit	Qiagen
1kb DNA Ladder	NEB
2-Log DNA Ladder	NEB

2.1.2 Buffers and Solutions

The details of all buffers and solutions used in this study are provided in the

following table (Table 2.2).

Table 2.2 List of Buffers and Solutions used in this study

Name	Description
3 % BSA Blocking buffer	3 g BSA TBS/T to 100 mL
Lysis buffer (DNA)	10 nM Tris-HCl, pH 7.5 10 mM EDTA 10 mM NaCl 0.5 % SDS 1 mg/mL proteinase K Up to 100 mL ddH$_2$0
Lysis buffer (protein)	1 mM Tris-HCl 1 mM EDTA 1 % Triton X-100 0.1 % Sodium deoxycholate 0.1 % SDS 140 nM NaCl Protease inhibitor
Nicoletti buffer	0.1 g sodium citrate 5 mg propidum idodide 1 mL Triton x100
1 x Phosphate buffered saline (PBS)	1 x PBS tablet (MELFORD) dissolved in 100 mL ddH$_2$0.

4 % PFA	4 g Parformaldehyde dH$_2$0 to 100 mL
Luria Broth (LB)	20 g LB (Miller, granulated, Thermo Fisher) dissolved in 1 L of ddH$_2$O. Supplemented if required using antibiotics.
LB Agar plates	8.75 g of LB Agar (Sigma-Aldrich) dissolved in 250 mL ddH$_2$O, supplemented if required with antibiotics. Melted prior to use and poured to make agar plates whilst still molten.
1 x TAE buffer	40 mM Tris 20 mM Acetate 1 mM EDTA
TBS/T	6.05 g Tris 8.76 g NaCl 0.05 % Tween 20 dH$_2$0 to 1 L
Transfer buffer (WB)	22.52 g Glycine 4.88 g Tris 400 mL Methanol Up to 2 L ddH$_2$0
Propidium iodide staining solution	1 mL PBS 20 µl RNAse A (10 mg/mL) 10 µL propidium iodide (1 mg/mL)
Wash buffer (WB)	15.76 g Tris HCl 87.66 g NaCl 5 mL Tween-20 Up to 1 L ddH$_2$0

2.1.3   Antibodies

Details of the antibodies used in this study are outlined in Table 2.3.

Table 2.3 List of antibodies used in this study

Antibody	Supplier	Lot no	Dilution
2 Goat anti-rabbit IgG – HRP	Santa Cruz	SC-2030	1: 10 000
PCNA (FL-261/PC10)	Santa Cruz	SC-7907	1: 10 000
PSIP1/p75 antibody	Bethyl Laboratories Inc	A300-848A	1:5000

2.1.4   RT qPCR primers.

All primers (Table 2.4) were obtained from Sigma-Aldrich, UK. Primers were used at a working concentration of 1 µM per reaction.

Table 2.4 List of RT qPCR primers used in this study

Primer	Sequence (5' -3')	
GAPDH	F	ACCCAGAAGACTGTGGATGG
	R	TTCTAGACGGCAGGTCAGGT
HOTTIP F + INT R	F	ATGGGTGTTTCTTGGAGCCT
	R	GTGGACAGGGAAGGGATAGG
HOTTIP F + R	F	ATGGGTGTTTCTTGGAGCCT
	R	AGGGGAGAAGTTGTGCTGAA
HOTTIP FULL	F	CCTAAAGCCACGCTTCTTTG
	R	TGCAGGCTGGAGATCCTACT
HOTTIP INT F + R	F	GGTTCACCCAGGAGTAAGCT
	R	AGGGGAGAAGTTGTGCTGAA
HOXA1	F	ACCCCTCGGACCATAGGATTAC

	R	AAGGCGCACTGAAGTTCTGTG
HOXA9	F	AAAAGCGGTGCCCCTATACA
	R	CGGTCCCTGGTGAGGTACAT
HOXA11	F	CGGCAGCAGAGGAGAAAGA
	R	CGGATCTGGTACTTGGTATAGGG
HOXA13	F	GGATATCAGCCACGACGAAT
	R	ATTATCTGGGCAAAGCAACG
L19	F	GCAGCCGGCGCAAA
	R	GCGGAAGGGTACAGCCAAT
PSIP/P52	F	CATGTTGGCCTTTCAGCATA
	R	TCATTTTGGGCTCAAAGCAT
PSIP1/P75	F	TGCTTTTCCAGACATGGTTGT
	R	CCCACAAACAGTGAAAAGACAG

2.1.5 RNA sequences

Guide RNA sequences (Table 2.5) and siRNA sequences (Table 2.6) used in this study are detailed below.

Table 2.5 CRISPR gRNA sequences used in this study

CRISPR gRNA	Sequence (5' -3')	
HOTTIP CRISPR KO	3P*	CACCgcgcaactccatcgaagccga
	5P	CACCgttaggacacactaaggactg
PSIP CRISPR KO	CACCgctactccaaaagctgccaga	

* Some blast sequence overlap with *HOXA13*

Table 2.6 siRNA sequences.

siRNA target	Sequence (5' -3')
HOXA13 KD 1	GGG AAU ACG CCA CGA AUA A UU
HOXA13 KD 2	CAG GAG GGU UAA AGA GAA A UU
HOTTIP KD 1	GCA CUG AAU UGA UGG CUU A UU
HOTTIP KD 2*	CGG CAG GAG CCC AAG GAA A UU
PSIP1 KD 1	GCA AUG AGG AUG UGA CUA A UU
PSIP1 KD 2	GAC UAA AGC AGU UGA CAU A UU
NTC 1	UAA UGU AUU GGA ACG CAU A
NTC 2	AGG UAG UGU AAU CGC CUU G

* Some blast sequence overlap with *HOXA13*

2.1.6   Software

The computer software used in this study is outlined in Table 2.7.

Table 2.7 Computer Software.

Computer software	Version
Acurri C6	V3.0
GraphPad Prism	V6
Image J Fiji	1.52
MobaXterm	V 12.4
Microsoft Excel	Microsoft Office 2016
NIS-Elements	V 4.11.0
R studio	V 3.3.6
SeqMonk	V 1.46

2.1.7 Plasmid vectors

The details of all plasmid vectors used in this study is outlined in Table 2.8.

Table 2.8 Plasmid vectors used in this study.

Plasmid	Source
pSpCas9(BB)-2A-Puro (PX459)	Addgene #62988 (Feng Zhang lab)
PSIP KO	P.Madapura/F.McKenna (PX459 backbone)
HOTTIP KO 3p	F.McKenna (PX459 backbone)
HOTTIP KO 5p	F.McKenna (PX549 backbone)

2.2 Methods.

2.2.1 Cell Culture.

2.2.1.1 Safety and Sterility

All tissue culture experiments were carried out aseptically in a Class 2 cabinet. All laboratory consumables were cleaned with 4 % Virkon disinfectant to destroy potential contaminants prior to use.

2.2.1.2 Cell lines

In these studies, the following adherent cell lines were used (Table 2.9).

Table 2.9 Cell lines used in these studies and corresponding growth media.

Cell Line	Description	Media and additional supplements
DU145	Epithelial prostate cancer cell line derived from a metastatic site in the brain.	RPMI + 10 % FBS + 5 % P/S
HCT116	Epithelial colorectal cancer cell line.	DMEM + 10 % FBS + 5 % P/S
HCT116 *HOTTIP* KO	Epithelial colorectal cancer cell line where the lncRNA *HOTTIP* has been deleted via CRISPR-Cas9.	DMEM + 10 % FBS + 5 % P/S
HCT116 *HOTTIP* WT	Epithelial colorectal cancer cell line. Control cell line that was subjected to transfection reagents but no gene editing.	DMEM + 10 % FBS + 5 % P/S
HCT116 PSIP1 KO	Epithelial colorectal cancer cell line where the PSIP1 protein has been deleted via CRISPR-Cas9.	DMEM + 10 % FBS + 5 % P/S
HCT116 PSIP1 WT	Epithelial colorectal cancer cell line. Control cell line that was subjected to transfection reagents but no gene editing.	DMEM + 10 % FBS + 5 % P/S
RKO1	Epithelial colorectal cancer cell line.	DMEM + 10 % FBS + 5 % P/S

2.2.1.3   Cell culture

Initially, all cell lines were seeded in pre-warmed growth media (37 °C) in a T25 cell culture flask. Cells were passaged for two weeks prior to initiation of experiments. Upon reaching confluency, growth media was removed from cells using an aspirator and cells were washed with pre-warmed PBS. 500 µl of pre-warmed trypsin was

added to the cells and the flask was placed in an incubator at 37 °C for 5 min or until

cells detached from the surface of the flask. After cells had detached from the flask,

trypsin was neutralised with 2 mL growth media and the cell suspension was

transferred to a 15 mL falcon. The cell suspension was spun down at 1400 rpm for 5

min. Meanwhile a T25 tissue culture flask containing 5 mL of pre-warmed 37 °C

relevant growth media was prepared aseptically. The supernatant was discarded,

and the cell pellet was re-suspended in 1 mL of the appropriate growth media. Cells

were then counted and seeded according to the volumes required for each

experiment.

2.2.1.4   Cryopreservation of cells

Cells were detached using Trypsin and pelleted (1400 rpm for 5 min). The

supernatant was removed, and the pellet was re-suspended in 1 mL of growth

media. 1 mL of freezing media (400 µL growth media + 400 µL FBS + 200 µL dimethyl

sulfoxide (DMSO) was added to the cell suspension and the cell suspensions were

added into cryovials for freezing. Cryovials were placed in polystyrene biofreezing

boxes to assist with slowing down the freezing process and were kept overnight at -

80 °C before long-term storage in liquid nitrogen at -196 °C.

2.2.1.5   Thawing and re-culturing of cells

A cryovial of cells was safely removed from a liquid nitrogen freezer, using the

appropriate safety precautions. After the vial was removed, it was immediately

placed inside a water bath heated to 37 °C for 5 min until the cells had thawed.

Meanwhile a T25 tissue culture flask containing 5 mL of pre-warmed (37 °C) growth

media was prepared aseptically. Once the vial of cells had thawed it was spun down at 1400 rpm for 5 min. The supernatant was removed and pelleted cells were re-suspended in 1 mL of the appropriate growth media. The whole re-suspension was added to the T25 tissue culture flask and once cells had settled, the flask was checked under a microscope to assess the condition of the cells and to confirm the absence of microbial contamination.

2.2.2 Using Clustered regularly interspaced short palindromic repeats (CRSIPR) Cas9 to create knock out stable cell lines

2.2.2.1 Guide RNA design

Guide RNAs (gRNAs) were designed using the UCSC genome browser (https://genome.ucsc.edu/) and the Zhang lab (MIT) online CRISPR design tool (http://crispr.mit.edu/). 20 bp gRNAs were designed in the region of interest.

2.2.2.2 Cloning of gRNAs into vectors

gRNA oligos were phosphorylated and annealed at 37 °C for 30 min, 95 °C for 5 min and ramped down to 25 °C in the following reaction (Table 2.10).

Table 2.10 Phosphorylation/annealing reaction.

Phosphorylation/annealing reaction
100 µM oligo1
100 µM oligo 2
1 µl 10X T4 Ligation Buffer
6.5 µl dH$_2$0
0.5 µl T4 PNK

The annealed oligo was diluted 1:500 with dH_2O and the following digestion-ligation reaction was set up (Table 2.11).

Table 2.11 Digestion-ligation reaction.

Digestion-ligation reaction
100 ng backbone vector
2 µl diluted phosphorylated and annealed duplex from previous step
2 µl 10X Tango buffer
1 µl 1M DTT
1 µl 10mM ATP
1 µl 10U/µL FastDigest *Bbs*I
0.5 µl T7 ligase
dH_2O up to 20 µl

The ligation reaction was incubated in a thermocycler under the following conditions (Table 2.12).

Table 2.12 Ligation reaction temperature conditions.

Ligation reaction		
37 °C	5 min	
23 °C	5 min	Repeat for 6 cycles
4 °C	Hold	

Once ligated, the vectors were transformed into competent cells.

2.2.2.3 Transformation of vectors

After gRNAs had been successfully cloned into vectors, they were transformed into *Escherichia coli* (*E. coli)* competent cells (DH5α or XL1-Blue strain). Competent cells

were thawed on ice for 30 min before use. 50 ng of plasmid DNA was incubated with 50 μl of competent cells on ice for a further 30 min. Cells were heat-shocked at 42 $^\circ$C for 45 secs and then placed on ice for a further 2 min. 500 μl of pre-warmed LB broth was added to the cells and the sample was incubated whilst shaking at 37 $^\circ$C for 60 min. Agar plates had been previously prepared with the appropriate antibiotic for selection added. 100 μl of sample was spread aseptically onto the agar plate using a sterile spreader. Plates were incubated overnight at 37 $^\circ$C and the next day bacterial colonies were picked for plasmid isolation.

2.2.3   Isolation of plasmids

Plasmids were isolated from bacterial cultures using the Monarch® Plasmid Miniprep Kit (NEB) or the GeneJET Plasmid Midiprep Kit (Thermo Fisher) depending on the desired end concentration required. The concentration and purity of each plasmid was quantified using a nanodrop before continuation.

2.2.3.1   Transfection

Cells were grown to ~80 % confluency and seeded into 6-well plates with 800 000 cells per well. 2 μg of gRNA plasmid was transfected into cells using the Lipofectamine® 3000 (Thermo Fisher) reagents following the manufacturer's protocol. A separate control well was also set up that included all transfection reagents except the gRNA plasmid (mock transfection control). 2 mL of growth media containing 2.5 μg/μl puromycin was added to each well of cells 24 h and 48 h after initial transfection to select for successfully transfected cells. After 72 h, 5000

transfected cells were seeded into 10 cm dishes by counting with a haemocytometer and cultured until colonies formed.

2.2.3.2 Colony picking

Cells were cultured for 8-10 days or until clear colonies of cells had formed. A 96-well plate was prepared with 35 µl room temperature trypsin per well, using a multichannel pipette. The plate was kept on ice throughout the duration of colony picking. Media was removed from the 10 cm dish of colonies using an aspirator, and then washed once with pre-warmed PBS. The bottom of the plate was covered with ~7 ml PBS. Using a microscope, colonies were picked from the plate using a P20 set to 4 µl using filter tips. The tip was used to scrape around the colony to ensure it is fully detached from the plate; then the detached colony was collected in the tip. Each colony was transferred into 35 µl of trypsin and pipetted up and down to break up the colony. After picking a sufficient number of colonies the 96-well plate was placed in a 37 °C incubator for 10 min to allow the trypsin to break up the colony into single cells. 200 µl of appropriate growth media was added to each trypsinised colony and pipetted up and down to break up the colony further using a multichannel pipette. The cells were then cultured in the 96-well plate refreshing media every two days. With sufficient growth, plates were then used to validate positive colonies.

2.2.4   Validation of positive clones

2.2.4.1   Genomic DNA extraction

Upon confluency of cells, media was removed and wells were washed 2x with 100 µl of PBS. The edges of the plates were sealed with parafilm and frozen at -80 °C overnight to help with cellular lysis. The next day plates were left to thaw on the bench for 5 min. 50 µl of DNA lysis buffer was added to each well using a multichannel pipette. The edges of the plate were then sealed with parafilm and it was placed in a humidified chamber and incubated overnight at 55 °C. Plates were removed from the incubator and spun down at 1000 rpm for 5 min. 150 µl of 5 M NaCl was added to 10 mL of cold ethanol (EtOH) and 100 µl of this solution was added to each well. The plate was tapped gently to mix and left at room temperature for 30 min. The plate was spun at 1500 rpm for 5 min and the NaCl/EtOH solution was removed by inverting the plate allowing the solution to drain. The plate was then blotted gently on paper towels to remove any excess ethanol. The wells were then washed 3x with 150 µl of freshly prepared 70 % EtOH, blotting the plate gently on paper towels in between each wash. The plate was air dried at RT for ~30 min and the remaining DNA was resuspended in 50 µl dH$_2$0.

2.2.4.2   Validation of HOTTIP KO clones via PCR

Positive clones with a deletion of HOTTIP were identified via PCR. The following PCR reaction (Table 2.13) was prepared using the previously isolated DNA.

Table 2.13 PCR reaction reagents.

Reagent	Quantity
Primers (4µM)	2 µl
DNA (50 ng)	2 µl
DreamTaq 3x master mix	5 µl
dH$_2$0	1 µl
Total Volume	10 µl

The reaction was incubated in a thermal cycler under the following conditions (Table 2.14).

Table 2.14 Thermal cycler conditions for DreamTaq PCR.

Number of cycles	Step duration	Temperature (°C)
1	3 min	95
35	20 sec	95
	30 sec	58
	30 sec	72
1	5 min	72
Hold		4

The resulting mixture was separated on a 1.5 % agarose gel at 80 V for 40 min. The gel was imaged on a BioRad EZ Gel Doc system.

2.2.4.3   Validation of PSIP KO clones via Western blotting

2.2.4.3.1.1 Protein extraction

The following steps were carried out on ice and all buffers were pre-chilled to 4 °C. Clones were grown until confluency was achieved in 6-well plates. Media was removed and cells were washed once with PBS. 100 µl of cold lysis buffer was added

59

to each well and the plate was incubated on ice for 30 min with occasional mixing. Samples were transferred to 1.5 mL tubes and placed in -20 °C for storage. Prior to western blotting, samples were thawed on ice then spun at 13000 rpm for 10 min at 4 °C.

2.2.4.4   SDS-Polyacrylamide Gel Electrophoresis (SDS-PAGE)

2.2.4.4.1.1   Gel preparation

Gels consisted of two layers; the resolving gel and the stacking gel and both were prepared using the SDS Gel Preparation Kit (Sigma Aldrich, 08091). 1.5 mm glass plates were assembled in a casting stand. The resolving gel was added via pipetting, leaving a 2 cm space at the top of the plate, and left to polymerize for 20 min. 1 mL of dH_2O was pipetted onto the top of the gel surface to ensure the gel was level and to remove any bubbles. Following polymerization, the dH_2O was removed and the stacking gel and 1.5 mm comb were applied to the cast. The gel was left for a further 30 min to ensure full polymerization of the stacking gel. The fully polymerized gel was then covered with a damp paper towel and stored at 4 °C for at least 2 h before use. The gels were stored at 4 °C for no longer than two weeks.

2.2.4.4.1.2   Preparation of protein samples and gel electrophoresis

Protein samples were transferred from storage (-20 °C) and defrosted on ice. Once thawed, the protein samples were spun briefly and mixed in a 1:1 ratio with sample incubation buffer (SDS gel preparation kit, Sigma Aldrich) making 20 µl total volume. Samples were incubated for 5 min at 95 °C allowing them to denature, prior to being loaded into the wells of the gel. 2 µl of the PageRuler™ protein ladder (Thermo Fisher) was also loaded into the gel to check the molecular weight of each protein

60

band. The protein samples were then separated on the gel at 200 V until the dye front reached the base of the resolving gel (approximately 120 min).

2.2.4.4.1.3 Membrane transfer

Prior to the start of transfer, the membrane was soaked in methanol for 5 min. The PVDF membrane (Roche), blotting paper and the SDS gel were soaked in transfer buffer for a further 5 min to equilibrate. The transfer was carried out using the Bio-Rad Trans-Blot machine at 0.7 A, 25 V for 30 min. After the transfer had taken place, the gel was discarded, and the membrane was collected.

2.2.4.4.1.4 Membrane blocking and antibody incubations

Following transfer, the membranes were carefully removed from the transfer cassette and incubated in blocking buffer (3 % BSA/TBST) overnight at 4 ^{o}C with gentle agitation to reduce non-specific binding. The next day, blocking buffer was removed and membranes were incubated with primary antibody (PSIP1/p75 antibody (A300-848A) and PCNA (FL-261/PC10)), diluted in 1:5000 in 1 % BSA/TBST for 2 h at RT with gentle agitation. Membranes were then washed with TBST for 3x5 min at RT with agitation and incubated for 1 h with Goat anti-rabbit IgG – HRP (Santa Cruz, lot no. A0615, SC-2030) secondary antibody with gentle agitation at room temperature. Before protein detection, the membranes were once again washed 3x5 min with TBST with strong agitation at room temperature.

2.2.4.4.1.5 Protein detection

In order to detect protein presence, the Clarity^{TM} Western ECL Blotting buffers (Bio-Rad) were added to membranes just before imaging as per the protocol provided.

Membranes were imaged using the FUSION -FX7 (VILBER LOURMAT) advanced analysis camera system.

2.2.5 RNA expression analysis

2.2.5.1 RNA extraction

Total RNA was extracted from each cell line using the Qiagen RNeasy mini kit (Qiagen, UK).

2.2.5.2 Reverse transcription

In order to reverse transcribe RNA to cDNA, the SuperScript II Reverse Transcriptase (Invitrogen), QuantiNova Reverse Transcription Kit (Qiagen, UK), or LunaScript® RT SuperMix kit (NEB) was used as per the manufacturers protocol. Resulting cDNA was diluted 1:10 in dH_2O before proceeding with qPCR.

2.2.5.3 Quantitative Real-Time PCR (qPCR)

Mastermixes containing SYBR green, primer concentration and dH_2O were prepared for all reactions to ensure equal distribution of components between wells. After mastermixes were prepared, they were gently mixed and spun. 2 µl of cDNA was added to each well in a 96-well plate that was placed in a cool block. 8 µl of mastermix was then added to the well. All reactions were performed in triplicate. After the plate was loaded, it was sealed with adhesive film and centrifuged at 1000 rpm for 1 min. The CFX connect™ Real-Time PCR Detection System (Bio-Rad) was used under the following conditions (Table 2.15).

Table 2.15 qPCR reaction conditions.

Number of cycles	Step duration	Temperature (°C)
1	5 min	95
39	10 sec	95
	30 sec	60
1	1 min	95
-	1 min	55
	10 sec at each 0.5 ˚C increment between 55 ˚C and 95 ˚C	

2.2.5.4   Data analysis

Samples were loaded in triplicate for each gene to be analysed by qPCR. Any anomalies (replicate wells that did not fall into 1 cycle of other replicates) were excluded from future analysis. The delta-delta Ct ($2^{-\Delta\Delta Ct}$) of each sample was calculated and samples were plotted on a graph based on fold change. Samples were normalised to a housekeeping gene (*GAPDH, L19*).

2.2.6 siRNA knockdown

2.2.6.1   siRNA design

siRNA duplexes were designed using the Dharmacon siDESIGN Center (https://dharmacon.horizondiscovery.com/design-center/) against each target gene, including rUrU overhangs.

2.2.6.2 siRNA transfection

Cells were transfected 24 h after seeding with 10 nM of siRNA diluted in Opti-MEM medium and mixed with Lipofectamine RNAiMAX transfection reagent. The siRNA-lipid complex solutions were incubated for 5min prior to adding to cells and the cultures were incubated for 48-72 h.

2.2.6.3 siRNA knockdown validation

2.2.6.3.1.1 RNA expression analysis

To ensure successful knockdown of each target gene, cells transfected with siRNAs were validated by extracting RNA from samples. Media was removed from cells and 500 μL TRIzol reagent was added to each well (12-well plate) and the subsequent solution was transferred to a 1.5 mL microcentrifuge tube. 100 μL of chloroform was added and each sample was gently shaken and then incubated at room temperature for 3 min. Samples were centrifuged at 12,000 x g for 15 min at 4 $^{\circ}$C. After spinning, 200 μL of the clear top phase was transferred to a fresh microcentrifuge tube. 250 μL of cold isopropanol was added to each tube, mixed, and samples were incubated for 10 min at room temperature. Samples were centrifuged at 12,000 x g for 10 min at 4 $^{\circ}$C. The supernatant was removed and pellets were washed twice with 75 % EtOH. After removing excess EtOH with a pipette tip, samples were left to air dry for 10 min at room temperature before being resuspended in 20 μL dH_2O. Samples were reverse transcribed (2.2.5.2) and mRNA levels were analysed via qPCR (2.2.5.3).

2.2.6.3.1.2 Validation of protein knockdown via siRNA

To validate PSIP1 knockdown, protein lysate was extracted and samples were checked for sufficient knockdown via Western blotting as per section 2.2.4.3

2.2.7   Cell assays

2.2.7.1   Cell proliferation growth assay

4000 cells were seeded in triplicate in a 96-well plate with 100 µl of growth media and incubated for the desired timepoints. Cells were fixed with 100 µl 4 % Paraformaldehyde (PFA) for 1 h at each time point. The fixative was removed, cells were washed twice with PBS and plates were left to dry at RT. Cells were stained with 50 µl 0.04 % crystal violet per well. After a 1 h incubation at RT, the stain was removed, and cells were washed 3x with dH_2O. Plates were left to dry and then 10 % acetic acid was added to each well and plates were placed on a rocker for 1 h at RT. Absorbance levels were then measured at OD490 with a CalrioStar multiwall plate reader (BMG Labtech).

2.2.7.2   Scratch/wound healing assay

Cells were seeded into 96-well plates so that they reached 100 % confluency after 24 h. At this point, scratches were made in each well with a 20 µl sterile tip. Media and any detached cells were then removed with an aspirator and 100 µL fresh media was slowly added to each well. Images of the scratched wells were obtained at intervals between 0 and 24 h. The subsequent migration of cells into the 'scratched' areas was measured using ImageJ software (https://imagej.nih.gov/ij) over this 24 h period.

2.2.7.3　Colony formation assay

1000 cells were seeded into a 6-well plate. Cells were cultured for ~2 weeks with regular media changes until colonies formed. Cells were fixed with 4 % PFA and stained with 0.04 % crystal violet. Colony numbers were analysed using ImageJ software (https://imagej.nih.gov/ij/).

2.2.7.4　Cell tracking assay

1000 cells per well were seeded in a 96-well plate 24 h prior to transfection or treatment. 100 µl of PBS was added to the outer wells of the plate to prevent evaporation. A Wide-Field microscope (Eclipse T*i*, Nikon) with a motorized stage and humidified chamber (Model:H301, OkoLab, Italy) set at 37 °C with 5 % CO_2 was used to acquire images 24 h after treatment/seeding. A 10X 0.3 N.A objective lens was used. Two-dimensional (2D) time series frames were captured with an Andor camera (Model: Luca-R-DL-626, *Andor* Techology, UK) using NIS-Elements software every 20 min for 24 h.

2.2.7.5　Flow cytometric analysis of apoptotic cells (DNA hypodiploidy staining).

Cells were seeded in a 6-well plate and subsequently treated and cultured for 3 days. Culture media was removed and transferred to 1.5 mL tubes. Samples were washed with PBS and this was also transferred to the same tube. 500 µl of trypsin was added to cells and incubated for a few min to allow cell dissociation. 500 µl of the collected media and PBS mixture was added to cells and pipetted gently up and down and transferred to the corresponding tube. Cell suspensions were centrifuged

for 3 min at 5000 rpm and the supernatant was removed. Pellets were suspended in 100 μl of Nicoletti buffer and tubes were immediately vortexed to avoid cell clumping. The percentage of apoptotic cells was quantified using an Accuri C6 flow cytometer. 1000 cells in total were measured per sample.

2.2.7.6   Cell cycle analysis

Cells were seeded in 6-well plates and grown until 80 % confluent. Cells were harvested, washed twice with PBS and fixed by dropwise addition of 500 μl 70 % ethanol with a gentle vortexing for 30 min. After fixation, cells were washed twice with PBS and pelleted (3000 rpm, 5 min) each time to remove excess ethanol. Cells were resuspended in 500 μl PI staining solution which includes a ribonuclease element (RNAse A) to ensure only DNA was stained. The number of cells in each stage of the cell cycle were quantified using an Acurri C6 flow cytometer. 10 000 cells in total were measured per sample.

2.2.7.7   Cell treatment with chemotherapeutic drugs

The chemotherapeutic drugs fluorouracil, oxaliplatin, and docetaxel were used to test the sensitivity of colorectal and prostate cancer cells to chemotherapeutic drugs when *HOTTIP, HOXA13,* and PSIP1 expression is reduced. A dose response curve was carried out to determine the optimal concentration of drug to use for each cell line. Drugs were added to cells in 96-well plates and cells were allowed to grow for three days prior to measurements being taken.

2.2.8 RNA preparation for sequencing analysis

2.2.8.1 RNA preparation

Total RNA was extracted from knock out and control cell lines using the Qiagen RNeasy Mini Kit (74104). cDNA was synthesised and qPCR carried out as described in 2.2.5.2 and 2.2.5.3 to validate the gene expression levels of knock out cell lines.

2.2.8.2 RNA quality check

The quality of RNA was checked by running samples on a 1.2 % agarose/TBE RNA gel. RNA samples were diluted 1:1 with loading dye and denatured by boiling for 10 min at 70 °C before immediately being placed on ice for a further 2 min. Samples were ran on an agarose gel by electrophoresis at 80 V for 60 min. The RNA integrity number (RIN) of each sample was quantified by Qubit RNA IQ assay (Thermo Scientific) prior to diluting samples to the sequencing company's (Novagene, Cambridge, UK) requirements.

2.2.9 Bioinformatics

RNA-Seq data analysis was completed using the linux/bash shell platform, Python, R, SeqMonk (Babraham Institute), and Gorilla gene ontology database (Bolha, Ravnik-Glavač and Glavač, 2017). The following packages were used: ''TopHat2' to align RNA-Seq reads to the human genome (Yang *et al.*, 2017), 'HTSeq' to count how many reads map to each gene (Hajjari and Salavaty, 2015) and 'DESeq2' to calculate the differential expression of RNA-Seq data (Hajjari and Salavaty, 2015). The data was filtered for genes P<0.01 and a Log2FC >0.5.

2.2.10 Statistical analysis

All statistical analysis was carried out using Graphpad prism 8, Rstudio or SeqMonk. A summary table of the statistical test used for each experiment is included below (Table 2.16). All experiments were the standard error of the mean (S.E.M) or standard deviation (S.D) of 3 biological repeats.

Table 2.16 Statistical analysis summary table

Assay	Statistical test	Description
Apoptosis assay	Two way ANOVA	-
Cell cycle assay	Two way ANOVA	-
Cell tracking assay	Kruskal-Wallis	siRNA vs NTC
Cell tracking assay	Mann-Whitney	WT vs KO
Colony formation assay	Unpaired t test	WT vs KD/KO
Colony formation assay	Two way ANOVA	Treatment vs no treatment
Dose response	Two way ANOVA	-
Growth assay	Two way ANOVA	-
qPCR	Unpaired t-test	WT vs KD/KO
qPCR	Two way ANOVA	Multiple gene comparison
Wound healing assay	Unpaired t test	-

3 Investigating the role of *HOTTIP* in the progression of cancer.

3.1 Introduction

HOXA transcript at the distal tip (*HOTTIP*) is a long non-coding RNA (lncRNA) located at the 5' end of the *HOXA* cluster and is involved in the regulation of nearby *HOXA* genes, in particular *HOXA13,* which is located in the closest proximity to *HOTTIP* (Qi, Zhou and Du, 2016). *HOTTIP* interacts with DNA through chromosomal looping, which results in these nearby *HOXA* genes being regulated in a *cis* fashion (Qi, Zhou and Du, 2016). *HOTTIP* binds to the WDR5 adapter protein enabling it to target *WDR5/MLL* complexes across the 5' end of the *HOXA* cluster, resulting in increased H3K4me3 levels which in turn maintains active expression of 5' *HOXA* genes (Bridges and Morgan, 1923).

HOTTIP expression is up-regulated in many cancers, including colorectal (Lappin *et al.*, 2006), pancreatic (Holland, 2013), hepatocellular carcinoma (HCC) (Quagliata *et al.*, 2015), breast (Yang *et al.*, 2017), gastric, lung, osteosarcoma and prostate cancer (Joo, Park and Chun, 2016). *HOTTIP* has been implicated in the development of some of these cancers alongside the nearby *HOXA13* gene (e.g. HCC, prostate, gastric), and together they have been associated with metastasis, increased cell proliferation and poor prognosis (Quagliata *et al.*, 2015; Chang *et al.*, 2016; Zhang *et al.*, 2016). A role for *HOTTIP* in promoting chemoresistance in cancer has also started to emerge (Joo, Park and Chun, 2016). However, this has only been documented once in prostate cancer (PCa) (De Kumar and Krumlauf, 2016) and no studies investigating the role of *HOTTIP* in colorectal cancer (CRC) chemosensitivity have so far been published.

This chapter will outline the role of *HOTTIP* in the progression of CRC and PCa cancer and investigate whether *HOTTIP* has a role in chemosensitivity. Global gene expression will also be explored following *HOTTIP* knock-out in HCT116 cells to determine the role of this lncRNA in the CRC transcriptome.

3.2   Validating siRNA mediated *HOTTIP* depletion and stable CRISPR-Cas9 *HOTTIP* knock out in cancer cell lines.

3.2.1   siRNA mediated depletion of HOTTIP

In order to determine the role of *HOTTIP* in CRC and PCa, siRNAs were employed to knockdown (KD) *HOTTIP* levels in three cell lines: HCT116 (Wang *et al.*, 2011), RKO1 (Wang *et al.*, 2011) (CRC) and DU145 (Kingston and Tamkun, 2014) (PCa). Two siRNAs (termed HOTTIP KD 1 and HOTTIP KD 2) targeted to transiently knockdown the expression of *HOTTIP* have been used throughout this study. These siRNA were compared to a non-targeting (NTC) siRNA control to reduce false-positive results or any changes occurring due to off-target effects.

Firstly, to confirm successful *HOTTIP* depletion in each cell line, cells were seeded in 6-well plates and transfected with either *HOTTIP* targeting or NTC siRNA. After 72 h, RNA was extracted and reverse transcribed to synthesise cDNA prior to qPCR analysis. Gene expression levels were quantified and data normalised to the ribosomal protein gene *L19.* The effect of siRNA mediated *HOTTIP* depletion upon nearby *HOXA* genes (*HOXA13, HOXA11*) was also quantified, due to the role of *HOTTIP* in regulating nearby *HOX* gene expression (Kingston and Tamkun, 2014).

A reduction in *HOTTIP* expression was observed in *HOTTIP* depleted HCT116 cells compared to NTC indicating successful *HOTTIP* KD (Figure 3.1A), as well as a reduction in *HOXA13* and *HOXA11* expression. A reduction in *HOTTIP* and *HOXA13* expression was also observed in *HOTTIP* depleted RKO1 cells, however this was not found to be significant (Figure 3.1B).

In *HOTTIP* depleted DU145 cells, both *HOTTIP* and *HOXA13* expression were reduced (Figure 3.1C), although this was not significant. siRNA mediated knockdown of *HOTTIP* in these cell lines followed the pattern stated in the literature where *HOXA13* expression is also reduced upon *HOTTIP* is depletion (Smith, Zyoud and Allegrucci, 2019). Therefore, these data can confirm successful siRNA mediated depletion in these cell lines. Successful siRNA depletion was regularly confirmed alongside functional assays to investigate the role of *HOTTIP* in HCT116, RKO1 and DU145.
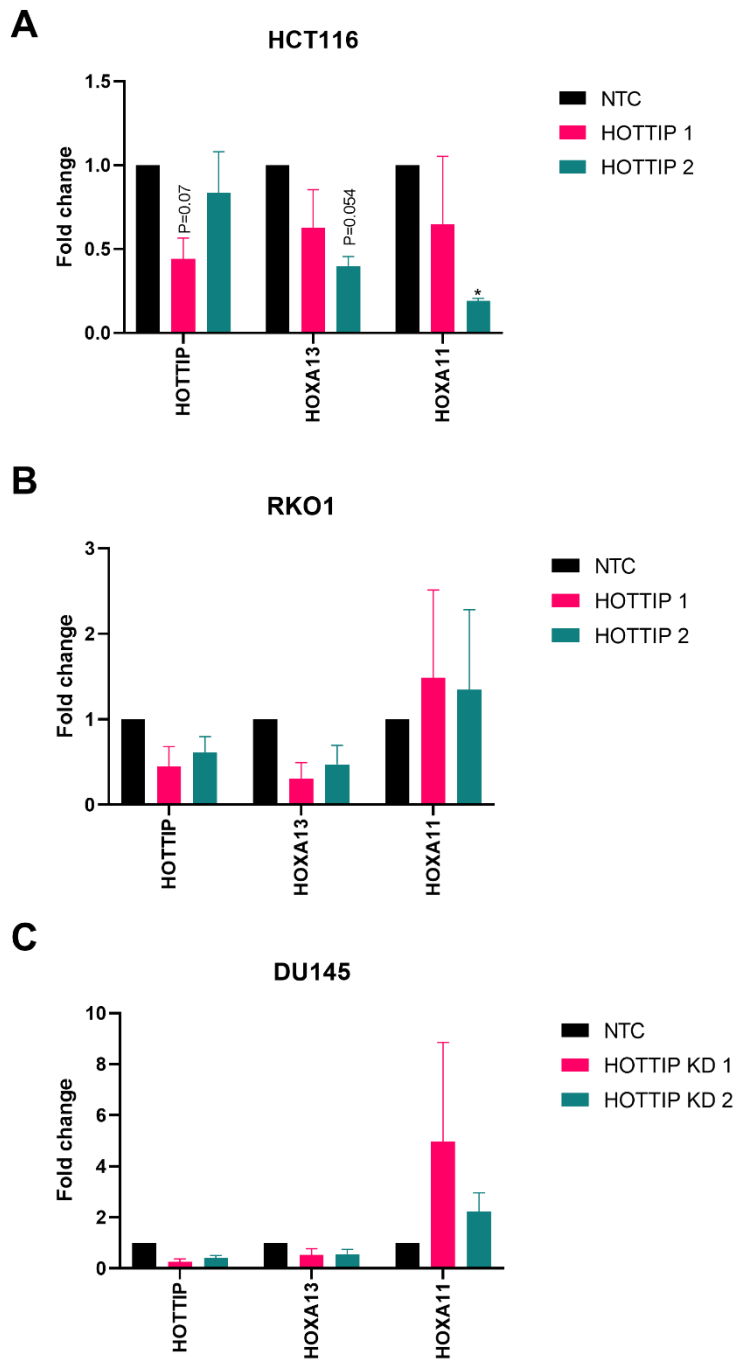
Figure 3.1 siRNA mediated HOTTIP depletion gene expression

(A) HCT116, (B) RKO1 and (C) DU145 cells were transfected with HOTTIP targeting or NTC siRNA for 72 h. RNA was subsequently extracted and cDNA synthesised. Gene expression levels of target genes (HOTTIP, HOXA13, HOXA11) were quantified and compared to NTC via qPCR. Data are mean (± S.E.M) fold change of relative expression of 3 biological replicates (N=3), analysed by qPCR and normalized to L19. Two-way ANOVA with Dunnett's multiple comparison test was used to quantify the statistical significance (*P<0.05).

3.2.2   Creating stable HOTTIP knock out lines using CRISPR-Cas9.

To validate the findings from the siRNA KD studies, stable CRISPR-Cas9 *HOTTIP* knock

out (KO) and wild type (WT) control HCT116 cell lines were created (as per Chapter 2,

section 2.2.2). Two guide RNAs (gRNAs) were designed to target each end of the

HOTTIP transcript (5' and 3'). This resulted in a deletion at each end (Figure 3.2A) and

a truncated, non-functional version of the *HOTTIP* transcript. The 5' gRNA was

designed, slightly downstream of the transcription start site (TSS), to avoid removing

any transcriptional machinery that could be acting on nearby genes.

After CRISPR-Cas9 selection, DNA was extracted from cells and a PCR screen

was performed to identify WT (empty plasmid backbone) and *HOTTIP* KO clones.

Three primer sets were designed to screen for positive *HOTTIP* KO CRISPR clones

(Figure 3.2A). A total of 48 possible clones were screened via PCR for the desired

HOTTIP KO genotype. After successful PCR screening, positive clones (1 x WT and 3 X

HOTTIP KO) were sent for Sanger sequencing analysis (Figure 3.2B). One WT and one

HOTTIP KO clone (Figure 3.2C) were selected for further work.

To confirm *HOTTIP* depletion at the RNA level, RNA was extracted from the

WT and KO clones and reverse transcribed to synthesise cDNA. Gene expression

levels were quantified via qPCR and data normalised to the ribosomal protein gene

L19. A highly significant loss of *HOTTIP* (Figure 3.2D) was observed indicating loss of

the *HOTTIP* transcript on the gene expression level. As well as loss of *HOTTIP*

expression, the nearby *HOXA13* gene was also significantly down regulated. *HOXA1*

expression is unaffected when *HOTTIP* expression is KO, which may be explained by

the fact that it is the *HOXA* gene located furthest away from *HOTTIP*. This is in line

with previous studies confirming that *HOTTIP* only regulates expression of nearby

HOX genes in *cis* (Kingston and Tamkun, 2014)*.* Overall, these data confirm

successful CRISPR-Cas9 mediated *HOTTIP* KO in HCT116 cells. These cell lines will be

used in conjunction with siRNA mediated *HOTTIP* depletion to further understand

the role of *HOTTIP* in CRC and PCa.
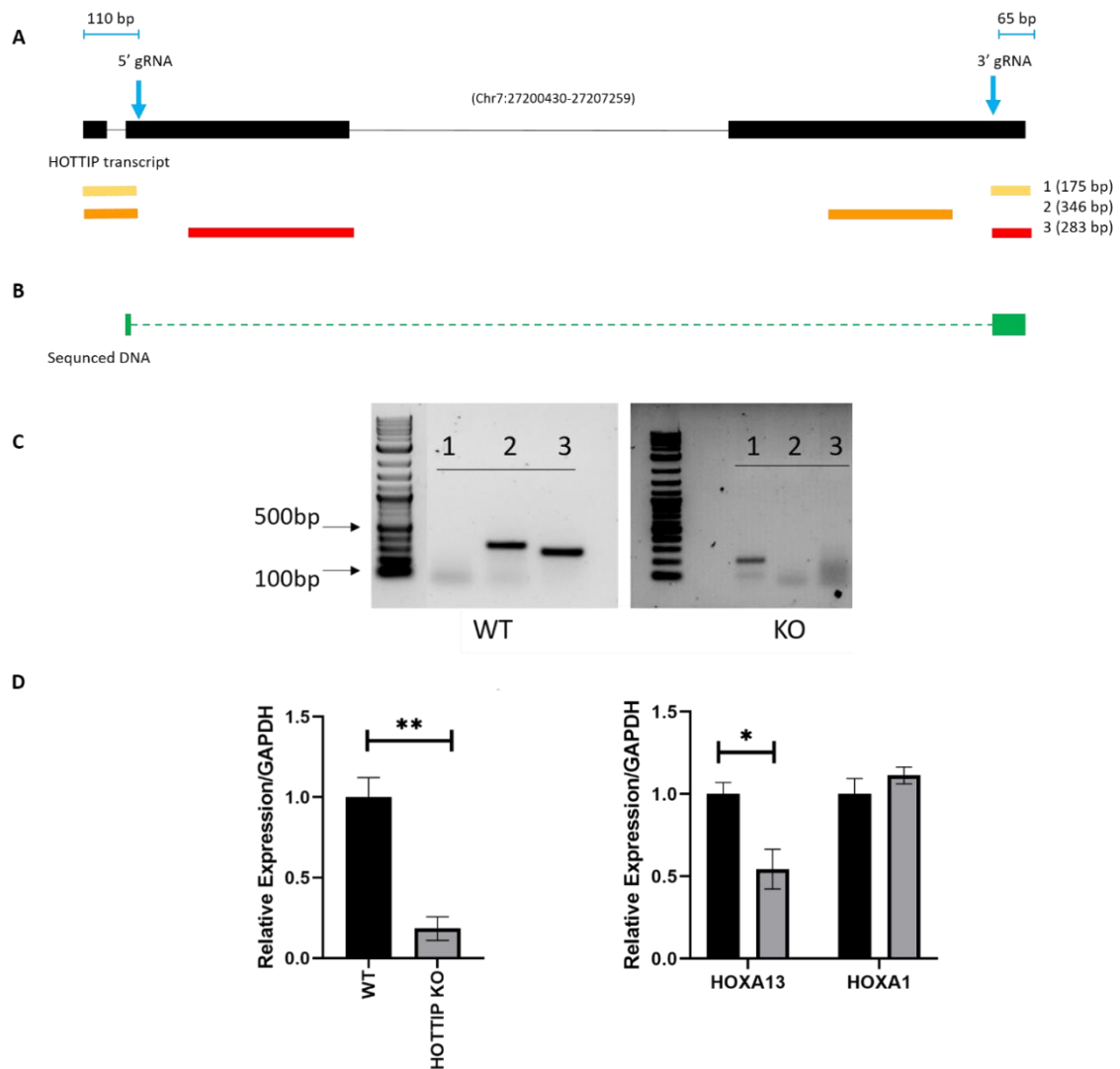
Figure 3.2 CRISPR-Cas9 mediated HOTTIP KO validation

(A) Schematic of 5' and 3' gRNA design targeted to delete HOTTIP DNA. Three primer pairs used to validate CRISPR KO clones were designed around the gRNA cut sites. Primer 1 (175 bp amplification) represents a KO clone, Primer 2 (346 bp amplification) represents a WT/HET clone. Primer 3 (283 bp amplification) represents a WT/HET clone. (B) Sequence data of a positive HOTTIP KO HCT116 clone that was analysed via Sanger sequencing. (C) DNA was extracted from WT and HOTTIP KO HCT116 clones and genotyped by PCR with three primer sets, primer 1 (175 bp = KO clone), primer 2 (346 bp = WT/HET clone), primer 3 (283 bp = WT/HET clone). (D) RNA was extracted from positive WT and HOTTIP KO HCT116 clones and cDNA subsequently synthesised. HOTTIP, HOXA13 and HOXA1 gene expression levels in both clones were analysed via qPCR. Data are mean (± S.E.M) expression of 3 biological replicates (N=3), analysed by qPCR and normalised to L19. Two-way ANOVA with Dunnett's multiple comparison test was used to quantify the statistical significance (*P<0.05, **P<0.01).

3.3   Investigating the role of HOTTIP deletion on the movement and migration of CRC and PCa cells.

Previous studies have described *HOTTIP* having roles in cell proliferation, migration and invasion in cancer (Kingston and Tamkun, 2014). Through *HOTTIP* depletion/deletion studies, this work will investigate this further in CRC and PCa cell lines and attempt to add to the knowledge of *HOTTIP*'s potential role as promoting oncogenesis.

3.3.1   Reduction of *HOTTIP* leads to a reduction in CRC and PCa single cell motility.

Single cell tracking analysis was used to analyse average cell speeds in *HOTTIP* depleted CRC and PCa cells. Prior to seeding, CYTO-ID dye (Enzo life sciences) was used to label cells, allowing fluorescence detection. Dyed cells were seeded sparsely in 96-well plates to enable individual analysis of a single cell to be possible. A Nikon Widefield microscope was used to capture images of each well every 20 minutes over a 24 h period. Cells were placed in a humidified CO_2 chamber to retain their optimum culturing conditions during this time. Average cell speeds were calculated using the Trackmate plugin on ImageJ Fiji (Milne *et al.*, 2002; Smith, Zyoud and Allegrucci, 2019).

Firstly, the average speed of siRNA mediated *HOTTIP* depleted CRC and PCa cells were tested. HCT116 cells transfected with HOTTIP KD 1 siRNA exhibited a slightly slower average cell speed and a smaller range of average speeds, although, these observations were not found to be significant (Figure 3.3A). An increase in average speed was observed in HCT116 cells transfected with HOTTIP siRNA 2; as

well as a larger range of average speeds. However, this was also not found to be significant (Figure 3.3A). *HOTTIP* depleted RKO1 cells exhibited a reduction in the range of average cell speeds, however, the mean average cell speed was similar to that of NTC and was non-significant (Figure 3.3B). *HOTTIP* depleted DU145 cells exhibited a slightly higher average cell speed than control; again, this was also not significant (Figure 3.3C). A reduction in average cell speed was observed in CRISPR-Cas9 mediated *HOTTIP* KO cells compared to WT (Figure 3.4); this was also not found to be statistically significant. Together, these data do not indicate a role of *HOTTIP* in promoting cell motility.
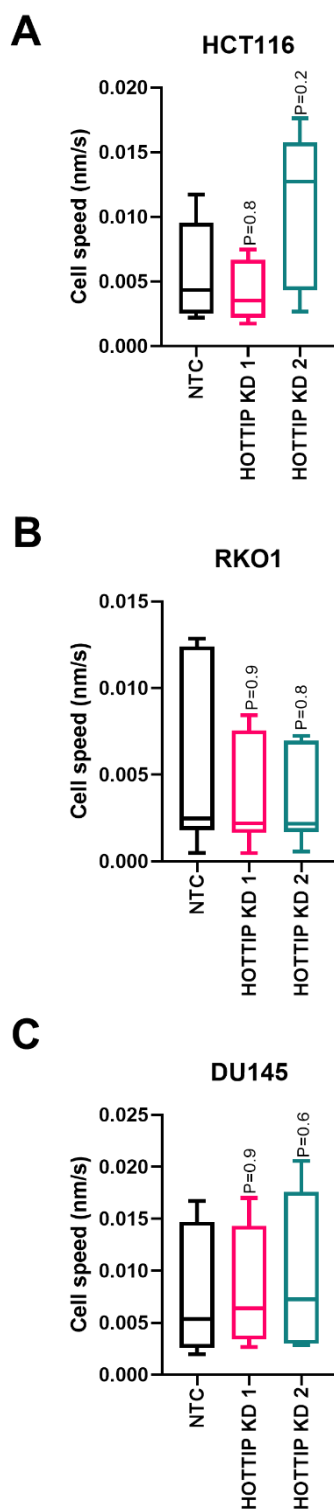
Figure 3.3 Single cell tracking analysis of siRNA mediated HOTTIP depleted cancer cells.

(A) HCT116, (B) RKO1 and (C) DU145 cells were transfected with HOTTIP targeting or NTC siRNA for 72 h. After being sparsely being seeded in 96-well plates, cells were placed in a humidified CO_2 chamber attached to a Nikon Widefield microscope where images were taken every 20 min for 24 h. Individual cells were tracked and average speeds were calculated using ImageJ Fiji. Data are mean (± S.E.M) expression of 3 biological replicates (N=3). Kruskal-Wallis test with Dunn's post-hoc test was used to quantify the statistical significance.
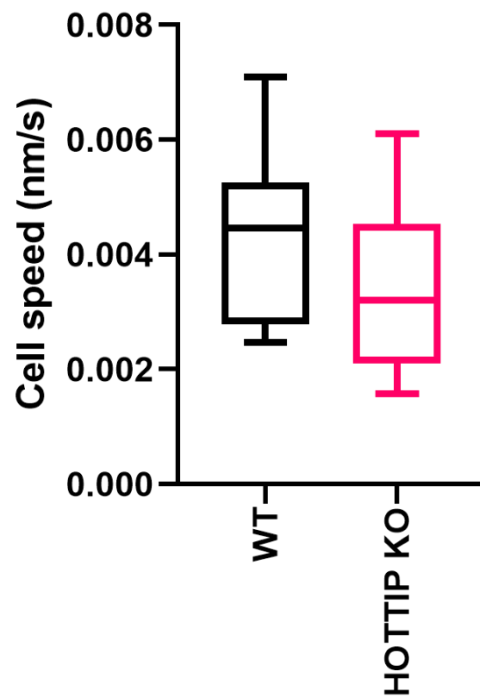
Figure 3.4 Single cell tracking of CRISPR-Cas9 HOTTIP KO HCT116 cells.

CRISPR-Cas9 mediated HOTTIP KO and WT HCT116 cells were seeded sparsely in 96-well plates and placed in a humidified CO_2 chamber attached to a Nikon Widefield microscope where images were taken every 20 min for 24 h. Individual cells were tracked and average speeds were calculated using ImageJ Fiji. Data are mean (± S.E.M) of 3 biological replicates (N=3). Mann Whitney test was used to test statistical significance (P=0.3).

3.3.2 *HOTTIP* depletion results in reduced migration of CRC and PCa cells.

To measure the migration rates of *HOTTIP* depleted cancer cells, wound healing assays were implemented. Cells were seeded in 6-well plates so they reached 100 % confluency within 24 h. A 'wound' was created in each well using a P20 pipette tip. A Nikon Widefield microscope was used to take pictures of each well every 20 minutes over a 24 h period. Cells were placed in a humidified CO_2 chamber to retain their optimum culturing conditions during this time. The percentage of cell coverage at each time point was analysed using Image J software (De Kumar and Krumlauf, 2016).

A reduction in cell migration was observed in *HOTTIP* depleted HCT116 and DU145 cells (Figure 3.5A/C), however, this was not significant for either cell line. RKO1 cells transfected with HOTTIP KD 1 exhibited an increase in migration, whereas RKO1 cells transfected with HOTTIP KD 2 resulted in a decrease in migration (P=0.07) (Figure 3.5B). Migration was also reduced in CRISPR-Cas9 *HOTTIP* KO compared to WT HCT116 cells, but again, this failed to reach diagnosis (P=0.08) (Figure 3.6). As no significant reduction in cell migration was observed, it cannot be confirmed that *HOTTIP* promotes cell migration in HCT116, RKO1 or DU145 cells.
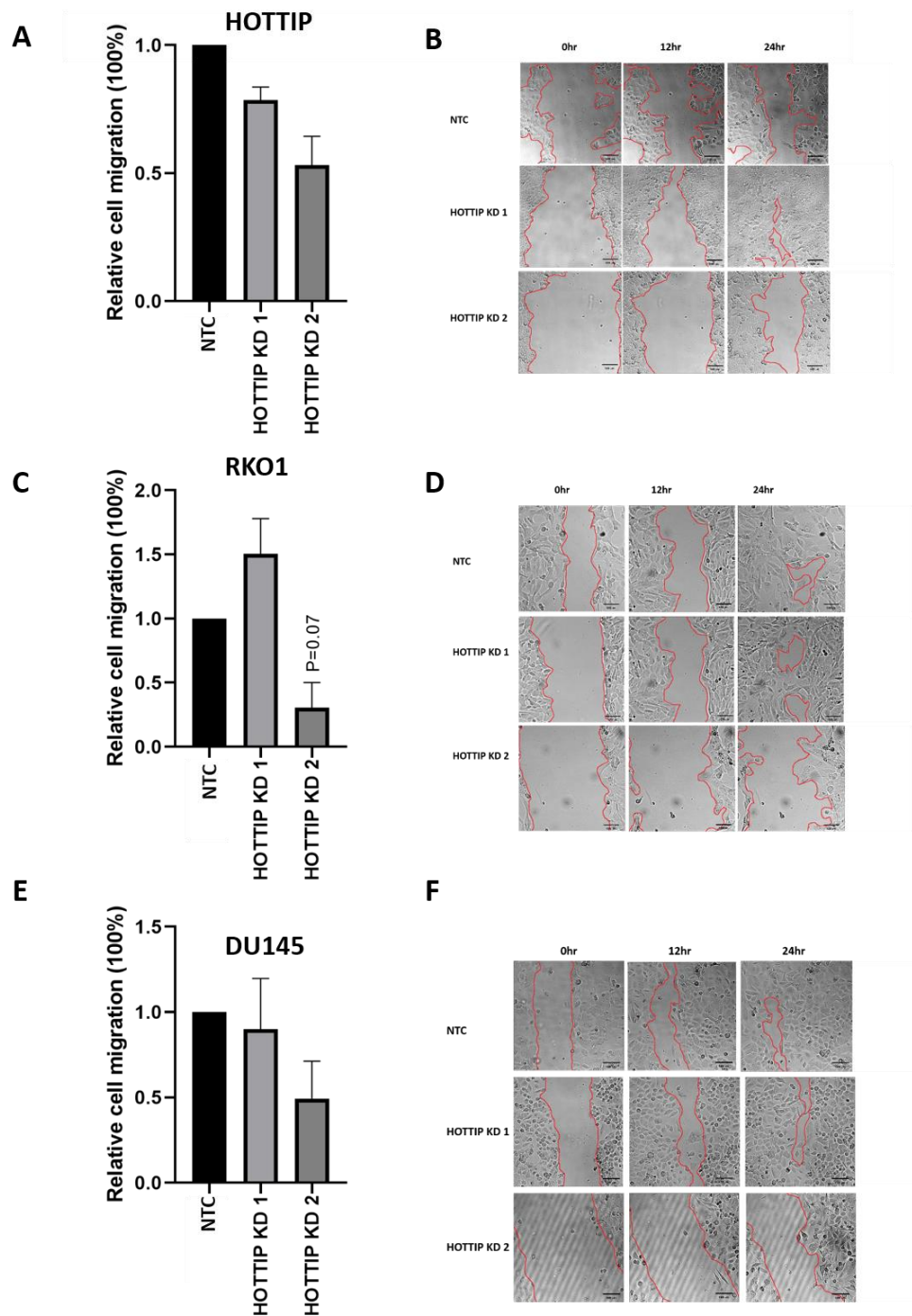
Figure 3.5 Cell migration rates of HOTTIP depleted cancer cells.

Wound healing assays were carried out to measure the migration rates of siRNA mediated HOTTIP depleted cancer cells. 'Wounds' were tracked over 24 h and HOTTIP depleted cell migration was calculated relative to NTC. Cell migration of HOTTIP depleted (A) HCT116 (B) RKO1 (C) DU145 cells. Data are mean (± S.E.M) of 3 biological replicates (N=3). One-way ANOVA with Dunnett's multiple comparison was used to test statistical significance. Representative images of WT and HOTTIP KD 'wounds' at 0 h, 12 h, and 22 h after initial scratching of confluent (D) HCT116 (E) RKO1 (F) DU145 cells taken using a Nikon Widefield microscope and analysed with ImageJ Fiji.
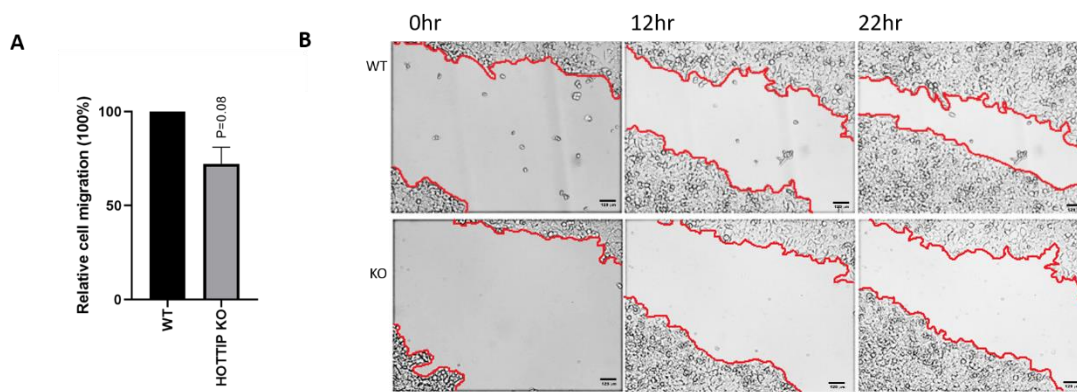
Figure 3.6 Cell migration rates of CRISPR-Cas9 mediated HOTTIP KO HCT116 cells.

Wound healing assays were carried out to measure the migration rates of CRISPR-Cas9 mediated HOTTIP KO HCT116 cells. (A) 'Wounds' were tracked over 24 h and HOTTIP KO cell migration was calculated relative to WT. Data are mean (± S.E.M) of 3 biological replicates (N=3). Unpaired t-test with Welch's correction was used to quantify statistical significance. (B) Representative images of WT and HOTTIP KO 'wounds' at 0 h, 12 h and 24 h after initial scratching of confluent cells taken using a Nikon Widefield microscope and analysed with ImageJ Fiji.

3.3.3 Investigating the effect of *HOTTIP* on cell viability and proliferation in HCT116 cells.

Colony formation assays were used to investigate the effect of *HOTTIP* on cancer cell growth; this assay allows measurement of cell viability and the ability of cells in a population to continually divide (De Kumar and Krumlauf, 2016). CRISPR-Cas9 mediated *HOTTIP* KO and WT HCT116 cells were seeded sparsely into 12-well plates and grown for ~10 days to allow single cells to form colonies. The number of colonies formed was quantified using ImageJ Fiji software (Schindelin *et al.*, 2012). No significant difference in the number of colonies was observed in *HOTTIP* KO cells compared to WT (Figure 3.7), indicating that *HOTTIP* does not have a role in maintaining HCT116 cell viability and proliferation.

The proliferation rates of CRISPR-Cas9 *HOTTIP* KO and WT HCT116 cells were then compared. Cells were seeded in 96-well plates and grown over a time series for 8 days. After each time point, cells were fixed and stained with crystal violet prior to colorimetric measurement (OD 490 nm) and growth rates were calculated relative to day 0 (no growth). A reduction in proliferation was observed in *HOTTIP* KO cells compared to WT (P=0.06) (Figure 3.8), suggesting *HOTTIP* may promote proliferation in HCT116 cells.
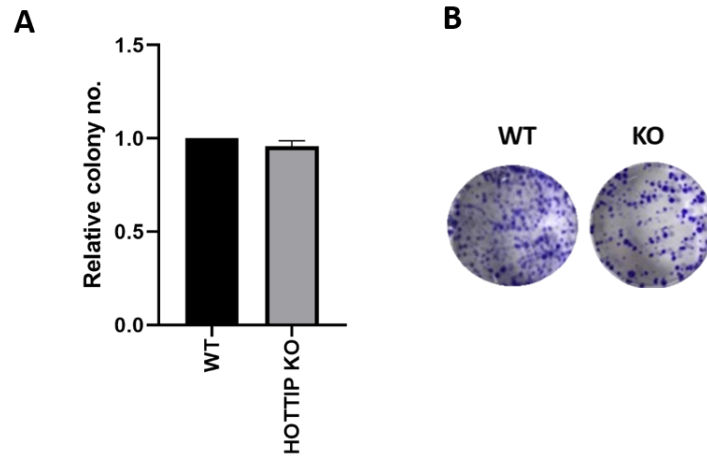
Figure 3.7 Colony formation ability in CRISPR-Cas9 mediated HOTTIP KO HCT116 cells compared to WT.

CRISPR-Cas9 mediated HOTTIP KO and WT HCT116 cells were seeded and allowed to form colonies for ~10 days. (A) Relative colony number of HOTTIP KO cells compared to WT. Data are mean (± S.E.M) of 3 biological replicates (N=3) relative to control WT cells. Unpaired t-test with Welch's correction was used to quantify the statistical significance. (B) Representative wells of colonies stained with crystal violet after fixation with 4 % PFA.
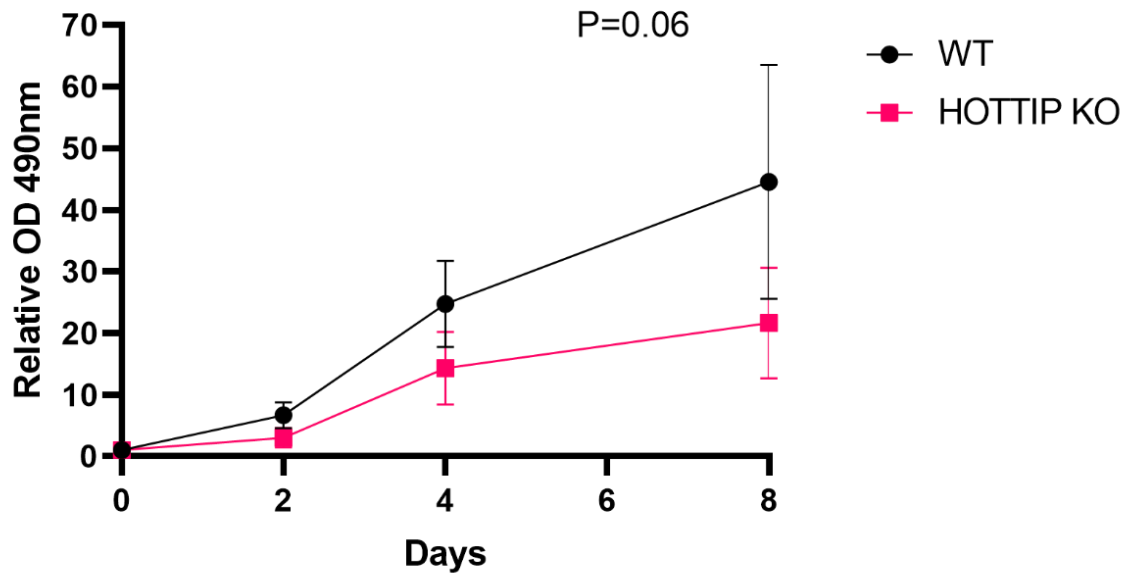
Figure 3.8 HOTTIP KO proliferation assay

CRISPR-Cas9 mediated HOTTIP KO and WT HCT116 cells were seeded in 96-well plates and growth rates were measured over an 8-day time series. Growth rates were calculated relative to day 0 (no growth). Data are mean (± S.E.M) of 3 biological replicates (N=3). A paired t-test was used to calculate statistical significance, P=0.06.

3.3.4 HOTTIP has no significant effect on apoptosis in cancer cells.

Flow cytometry was used to assess whether *HOTTIP* depletion alters the levels of apoptosis in HCT116, RKO1 and DU145 cells. Again, siRNAs were used to knockdown *HOTTIP* expression. 72 h after transfection, all cells and media were collected and pelleted. Pelleted cells were re-suspended in Nicoletti buffer (De Kumar and Krumlauf, 2016) containing propidium iodide (PI), used to stain apoptotic cells. During the process of apoptosis DNA becomes fragmented. As a result, rates of apoptosis can be measured by the identification of hypodiploid cells using a DNA stain such as PI. Cellular PI intensity was quantified using flow cytometry and rates of apoptosis were compared to NTC siRNA controls.

In *HOTTIP* depleted HCT116 cells, a decrease in apoptosis was observed compared to NTC (Figure 3.9A). *HOTTIP* depleted RKO1 and DU145 cells exhibited an increase in apoptosis (Figure 3.9B/C). In all cases, this was not found to be significant. The apoptosis rates of CRIPSR-Cas9 *HOTTIP* KO HCT116 cells were then examined, and whilst they were found to increase compared to WT, this was again a non-significant result (Figure 3.10). Overall, depletion of *HOTTIP* in these cell lines does not appear to contribute to increased cell death.
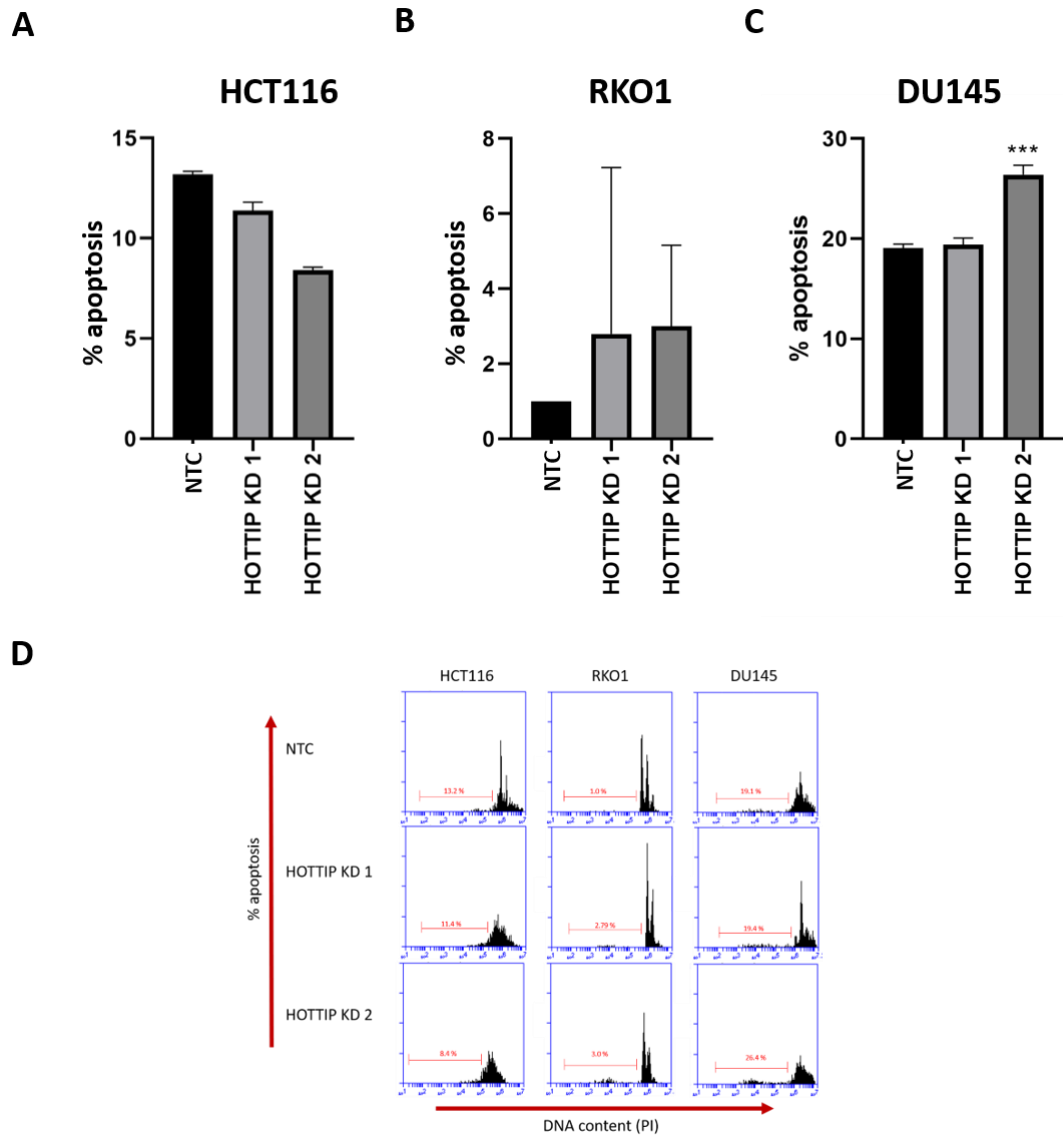
Figure 3.9 Investigating the apoptosis rates of siRNA mediated HOTTIP depleted cancer cells.

After transfection for 72 h with siRNA targeting HOTTIP or NTC, all cells and media were collected and pelleted. Pellets were re-suspended in Nicoletti buffer and percentage apoptosis of HOTTIP depleted (A) HCT116, (B) RKO1 and (C) DU145 cells were analysed for DNA hypodiploidy via flow cytometry. (D) Representative flow cytometry plots of HOTTIP depleted and NTC HCT116, RKO1 and DU145 cells, average Sub-G1 percentages highlighted in red. Data are mean (±S.E.M) of 3 biological replicates (N=3). Two-way ANOVA with Dunnett's multiple comparisons test was used to quantify statistical significance.
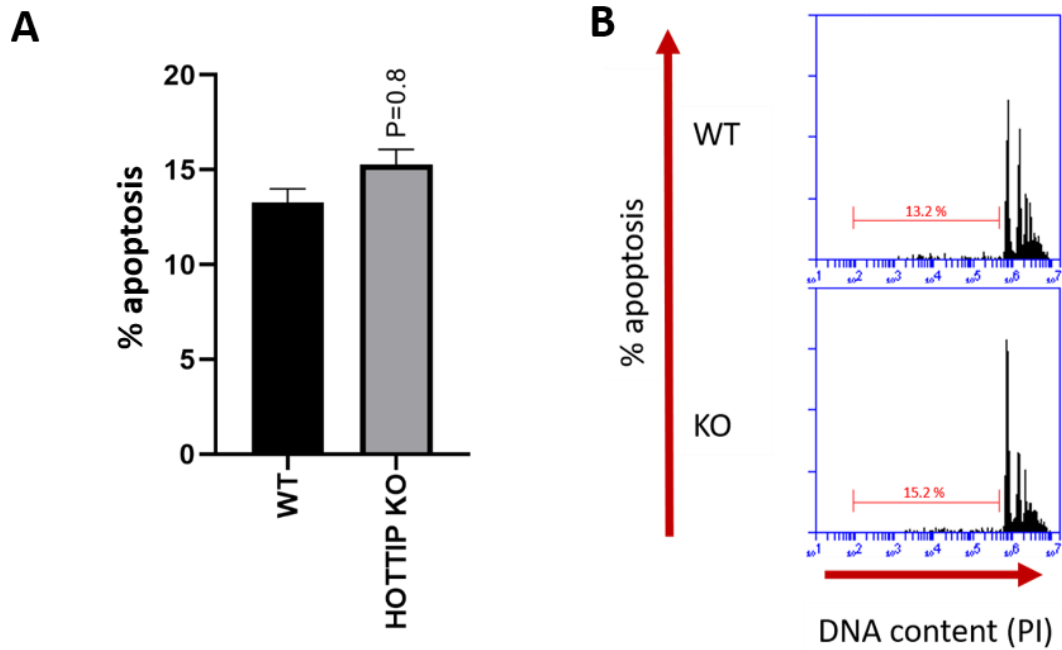
Figure 3.10 Investigating the apoptosis rates of CRISPR-Cas9 mediated HOTTIP KO HCT116 cells.

CRISPR-Cas9 mediated HOTTIP KO and WT cells were cultured in 6-well plates prior to all cells and media being collected and pelleted. Pellets were re-suspended in Nicoletti buffer and percentage apoptosis was analysed for DNA hypodiploidy via flow cytometry. (A) Percentage apoptosis of CRISPR-Cas9 mediated HOTTIP knockout HCT116 cells. (B) Representative flow cytometry plots of HOTTIP KO and WT HCT116 cells, average Sub-G1 percentages highlighted in red. Data are mean (±S.E.M) of 3 biological replicates (N=3). Two-way ANOVA with Sidak's multiple comparisons test was used to quantify statistical significance.

3.3.5　HOTTIP does not drive cell cycle progression in cancer cells.

HOTTIP has previously been described to promote cell cycle progression in leukaemia (Rinn *et al.*, 2007; Wang *et al.*, 2011). Flow cytometry was used to investigate if this is also seen in HCT116, RKO1 and DU145 cells. Cell cycle assays assess cellular DNA content and indicate what percentage of cells in a sample are in each stage of the cell cycle (Wang *et al.*, 2011). Cells were transfected with HOTTIP KD or NTC siRNA for 72 h, after which point all cells and media were pelleted and fixed so the cell cycle stage of each cell could be analysed. The fixative was removed, and samples were re-suspended in a stain containing PI. A flow cytometer was used to measure the percentage of cells in each stage of the cell cycle (G1 vs S vs G2/M) to see if there is a change in this distribution when *HOTTIP* is depleted in HCT116, RKO1 and DU145 cells. The percentage of cells in each phase of the cell cycle was analysed and *HOTTIP* depleted cells were compared to NTC.

　　　HOTTIP depleted HCT116 cells resulted in an increase in S phase and a decrease in G2/M and G1 phase compared to NTC (Figure 3.11A). An increase in G2/M and S phase was observed in *HOTTIP* depleted RKO1 cells, however, no difference in G1 phase was observed (Figure 3.11B). In DU145 cells, *HOTTIP* depletion led to an increase in G2/M and a decrease in G1 phase, nevertheless, no change in S phase was observed (Figure 3.11C). None of these data were found to be significant. In CRISPR-Cas9 *HOTTIP* KO HCT116 cells, an increase in G1 phase and a decrease in G2/M and S phase was observed (Figure 3.12), again this was not found to be significant. Overall, these data suggest that *HOTTIP* does not influence cell cycle progression in HCT116, RKO1 and DU145 cell lines.
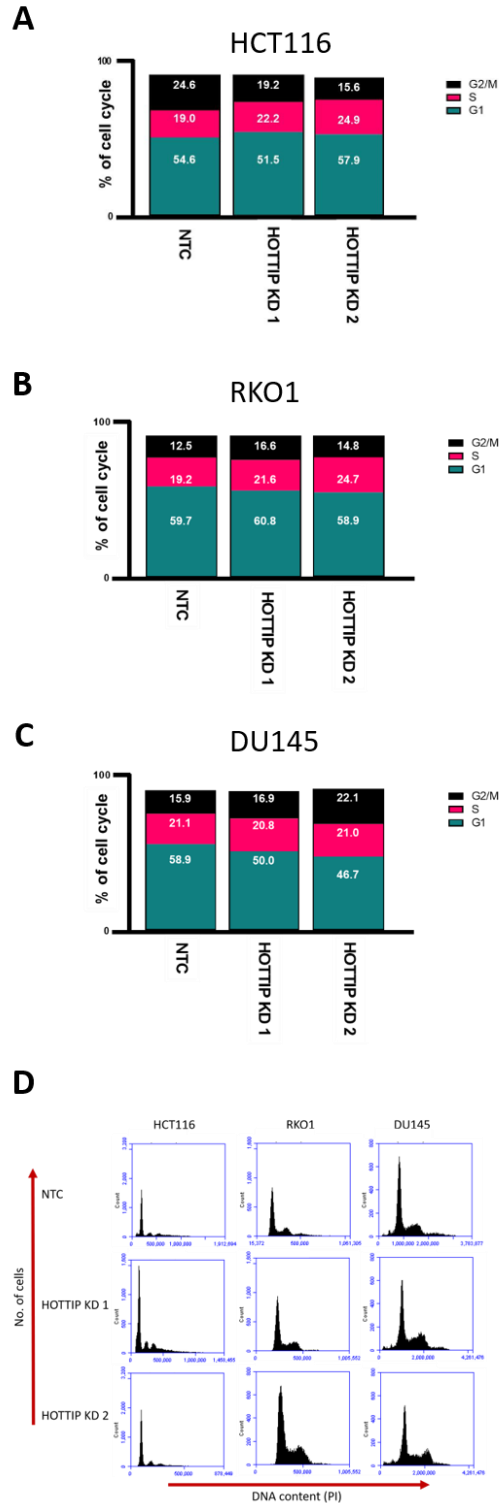
Figure 3.11 Cell cycle analysis of siRNA mediated HOTTIP depletion in cancer.

siRNA mediated HOTTIP depleted and NTC cells were analysed via flow cytometry to measure the percentage of (A) HCT116 (B) RKO1 (C) DU145 cells in each stage of the cell cycle. Data are mean (± S.E.M) of 3 biological replicates (N=3). Two-way ANOVA with Dunnett's multiple comparisons test was used to quantify statistical significance. (D) Representative flow cytometry plots of HOTTIP depletion and NTC HCT116, RKO1, and DU145 cells.
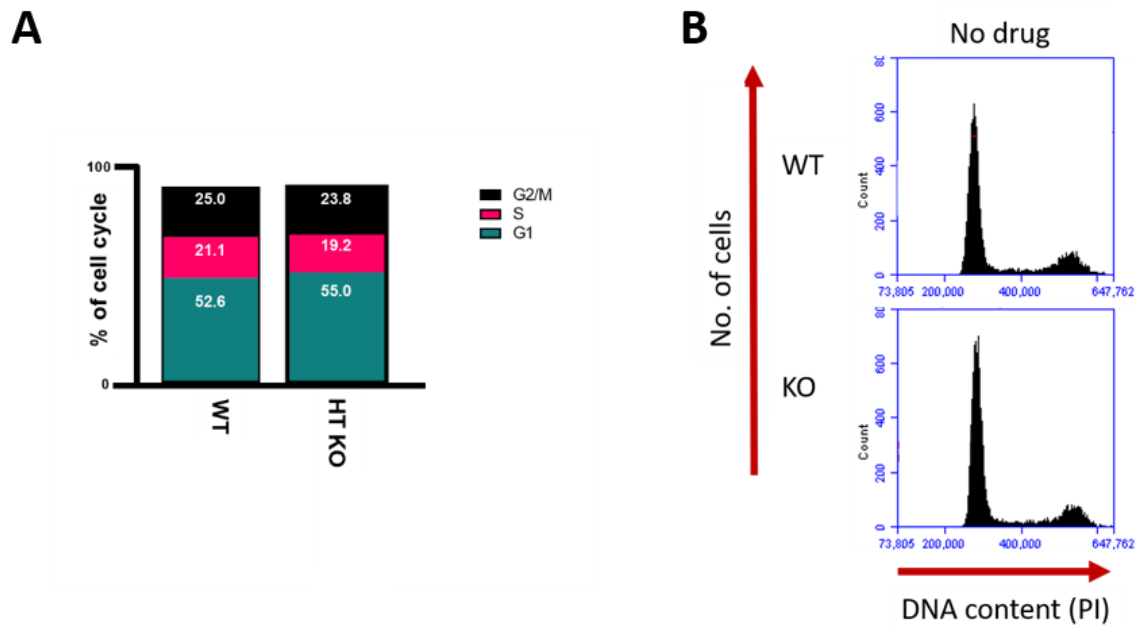
Figure 3.12 Cell cycle analysis of CRISPR-Cas9 mediated *HOTTIP* knockout in HCT116.

(A) Cell cycle analysis was carried out on CRISPR-Cas9 mediated HOTTIP KO and WT HCT116 cells using flow cytometry. Data are mean (± S.E.M) of 3 biological replicates (N=3). Two-way ANOVA with Tukey's multiple comparisons test was used to quantify statistical significance. (B) Representative flow cytometry plots of HOTTIP KO and WT HCT116 cells.

3.4 *HOTTIP* protects colorectal and prostate cancer cells against chemotherapeutic drugs.

Previous studies have suggested a role of *HOTTIP* in protecting cancer cells (small cell lung cancer and pancreatic cancer) from death when exposed to chemotherapy (Wang *et al.*, 2011). Two commonly used colorectal cancer chemotherapeutic drugs; Fluorouracil (5FU) (Li *et al.*, 2018) and Oxaliplatin (OX) (Wang *et al.*, 2011), and a prostate cancer drug; Docetaxel (DOC) (Ito *et al.*, 2018) were selected to investigate whether *HOTTIP* expression protects CRC and PCa cells against chemotherapy toxicity.

3.4.1 *HOTTIP* depletion results in sensitivity of cells towards chemotherapy in cancer.

Initially, the dose response of siRNA mediated *HOTTIP* depletion and CRISPR *HOTTIP* KO cells to chemotherapeutic drugs was tested in order to investigate whether *HOTTIP* has a role in promoting chemoresistance in cancer cells. Cells were seeded in 96-well plates and treated with a dose range of either 5FU, OX or DOC for 72 h prior to being fixed and stained with crystal violet for colorimetric measurement (OD 490 nm). The optical density was calculated relative to no drug treatment (0 µM). Proliferation rates were calculated for both control and *HOTTIP* depleted cells treated with each drug.

Both 5FU and OX were found to inhibit HCT116 and RKO1 NTC growth across all concentrations tested. A reduction in cell growth was observed in *HOTTIP* depleted HCT116 cells when treated with lower concentrations of 5FU (0.1 µM and 1

µM), indicating increased sensitivity to 5FU compared to NTC at these doses (Figure 3.13A). When treated with OX, HCT116 cells transfected with HOTTIP KD 1 exhibited greater sensitivity to the drug than both HOTTIP KD 2 and NTC (Figure 3.13B). However, this was not significant for either drug. A significant sensitivity in RKO1 cells transfected with HOTTIP KD 1 and treated with 0.1 µM 5FU was observed (Figure 3.14A). No sensitivity to OX was observed in *HOTTIP* depleted RKO1 cells (Figure 3.14B). Unexpectedly, no sensitivity to DOC was observed in DU145 NTC cells. However, there was increased sensitivity to DOC observed in *HOTTIP* depleted DU145 cells (Figure 3.15), although this was not a significant effect.

An increase in sensitivity of CRISPR-Cas9 *HOTTIP* KO HCT116 cells to 5FU was observed at the 0.1 and 1 µM concentrations (Figure 3.16A). However, a rise in *HOTTIP* KO cell growth was evident when both KO and WT cells were treated with 10 µM 5FU. An increase in sensitivity was also observed in *HOTTIP* KO HCT116 cells when treated with OX at the 10, 100 and 1000 µM doses (Figure 3.16B). Overall, siRNA mediated depletion of *HOTTIP* in HCT116 or DU145 did not result in significant increase in sensitivity of the cells to chemotherapy. The exception was *HOTTIP* depleted RKO1 cells, where significant sensitivity was observed when treated with 0.1 µM 5FU. When *HOTTIP* was permanently deleted in CRISPR-Cas9 KO HCT116 cells, significant sensitivity of the cells was observed when treated with either 5FU or OX, indicating chemosensitive properties of *HOTTIP* in this cell line.

A
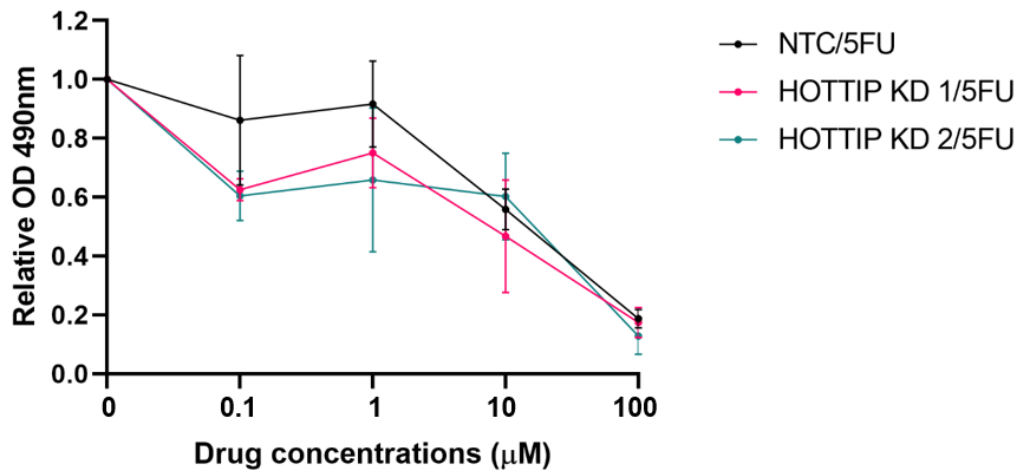
B
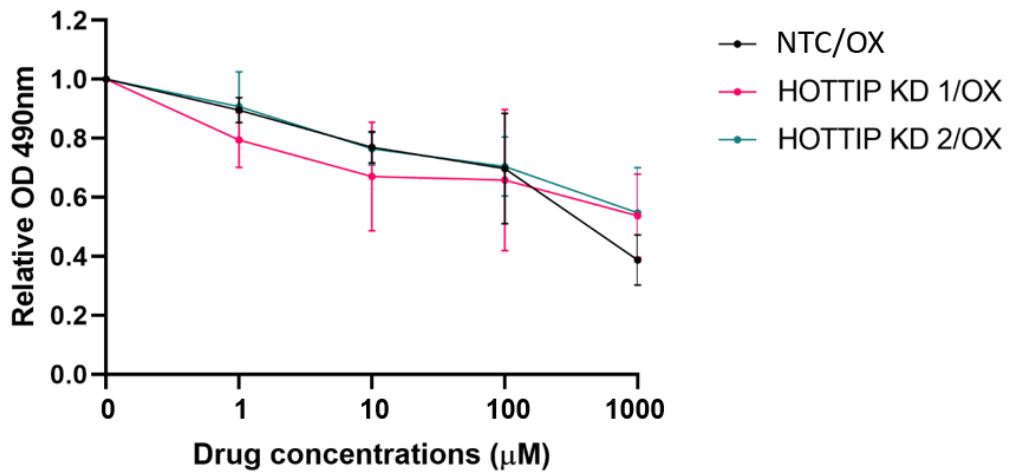
Figure 3.13 Dose response of siRNA mediated HOTTIP depleted HCT116 cells to chemotherapeutic drugs.

HCT116 cells were transfected with *HOTTIP* targeting and NTC siRNA for 72 h. Cells were then seeded in 96-well plates and subsequently treated with a dose response of (A) 5FU (0, 0.1, 1, 10, 100 μM) or (B) OX (0, 1, 10, 100, 1000 μM) for a further 72 h. The dose response of siRNA mediated *HOTTIP* depleted HCT116 cells to chemotherapeutic drugs was examined and compared to NTC. All data are mean (± S.E.M) of 3 biological replicates (N=3). Two-way ANOVA with Dunnett's multiple comparisons test was used to quantify statistical significance.
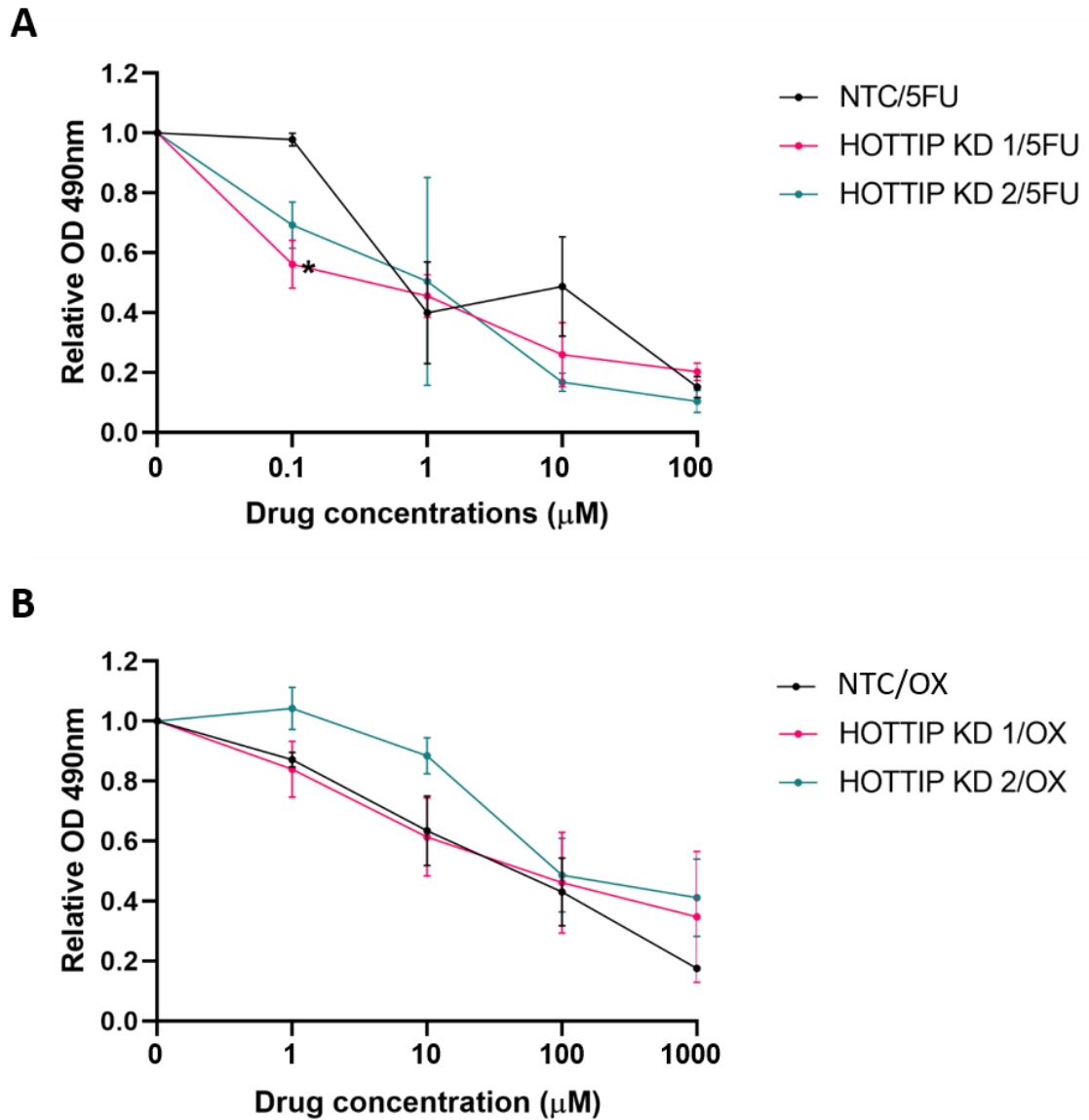
Figure 3.14 Dose response of siRNA mediated HOTTIP depleted RKO1 cells to chemotherapeutic drugs.

RKO1 cells were transfected with HOTTIP targeting and NTC siRNA for 72 h. Cells were then seeded in 96-well plates and subsequently treated with a dose response of (A) 5FU (0, 0.1, 1, 10, 100 µM) or (B) OX (0, 1, 10, 100, 1000 µM) for a further 72 h. The dose response of siRNA mediated HOTTIP depleted RKO1 cells to chemotherapeutic drugs was examined and compared to NTC. All data are mean (± S.E.M) of 3 biological replicates (N=3). Two-way ANOVA with Dunnett's multiple comparisons test was used to quantify statistical significance (*P<0.05).
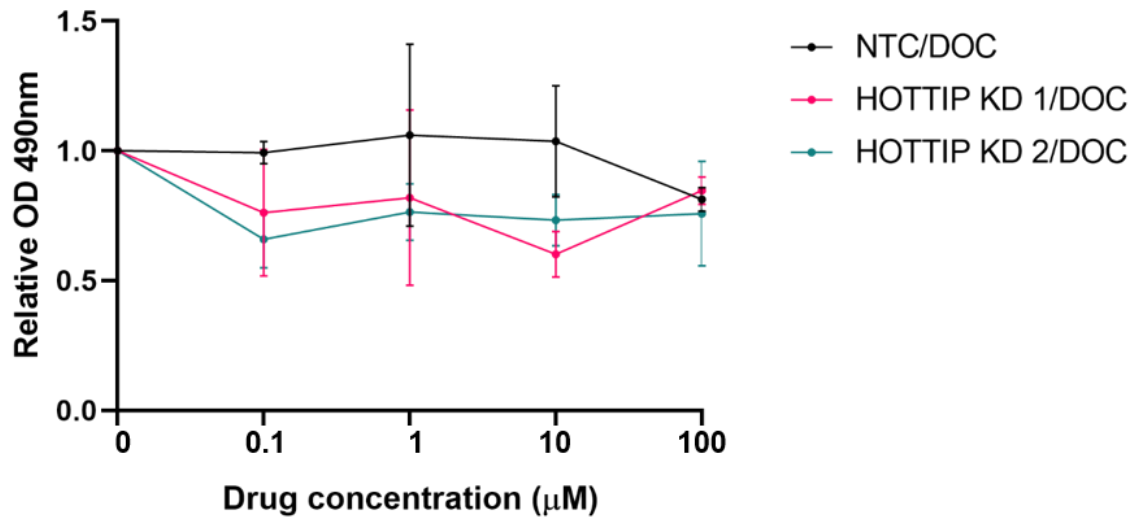
Figure 3.15 Dose response of siRNA mediated HOTTIP depleted DU145 cells to chemotherapeutic drugs.

DU145 cells were transfected with HOTTIP targeting and NTC siRNA for 72 h. Cells were then seeded in 96-well plates and subsequently treated with a dose response of DOC (0, 0.1, 1, 10, 100 μM) for a further 72 h. The dose response of siRNA mediated HOTTIP depleted HCT116 cells to chemotherapeutic drugs was examined and compared to NTC. All data are mean (± S.E.M) of 3 biological replicates (N=3). Two-way ANOVA with Dunnett's multiple comparisons test was used to quantify statistical significance.
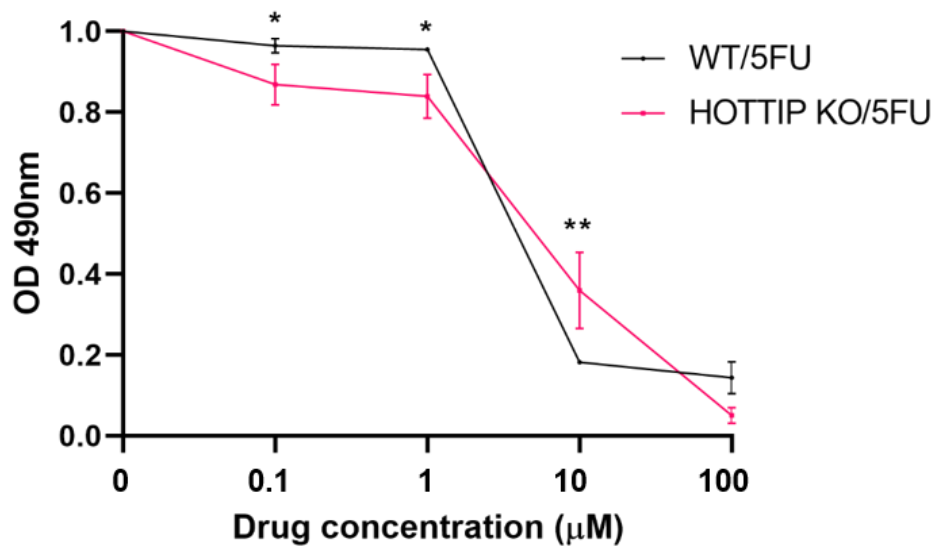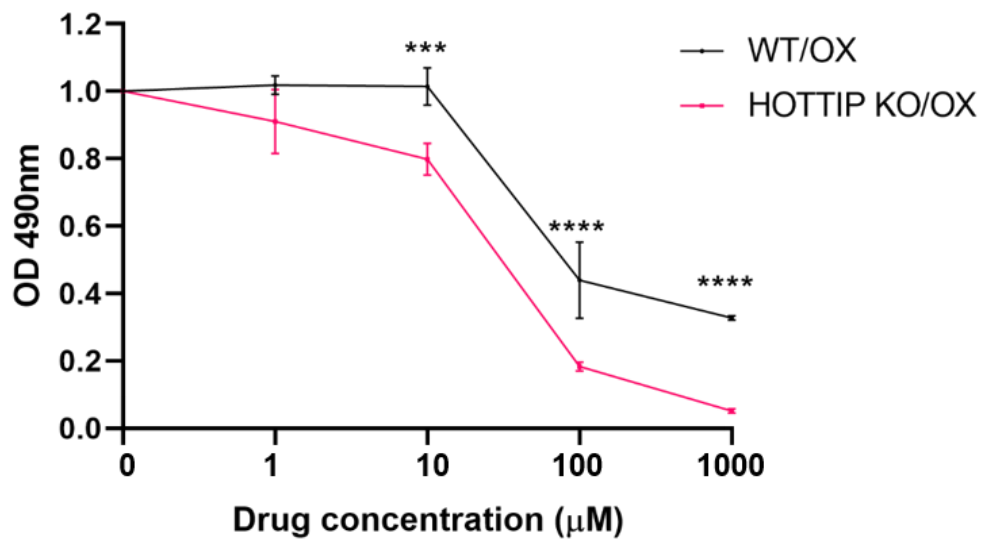
Figure 3.16 Dose response of CRISPR-Cas9 mediated *HOTTIP* KO HCT116 cells to chemotherapeutic drugs.

CRISPR-Cas9 mediated HOTTIP KO and WT HCT116 cells were seeded in 96-well plates and subsequently treated with a dose response of (A) 5FU (0, 0.1, 1, 10, 100 µM) or (B) OX (0, 1, 10, 100, 1000 µM) for 72 h. The dose response of HOTTIP KO HCT116 cells to chemotherapeutic drugs was examined and compared to WT. All data are mean (± S.E.M) of 3 biological replicates (N=3). Two-way ANOVA with Sidak's multiple comparisons test was used to quantify statistical significance (*P<0.05, ***P<0.001, ****P<0.0001).

3.4.2   Reduction in *HOTTIP* leads to an increase in cell death when CRC cells are treated with chemotherapeutic drugs.

After investigating sensitivity to chemotherapy in cancer cells with reduced *HOTTIP* expression, the rates of cell death (apoptosis) after exposure to 10 µM 5FU, 10 µM OX or 1 µM DOC was tested. Cells were treated with chemotherapeutic drugs and incubated for different time points: 24 h, 48 h, 72 h. A no drug comparison was also included for each cell line. Flow cytometry was used to quantify the percentage of cells undergoing apoptosis as described above (Section 3.3.4). *HOTTIP* depleted cells were compared to NTC and no drug controls.

After 72 h siRNA knockdown, *HOTTIP* depleted HCT116 cells exhibited a reduction in the percentage of cells undergoing apoptosis. With the addition of chemotherapy treatment, a significant increase in apoptosis was observed in *HOTTIP* depleted HCT116 cells treated with both 5FU (Figure 3.17A) and OX (Figure 3.17B). An increase in the percentage of RKO1 cells undergoing apoptosis was seen upon siRNA mediated *HOTTIP* depletion. This pattern was also observed when RKO1 cells were treated with 5FU (Figure 3.18A) or OX (Figure 3.18B). *HOTTIP* depleted DU145 cells showed an increase in apoptosis compared to NTC (Figure 3.19A), and this was sustained with the addition of DOC treatment.

Stable *HOTTIP* KO HCT116 cells exhibited a slight increase in the percentage of cells undergoing apoptosis compared to WT HCT116 cells (Figure 3.20). With the addition of 5FU treatment, no significant difference in apoptosis was observed for *HOTTIP* KO cells (Figure 3.20A). However, when treated with OX, *HOTTIP* KO cells

exhibited a significant increase in apoptosis at the 24 and 48 h time points (Figure 3.20B). Together, these data suggest a chemosensitive role for *HOTTIP* in HCT116 and DU145 cells but not RKO1 cells.
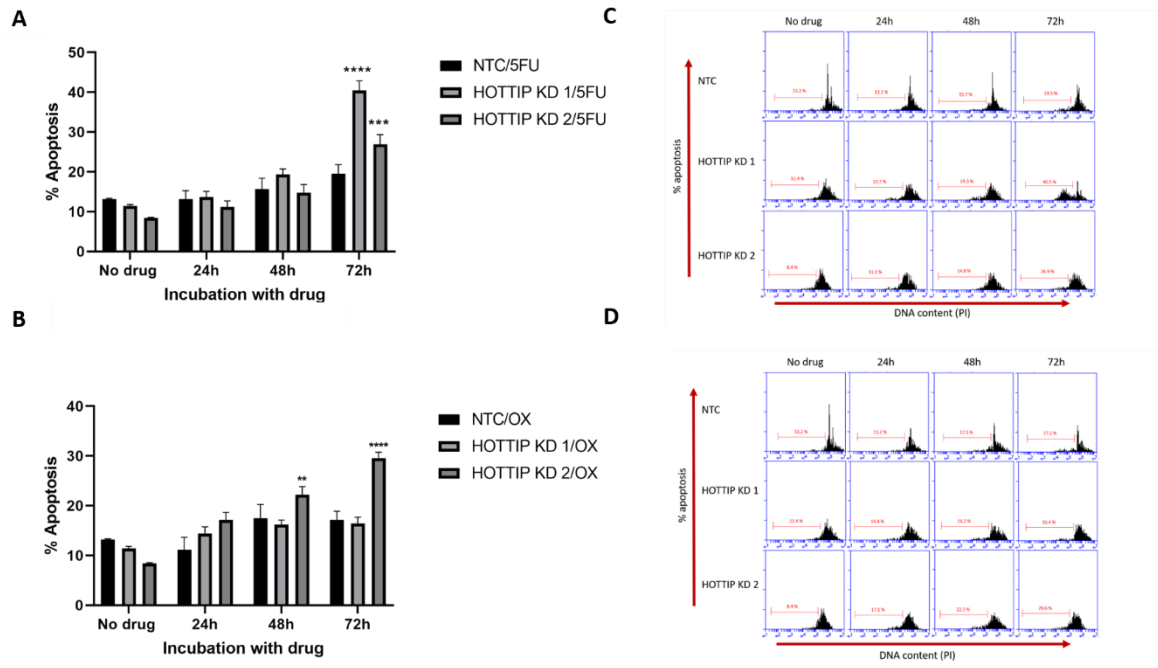
Figure 3.17 Apoptosis of HOTTIP depleted HCT116 cells to chemotherapeutic drugs.

HCT116 cells were transfected with HOTTIP targeting or NTC siRNA for 72 h and subsequently treated with chemotherapeutic drugs for DNA hypodiploidy analysis using a flow cytometer at 24 h, 48 h and 72 h after initial treatment. No drug controls were also included. Data are mean ($\pm$ S.E.M) of 3 biological replicates (N=3). Two-way ANOVA via Dunnett's comparison test was used to quantify the statistical significance (**P<0.01, ***P<0.001. ****P<0.0001). HOTTIP depleted HCT116 cells were treated with 10 μM (A) 5FU or (B) 10 μM OX for up to 72 h. Representative flow cytometry plots of HOTTIP depleted and NTC HCT116 cells treated with (C) 10 μM 5FU or (D) 10 μM OX, average Sub-G1 percentages are highlighted in red.
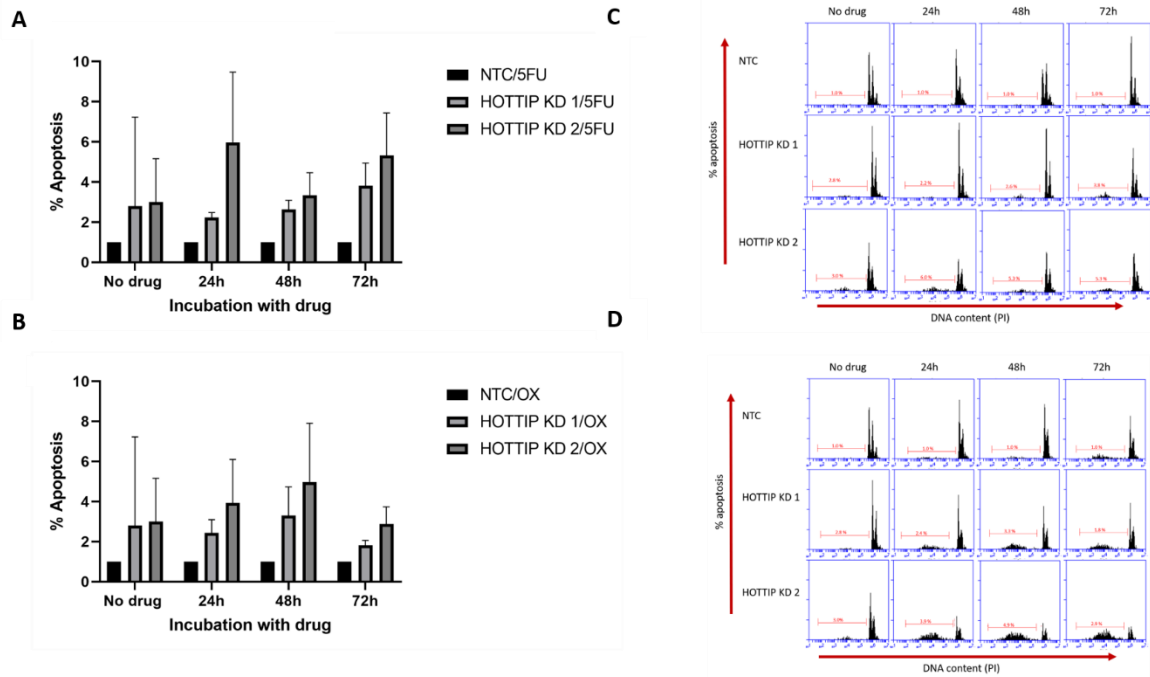
Figure 3.18 Apoptosis of HOTTIP depleted RKO1 cells to chemotherapeutic drugs.

RKO1 cells were transfected with HOTTIP targeting or NTC siRNA for 72 h and subsequently treated with chemotherapeutic drugs for DNA hypodiploidy analysis assay using a flow cytometer at 24 h, 48 h and 72 h after initial treatment. No drug controls were also included. Data are mean (± S.E.M) of 3 biological replicates (N=3). Two-way ANOVA via Dunnett's comparison test was used to quantify the statistical significance. (A) HOTTIP depleted RKO1 cells were treated with (A) 10 µM 5FU or (B) OX for up to 72 h. Representative flow cytometry plots of HOTTIP depleted and NTC RKO1 cells treated with (C) 5FU or (D) OX, average Sub-G1 percentages are highlighted in red.
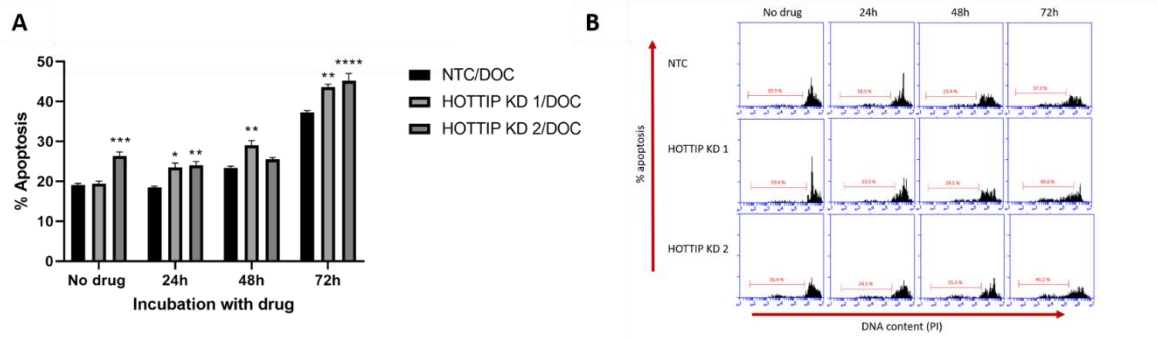
Figure 3.19 Apoptosis of *HOTTIP* depleted DU145 cells to chemotherapeutic drugs.

DU145 cells were transfected with HOTTIP targeting or NTC siRNA for 72 h and subsequently treated with chemotherapeutic drugs for DNA hypodiploidy analysis using a flow cytometer at 24 h, 48 h and 72 h after initial treatment. No drug controls were also included. Data are mean (± S.E.M) of 3 biological replicates (N=3). Two-way ANOVA via Dunnett's comparison test was used to quantify the statistical significance (*P<0.05, **P<0.01, ***P<0.001. ****P<0.0001). (A) HOTTIP depleted cells were treated with 1 µM DOC for up to 72 h. (B) Representative flow cytometry plots of HOTTIP depleted and NTC cells treated with DOC, average Sub-G1 percentages are highlighted in red.
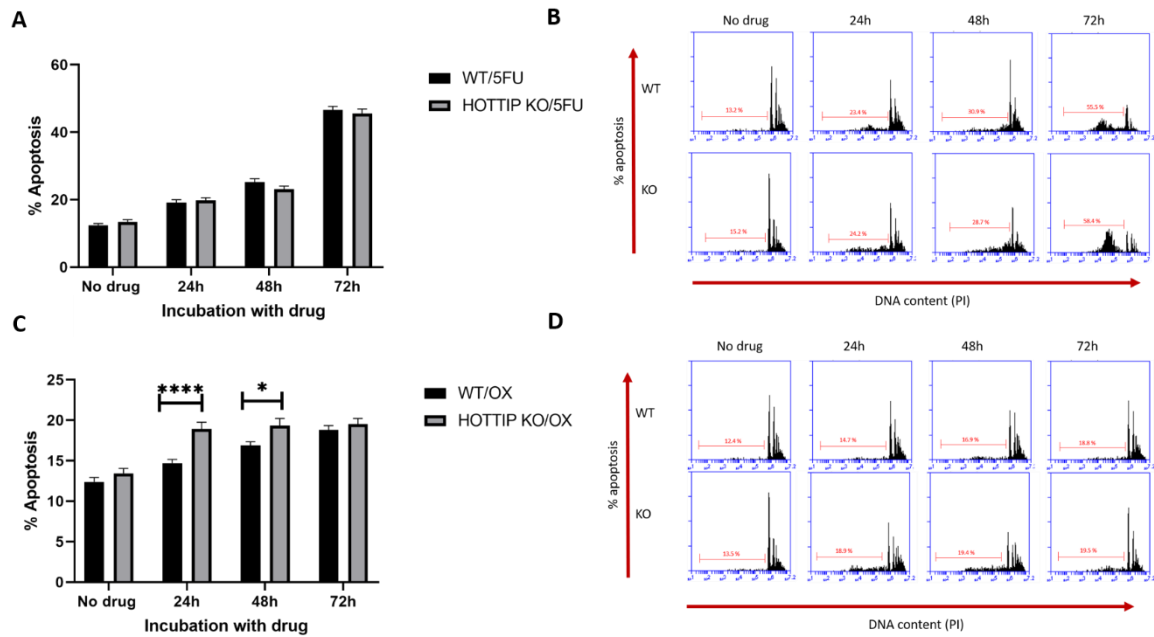
Figure 3.20 Apoptosis of CRISPR-Cas9 mediated HOTTIP KO cells to chemotherapeutic drugs.

CRISPR-Cas9 mediated HOTTIP KO and WT cells were treated with chemotherapeutic drugs for DNA hypodiploidy analysis using a flow cytometer at 24 h, 48 h and 72 h after initial treatment. No drug controls were also included. Data are mean (± S.E.M) of 3 biological replicates (N=3). Two-way ANOVA with Sidak's multiple comparisons test was used to quantify statistical significance (*P>0.05, ****P<0.0001). Stable HOTTIP KO and WT HCT116 cells treated with (A) 10 µM 5FU or (C) OX. Representative flow cytometry plots of stable HOTTIP KO and WT HCT116 cells treated with (B) 5FU or (D) OX, average Sub-G1 percentages are highlighted in red.

3.4.3   Reduction in *HOTTIP* expression reduces HCT116 colony forming ability when exposed to chemotherapeutic drugs.

Colony formation assays were used to further investigate the effect of *HOTTIP* on cancer cell survival when exposed to chemotherapeutic drugs. CRISPR-Cas9 *HOTTIP* KO and WT stable cells were seeded sparsely in 12-well plates. After 3-4 days, cells were treated with 10 µM 5FU or 10 µM OX. A no drug control was also included to measure the colony growth without the addition of chemotherapy treatment. There was no significant difference in the number of colonies present in the *HOTTIP* KO and WT HCT116 cells prior to the introduction of chemotherapy. When treated with 5FU or OX, a significant reduction in colonies was observed in *HOTTIP* KO compared to WT (Figure 3.21).

The proliferation rate of CRISPR-Cas9 *HOTTIP* KO HCT116 cells when treated with 10 µM 5FU or 10 µM OX were investigated over a 4-day time series. Proliferation rates were calculated relative to day 0. Prior to the addition of chemotherapy, reduced proliferation of CRISPR-Cas9 mediated stable *HOTTIP* KO HCT116 cells was observed compared to WT (P=0.06) (Figure 3.22A). Reduced proliferation was also observed in *HOTTIP* KO cells treated with 5FU; this was found to be significant at for HOTTIP KO compared to WT at day 4 (Figure 3.22B). When treated with OX, *HOTTIP* KO cells also exhibited reduced growth; however, this was not a significant result (Figure 3.22C). This loss in proliferation may be a result of *HOTTIP* KO rather than the introduction of OX as there is a similar pattern observed in *HOTTIP* KO samples when compared to WT, regardless of whether cells have been

treated with OX. Together, these data may further indicate sensitivity of *HOTTIP* KO

cells to chemotherapy, particularly 5FU as reduced growth is observed in *HOTTIP* KO

HCT116 cells compared to WT.
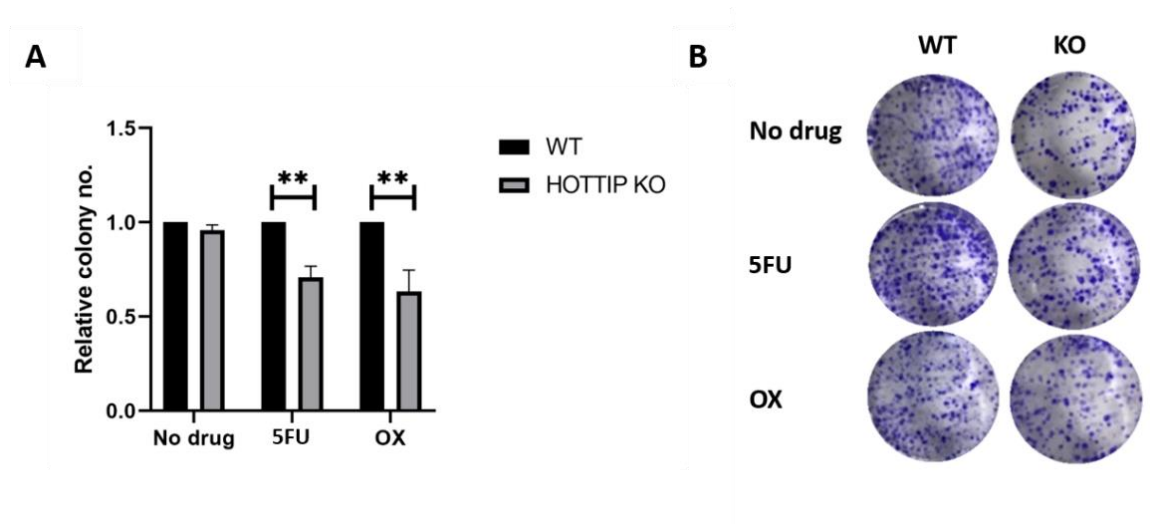
Figure 3.21 CRISPR-Cas9 mediated HOTTIP KO cells exhibit significant loss of colony formation ability in HCT116 cells.

(A) Relative colony number of CRISPR-Cas9 mediated *HOTTIP* KO and WT HCT116 cells were compared with no drug, treatment with 10 μM 5FU or 10 μM OX. Data are mean (± S.E.M) of 3 biological replicates (N=3) relative to control WT cells. Two-way ANOVA with Sidak's multiple comparisons test was used to quantify statistical significance (** P<0.01). (B) Representative wells of colonies formed and stained with crystal violet after treatment with 5FU or OX.
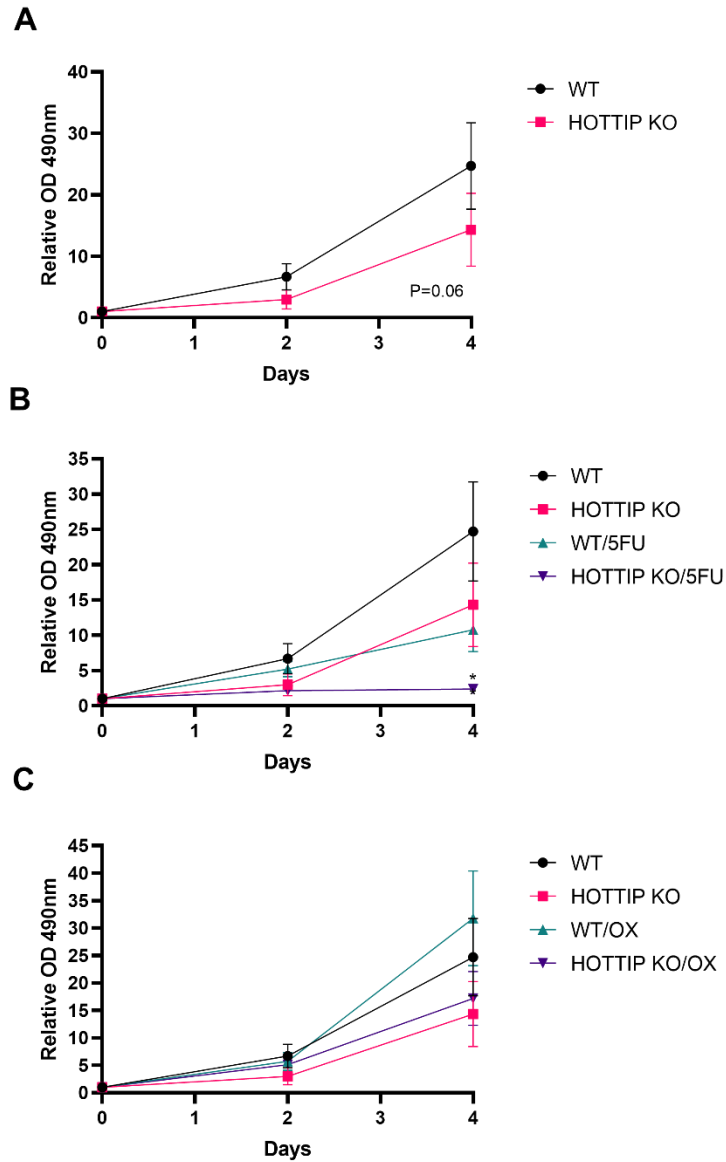
Figure 3.22 Proliferation of CRISPR-Cas9 mediated HOTTIP KO and WT HCT116 cells when treated with chemotherapeutic drugs.

CRISPR-Cas9 mediated HOTTIP knockout and WT HCT116 cells were grown over a 4-day time course in the presence of (A) no drug, (B) 10 μM 5FU and (C) 10 μM OX. Cells were fixed with 4% PFA and stained with crystal violet prior to colorimetric assay measurement (OD 490 nm). Growth rates were calculated relative to day 0 (no growth or drug treatment). No significant change in growth rate was observed. Data are mean (± S.E.M) of 3 biological replicates (N=3). Two-way ANOVA with Sidak's multiple comparisons test was used to quantify statistical significance (P<0.05).

3.4.4 Chemotherapeutic drugs do not induce cell cycle arrest when *HOTTIP* is depleted in CRC and PCa cells.

After sensitivity to chemotherapy was observed in *HOTTIP* depleted cells, it was decided to investigate whether 5FU, OX or DOC treatment influences changes in the cell cycle upon *HOTTIP* depletion. siRNA mediated *HOTTIP* KD or CRISPR-Cas9 *HOTTIP* KO cells and their respective controls were treated with 10 μM 5FU, 10 μM OX or 1 μM DOC for 72 h. No drug controls were also included in this analysis. A flow cytometer was used to measure the percentage of cells in each stage of the cell cycle as outlined previously (Section 3.3.5).

Upon siRNA mediated *HOTTIP* depletion, HCT116 cells exhibited an increase in G1 and S phase, as well as a reduction in the percentage of cells undergoing G2/M phase (Figure 3.23A). After treatment with 5FU, no changes in the cell cycle were observed for HCT116 cells transfected with HOTTIP 1 siRNA. However, when transfected with HOTTIP 2 siRNA HCT116 cells exhibited a slight increase in G1 phase (Figure 3.23B) compared to NTC (Figure 3.23A). *HOTTIP* depleted HCT116 cells treated with OX resulted in a higher percentage of cells in G1 phase, and a reduction of cells in G1 and G2/M phase compared to NTC (Figure 3.23C).

RKO1 cells exhibited an increase in cells in G2/M and S phase after siRNA mediated depletion (Figure 3.24A). When treated with 5FU, no change was observed for RKO1 cells transfected with HOTTIP KD 1. However, an increase in the percentage of cells undergoing G2/M and S phase, as well as a reduction in G1 phase was observed for RKO1 cells transfected with siRNA HOTTIP KD 2 (Figure 3.24B).

When treated with OX, *HOTTIP* depleted RKO1 cells underwent an increase in the percentage of cells in G2/M and S phase, as well as a reduction in cells undergoing G1 phase (Figure 3.24C).

After siRNA mediated *HOTTIP* depletion, DU145 cells showed no change in cells in S phase; although, an increase in G2/M and decrease in G1 phase was observed (Figure 3.25A). When treated with DOC, there were no differences in cell cycle stages seen between NTC and DU145 cells transfected with siRNA HOTTIP KD 1, with the exception of S phase, where a decrease in the number of cells at this stage of the cell cycle was observed. However, a decrease in the percentage of cells in S and G1 phase and an increase in the percentage of cells in G2/M was observed in DU145 cells transfected with HOTTIP KD 2, also treated with DOC (Figure 3.25B). Despite these observations, none of the above data for either cell line was found to be significant.

The cell cycle of stable CRISPR-Cas9 *HOTTIP* KO and WT cells treated with 10 µM 5FU or 10 µM Ox was investigated next. A time series was established for each drug treatment: 0 h (no drug control), 24 h, 48 h and 72 h to investigate if any shifts in the cell cycle were occurring before the 72 h time point used in the siRNA experiments. Prior to the addition of chemotherapy, an increase in cells in G1 phase, and a decrease in G2/M and S phase was observed for *HOTTIP* KO HCT116 cells. When treated with 5FU for 24 h, the same pattern was observed, with the exception of increased *HOTTIP* KO cells undergoing G2/M phase compared to WT. After longer incubation with 5FU (48 h – 72 h), there was no difference in cell cycle stages

between *HOTTIP* KO and WT cells seen (Figure 3.26A), suggesting 5FU was equally affecting the cell regardless of level of *HOTTIP* expression.

When treated with OX, an increase in the percentage of cells in G2/M and G1 phase was observed in *HOTTIP* KO cells over the time course. Similarly, a reduction in *HOTTIP* KO cells undergoing S phase was also seen at each time point (Figure 3.26B). However, in both instances, any changes in cell cycle stages, as a result of chemotherapy treatment was found to be non-significant.
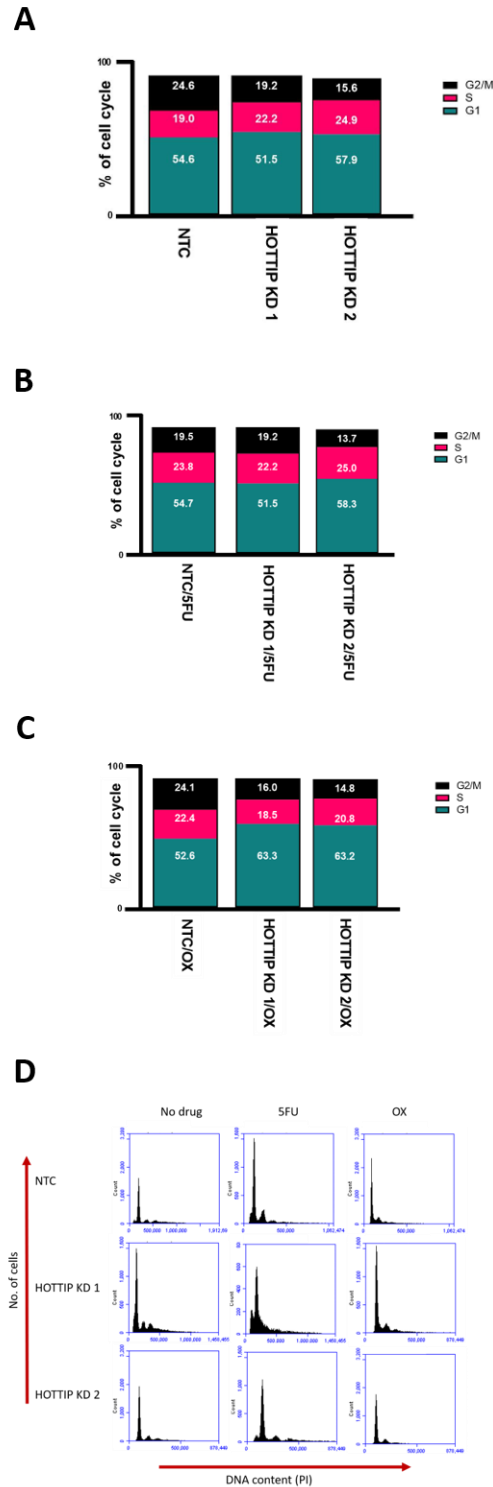
Figure 3.23 Cell cycle analysis of siRNA mediated *HOTTIP* depletion in HCT116 cells.

Cell cycle analysis of (A) siRNA mediated *HOTTIP* depleted and NTC HCT116 cells treated with (B) 10 µM 5FU or (C) 10 µM OX for 72 h. A no drug control was also included. Data are mean (± S.E.M) of 3 biological replicates (N=3). Two-way ANOVA with Dunnett's multiple comparisons test was used to quantify statistical significance. (D) Representative flow cytometry plots of siRNA mediated HOTTIP depleted and NTC HCT116 cells with and without drug treatment.
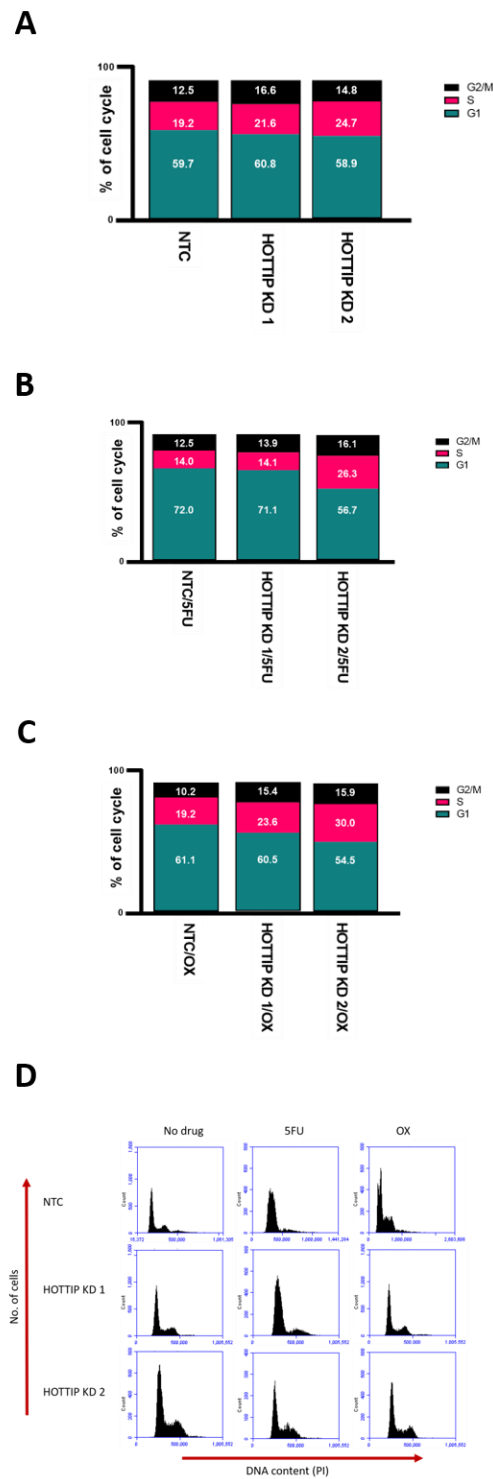
Figure 3.24 Cell cycle analysis of siRNA mediated *HOTTIP* depletion in RKO1 cells.

Cell cycle analysis of (A) siRNA mediated *HOTTIP* depleted and NTC RKO1 cells treated with (B) 10 µM 5FU or (C) 10 µM OX for 72 h. A no drug control was also included. Data are mean (± S.E.M) of 3 biological replicates (N=3). Two-way ANOVA with Dunnett's multiple comparisons test was used to quantify statistical significance. (D) Representative flow cytometry plots of siRNA mediated HOTTIP depleted and NTC RKO1 cells with and without drug treatment.
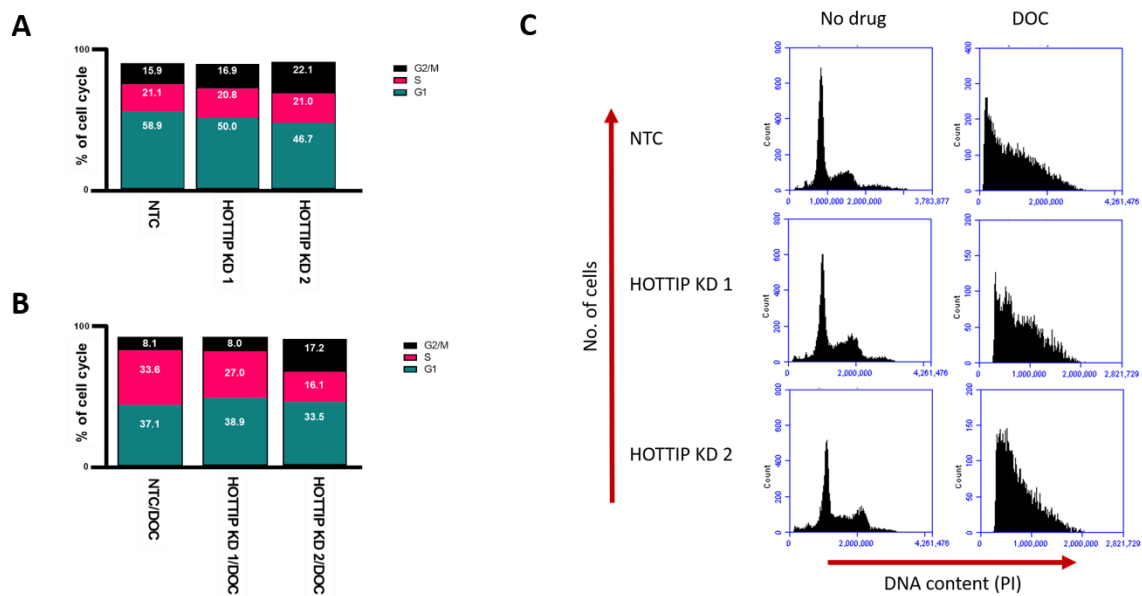
Figure 3.25 Cell cycle analysis of siRNA mediated HOTTIP depletion in DU145 cells.

Cell cycle analysis of (A) siRNA mediated *HOTTIP* depleted and NTC DU145 cells treated with (B) 1 µM DOC for 72 h. A no drug control was also included. Data are mean (± S.E.M) of 3 biological replicates (N=3). Two-way ANOVA with Dunnett's multiple comparisons test was used to quantify statistical significance. (C) Representative flow cytometry plots of siRNA mediated HOTTIP depleted and NT cells with and without drug treatment.
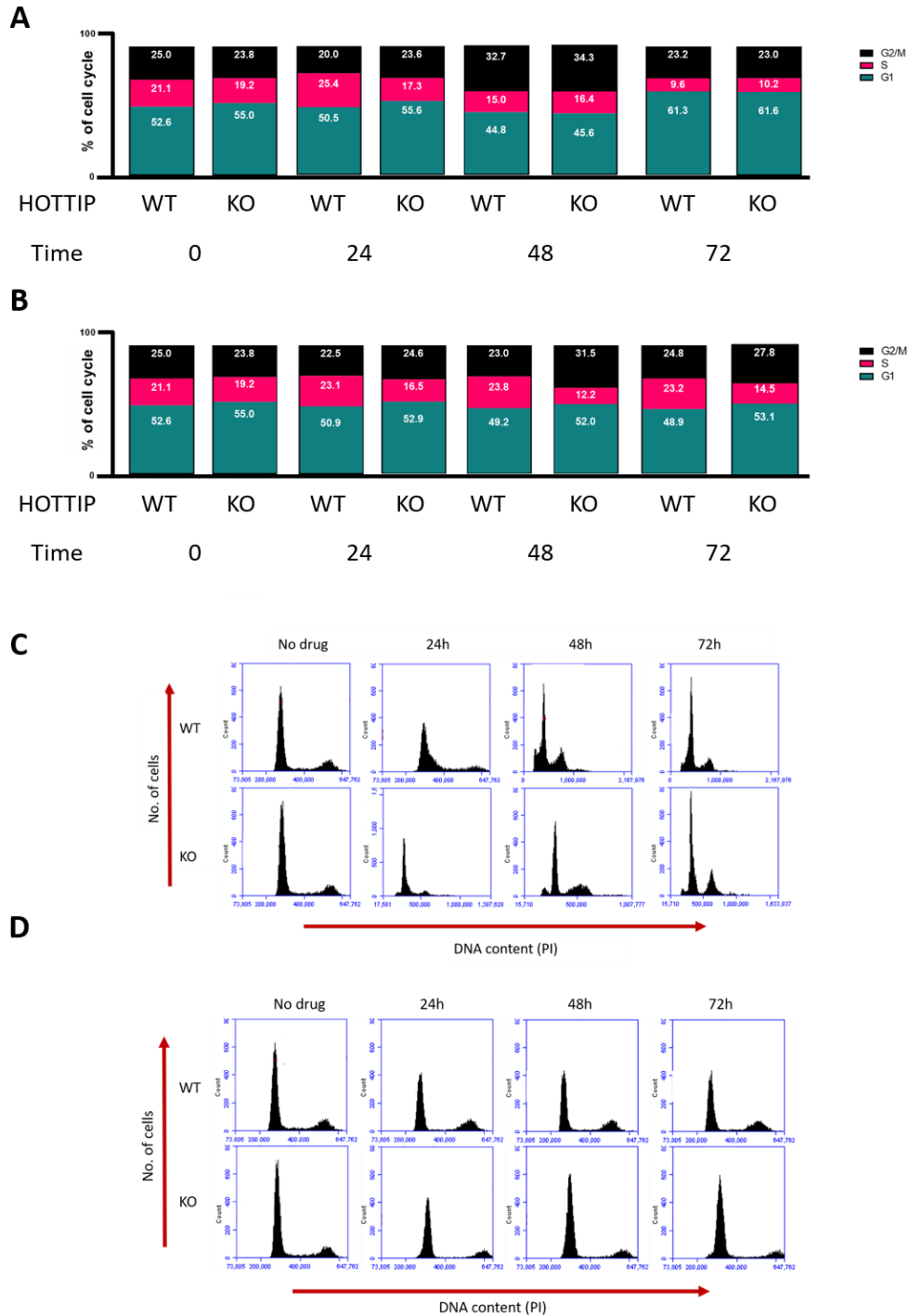
Figure 3.26 Cell cycle analysis of CRISPR-Cas9 mediated *HOTTIP* knockout in HCT116 cells treated with chemotherapeutic drugs.

CRISPR-Cas9 mediated HOTTIP KO and WT HCT116 cells were treated with (A) 10 μM 5FU or (B) 10 μM OX for 24 h, 48 h, 72 h and the percentage of cells in each stage of the cell cycle was analysed via flow cytometry. A no drug control was also included (0h). Data are mean (± S.E.M) of 3 biological replicates (N=3). Two-way ANOVA with Tukey's multiple comparisons test was used to quantify statistical significance. Representative flow cytometry plots of HOTTIP KO and WT cells treated with (C) 5FU or (D) OX.

115

3.5   RNA-Seq analysis of stable *HOTTIP* KO cell lines

After the above functional assays investigating the role of *HOTTIP* in CRC and PCa were carried out, it was decided to look at the transcriptome when *HOTTIP* is deleted in HCT116 cells in more detail. The CRISPR-Cas9 *HOTTIP* KO and WT HCT116 cell lines were used once again for this work. RNA extracted from *HOTTIP* KO and WT cells was sent for RNA-Sequencing (RNA-Seq) (Novogene, UK), where all further library preparations for sequencing were completed. FASTA files of each genotype (triplicate independent repeats) were returned for analysis. Firstly, FASTQC analysis was carried out to ensure each raw sequence data file had good quality reads. The raw data files were subsequently mapped to the genome (hg38), reads were counted and differential expression of genes in each sample calculated using statistical analysis packages: TopHat2 (Kim *et al.*, 2013), HTSeq (Wen *et al.*, 2018) and DESeq2 (Chang *et al.*, 2016; Qin *et al.*, 2019). Genomic tracks of WT and *HOTTIP* KO samples were compared at the *HOXA* cluster (Figure 3.27). A clear deletion of the *HOTTIP* transcript in the KO lines was identified. In agreement with previous results, (Section 3.2.2), a reduction in *HOXA13* was also seen in *HOTTIP* KO compared to WT. Interestingly, an increase in *HOXA3* was observed in the KO lines compared to WT.

After *HOTTIP* deletion was confirmed, the differential expression of *HOTTIP* KO and WT genes was explored. Differentially expressed genes were filtered to include only those with P<0.01 and Log2Fold Change (Log2FC) >0.5 values. A heatmap of all filtered genes was produced (Figure 3.28) to compare gene expression patterns across all replicates. A change in gene expression of 431

upregulated (Supplementary Table 8.1) and 494 downregulated (Supplementary

Table 8.2) genes was observed in *HOTTIP* KO compared to WT HCT116 cells.
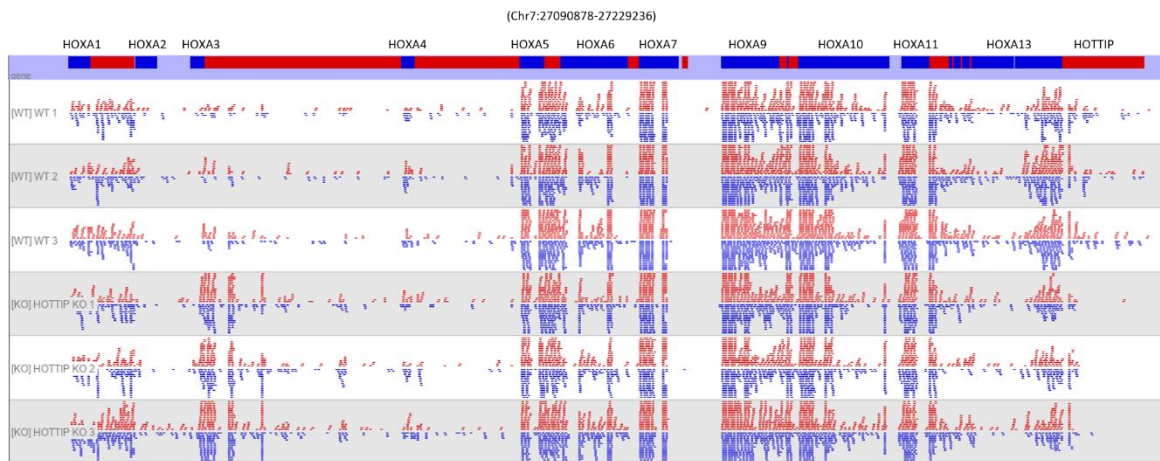
Figure 3.27 Seqmonk visualisation of WT and HOTTIP KO genome tracks at the HOXA cluster generated from RNA-Seq analysis.

The transcriptome of WT and HOTTIP KO HCT116 cells was analysed in triplicate by RNA-Seq. Differential expression of genes was analysed through using the statistical packages 'TopHat2', 'HTSeq' and 'DESeq2'. After analysis, BAM files were loaded in to the SeqMonk programme (Babraham Institute) to visualise the mapped sequence data. Genomic tracks of HOTTIP KO and WT replicates were compared at the HOXA cluster. Red tracks represent DNA found on the forward strand, blue tracks represent DNA found on the reverse strand.
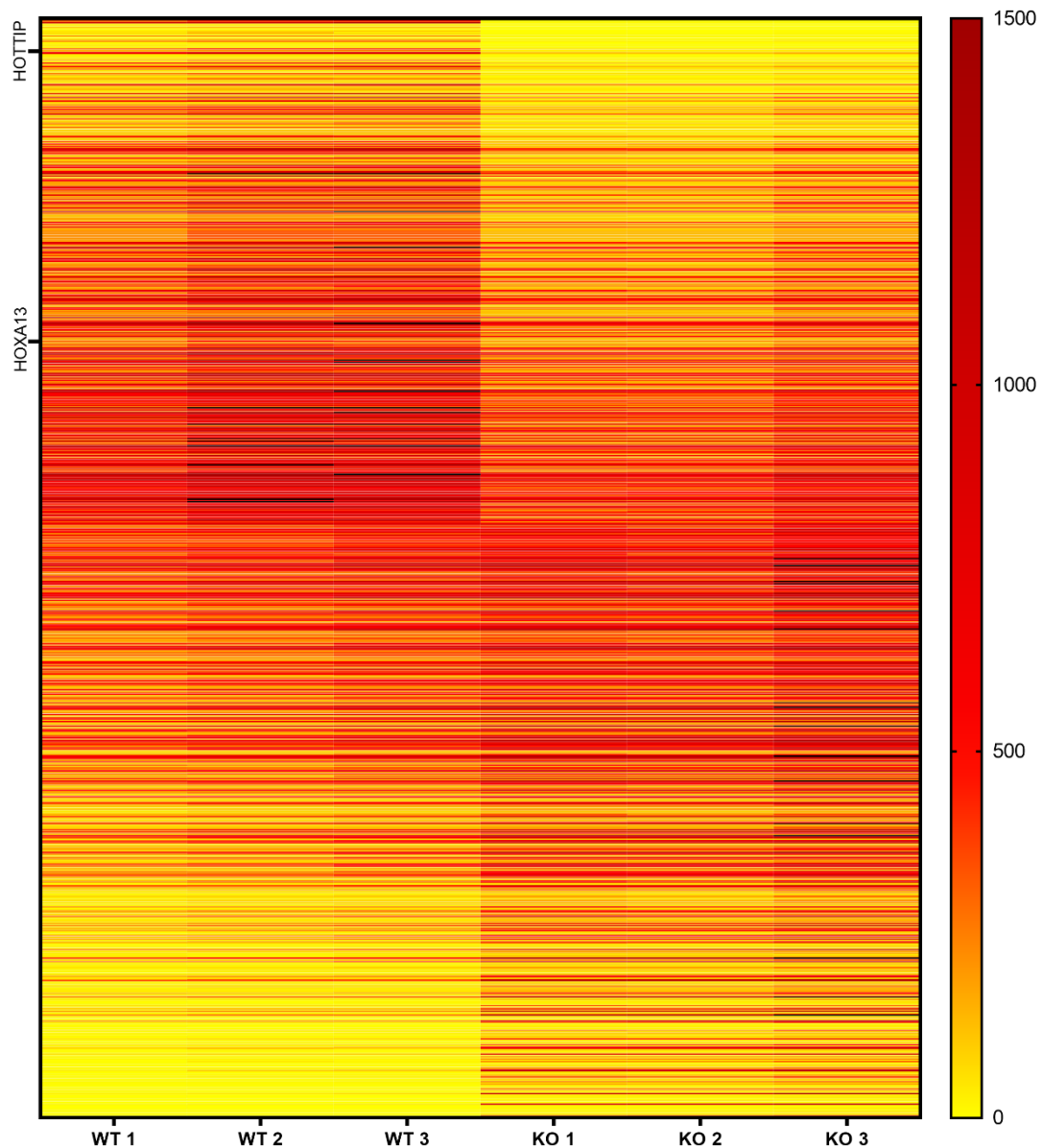
Figure 3.28 Heat map of differentially expressed genes identified through HOTTIP KO HCT116 RNA-Seq analysis.

The transcriptome of WT and HOTTIP KO HCT116 cells was analysed by RNA-Seq. Differential expression of genes was analysed through using the statistical packages 'TopHat2', 'HTSeq' and 'DESeq2'. After analysis, BAM files were loaded in to the SeqMonk programme (Babraham Institute) to visualise and analyse the mapped sequenced data further. Data was filtered by only accepting genes P<0.01 and a Log2FC >0.5 (925 genes total). A heat map indicating differential expression of genes in WT and HOTTIP KO replicates was produced and colour coded depending on differential expression value. Y-axis labels are a subset of all 925 differentially expressed genes although all genes were included in analysis.

To explore differential expression further, all significant *HOX* genes from the filtered data were plotted. Again, this was compared across all replicates of the *HOTTIP* KO and WT samples (Figure 3.29). *HOTTIP, HOXA13* and *HOXD8* were all found to be downregulated in *HOTTIP* KO samples. All other *HOX* genes were upregulated upon *HOTTIP* deletion. Interestingly, many *HOXB* genes (*HOXB3, HOXB4, HOXB6, HOXB8, HOXB9*) were subject to this upregulation. Many *HOXB* genes have been associated with cancer; in particular *HOXB8* has been described as being oncogenic and promoting CRC invasiveness (Li *et al.*, 2015).

HOTTIP is known to directly regulate 5' *HOXA* genes (*HOXA13, HOXA11, HOXA10* and *HOXA9*), as *HOTTIP* is located on the 5' end of the *HOXA* cluster (Quagliata *et al.*, 2018) and acts in *cis* to regulate expression of nearby genes (Zhang *et al.*, 2016). Altered *HOXB* expression could be due to an indirect effect of *HOXA13* downregulation, as *HOX* transcription factors (TFs) are known to regulate expression of each other (Quagliata *et al.*, 2018). *HOXA3* expression is highly upregulated in *HOTTIP* KO samples compared to WT, which follows what was observed when genomic tracks were previously compared (Figure 3.27). Although not found in close proximity to *HOTTIP*, the lncRNA HOXA cluster antisense RNA 2 (*HOXA-AS2*) was also found to be upregulated in *HOTTIP* KO samples and is located between *HOXA3* and *HOXA4* in the *HOXA* cluster (Qin *et al.*, 2019). The upregulation of *HOXA3* observed could be a direct effect of *HOXA-AS2* upregulation rather than *HOTTIP* KO.

All differentially expressed genes were then visualised using a scatter plot to further determine which genes were upregulated in either *HOTTIP* KO or WT samples (Figure 3.30). The filtered *HOX* genes are highlighted in red; higher

expression was observed for *HOTTIP, HOXA13* and *HOXD8* in WT samples and higher

expression of all remaining significant *HOX* genes was observed in *HOTTIP* KO

samples. This follows what was seen previously (Figure 3.29).
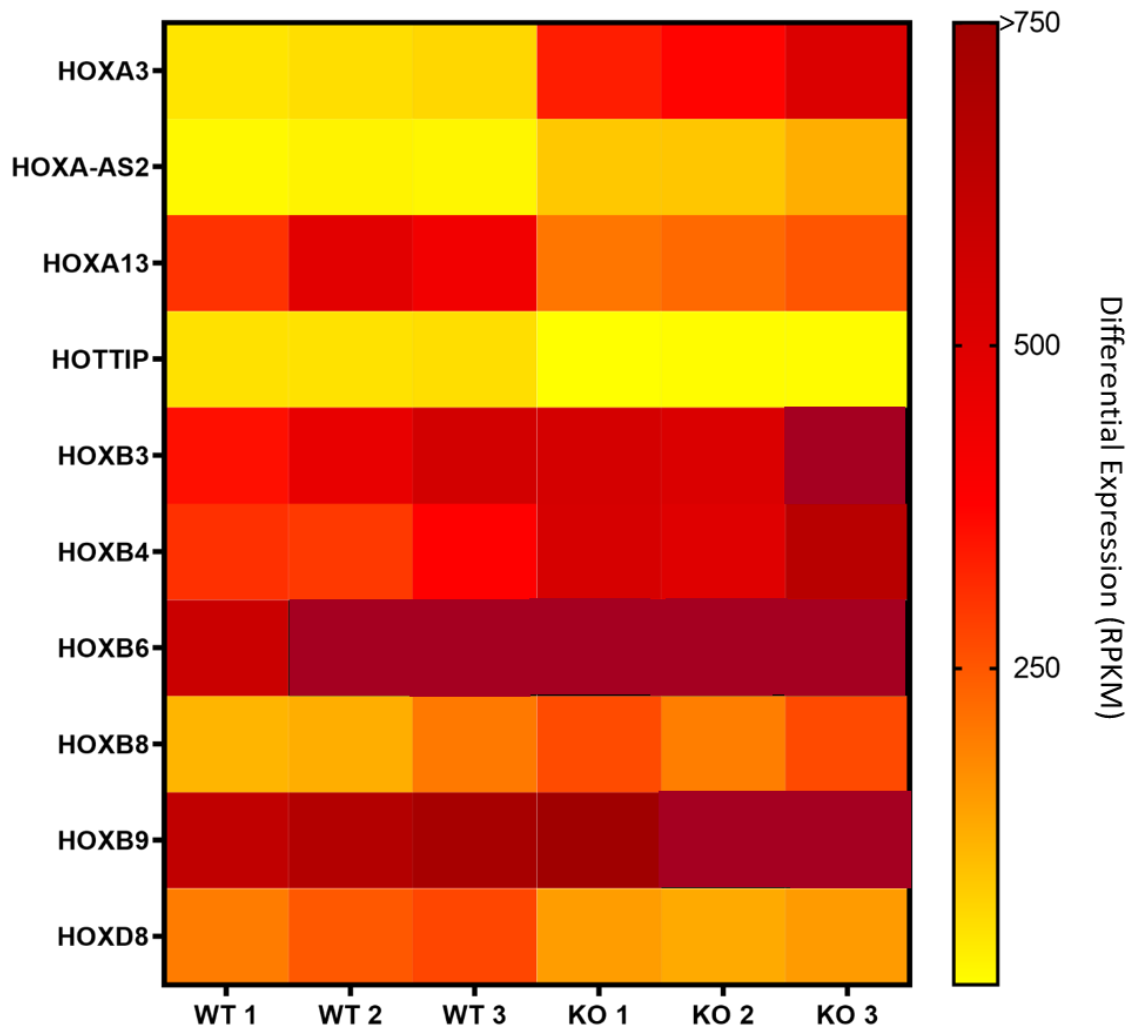
Figure 3.29 Heat map of differentially expressed HOX genes identified through HOTTIP KO HCT116 RNA-Seq analysis.

The transcriptome of WT and HOTTIP KO HCT116 cells was analysed by RNA-Seq. Differential expression (RPKM) of genes was analysed through using the statistical packages 'TopHat2', 'HTSeq' and 'DESeq2'. After analysis, BAM files were loaded in to the SeqMonk programme (Babraham Institute) to visualise and analyse the mapped sequenced data further. Data was filtered by only accepting genes P<0.01 and a Log2FC >0.5 (925 genes total). A heat map of target genes only (N=10) indicating differential expression of HOTTIP and HOX genes in WT and HOTTIP KO replicates was produced and colour coded depending on differential expression value.
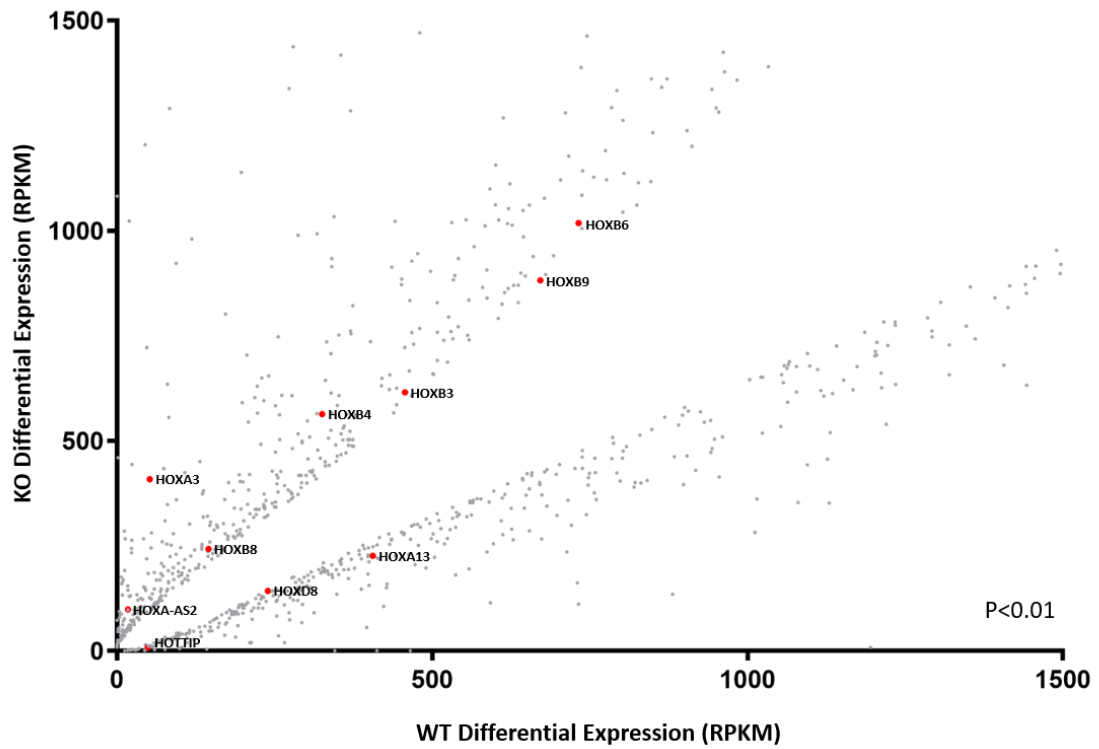
Figure 3.30 Differential expression of genes identified through analysis of the WT and HOTTIP KO HCT116 cell transcriptomes.

The transcriptome of WT and HOTTIP KO HCT116 cells was analysed by RNA-Seq. Differential expression of genes was analysed through using the statistical packages 'TopHat2', 'HTSeq' and 'DESeq2'. Data was filtered by only accepting genes P<0.01 and a Log2FC >0.5 (925 genes total). A scatter plot was drawn indicating differential expression of genes and whether the expression was greater in WT (x-axis), or HOTTIP KO (y-axis) cells. Genes of interest are highlighted in red and labelled.

It was then decided to further investigate the potential importance of these differentially expressed *HOX* genes in CRC. Kaplan-Meier (K-M) survival plots were generated using an online database (kmplot.com) (Falaschi, Abdurashidova and Biamonti, 2010) to examine if their expression levels correlate with patient survival (Figure 3.31). Rectal adenocarcinoma RNA-Seq data from 165 patients was chosen for this analysis as it falls into the CRC classification. Higher levels of *HOXA3* (P=0.036) and *HOXB4* (P=0.015) were significantly correlated with poorer survival in rectal adenocarcinoma, whereas higher *HOXA13* (P=0.066) and *HOXB9* (P=0.078) expression were correlated with better patient survival. Both *HOXA3* and *HOXB4* were upregulated when *HOTTIP* was deleted in HCT116 cells; indicating *HOTTIP* may have tumour suppressive properties in preventing overexpression of *HOXA* (or its regulatory lncRNA *HOXA-AS2*) and *HOXB4* in CRC.

After exploring *HOX* gene expression, all significant differentially expressed genes were investigated further by performing gene ontology (GO) analysis. The GOrilla online tool (Han *et al.*, 2018; Shi *et al.*, 2018) was used to analyse all genes and determine what biological pathways or processes they may be involved in. A total of 987 genes out of 1291 were associated with a GO term. From this list, 32 genes (Supplementary Figure 3) associated with the most significant biological processes (Figure 3.32) were selected for further analysis. Two main groups of genes were highlighted as a result of this analysis: peptidyl arginine deiminase 2 and 3 (*PADI2/3*) and the protocadherin alpha cluster (*PCDHA1-13*), including the protocadherin alpha subfamily c 1 and 2 (*PCDHAC1/2*).
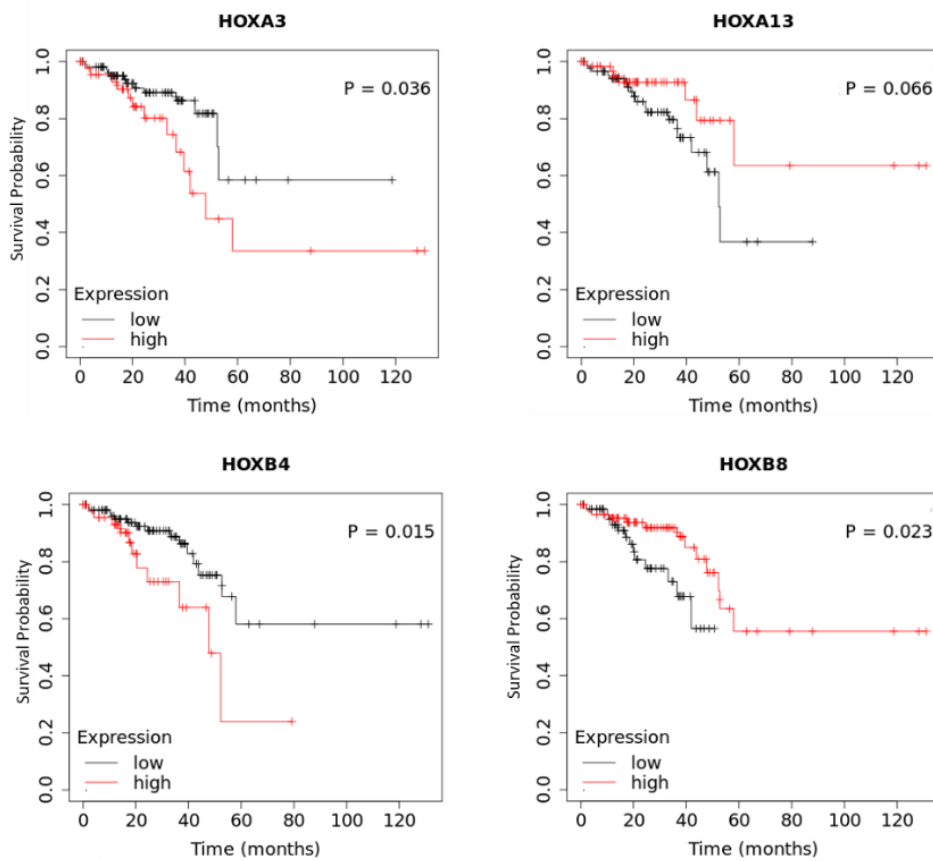
Figure 3.31 Kaplan-Meier survival plots of differentially expressed HOX genes identified through HOTTIP KO HCT116 RNA-Seq analysis.

Kaplan-Meier survival plots generated by a meta-analysis of rectal adenocarcinoma RNA-Seq data using kmplot online software (kmplot.com) to determine if differentially expressed HOX genes identified through RNA-Seq analysis of WT and *HOTTIP* KO HCT116 cells is correlated with increased or decreased survival rates in CRC. The probability of survival (y-axis) is plotted against the time (months) a patient is estimated to survive the disease (x-axis). Black lines indicate low gene expression and red lines indicate high gene expression. N=165 patient samples were analysed in the rectal adenocarcinoma RNA-Seq dataset.
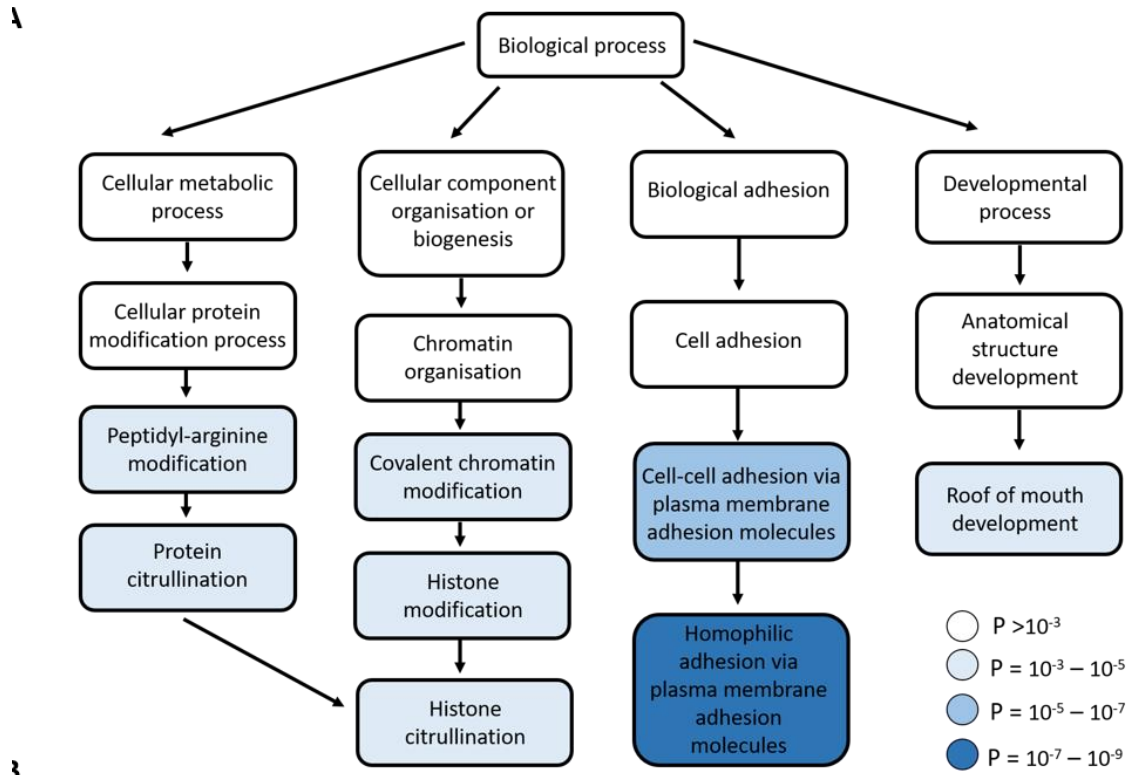
Biological process	Genes
Cell-cell adhesion via plasma-membrane adhesion molecules	AMIGO1, FAT2, FAT4, IL1RAP, PCDHA1, PCDHA10, PCDHA11, PCDHA12, PCDHA13, PCDHA2, PCDHA3, PCDHA4, PCDHA5, PCDHA6, PCDHA7, PCDHA8, PCDHA9, PCDHAC1, PCDHAC2, PCDHG10, PCDHGB2, PVRL4, TENM3, TGFB2
Covalent chromatin modification	CDH5, PADI2, PADI3
Histone citrullination	PADI2, PADI3
Histone modification	CDH5, PADI2, PADI3
Homophilic cell adhesion via plasma membrane adhesion molecules	AMIGO1, FAT2, FAT4, PCDHA1, PCDHA10, PCDHA11, PCDHA12, PCDHA13, PCDHA2, PCDHA3, PCDHA4, PCDHA5, PCDHA6, PCDHA7, PCDHA8, PCDHA9, PCDHAC1, PCDHAC2, PCDHG10, PCDHGB2, PVRL4, TENM3
Peptidyl-arginine modification	PADI2, PADI3
Protein citrullination	PADI2, PADI3
Roof of mouth development	CSRNP1, DH5S3, SATN2, TGFB2, TGFBR3, WNT3A

Figure 3.32 Gene ontology analysis of HOTTIP KO HCT116 RNA-Seq data.

The transcriptome of WT and HOTTIP KO HCT116 cells was analysed by RNA-Seq. Differential expression of genes was analysed through using the statistical packages 'TopHat2', 'HTSeq' and 'DESeq2'. Data was filtered by only accepting genes P<0.01 and a Log2FC >0.5 (925 genes total). Gene ontology analysis on filtered genes executed using the GOrilla database (http://cbl-gorilla.cs.technion.ac.il/). Biological processes (A) and a list of genes associated with these processes were identified (B). The colour chart reflects the degree of gene enrichment.

Firstly, to visualise differential expression patterns, genomic tracks of the *PADI* and *PCDHA* genes were compared between *HOTTIP* KO and WT samples. An increase in *PADI2* and *PADI3* can be observed in *HOTTIP* KO replicates compared to WT (Figure 3.33A). The *PCDHA* genes are found in a closely linked cluster (Watanabe *et al.*, 2018) and as many of this gene family overlap, it is hard to distinguish genomic patterns by visualizing genomic tracks. An overall pattern was observed where 3' *PCDHA* genes are upregulated in the *HOTTIP* KO replicates whereas 5' *PCDHA* genes are downregulated in *HOTTIP* KO (Figure 3.33B).

More in-depth comparisons of these genes were then carried out by looking at the differential expression of each gene in *HOTTIP* KO and WT samples. Upregulation of *PADI2/3* was observed in *HOTTIP* KO cells (Figure 3.38A) which supports what was seen previously (Figure 3.33A). Downregulation of the *PCDHA* family was observed in *HOTTIP* KO samples, however this effect is less pronounced for *PCDHAC1/2* genes located on the 5' end of the cluster (Figure 3.34A). Again, when looking at this data on a scatter plot, *PADI2/3* are upregulated and the *PCDHAC* family are downregulated in *HOTTIP* KO (Figure 3.34B). All *PCDHA* genes exhibited a similar differential pattern and were found to also form a cluster when visualised (Figure 3.34B).
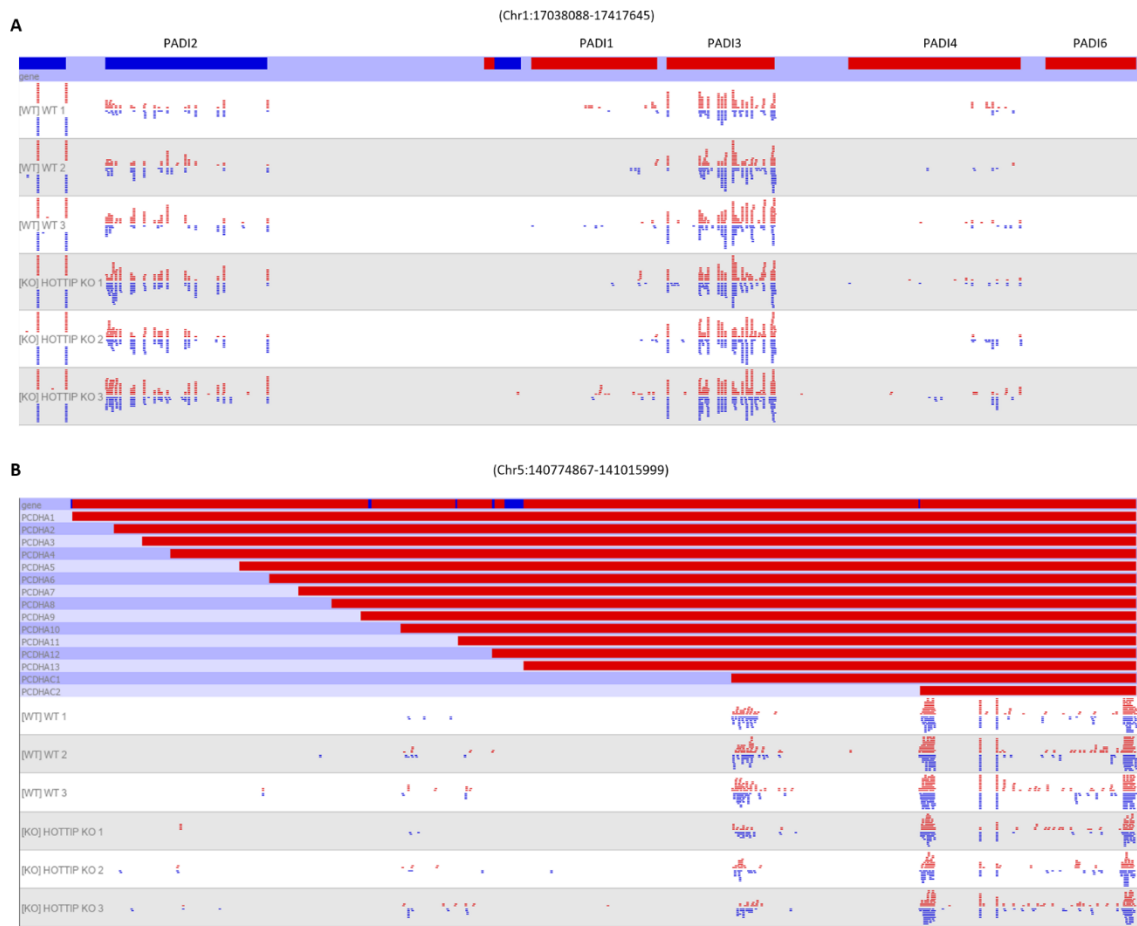
Figure 3.33 Seqmonk visualisation of differential expressed genes identified after gene ontology analysis of HOTTIP KO HCT116 RNA-Seq data.

The transcriptome of WT and HOTTIP KO HCT116 cells was analysed by RNA-Seq. Differential expression of genes was analysed through using the statistical packages 'TopHat2', 'HTSeq' and 'DESeq2'. Data was filtered by only accepting genes P<0.01 and a Log2FC>0.5 (925 genes total). After gene ontology analysis (GOrilla), tracks of newly identified genes of interest were visualised in SeqMonk (Babraham Institute). The tracks of HOTTIP KO and WT replicates were compared when looking at (A) the PADI family and (B) the PCDHA cluster.

A
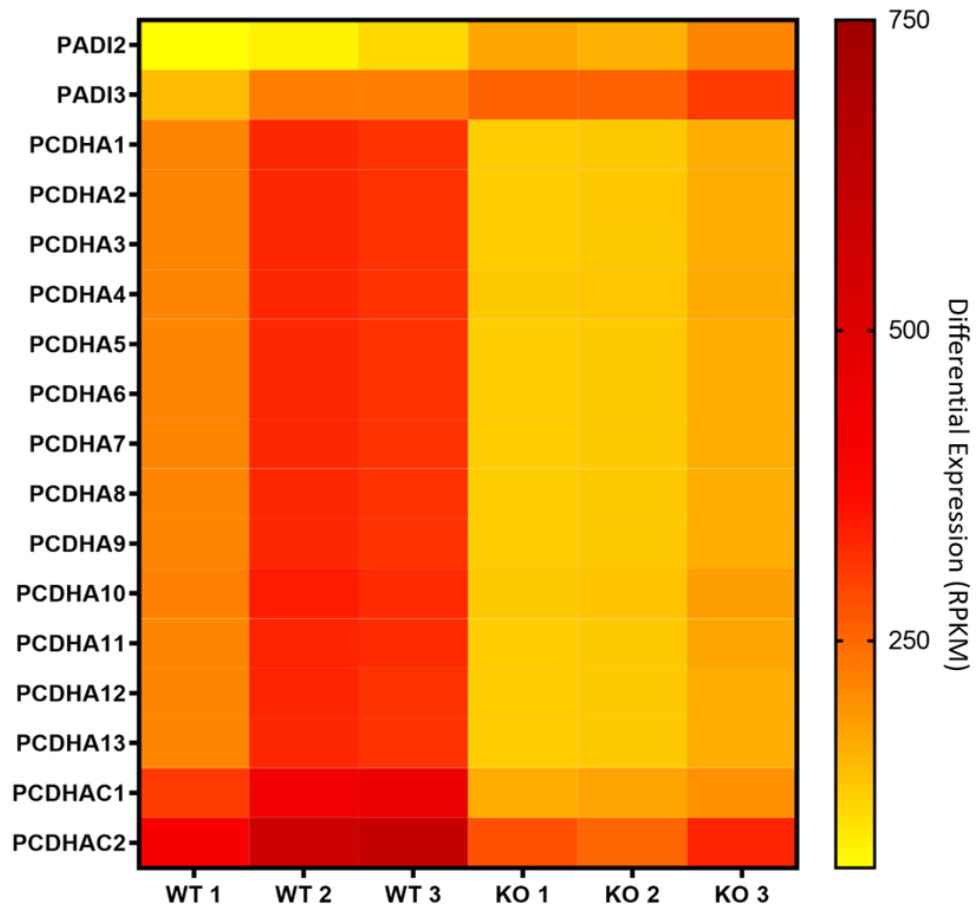
B
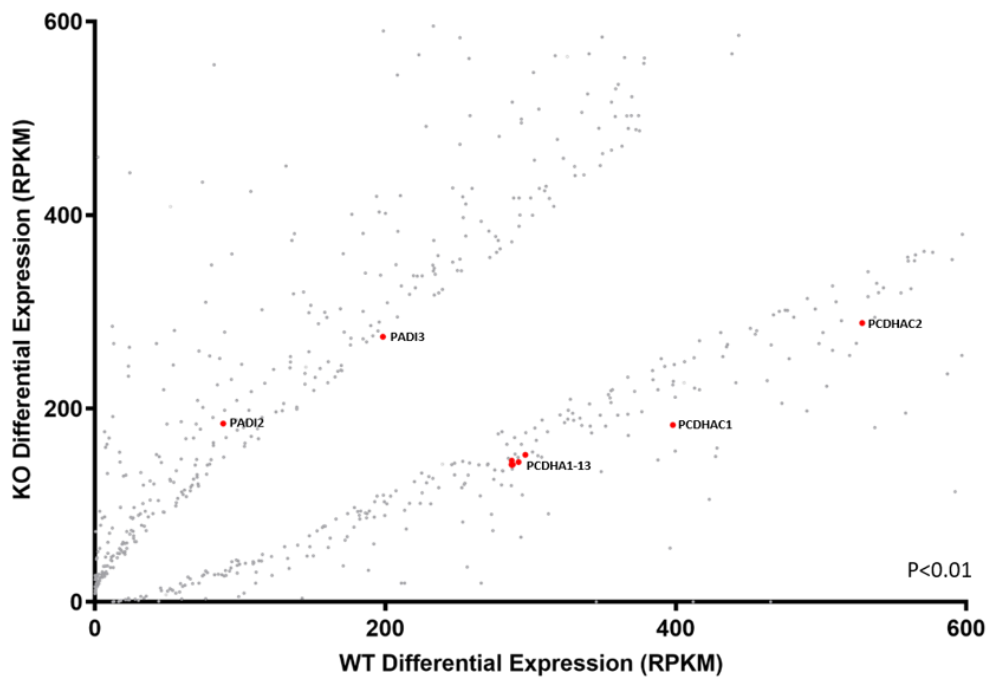
Figure 3.34 Gene ontology analysis of HOTTIP KO HCT116 RNA-Seq data.

The transcriptome of WT and HOTTIP KO HCT116 cells was analysed by RNA-Seq. Differential expression of genes was analysed through using the statistical packages 'TopHat2', 'HTSeq' and 'DESeq2'. Data was filtered by only accepting genes P<0.01 and a Log2FC >0.5 (925 genes total). After gene ontology analysis (GOrilla), differentially expressed genes involved in highlighted biological processes were visualised. (A) A heatmap showing differentially expressed genes in WT and HOTTIP KO samples. (B) A scatterplot indicating where these genes (highlighted in red) sit in relation to all other differentially expressed genes and whether the expression was greater in WT (x-axis), or HOTTIP KO (y-axis) cells.

The potential importance of these differentially expressed *PADI* and *PCDHA* genes was then explored further in CRC. Kaplan-Meier (K-M) survival plots were generated using an online database (kmplot.com) (Joo, Park and Chun, 2016) to examine if expression levels of the selected genes correlate with patient survival (Figure 3.35). Renal adenocarcinoma RNA-Seq data from 165 patients was again used for this analysis. High expression of *PADI3* (P=0.047), *PCDHA9* (P=0.029) and *PCDHA12* (P=0.01) were significantly correlated with poorer survival in rectal adenocarcinoma. However, *PCDHA10* (P=0.037) was found to have a similar effect on patient survival regardless of expression level.

Overall, two groups of genes were identified from GO analysis: *PADI* and *PCDHA*. *PADI2* and *PADI3* were upregulated in *HOTTIP* KO samples and have previously been reported in colorectal cancer. They are markers of citrullination, a post-translational modification that has been found to promote cancer progression by altering gene expression through rearranging methylation patterns (Chang *et al.*, 2016; He *et al.*, 2017). The *PCDHA* cluster genes were downregulated in *HOTTIP* KO HCT116 cells. Protocadherins have important roles in specific cell-cell connections and in promoting tumour development (Yang *et al.*, 2017). In cancer, the methylation pattern of *PCDHA* clusters is often altered so their expression is silenced (Fu *et al.*, 2017).
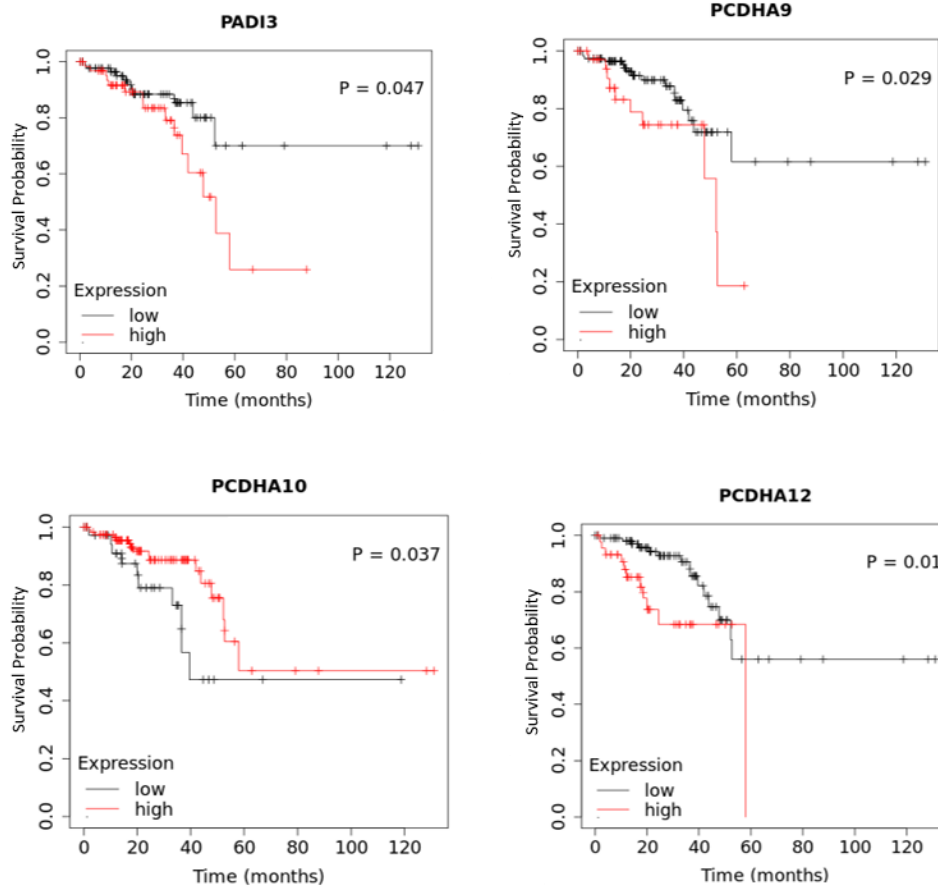
Figure 3.35 Kaplan-Meier survival plots of differentially expressed genes identified through gene ontology analysis of HOTTIP KO HCT116 RNA-Seq data.

Kaplan-Meier survival plots generated by a meta-analysis of rectal adenocarcinoma RNA-Seq data using kmplot online software (kmplot.com) to determine if differentially expressed PADI and PCDHA genes identified through gene ontology analysis of HOTTIP KO HCT116 RNA-Seq data is correlated with increased or decreased survival rates in CRC. The probability of survival (y-axis) is plotted against the time (months) a patient is estimated to survive the disease (x-axis). Black lines indicate low gene expression and red lines indicate high gene expression. N=165 patient samples were analysed in the rectal adenocarcinoma RNA-Seq dataset.

3.6 Discussion

HOTTIP expression is up-regulated in many cancers, including colorectal (Pradeepa *et al.*, 2017) and prostate (Wang *et al.*, 2011). Alongside *HOXA13* it has been associated with metastasis, increased cell proliferation, poor prognosis (Pradeepa *et al.*, 2017) and chemoresistance (Cheng *et al.*, 2015).

3.6.1 *HOTTIP* regulates *HOXA13* expression in CRC and PCa.

Upon *HOTTIP* depletion via siRNA knockdown in HCT116, RKO1 and DU145 cells, *HOXA13* expression was reduced. This was also observed in stable CRISPR-Cas9 mediated *HOTTIP* KO HCT116 cells. These data support what has been previously described in mouse models where *HOTTIP* regulates the expression of nearby *HOXA* genes in *cis* (Wang *et al.*, 2011). However, it should be noted that there was some BLAST sequence overlap for CRISPR gRNA HOTTIP 3P and siRNA HOTTIP KD 2 with *HOXA13*. Therefore, the reduction in *HOXA13* expression observed could be a result of an off-target effect of the CRISPR gRNA or siRNA rather than a direct effect of *HOTTIP* depletion*.

3.6.2 *HOTTIP* does not contribute to the proliferation, movement and migration of CRC and PCa cells.

Previous studies have described *HOTTIP* having roles in cell proliferation, migration and invasion in cancer (Kim and Shiekhattar, 2016). This was not replicated in this study. When *HOTTIP* was stably deleted from HCT116 cells a loss in cell motility was observed as well as a reduction in cell proliferation (P=0.06). This was not replicated

in the siRNA *HOTTIP* KD experiments in either of the cell lines (HCT116, RKO1, DU145). As a result, a strong role for *HOTTIP* in promoting cell movement and migration in these cell lines cannot be confirmed in this study.

3.6.3 *HOTTIP* may protect colorectal cancer cells against chemotherapeutic drugs.

Previous studies have suggested a role of *HOTTIP* in protecting cancer cells from death when exposed to chemotherapy (Li *et al.*, 2011; Cheng *et al.*, 2015). Commonly used CRC chemotherapeutic drugs 5-Fluoracil (5FU) (Carethers *et al.*, 2004) and Oxaliplatin (OX) (Comella *et al.*, 2009), and a PCa drug Docetaxel (DOC) (Ito *et al.*, 2018) were used to investigate whether *HOTTIP* expression protects CRC and PCa cells against chemotherapy toxicity.

When investigating sensitivity of *HOTTIP* depleted/KO cells to chemotherapeutic drugs, more consistent results were observed when *HOTTIP* was permanently deleted from HCT116 cells. Sensitivity to both 5FU and OX was observed when exploring the dose response, colony formation ability and proliferation rates of cells. There is no known report of *HOTTIP* playing a role in preventing apoptosis in PCa, however it has been reported once in CRC in HCT116 and SW620 cell lines (T. Liu *et al.*, 2018) which supports the findings observed in this study.

With the introduction of chemotherapy treatment, a significant increase in apoptosis was observed in *HOTTIP* depleted HCT116 cells treated with chemotherapeutic drugs. This was replicated in stable CRISPR *HOTTIP* KO HCT116 cells treated with OX, but not 5FU. A significant increase in apoptosis was observed

in *HOTTIP* depleted DU145 cells treated with DOC. However, this was also seen in *HOTTIP* depleted DU145 cells without DOC treatment; indicating that the increase in apoptosis is due to absence of *HOTTIP* rather than treatment with the drug.

In contrast, no significant shifts in the percentage of cells in each stage of the cell cycle were identified in *HOTTIP* depleted or stably deleted cells treated with chemotherapeutic drugs. 5FU is expected to induce arrest in both G1 and S phases of the cell cycle (Guo *et al.*, 2008; Focaccetti *et al.*, 2015); this arrest was increased in HCT116 and RKO1 cells transfected with siRNA HOTTIP KD 2, but not observed with siRNA HOTTIP KD 1 or the stable *HOTTIP* CRISPR KO HCT116 cell line. OX premdominantly induces arrest in G2/M phase and this was replicated here. Arrest during both S and G2/M phase is expected in cells treated with DOC (Tabaczar *et al.*, 2010; Nader, El Amm and Aragon-Ching, 2018), this was only observed for G2/M in DU145 cells. Together, this suggests OX is acting as expected, whereas 5FU and DOC have exhibited some shifts in their mechanisms of action. This could be a result of *HOTTIP* depletion, although more investigative work would need to be carried out before concluding this. There is no literature examining the role of *HOTTIP* on the cell cycle in the presence of chemotherapeutic drugs. There have been reports of *HOTTIP* promoting cell cycle progression in leukaemia (Zhuang, Li and Ma, 2019) which has not been observed in CRC or PCa in this study.

Overall, some sensitivity to chemotherapy was observed for CRC cells upon *HOTTIP* depletion. The strongest effect was observed in HCT116 *HOTTIP* KO cells, indicating that *HOTTIP* may exhibit chemosensitive properties in this cell line. This supports what has previously been reported in the literature (Li *et al.*, 2011; Sun, Hu,

et al., 2018). This is the first time a potential role for *HOTTIP* in promoting

chemosensitivity in *HOTTIP* has been described in CRC.

3.6.4   Global analysis of *HOTTIP* deletion in HCT116 CRC cells.

After exploring the functional role of *HOTTIP* in CRC and PCa, the transcriptome of

HOTTIP deleted HCT116 cells was investigated through RNA-Seq analysis. *HOTTIP,*

HOXA13 and *HOXD8* were all downregulated upon *HOTTIP* deletion. The *cis*

regulatory relationship between *HOTTIP* and the nearby *HOXA13* gene has been well

established (Wang *et al.*, 2011; Pradeepa *et al.*, 2017) and re-created earlier in this

study. However, *HOXD8* has not yet been described in relation to *HOTTIP*, although

it has been described as a tumour repressor in CRC (Mansour and Senga, 2017).

      HOXA3 and many genes belonging to the *HOXB* cluster were found to be

upregulated in *HOTTIP* KO cells (Figure 3.29). Although *HOTTIP* has not been directly

implicated in *HOXB* regulation, many *HOXB* genes have been described as promoting

CRC cell proliferation and metastasis (Iman *et al.*, 2016; Huang *et al.*, 2017; Ying *et*

al., 2020). *HOXA3* is known to be regulated by another lncRNA, *HOXA-AS2* (Ding *et*

al., 2017) that was also found to be up-regulated in HCT116 upon *HOTTIP* deletion

(Figure 3.29). *HOTTIP* may have a role in regulating *HOXA-AS2* which in turn affects

HOXA3 expression.

      During GO analysis, two main sets of genes were highlighted as being

differentially expressed in *HOTTIP* KO HCT116 cells: the *PADI* and *PCDHA* clusters.

Upregulation of *PADI2/3* was observed in *HOTTIP* KO cells. *PADI2/3* are usually

found to suppress proliferation and act as tumour suppressors in CRC (Funayama *et*

al., 2017; Chai *et al.*, 2019; Chang *et al.*, 2019). Although, there is contradicting literature describing the role of *PADI2.* Some studies have shown it is correlated with poor prognosis (Cantarino *et al.*, 2016) as well as promoting liver metastasis (Chen *et al.*, 2017), a common secondary CRC site. However, other work has shown that *PADI2* is downregulated in CRC (Cantarino *et al.*, 2016) and can suppress the proliferation of CRC cells through protein citrullination (Funayama *et al.*, 2017). This tumour suppressive role fits with what is observed in this data as *PADI3* has previously been described as a tumour suppressor gene in CRC (Chai *et al.*, 2019; Chang *et al.*, 2019). A relationship between *HOTTIP* and *PADI2/3* has not yet been described; nevertheless, these data suggest that *HOTTIP* may also act as a tumour suppressor via the regulation of *PADI2* and *PADI3,* as upon loss of *HOTTIP* these genes are upregulated in HCT116 cells.

Alternatively, expression of the *PCDHA* cluster was downregulated in *HOTTIP* KO samples compared to WT. Protocadherins have important roles in specific cell-cell connections and in promoting tumour development (Berx and van Roy, 2009) so when depleted in *HOTTIP* KO cells this may prevent cancer progression. On the other hand, *PCDHA* genes are also involved in development, as regulators of the neural circuit formation (Peek, Mah and Weiner, 2017). As *HOX* expression was shown to be de-regulated with *HOTTIP* depletion, another possibility could be that the *HOX* TFs could be regulating the expression of *PCDHA's* in CRC rather than *HOTTIP* having a direct effect on their expression.

3.7   Summary

In summary, *HOTTIP* was found to exhibit some chemosensitive properties in the HCT116 cell line. This was observed in both siRNA mediated depleted cells and CRISPR-Cas9 mediated stable *HOTTIP* KO cells, although the stable cell line provided more significant and therefore conclusive results. This suggests that CRC patients exhibiting high levels of *HOTTIP* may not react to chemotherapy as well as those patients with lower levels; tumour cell testing for this gene may aid clinicians with deciding on treatment options for a patient. More study into the chemosensitive properties of *HOTTIP* in CRC will provide further clarification.

When investigating global expression patterns in *HOTTIP* KO HCT116 cells, a novel relationship where *HOXD8* expression is reduced upon *HOTTIP* deletion was observed. *HOTTIP* was also shown to negatively regulate *PADI2/3* and the *PCDHA* cluster. Overall, these data suggest a role for *HOTTIP* in promoting CRC cell progression through transcriptional regulation of *HOXA, PADI* and *PCDHA* genes. Further study may determine if regulation of these genes contributes to the chemosensitive role of *HOTTIP* in cancer.

Limitations of this work include the BLAST sequence overlap for CRISPR gRNA HOTTIP 3P and siRNA HOTTIP KD 2 with *HOXA13*. This raises the potential issue of off-target effects and the resultant data may be a result of *HOXA13* depletion as well as or instead of the intended *HOTTIP* depletion. Ensuring specificity would have improved the quality of the data in this chapter. Further optimisation of the chemotherapeutic drug assays (time points, concentrations, controls) would

improve the significance of the data observed in this chapter, adding confidence to

the suggestion of a potential chemosensitive role of *HOTTIP* in CRC and PCa. Knock-

down success was checked regularly but was not performed for every experiment;

therefore, providing confirmation of siRNA knockdown (via qPCR/Sanger

sequencing) for each of the cell assays would also add confidence to this data.

4 Investigating the role of *HOXA13* in the progression of cancer.

4.1 Introduction

Homeobox protein HOX-A13 (*HOXA13*) is one of the Homebox A Cluster (*HOXA*) genes involved in animal development and is located at the 5' end of the *HOXA* cluster (Yamamoto *et al.*, 2019) . The lncRNA *HOTTIP* is located in close proximity to HOXA13 (Wang *et al.*, 2011), as described in Chapter 3. *HOXA13* is a transcription factor (Qin *et al.*, 2019) and a highly conserved gene, and has roles in gene regulation during embryonic development (Wang *et al.*, 2016).

HOX genes are involved in many cellular functions and therefore any mutational changes or downregulation of *HOX* genes has the potential to contribute to tumour development and progression (Wang *et al.*, 2016). Upregulation of *HOXA13* has been associated with some cancers, including gastric (Chang *et al.*, 2016; Qin *et al.*, 2019), pancreatic (Li *et al.*, 2015), liver (Quagliata *et al.*, 2018) and prostate (Zhang *et al.*, 2016). This has been outlined further in Chapter 1 (Section 1.4.1).

Although having previously being described in gastrointestinal (GI) cancers, this study will focus specifically on outlining the role of *HOXA13* in the progression of colorectal cancer (CRC) which has not yet been investigated. The role of *HOXA13* in prostate cancer (PCa) will also be explored. It will be determined whether *HOXA13* has a role in protecting CRC and PCa cells from cell death as a result of

chemotherapy treatment and whether it influences the progression of the disease through promoting cell movement and migration.

4.2 siRNA mediated depletion of *HOXA13* results in reduced expression of other *HOXA* genes and the lncRNA *HOTTIP* in CRC and PCa.

Two siRNAs targeted to transiently knockdown (KD) the expression of *HOXA13* have been used throughout this study to investigate the role of *HOXA13* in CRC and PCa. These have been named HOXA13 KD 1 and HOXA13 KD 2. All experiments have included non-targeting (NTC) siRNA controls to reduce false positive results or any changes occurring due to off-target effects. Three cell lines were used: HCT116 (Brattain *et al.*, 1981), RKO1 (Brattain *et al.*, 1984) (both CRC) and DU145 (Stone *et al.*, 1978) (PCa).

To confirm successful knockdown of *HOXA13* in each of the three cell lines, gene expression levels were checked for sufficient *HOXA13* depletion. The subsequent expression of other *HOXA* genes and the lncRNA *HOTTIP* (Chapter 3) were also measured. Cells were seeded in 6-well plates and transfected with either *HOXA13* targeting or NTC siRNA. RNA was extracted from cells 72 h after siRNA transfection and cDNA was subsequently reverse transcribed. Gene expression levels were quantified using qPCR and data normalised to the ribosomal protein L19 (*L19)* gene.

Over 60 % *HOXA13* depletion was observed in each of the three cell lines (Figure 4.1) indicating successful knockdown When *HOXA13* was depleted in HCT116

cells with siRNA HOXA13 KD 1, expression of all nearby genes (*HOTTIP, HOXA13, HOXA11, HOXA9* and HOXA1) was reduced (Figure 4.1A). This was found to be significant for both *HOXA13* and *HOXA11,* located adjacent to *HOXA13* on the *HOXA* cluster. HCT116 cells transfected with HOXA13 KD 2 resulted in reduced expression of *HOTTIP, HOXA13* and *HOXA9*, however this was not found to be statistically significant. In *HOXA13* depleted RKO1 cells, all nearby genes were significantly reduced (*HOTTIP, HOXA13, HOXA11, HOXA9, HOXA1)* with the exception of *HOXA11* when cells were transfected with HOXA13 KD 2 (Figure 4.1B). In *HOXA13* depleted DU145 cells, both *HOTTIP* and *HOXA13* expression was significantly reduced. Reduced *HOXA9* and *HOXA2* expression was observed in DU145 cells transfected with *HOXA13* siRNA 2 KD, however this was not significant (Figure 4.1C).

To summarise, in the CRC cell lines (HCT116 and RKO1), *HOXA13* depletion resulted in significant downregulation of *HOTTIP* and *HOXA* genes. In the PCa cell line (DU145), *HOXA13* depletion resulted in significant downregulation of *HOTTIP*. Together these data suggest that a reduction in *HOXA13* expression also results in a reduction in *HOTTIP* expression in HCT116, RKO1 and DU145 cell lines. *HOXA13* expression also influences other *HOXA* genes in CRC, with the most prominent effect seen in the RKO1 cell line, however *HOXA13* depletion does not influence the expression of other *HOXA* genes in the prostate cancer cell line (DU145). *HOTTIP* has previously been described as regulating nearby *HOXA* genes, including *HOXA13* in mouse models (Pradeepa *et al.*, 2017). This observation has now been replicated in the HCT116, RKO1 and DU145 cell lines. Significant *HOXA13* depletion in each cell line confirms successful siRNA knockdown. Successful siRNA depletion was regularly

confirmed alongside functional assays to investigate the role of *HOXA13* in HCT116,
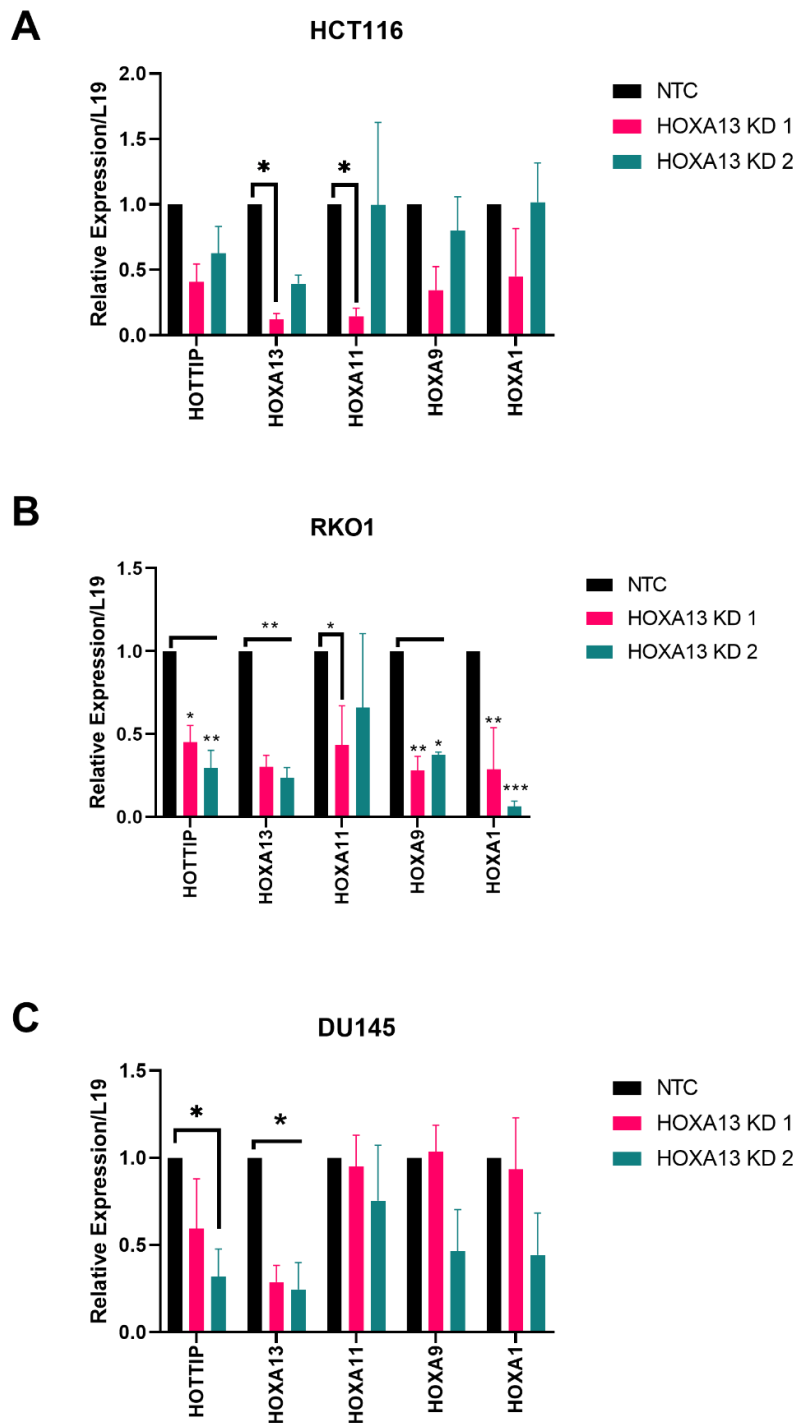
RKO1 and DU145.

Figure 4.1 siRNA mediated *HOXA13* depletion gene expression

(A) HCT116, (B) RKO1 and (C) DU145 cells were transfected with siRNA targeting *HOXA13* or NTC for 72 h. RNA was subsequently extracted and cDNA synthesised. Gene expression levels of target genes (*HOTTIP, HOXA13, HOXA11, HOXA9, HOXA1*) were quantified and compared to control via qPCR. Data are mean (± S.E.M) expression of 3 biological replicates (N=3), analysed by RT-qPCR and normalized to *L19*. Two-way ANOVA with Dunnett's multiple comparison test was used to quantify the statistical significance (*$P<0.05$, **$P<0.01$).

4.3   Investigating the role of *HOXA13* expression in the movement and migration of CRC and PCa cells.

HOXA13 has previously been described alongside *HOTTIP* (Chapter 3), to promote cell proliferation, migration and invasion in pancreatic (Li *et al.*, 2011), gastric (Chang *et al.*, 2016; Qin *et al.*, 2019), esophageal squamous cell (Shen and Chen, 2011), and prostate cancer (Zhang *et al.*, 2016; Dong *et al.*, 2017a). The functional role of *HOXA13* in HCT116, RKO1 and DU145 will be explored to understand if this is also found in these cell lines.

4.3.1   *HOXA13* does not influence single cell motility in CRC and PCa.

Single cell tracking analysis was used to analyse the motility of CRC and PCa cells following manipulation of *HOXA13* levels. This will indicate whether *HOXA13* has a role in cancer cell migration. To enable fluorescent detection, CYTO-ID dye (Enzo life sciences) was used to label cells. Dyed, siRNA transfected cells were seeded sparsely into 96 well plates so individual cells could be tracked with a Nikon Widefield microscope. Images were taken every 20 minutes for 24 h. Cells were placed in a humidified CO_2 chamber to retain their optimum culturing conditions whilst being imaged. Average cell speeds calculated using the Trackmate plug in on Image J (Tinevez *et al.*, 2017).

The range of cell speeds was reduced for *HOXA13* depleted HCT116 cells, however the change in motility was not found to be significant (Figure 4.2A). An increase in cell motility was observed for RKO1 cells transfected with HOXA13 KD 1; however, no change was seen for the same cells transfected with HOXA13 KD 2

(Figure 4.2B). No significant difference in cell motility was observed for *HOXA13* depleted DU145 cells, however the range of DU145 cells transfected with siRNA HOXA13 KD 1 was reduced compared to NTC (Figure 4.2C).

Overall, despite some differences in motility observed between *HOXA13* depleted and NTC cells, this was not significant in any cell line. Therefore, it cannot be concluded that *HOXA13* does not contribute to migration in HCT116, RKO1 or DU145 cells.
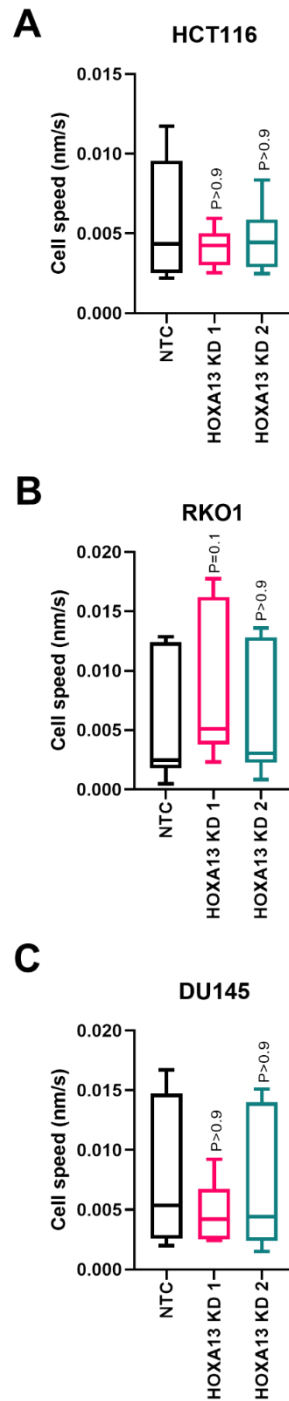
Figure 4.2 Single cell tracking analysis of siRNA mediated HOXA13 depletion.

Single cell tracking was used to measure the average speed of siRNA mediated *HOXA13* depleted and NTC (A) HCT116, (B) RKO1 and (C) DU145 cells. After sparsely being seeded in 96-well plates, cells were placed in a humidified CO2 chamber attached to a Nikon Widefield microscope where images were taken every 20 min for 24h. Individual cells were tracked and average speeds were calculated using ImageJ Fiji. Data are mean (± S.E.M) expression of 3 biological replicates (N=3). Kruskal-Wallis test with Dunn's post-hoc test was used to quantify the statistical significance.

4.3.2   *HOXA13* depletion has no significant effect of migration rate in CRC and PCa.

Wound healing assays were implemented to measure the migration rates of *HOXA13* depletion in HCT116, RKO1 and DU145 cancer cells. To do this, cells were seeded in 6-well plates so they reached 100% confluency within 24 h. A 'wound' was created in each well by scratching a gap in the confluent cells with a P20 pipette tip. A Nikon Widefield microscope was used to take pictures of each well every 20 minutes over a 24 h period. Cells were placed in a humidified CO_2 chamber to retain their optimum culturing conditions. The percentage of cell coverage at each time point was analysed using ImageJ (Schindelin *et al.*, 2012).

HOXA13 depleted HCT116 cells exhibited a reduction in cell migration when transfected with HOXA13 KD 1 (41 % reduction) or HOXA13 KD 2 (58 % reduction) siRNAs, however this was not found to be significant (Figure 4.3A). *HOXA13* depleted RKO1 cells showed no significant difference in cell migration rate compared to control (Figure 4.3B). In DU145 cells, a reduction in migration was observed for *HOXA13* depleted cells, however this again was not significant (HOXA13 KD 1 = 38 % reduction, HOXA13 KD 2 = 33 % reduction), (Figure 4.3C). More data would have to be collected before it can be concluded whether *HOXA13* has a role in cell migration in HCT116, RKO1 or DU145 cell lines.
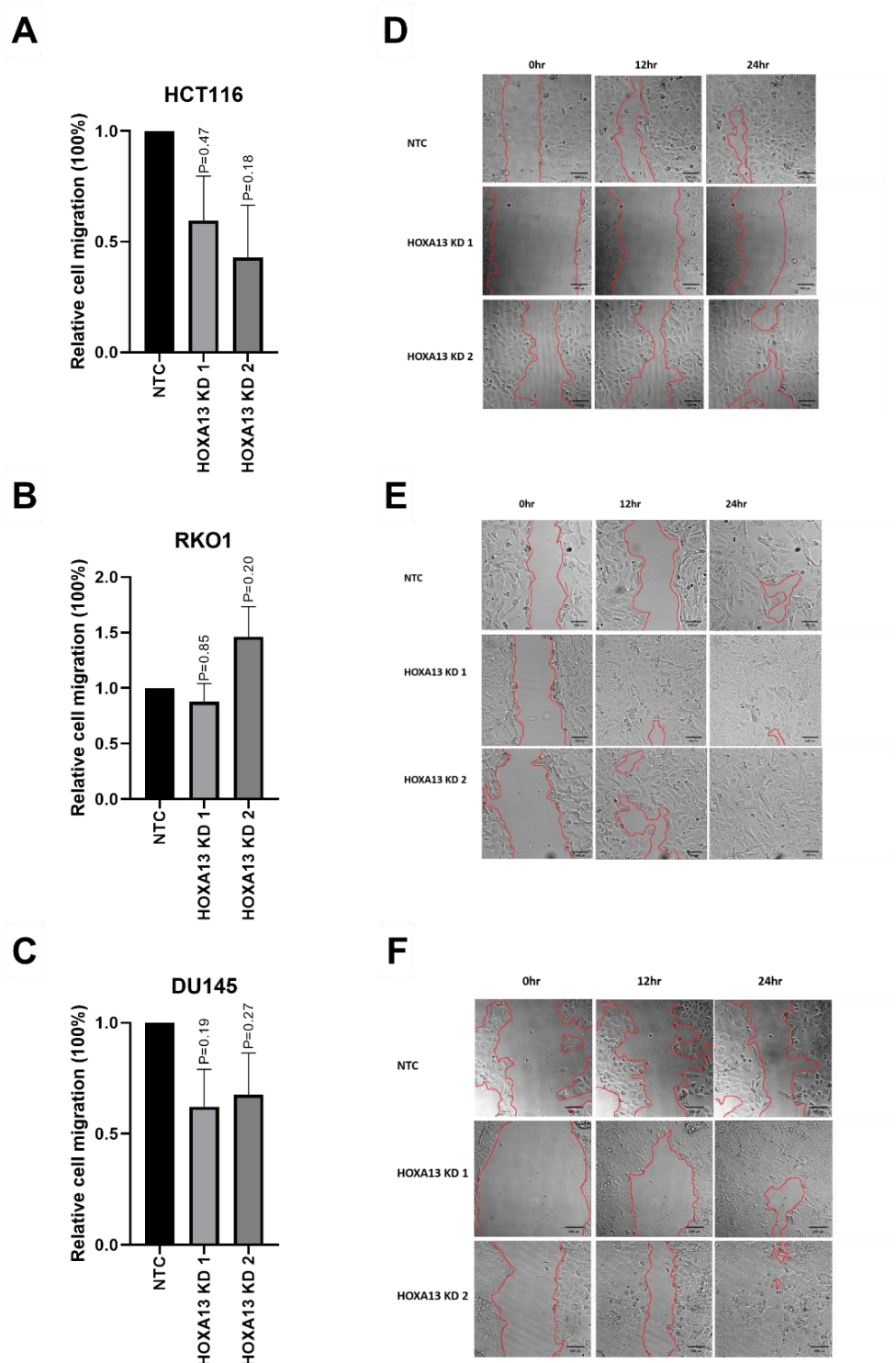
Figure 4.3 siRNA mediated HOXA13 depletion reduces migration of cancer cells.

Wound healing assays were carried out to measure the migration rates of siRNA mediated *HOXA13* depletion in (A) HCT116, (B) RKO1 and (C) DU145 cells. 'Wounds' were tracked over 24 h and *HOXA13* KD cell migration was calculated relative to NTC. Representative microscopy images of *HOXA13* KD and control 'wounds' in (D) HCT116, (E) RKO1 and (F) DU145 cells at 0 h, 12 h and 24 h after initial scratching of wound. All data are mean (± S.E.M) of 3 biological replicates (N=3) relative to 100% wound closure. One-way ANOVA with Dunnett's multiple comparisons test was used to quantify statistical significance.

4.3.3 Investigating the effect of *HOXA13* on CRC and PCa cell proliferation.

The effect of *HOXA13* depletion on growth rates was investigated. After siRNA transfection, cells were seeded in 96-well plates and grown for up to 8 days. After each time point, cells were fixed and stained with crystal violet prior to colorimetric analysis (OD 490nm), growth rates were calculated relative to day 0 (no growth).

In *HOXA13* depleted HCT116 cells a loss in proliferation was observed compared to control, although this was not significant (Figure 4.4A). Opposingly, a significant increase in proliferation was detected in *HOXA13* depleted in RKO1 cells (Figure 4.4B). In DU145 cells, growth rates are variable for siRNA depleted cells and no significant effect was found compared to NTC (Figure 4.4C). Overall, no significant effect on growth rate was found for *HOXA13* depleted HCT116 and DU145 cells indicating *HOXA13* does not contribute to proliferation in these cell lines. *HOXA13* depletion significantly increases the growth rate of RKO1 cells suggesting *HOXA13* expression may supress RKO1 cell proliferation.
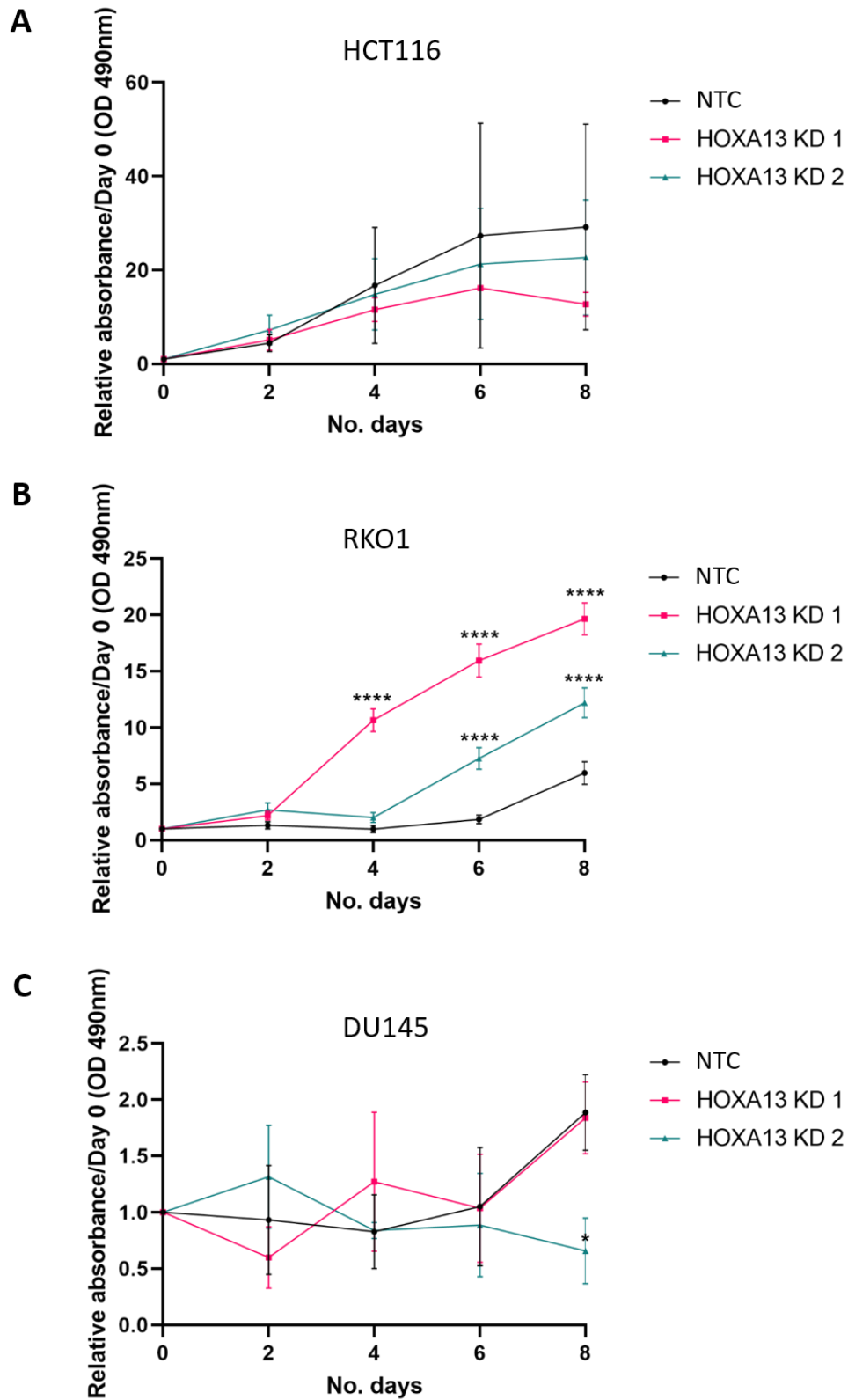
Figure 4.4 siRNA mediated HOXA13 depletion in vitro cell growth assay.

Proliferation of siRNA mediated HOXA13 depleted and NTC (A) HCT116, (B) RKO1, and (C) DU145 cells were seeded in 96-well plates and growth rates were measured over an 8-day time series. Growth rates are relative to day 0 (no growth). Data are mean (± S.E.M) of 3 biological replicates (N=3). Two-way ANOVA with Dunnett's multiple comparison test was used to quantify statistical significance (*P<0.05, ****P<0.0001).

4.3.4 *HOXA13* depletion does not induce increased apoptosis in cancer cells.

Flow cytometry was used to assess whether *HOXA13* depletion leads to an increase in apoptosis in HCT116, RKO1 and DU145 cells. After transfection with *HOXA13* targeted or NTC siRNAs, all cells and media were collected and pelleted. Pelleted cells were re-suspended in Nicoletti buffer (Riccardi and Nicoletti, 2006) containing propidium iodide (PI) that is used to stain apoptotic cells. During the process of apoptosis DNA becomes fragmented. As a result, rates of apoptosis can be measured by the identification of hypodiploid cells using a DNA stain such as PI. Cellular PI intensity was quantified using flow cytometry and rates of apoptosis were compared to that of NTC.

An increase in percentage apoptosis was observed for *HOXA13* depleted HCT116 cells (Figure 4.5A), however this was non-significant. The opposite was observed in RKO1 cells where *HOXA13* depletion resulted in a reduction in percentage apoptosis (Figure 4.7B); this was also not found to be significant. *HOXA13* depleted DU145 cells exhibited a significant increase in apoptosis (Figure 4.5C), suggesting that *HOXA13* may have a role in role in protecting DU145 cells from cell death.
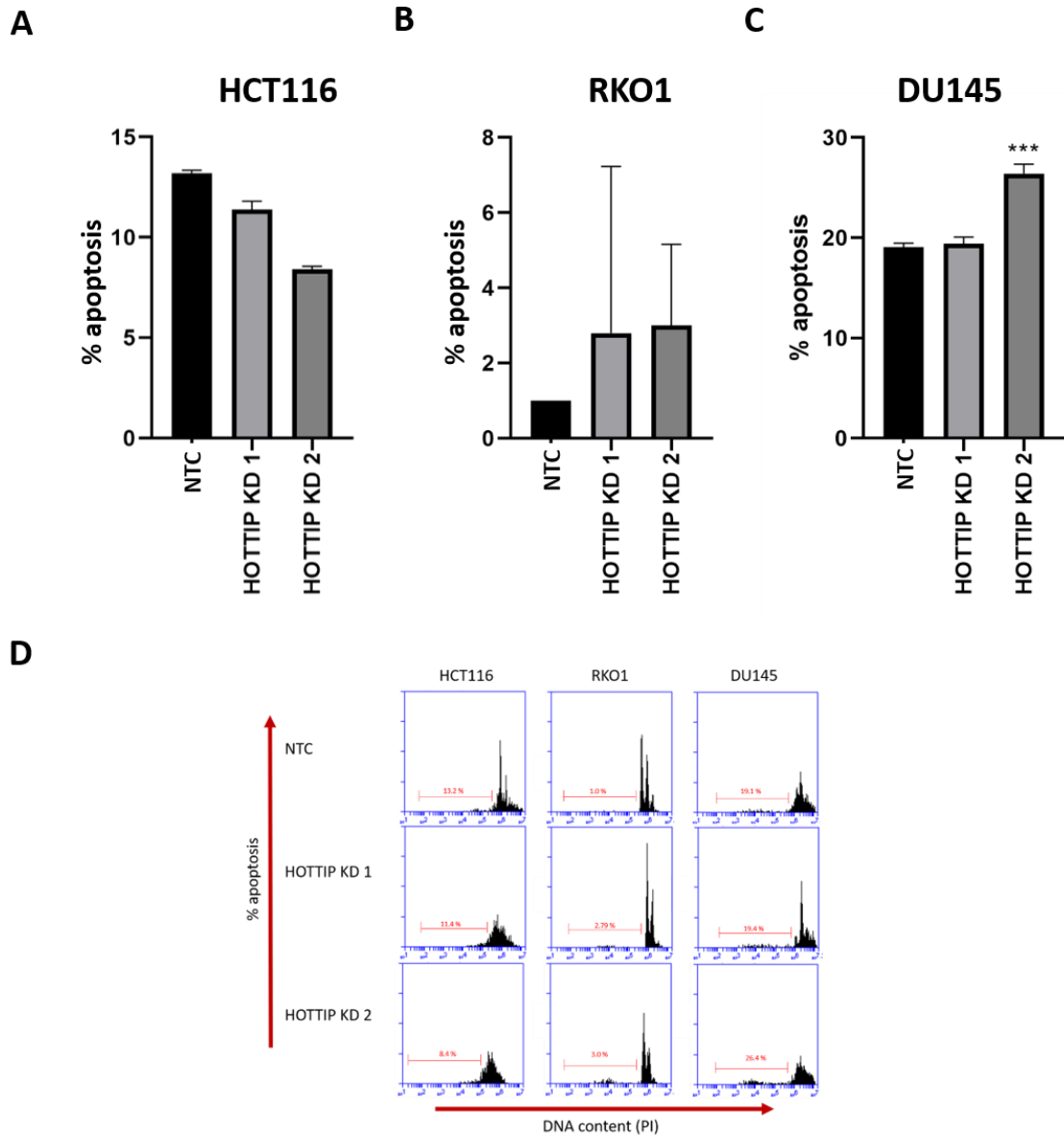
Figure 4.5 Apoptosis of siRNA mediated HOXA13 depleted CRC and PCa cells.

After transfection for 72 h with siRNA targeting *HOXA13* or NTC, all cells and media were collected and pelleted. Pellets were re-suspended in Nicoletti buffer and DNA hypodiploidy analysis was carried out using flow cytometry. Percentage apoptosis of *HOXA13* depleted (A) HCT116, (B) RKO1 and (C) DU145 cells. (D) Representative flow cytometry plots of *HOXA13* depleted and NTC HCT116, RKO1 and DU145 cells, average Sub-G1 percentages are highlighted in red. Data are mean (± S.E.M) of 3 biological replicates (N=3). Two-way ANOVA with Dunnett's multiple comparisons test was used to quantify statistical significance (**P<0.01, ****P<0.0001).

4.3.5 *HOXA13* depletion does not drive cell cycle progression

Flow cytometry was used to determine whether *HOXA13* has roles in cell cycle progression in CRC or PCa. Cell cycle assays assess cellular DNA content and indicate what percentage of cells in a sample are in each stage of the cell cycle (Kim and Sederstrom, 2015). Cells were transfected with *HOXA13* targetting or NTC siRNA for 72 h, after which point all cells and media were pelleted and fixed so the cell cycle stage of each cell could be analysed. The fixative was removed and samples were re-suspended in a stain containing PI. A flow cytometer was used to measure the percentage of cells in each stage of the cell cycle (G1, S, G2/M) to see if there is a change in this distribution when *HOXA13* is depleted in HCT116, RKO1 or DU145 cells.

In HCT116 cells, *HOXA13* depletion resulted in an increase in G1 and S phase, and a decrease in G2/M phase, although this was not a significant effect (Figure 4.6A). *HOXA13* depleted RKO1 cells exhibited an increase in G1 phase, however S phase was reduced. RKO1 cells transfected with HOXA13 KD 1 exhibited a loss in the number of cells in G2/M phase, however this remained unchanged for RKO1 transfected with HOXA13 KD 2 – again these changes were non-significant (Figure 4.6B). The percentage of cells in G1 phase was reduced whereas G2/M phase was increased in *HOXA13* depleted DU145 cells. DU145 cells transfected with HOXA13 KD 1 exhibited an increase in S phase whereas DU145 cells transfected with HOXA13 KD 2 exhibited a decrease in S phase (Figure 4.6C). No cell cycle changes were found to be significant in DU145 cells. Therefore, these data indicate that *HOXA13* does not contribute to cell cycle progression in HCT116, RKO1 or DU145 cells.
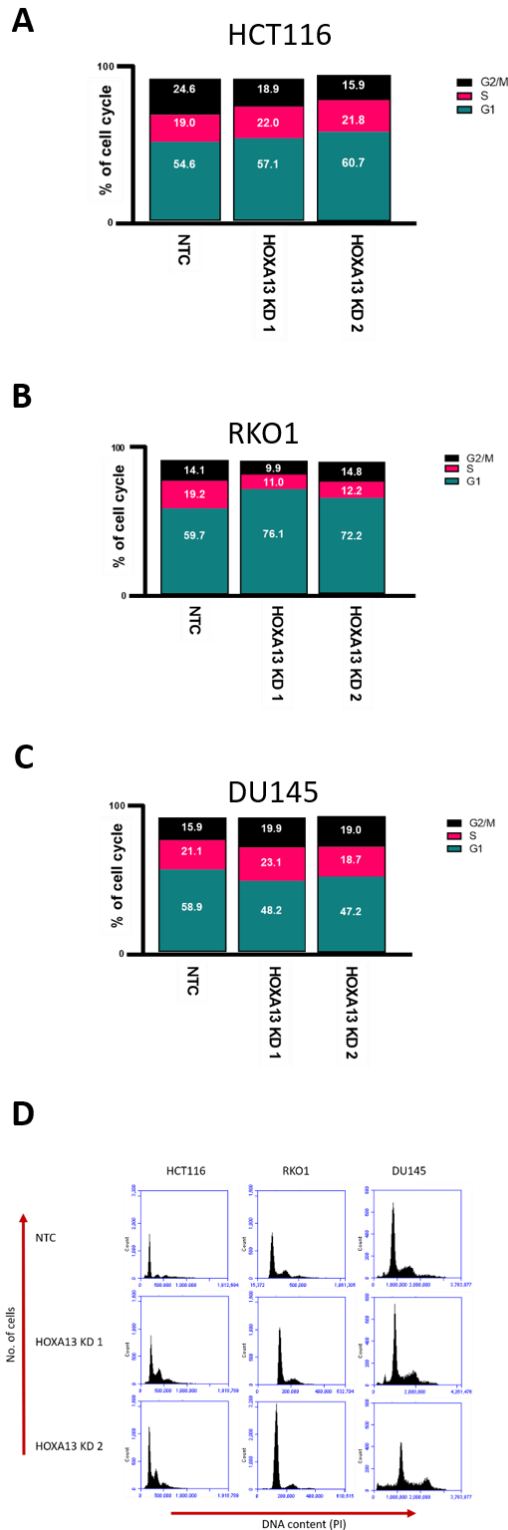
Figure 4.6 Cell cycle analysis of siRNA mediated HOXA13 depleted CRC and PCa cells.

siRNA mediated PSIP1 depleted and NTC HCT116, RKO1 and DU145 cells were analysed via flow cytometry to measure the percentage of cells in each stage of the cell cycle. Cell cycle analysis of HOXA13 depleted (A) HCT116 (B) RKO1 (C) DU145 cells. (D) Representative flow cytometry plots of HOXA13 depleted cells and NTC. Data are mean (± S.E.M) of 3 biological replicates (N=3). Two-way ANOVA with Dunnett's multiple comparisons test was used to quantify statistical significance.

155

4.4   *HOXA13* expression protects cancer cells against chemotherapeutic drugs.

High *HOXA13* expression has been linked to chemoresistance in esophageal squamous cell carcinoma (ESCC) (Shi *et al.*, 2018), hepatocellular carcinoma (Quagliata *et al.*, 2018), gastric cancer (Han *et al.*, 2018), and pancreatic cancer (Li *et al.*, 2011). However, this has not yet been documented in CRC or PCa. The following chemotherapeutic drugs have been used to investigate whether *HOXA13* has a role in chemoresistance in CRC or PCa: Fluorouacil (5FU) (Carethers *et al.*, 2004), Oxaliplatin (OX) (Comella *et al.*, 2009) that are both commonly used in CRC treatment, and Docetaxel (DOC) (Ito *et al.*, 2018) that is frequently used in the management of PCa.

4.4.1   The dose response of cancer cells to chemotherapy remains unchanged with *HOXA13* depletion.

Initially, the dose response of *HOXA13* depleted HCT116, RKO1 and DU145 cells to chemotherapeutic drugs was tested in order to investigate whether *HOXA13* depletion increases sensitivity of cells to chemotherapy, which would indicate chemoresistant properties of *HOXA13*. siRNA mediated *HOXA13* depleted cells were seeded in 96-well plates and treated with a dose range of either 5FU, OX or DOC for 72 h prior to being fixed and stained with crystal violet for colorimetric measurement (OD 490 nm). The optical density was calculated relative to no drug treatment (0 µM).

156

A significant increase in sensitivity to 0.1 µM 5FU was observed in HCT116 cells transfected with HOXA13 KD 2. There was no sensitivity to 5FU observed for the same cells transfected with HOXA13 KD 1 (Figure 4.7A). Sensitivity of *HOXA13* depleted HCT116 cells treated with OX was also observed. This was significant for cells transfected with HOXA13 KD 1 and treated with 10 µM OX (Figure 4.7B). Significant sensitivity was observed for *HOXA13* depleted RKO1 cells treated with 0.1 µM 5FU when transfected with HOXA13 KD 1 (Figure 4.8A). RKO1 cells transfected with HOXA13 KD 1 exhibited increased sensitivity when treated with 10 µM OX (Figure 4.8B). Unexpectedly, no sensitivity to DOC was observed in DU145 NTC cells, however DU145 cells transfected with HOXA13 KD 1 exhibited significant sensitivity to 10 µM of DOC (Figure 4.9). No significant difference was observed for DOC treated DU145 cells transfected with HOXA13 KD 2. Overall, these data suggest that *HOXA13* depletion may enhances chemosensitivity in these cell lines, particularly when does with 1 µM 5FU (HCT116, RKO1), 10 µM OX (HCT116, RKO1) or 10 µM DOC (DU145). Further experimental work would need to be carried out to confirm this observation.

A
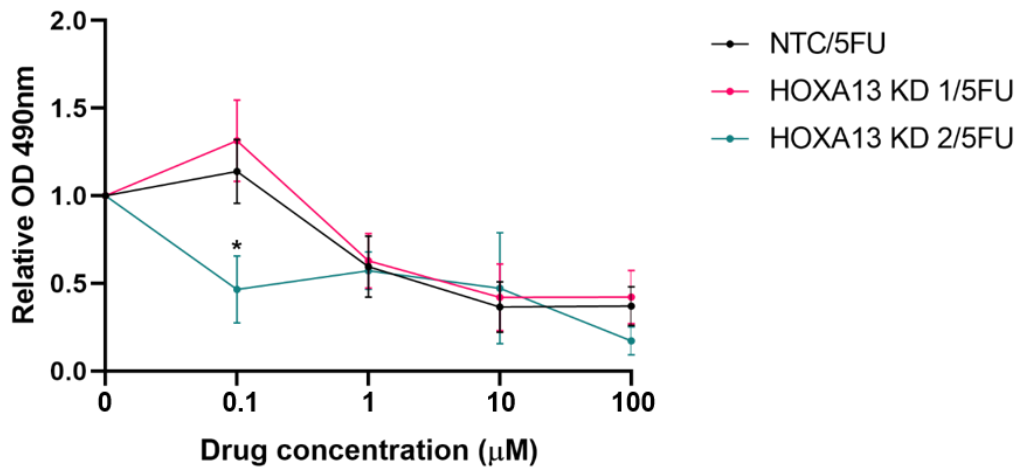
B
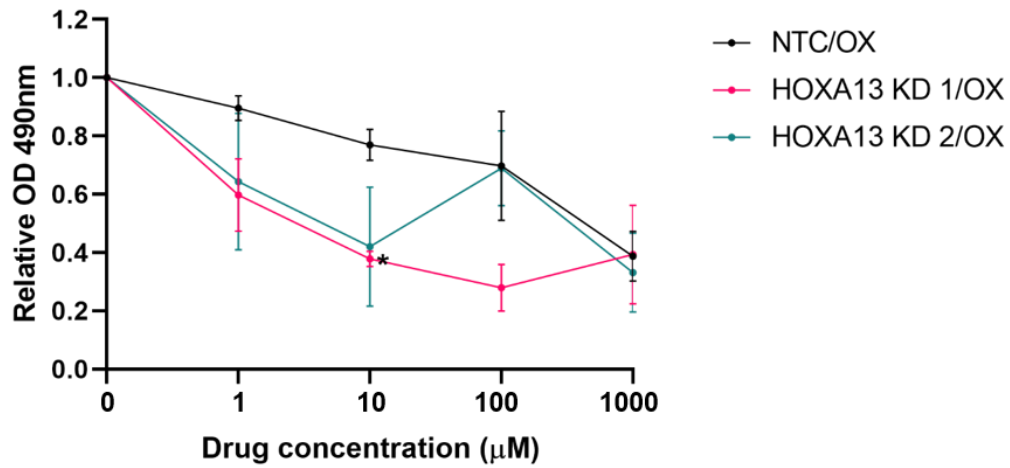
Figure 4.7 Dose response of siRNA mediated HOXA13 depleted HCT116 cells to chemotherapeutic drugs.

HCT116 cells were transfected with HOXA13 targeting or NTC siRNA for 72 h. Cells were then seeded in 96-well plates and subsequently treated with a dose response of (A) 5FU (0, 0.1, 1, 10, 100 µM) or (B) OX (0, 1, 10, 100, 1000 µM) for a further 72 h. All data are mean (± S.E.M) of 3 biological replicates (N=3). Two-way ANOVA with Dunnett's multiple comparisons test was used to quantify statistical significance (*$P<0.05$).
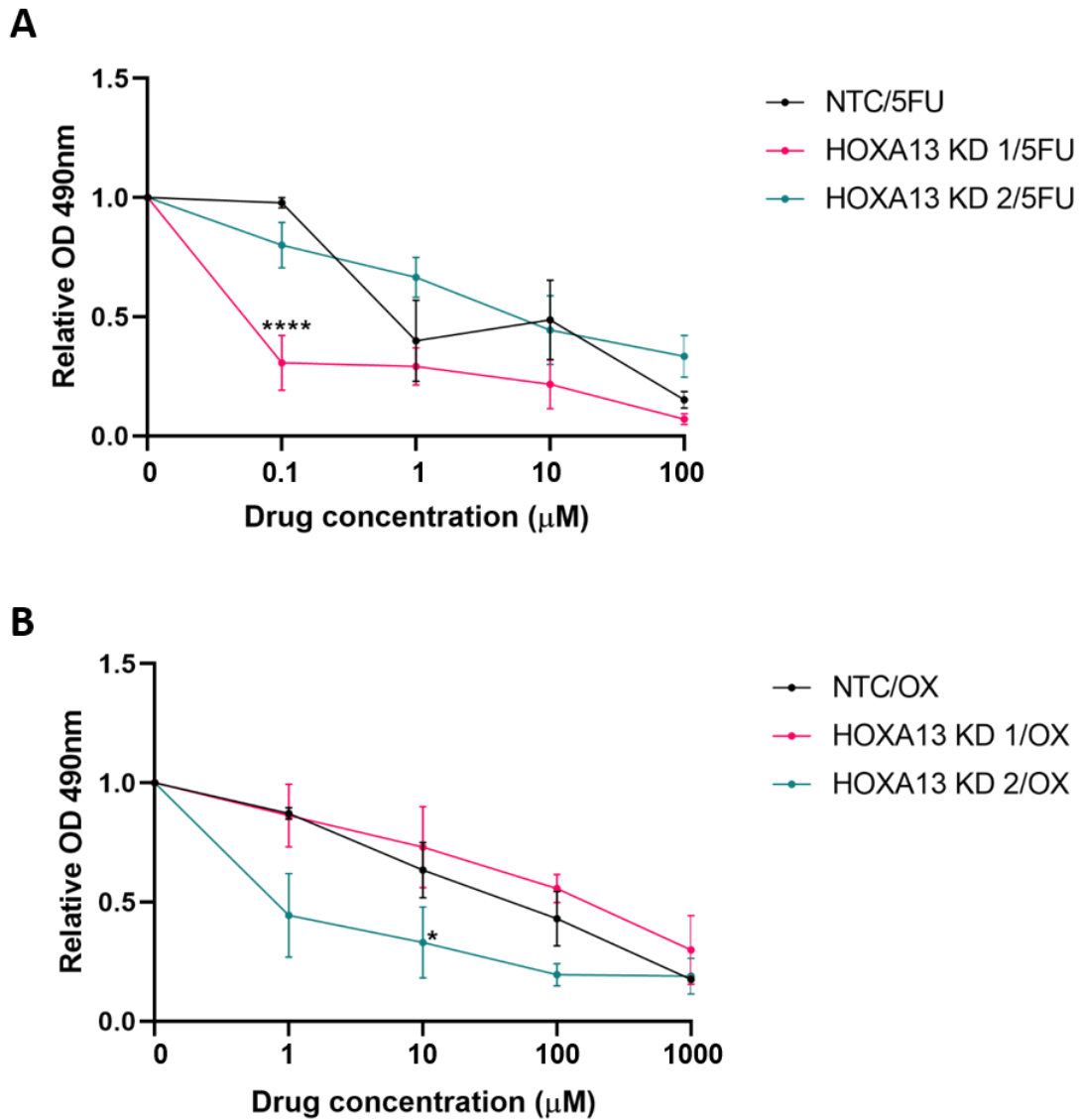
Figure 4.8 Dose response of siRNA mediated HOXA13 depleted RKO1 cells to chemotherapeutic drugs.

RKO1 cells were transfected with HOXA13 targeting or NTC siRNA for 72 h. Cells were then seeded in 96-well plates and subsequently treated with a dose response of (A) 5FU (0, 0.1, 1, 10, 100 μM) or (B) OX (0, 1, 10, 100, 1000 μM) for a further 72 h. All data are mean (± S.E.M) of 3 biological replicates (N=3). Two-way ANOVA with Dunnett's multiple comparisons test was used to quantify statistical significance (*$P<0.05$, ****$P<0.0001$).
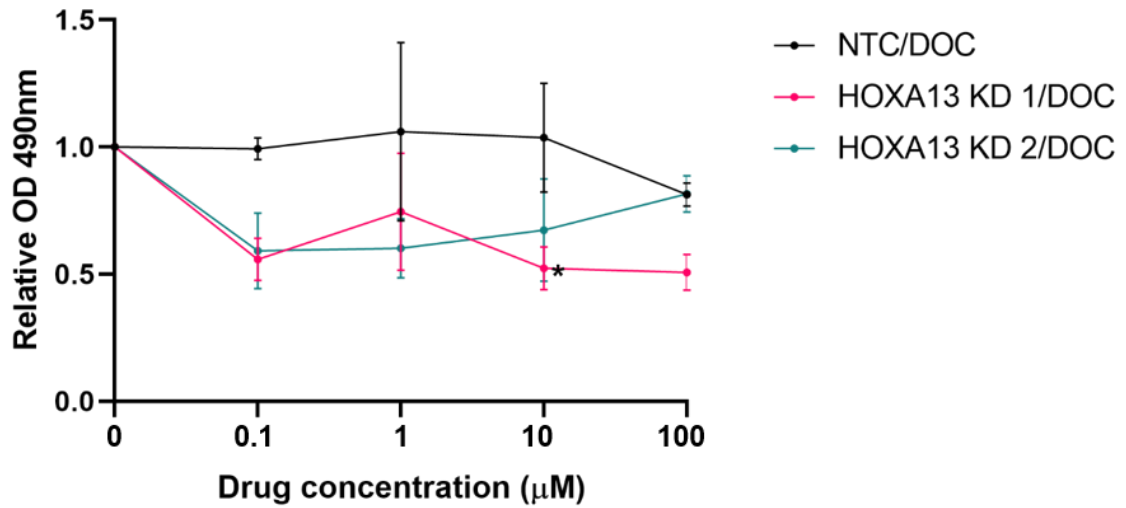
Figure 4.9 Dose response of siRNA mediated HOXA13 depleted DU145 cells to chemotherapeutic drugs.

DU145 cells were transfected with HOXA13 targeting or NTC siRNA for 72 h. Cells were then seeded in 96-well plates and subsequently treated with a dose response of DOC (0, 0.1, 1, 10, 100 µM) for a further 72 h. All data are mean (± S.E.M) of 3 biological replicates (N=3). Two-way ANOVA with Dunnett's multiple comparisons test was used to quantify statistical significance (*P<0.05).

4.4.2   Depletion of *HOXA13* leads to an increase in cell death when CRC and PCa cells are treated with chemotherapeutic drugs.

After investigating sensitivity to chemotherapy in cancer cells with reduced *HOXA13* expression, rates of cell death (apoptosis) of these cells after exposure to 10 μM 5FU, 10 μM OX or 1 μM DOC was tested. Cells were treated with chemotherapeutic drugs and incubated for different time points: 24 h, 48 h, 72 h. A no drug comparison was also included for each cell line. Flow cytometry was used to quantify the percentage of cells undergoing apoptosis as described above (Section 4.3.4). *HOXA13* depleted cells were compared to NTC and no drug controls.

After 72 h siRNA knockdown, *HOXA13* depleted cells exhibited an increase in the percentage of cells undergoing apoptosis. With the addition of chemotherapy, a significant increase in apoptosis was also observed for *HOXA13* depleted HCT116 cells treated with 5FU for 48 h or treated with OX for 48 h or 72 h (Figure 4.10). A reduction in apoptosis was observed in *HOXA13* depleted RKO1 cells prior to the addition of chemotherapy. This was also observed with the addition of 5FU and OX treatment (Figure 4.11), however this was not found to be significant. A significant increase in apoptosis was also observed in the PCa cell line (DU145) when *HOXA13* expression was depleted, and this was also witnessed when cells were treated with DOC (Figure 4.12). Together, these data further confirm that *HOXA13* depleted HCT116 cells exhibit sensitivity to chemotherapeutic drugs. DU145 cells exhibited an increase in apoptosis prior to chemotherapy treatment suggesting increased apoptosis may be a direct result of *HOXA13* depletion rather than treatment with chemotherapy.
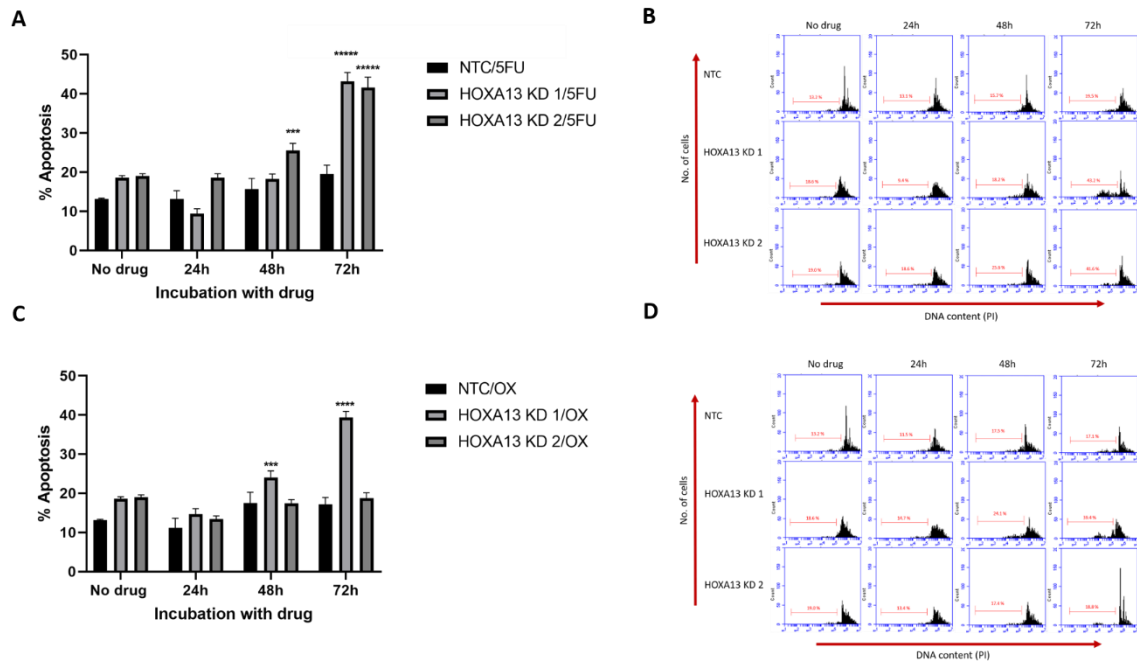
Figure 4.10 Sensitivity of siRNA mediated HOXA13 depleted HCT116 cells to chemotherapy.

HCT116 cells were transfected with HOXA13 targeting or NTC siRNA for 72 h and subsequently treated with (A) 10 μM 5FU or (C) 10 μM OX for DNA hypodiploidy analysis using a flow cytometer at 24 h, 48 h, 72 h after initial treatment. No drug controls were also included. Data are mean (± S.E.M) of 3 biological replicates (N=3). Two-way ANOVA with Dunnett's multiple comparisons test was used to quantify statistical significance (***P<0.001, ****P<0.0001). Representative flow cytometry plots of (B) 5FU and (D) OX treated cells, average Sub-G1 percentages are highlighted in red.

Figure 4.11 Sensitivity of siRNA mediated HOXA13 depleted RKO1 cells to chemotherapy.

RKO1 cells were transfected with HOXA13 targeting or NTC siRNA for 72 h and subsequently treated with (A) 10 μM 5FU or (C) 10 μM OX for DNA hypodiploidy analysis using a flow cytometer at 24 h, 48 h, 72 h after initial treatment. No drug controls were also included. Data are mean (± S.E.M) of 3 biological replicates (N=3). Two-way ANOVA with Dunnett's multiple comparisons test was used to quantify statistical significance (***P<0.001, ****P<0.0001). Representative flow cytometry plots of (B) 5FU and (D) OX treated cells, average Sub-G1 percentages are highlighted in red.
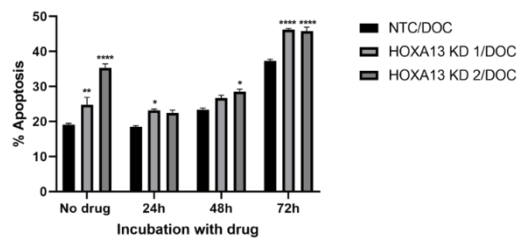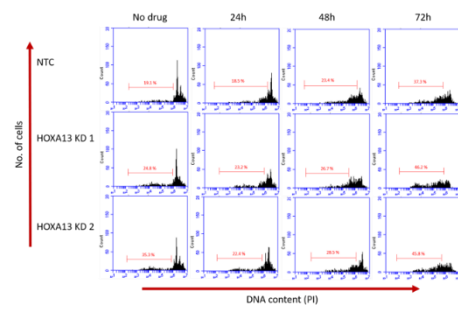
Figure 4.12 Sensitivity of siRNA mediated HOXA13 depleted DU145 cells to chemotherapy.

DU145 cells were transfected with HOXA13 targeting or NTC siRNA for 72 h and subsequently treated with (A) 1 µM DOC OX for DNA hypodiploidy analysis using a flow cytometer at 24 h, 48 h, 72 h after initial treatment. No drug controls were also included. Data are mean (± S.E.M) of 3 biological replicates (N=3). Two-way ANOVA with Dunnett's multiple comparisons test was used to quantify statistical significance (***P<0.001, ****P<0.0001). (B) Representative flow cytometry plots of DOC treated cells, average Sub-G1 percentages are highlighted in red.

4.4.3 Chemotherapeutic drugs do not induce arrest in cell cycle phases when *HOXA13* is depleted in CRC and PCa.

Cell cycle analysis of *HOXA13* depleted cancer cells treated with chemotherapeutic drugs was then investigated. HCT116, RKO1 or DU145 cells were transfected with *HOXA13* targeted or NTC siRNA for 72 h and subsequently treated with 10 µM 5FU, 10 µM OX or 1 µM DOC for a further 72 h. No drug controls were also included in this analysis. A flow cytometer was used to measure the percentage of cells in each stage of the cell cycle as outlined previously (4.3.5).

An increase in S and G1 phase and a decrease in G2/M phase was observed in *HOXA13* depleted HCT116 cells prior to the addition of chemotherapy treatment (Figure 4.13A). When treated with 5FU, *HOXA13* depleted HCT116 cells exhibited an increase in S phase, and a decrease in G2/M and G1 phase (Figure 4.13B). When treated with OX, HCT116 cells transfected with HOXA13 KD 1 siRNA did not exhibit any changes in the cell cycle (<1 %). However, when transfected with HOXA13 KD 2, an increase in S and a decrease in G2/M phase was observed (Figure 4.13C). However, these changes were not found to be statistically significant.

Prior to chemotherapy treatment, *HOXA13* depleted RKO1 cells displayed a decrease in S phase compared to NTC, as well as a decrease in G2/M observed in RKO1 cells transfected with HOXA13 KD 1. (Figure 4.14A). *HOXA13* depleted RKO1 cells exhibited a loss of cells in S and G2/M phase, and an increase in G1 phase when treated with 5FU (Figure 4.14B). When treated with OX, *HOXA13* depleted RKO1 cells

165

exhibited an increase in G1 phase and a decrease in G2/M phase (Figure 4.14C). Again, none of these changes were significant for *HOXA13* depleted RKO1 cells.

An increase in G2/M and a decrease in G1 phase was observed in *HOXA13* depleted DU145 cells that were not subjected to chemotherapy treatment. DU145 cells transfected with HOXA13 KD 1 exhibited an increase in S phase, however a reduction in S phase was observed with DU145 cells transfected with HOXA13 KD 2 (Figure 4.15A). When treated with DOC, *HOXA13* depleted DU145 cells exhibited an increase in G2/M, whereas a decrease in S phase was observed. The percentage of cells in G1 phase increased when DU145 cells were transfected with HOXA13 KD 1 and treated with DOC, whereas the opposite was observed for DU145 cells transfected with HOXA13 KD 2 and treated with DOC (Figure 4.15B). No changes in cell cycle stage of *HOXA13* depleted DU145 cells was found to be significant. Overall, no significant change in the percentage of cells in each stage of the cell cycle was observed for *HOXA13* depleted HCT116, RKO1 or DU145 cells exposed to chemotherapy.
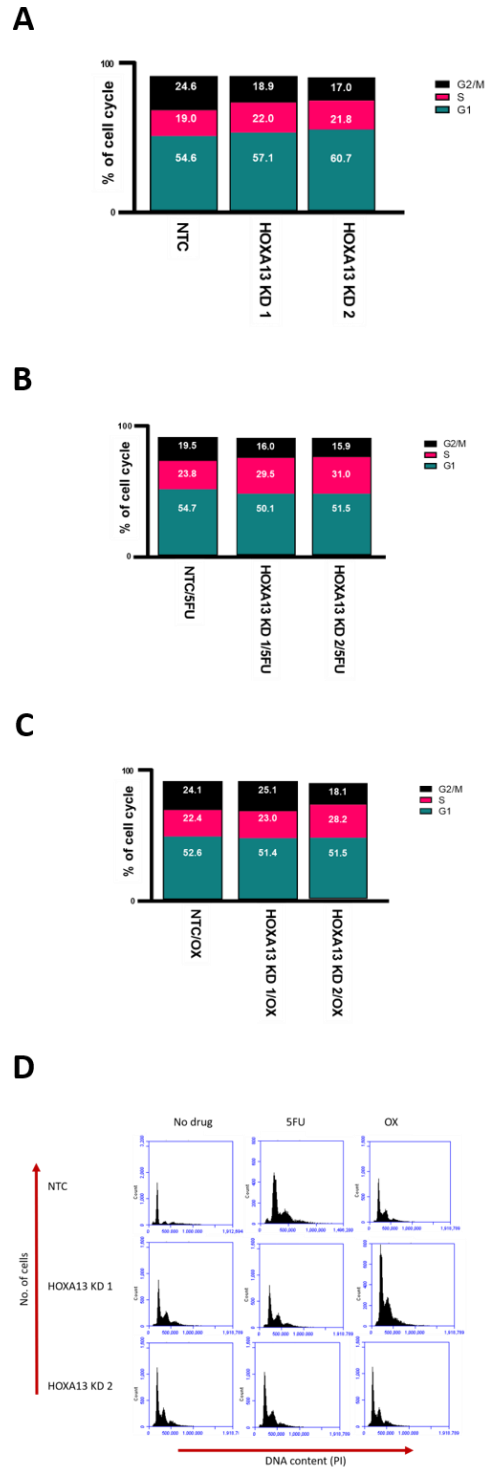
Figure 4.13 Cell cycle analysis of siRNA mediated HOXA13 depletion in HCT116 cells.

After 72 h of siRNA mediated *HOXA13* depletion, HCT116 cells were treated with (A) no drug (B) 10 μM 5FU or (C) 10 μM OX for 72 h and the percentage of cells in each stage of the cell cycle was analysed via flow cytometry. Data are mean (± S.E.M) of 3 biological replicates (N=3). Two-way ANOVA with Dunnett's multiple comparisons test was used to quantify statistical significance. (D) Representative flow cytometry plots of *HOXA13* depleted and NTC HCT116 cells with and without drug treatment.

167
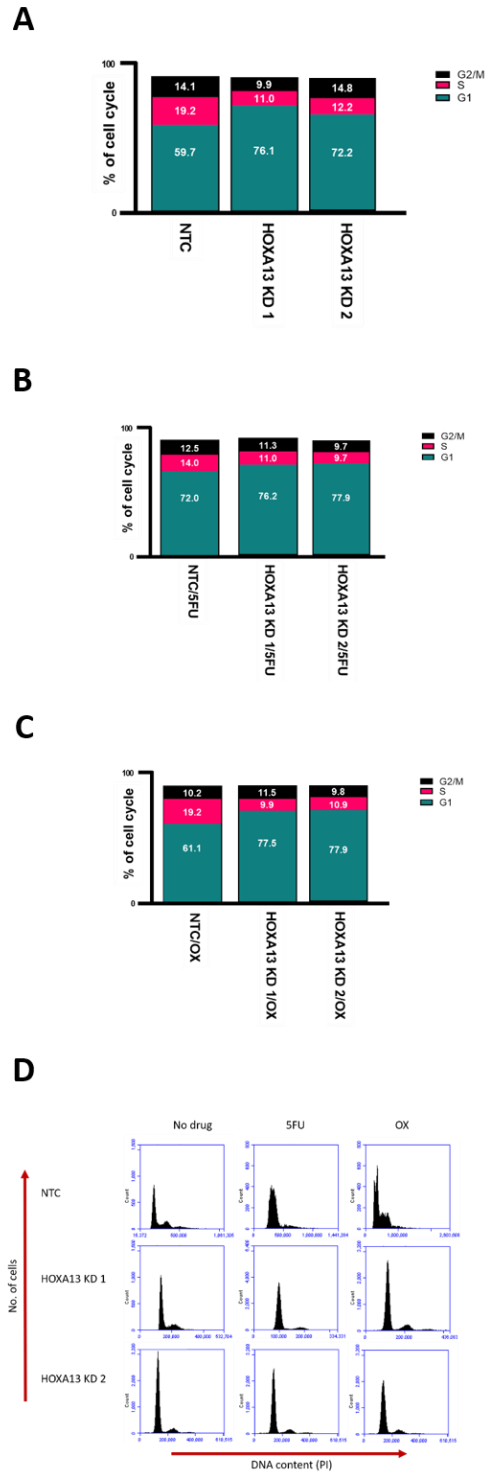
Figure 4.14 Cell cycle analysis of siRNA mediated HOXA13 depletion in RKO1 cells.

After 72 h of siRNA mediated *HOXA13* depletion, RKO1 cells were treated with (A) no drug (B) 10 µM 5FU or (C) 10 µM OX for 72 h and the percentage of cells in each stage of the cell cycle was analysed via flow cytometry. Data are mean (± S.E.M) of 3 biological replicates (N=3). Two-way ANOVA with Dunnett's multiple comparisons test was used to quantify statistical significance. (D) Representative flow cytometry plots of *HOXA13* depleted and NTC RKO1 cells with and without drug treatment.
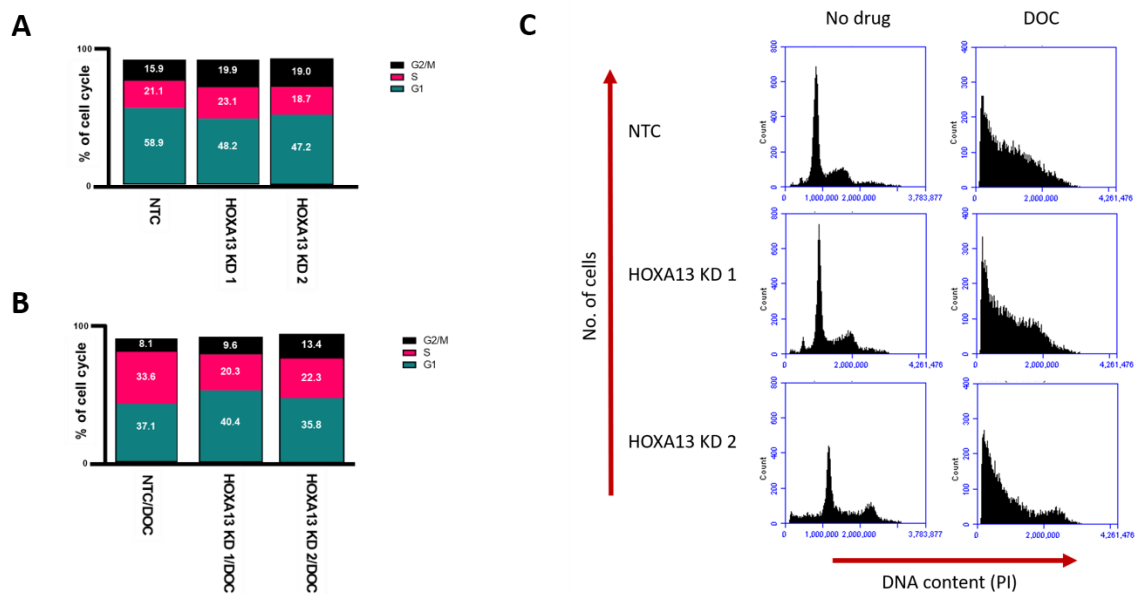
Figure 4.15 Cell cycle analysis of siRNA mediated HOXA13 depletion in DU145 cells.

After 72 h of siRNA mediated *HOXA13* depletion, cells were treated with (A) no drug or (B) 1 μM DOC for 72 h and the percentage of cells in each stage of the cell cycle was analysed via flow cytometry. Data are mean (± S.E.M) of 3 biological replicates (N=3). Two-way ANOVA with Dunnett's multiple comparisons test was used to quantify statistical significance. (C) Representative flow cytometry plots of *HOXA13* depleted and NTC HCT116 cells with and without drug treatment.

4.5 Discussion

In this chapter, the effect of *HOXA13* depletion on CRC and PCa cells was investigated. As mentioned previously, upregulation of *HOXA13* has be implicated in gastric (Chang *et al.*, 2016; Qin *et al.*, 2019), pancreatic (Li *et al.*, 2015), liver (Quagliata *et al.*, 2018) and prostate (Zhang *et al.*, 2016) cancer.

4.5.1 *HOXA13* depletion results in depletion of other *HOXA* genes in CRC.

Upon siRNA mediated *HOXA13* depletion, significant downregulation of *HOXA11* was observed in both CRC cell lines (HCT116, RKO1). In *HOXA13* depleted RKO1 cells, significant downregulation was also observed in all other *HOXA* genes tested (*HOXA9, HOXA1*) and the lncRNA *HOTTIP*. It has been previously described that multiple *HOX* genes can be aberrantly expressed at the same time in cancer (Bhatlekar, Fields and Boman, 2018; Tatangelo *et al.*, 2018). However, this is the first time a regulatory link between *HOXA13* and other *HOX* genes has been witnessed in CRC.

HOTTIP expression was reduced in *HOXA13* depleted RKO1 and DU145 cells. Other studies have shown that *HOTTIP* can contribute to the progression of cancer by regulating *HOXA13* (Li *et al.*, 2015; Zhang *et al.*, 2016); this study has shown that this may also work in the opposite fashion, where upon *HOXA13* depletion, *HOTTIP* expression is also reduced in RKO1 and DU145 cells. This could be a result of changes in occupancy of the WDR5/MLL protein complex that is known to regulate *HOXA* gene expression (Wang *et al.*, 2011; Pradeepa *et al.*, 2017).

4.5.2   *HOXA13* depletion has no effect on the migration and proliferation of CRC and PCa cell lines.

Previous literature has described *HOXA13* as promoting cell proliferation, migration and invasion in pancreatic (Li *et al.*, 2011), gastric (Chang *et al.*, 2016; Qin *et al.*, 2019), esophageal squamous cell (Shen and Chen, 2011), and prostate cancer (Zhang *et al.*, 2016; Dong *et al.*, 2017a). siRNA mediated *HOXA13* depletion had no significant effect on HCT116, RKO1 or DU145 motility and no significant difference was observed in *HOXA13* depleted HCT116 or DU145 cells; this opposes what has been previously reported in the literature, where *HOXA13* has been implicated in gastric cancer through promoting metastasis (Chang *et al.*, 2016). However, *HOXA13* depleted RKO1 cells exhibited a highly significant increase in proliferation compared to NTC. This may suggest a possible tumour suppressive role of *HOXA13* in this cell line. Other *HOX* genes have been described as having tumour suppressor-like properties in CRC, such as *HOXB13* (Xie *et al.*, 2019) and *HOXD8* (Mansour and Senga, 2017). However, further work will need to be carried out before confirming this in *HOXA13*.

No significant difference in apoptosis was observed in the CRC cell lines (HCT116, RKO1) when cells were depleted of *HOXA13.* In contrast, a significant increase in percentage apoptosis was observed for *HOXA13* depleted DU145 cells. This indicates that HOXA13 may inhibit apoptosis in PCa, supporting what has been observed in other studies (Dong *et al.*, 2017a). *HOX* genes have been found to interact with factors that promote cell cycle progression (Falaschi, Abdurashidova and Biamonti, 2010). Moreover, *HOXA13* has been shown to arrest G0/G1 phase by

activating the Wnt and TGF-β pathways when depleted in other tumours such as in glioma (Duan *et al.*, 2015). The Wnt pathway is a critical pathway that becomes hyperactivated and drives CRC progression (Schatoff, Leach and Dow, 2017) and is associated with late stage PCa (Yeh *et al.*, 2019). However, no involvement in cell cycle promotion in either CRC or PCa was observed for *HOXA13* in this study, contradicting what has previously been stated in the literature.

4.5.3   *HOXA13* has chemoresistant properties in CRC and PCa.

Chemoresistant properties of *HOXA13* has been described in cancers including esophageal squamous cell carcinoma (Shi *et al.*, 2018), gastric (Han *et al.*, 2018), and pancreatic (Li *et al.*, 2015). *HOXA13* has been described as contributing to 5FU resistance in gastric cancer, where affects the stomach and therefore is in close proximity to the colon (Han *et al.*, 2018). Here, *HOXA13* depleted HCT116 and RKO1 cells were more sensitive to both 5FU (0.1 µM) and OX (10 µM) treatment compared to NTC when testing dose response. Sensitivity to 10 µM DOC treatment was also observed in *HOXA13* depleted DU145 cells. These data therefore suggest *HOXA13* may also have a chemosensitive role in CRC and PCa. This is further aided by the significant increase in the percentage of cells undergoing apoptosis observed for *HOXA13* depleted HCT116 cells treated with 5FU for 48 h and OX for 48 and 72 h compared to NTC.

On the other hand, when treated with chemotherapeutic drugs, *HOXA13* depleted cells did not exhibit increased sensitivity. Discrepencies between each siRNA (HOXA13 KD 1 and HOXA13 KD 2) were observed across all cell lines, making it

difficult to draw conclusions. This highlights the importance of using a panel of siRNAs to knockdown target gene expression.

An interesting observation that has been made throughout this study is the difference between the CRC cell lines (HCT116 and RKO1). *HOXA13* depletion in RKO1 cells results in significant changes in cellular function when there are no changes observed in HCT116. Both cell lines are derived from similar stages of disease metastasis (Boyd *et al.*, 1988; Arango *et al.*, 2004) so it is not a result of differing disease stage. One explanation is the possibility of increased transfection efficiency of RKO1 cells – a greater *HOXA13* depletion could be causing the difference in results, rather than the difference in cell line. The addition of employing CRISPR-Cas9 to permanently delete *HOXA13* expression may provide further clarification to the role of *HOXA13* in HCT116, RKO1 and DU145.

4.6   Summary

In summary, *HOXA13* depletion resulted in depletion of other *HOXA* genes (HCT116, RKO1) and the lncRNA *HOTTIP* (RKO1, DU145), suggesting that *HOXA13* expression may influence the expression of other *HOXA* genes and *HOTTIP* in these cell lines. When exploring the functional role of *HOXA13*, no effect on cell migration or proliferation in HCT116 or DU145 cells was evident. The exception was RKO1 cells where *HOXA13* depletion resulted in an increase in cell motility and proliferation.

One observation from this study was the increased sensitivity of the cell lines to chemotherapy when *HOXA13* expression was depleted. This suggests a potential chemosensitive role of *HOXA13* in HCT116, RKO1 and DU145 cells. More work

should be carried out to confirm this role, particularly in CRC, as this has not yet been described in this cancer. If characterised further by other studies to have chemosensitive properties in CRC and PCa, *HOXA13* could be used as a prognostic biomarker to stratify patients who may or may not respond to treatment with these drugs, allowing alternative drugs or therapies to be investigated in order to achieve a more promising clinical result.

Limitations of this work include discrepancies between siRNAs targeting HOXA13. Including a larger panel of siRNAs would improve the quality of the data and ensure conclusions can be drawn confidently. Knock-down success was checked regularly but was not performed for every experiment; therefore, providing confirmation of siRNA knockdown (via qPCR/Sanger sequencing) for each of the cell assays would also add confidence to this data. Further optimisation of the chemotherapeutic drug assays (time points, concentrations, controls) would improve the significance of the data observed in this chapter, adding confidence to the suggestion of a potential chemosensitive role of *HOXA13* n CRC and PCa. As mentioned, producing a *HOXA13* stable KO cell line via CRISPR-Cas9 may provide further clarification to the role of *HOXA13* in HCT116, RKO1 and DU145.

5 Investigating the role of PSIP1 in the progression of colorectal cancer.

5.1 Introduction

PSIP1 (PC4 and SFRS1 Interacting Protein 1) or LEDGF (Lens epithelium-derived growth factor) is a chromatin binding protein (Singh *et al.*, 2017) involved in gene regulation. It encodes two isoforms: PSIP1/p52 and PSIP1/p75 that occur as a result of alternative splicing. These isoforms interact with the transcription factor PC4 (Positive Cofactor 4), where they act as transcriptional coactivators (Ge, Si and Roeder, 1998; Ge, Si and Wolffe, 1998). PSIP1 is an epigenetic reader of H3K36me2/me3 and preferentially binds to actively transcribed chromatin, promoting gene expression (Pradeepa *et al.*, 2012; El Ashkar *et al.*, 2017). It has been established in mouse models that Psip1 is involved in the transcriptional regulation of *Hox* genes (Pradeepa *et al.*, 2012, 2014). In humans, the PSIP1 gene is located on chromosome 9 (p22.3).

PSIP1 has been linked to multiple diseases; the most prominent being its role in promoting replication of the HIV-1 virus (Pradeepa *et al.*, 2012; Baid *et al.*, 2013). PSIP1 guides HIV-1 integration into host DNA through binding to integrase protein (IN) and tethering it to chromatin (Marshall et al. 2007). PSIP1 has also been implicated in cancer, including breast (Deepak K. Singh *et al.*, 2017), ovarian (French *et al.*, 2016) and prostate cancer (Basu et al. 2012; Ríos-Colón et al. 2017). PSIP1 has been well documented in leukaemia as a result of interacting with Mixed Lineage Leukaemia 1 (MLL1)/MEN1 (MENIN) to form an oncogenic complex that binds to target genes (Cermakova *et al.*, 2016; El Ashkar *et al.*, 2018). PSIP1 also interacts with the MLL1 complex to regulate the expression of *Hoxa distal transcript antisense RNA (Hottip)*

(Pradeepa *et al.*, 2017), as described in Chapter 3. However, there is a lack of information on whether PSIP1 has a role in promoting colorectal cancer (CRC).

This chapter will outline the role of PSIP1 in the progression of CRC and investigate whether PSIP1 has a role in protecting cancer cell death when put under stress from treatment with chemotherapeutic drugs.

5.2   The role of PSIP1 in cancer

To investigate the role of PSIP1 in cancer, and whether this protein is a valid target to investigate as a therapeutic option, online databases (kmplot.com) (Györffy *et al.*, 2010) were interrogated and Kaplan-Meier (K-M) survival plots generated to examine if PSIP1 expression levels correlate with patient survival in rectal adenocarcinoma (Figure 5.1A). This carcinoma was chosen as it can be classed as a type of CRC and can give a good indication if PSIP1 levels correlate with patient survival in other colorectal cancers. K-M plots of lung adenocarcinoma and cervical squamous cell carcinoma were also generated as a comparison to CRC. High levels of PSIP1 were correlated with lower survival in rectal adenocarcinoma (Figure 5.1A), however this was not found to be significant (P=0.06). On the other hand, lower PSIP1 expression is beneficial to survival in both lung adenocarcinoma (Figure 5.1B) and cervical squamous cell carcinoma (Figure 5.1C). This was found to have significant correlation (P=0.048) in lung carcinoma and highly significant correlation (P=0.0089) in cervical squamous cell carcinoma. Analysis of the literature and available online data such as in Figure 5.1, confirmed that there is an interesting case for investigating the role of PSIP1 in CRC.
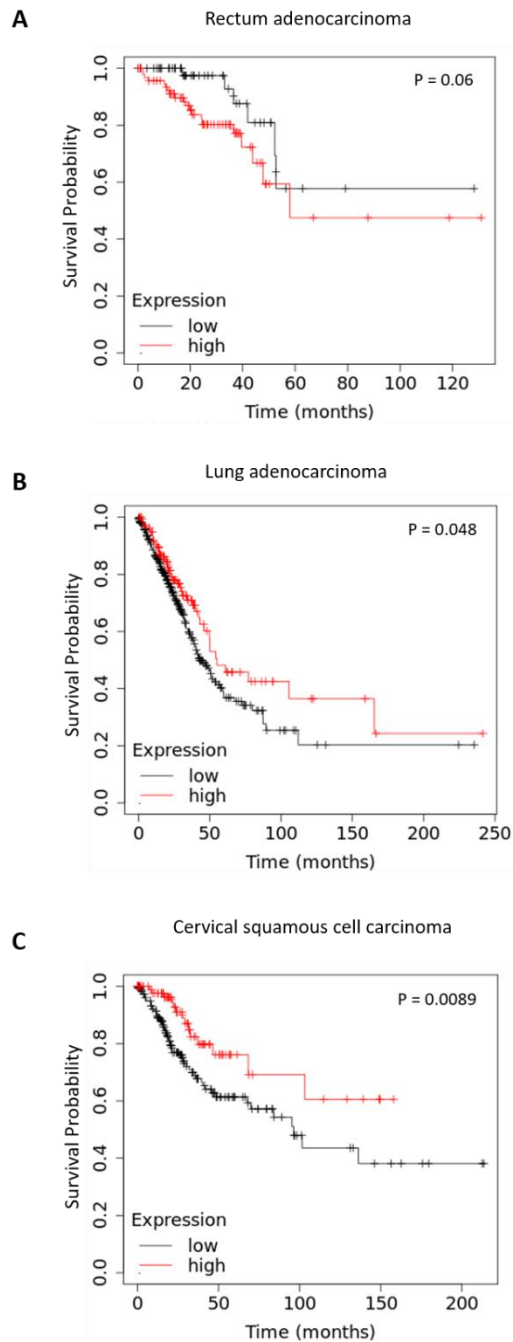
Figure 5.1 Kaplan-Meier survival plots of PSIP1 expression levels in cancer

Kaplan-Meier survival plots generated by a meta-analysis of RNA-seq data using kmplot online software (kmplot.com) to determine if PSIP1 is correlated with increased or decreased survival rates in cancer. The probability of survival (y-axis) is plotted against the time (months) a patient is estimated to survive the disease (x-axis). Black lines indicate low PSIP1 expression and red lines indicate high PSIP1 expression, N=number of patients in each dataset. (A) Rectum adenocarcinoma, P=0.06, N=165. (B) Lung adenocarcinoma, P=0.048, N=513. (C) Cervical squamous cell carcinoma, P=0.0089, N=304.

5.3   Validating siRNA mediated PSIP1 depletion and stable CRISPR-Cas9 PSIP1 knockout colorectal cancer cell lines.

5.3.1   siRNA mediated depletion of PSIP1.

In order to determine the role of PSIP1 in CRC, siRNAs were employed to knockdown (KD) PSIP1 levels in CRC cells. Two siRNAs were used to deplete PSIP1 and all experiments were carried out with non-targeting (NTC) siRNA controls to reduce false-positive results or any changes occurring due to off-target effects. siRNA mediated PSIP1 depletion was carried out in HCT116 CRC cells, a cell line derived from a human colonic carcinoma (Brattain *et al.*, 1981).

To confirm successful depletion of PSIP1 in HCT116, cells were seeded in 6-well plates and transfected with either PSIP1 targeting or NTC siRNA. After 72 h, cells were harvested, and the protein lysate was extracted. A protein quantification assay (BioRad DC assay) was used to quantify each protein sample prior to SDS-PAGE. Immunoblotting was performed using antibodies specific for PSIP1 or Proliferating cell nuclear antigen (PCNA) (housekeeping control protein). WT HCT116 total protein lysate was also used as an additional control.

PSIP1 depletion was successful at the protein level when transfected with both siRNAs (PSIP KD 1 and PSIP KD 2), compared to the controls (Figure 5.2). Densitometry analysis (Schindelin *et al.*, 2012) was used to determine the percentage knockdown of PSIP1 protein compared to non-transfected control (HCT116 WT). HCT116 cells transfected with PSIP KD 1 showed an 80 % depletion in PSIP1 protein levels. PSIP KD

2 siRNA was less efficient (36 % depletion) compared to HCT116 WT control. Non-targeting controls (NTC1 and NTC2) were also compared to HCT116 WT control. NTC1 showed some reduction in PSIP1 expression compared to HCT116 WT (20 %) indicating some loss of PSIP1 as a result of this transfection. However, when compared to HCT116 WT, NTC2 showed an increase in protein expression (49 % increase). Although care was taken to load equal protein concentrations, discrepancies in what was loaded could account for this increase in expression compared to WT. NTC1 and 2 will be averaged for experiments going forward to take in to account this fluctuation in protein expression between the two controls. This confirms successful siRNA mediated depletion of PSIP1 in HCT116 cells. This depletion was checked regularly for future siRNA knockdown experiments when investigating the functional role of PSIP1 in HCT116 cells.
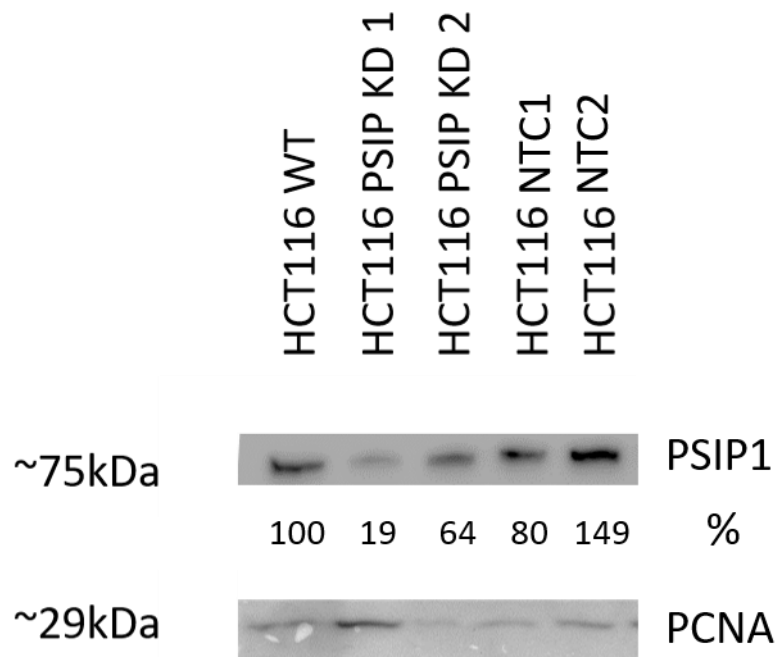
Figure 5.2 HCT116 siRNA mediated PSIP1 depletion validation via Western blot analysis.

HCT116 cells were seeded in 6-well plates and transfected with PSIP1 targeting (PSIP KD 1, PSIP KD 2) or NTC (NTC1, NTC2) siRNA. Protein lysate was extracted 72 h after transfection and expression levels were analysed via western blot. A total HCT116 protein lysate control was also included (HCT116 WT) and treated as 100% protein expression when calculating densitometry values. Protein expression was normalised to that of PCNA (29kDa) and all analysis was carried out using ImageJ Fiji.

After validation of siRNA mediated PSIP1 depletion in HCT116 cells, changes in gene expression levels of the lncRNA *HOTTIP* and nearby *HOXA* genes, as a result of this depletion, were investigated. It has been previously shown (Pradeepa *et al.*, 2017) that Psip1 regulates the expression of *Hottip* in mouse models and in turn, the expression of *HOXA13*, a *HOXA* gene that is located in close proximity to *HOTTIP* (Chapter 3 & 4). The expression levels of these target genes were measured to explore if this same regulation pattern is followed in CRC. Cells were therefore harvested 72 h after siRNA transfection, RNA was extracted, and cDNA synthesised subsequently. Target gene expression (*HOTTIP, HOXA13, HOXA1*) was quantified using qPCR and data normalised to the ribosomal protein gene *L19*.

Loss of *HOXA13* expression was observed in PSIP1 depleted samples compared to NTC (Figure 5.3). This was significant for cells transfected with PSIP KD 2. *HOTTIP* and *HOXA1* expression were also reduced as a result of PSIP1 depletion, however this was not found to be significant. This suggests that PSIP1 has a role in regulating *HOXA13* expression in HCT116, following the regulation pattern seen in other studies (Pradeepa *et al.*, 2017).
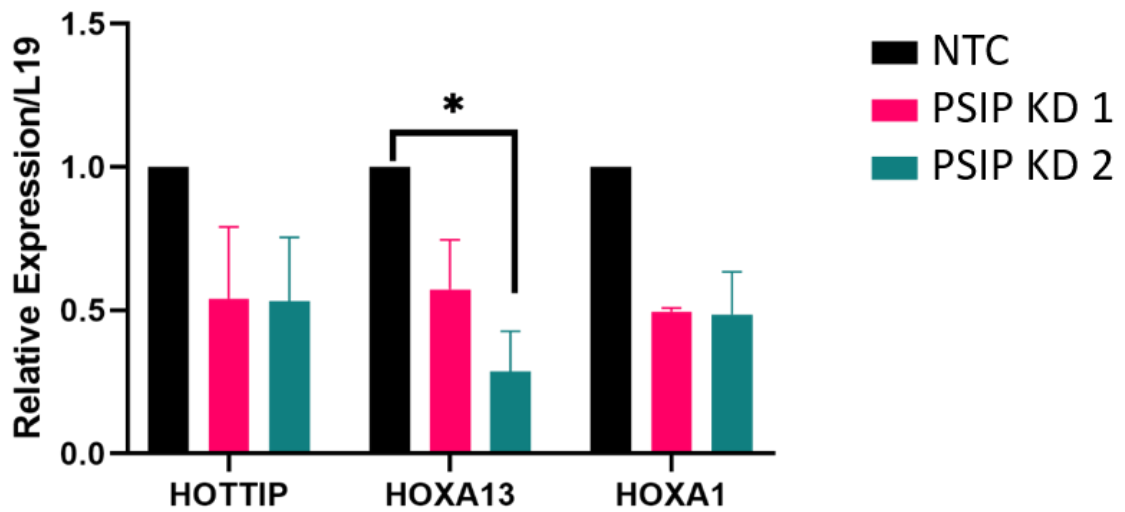
Figure 5.3 PSIP1 depletion results in reduction of HOTTIP and HOXA genes.

RNA was extracted from PSIP1 targeted (PSIP KD 1, PSIP KD 2), and NTC siRNA transfected HCT116 cells and cDNA was synthesized prior to qPCR analysis. Gene expression levels of target genes (HOTTIP, HOXA13, HOXA1) were quantified and compared to control. Data are mean (± S.E.M) expression of 3 biological replicates (N=3), analysed by qPCR and normalised to L19. Two-way ANOVA with Dunnett's multiple comparison test was used to quantify the statistical significance. (*P<0.05).

5.3.2 Creating stable PSIP1 knock out lines using CRISPR-Cas9.

To confirm the siRNA KD results, stable CRISPR-Cas9 PSIP1 knockout (KO) cell lines were created - again, the CRC HCT116 cell line was used. A guide RNA (gRNA) was designed to interrupt exon 6 of the PSIP1 protein (Figure 5.4), resulting in a frameshift mutation which prevents any functional PSIP1 protein from being synthesised.

After CRISPR-Cas9 selection, cells were harvested, and protein lysate was extracted. A screen was performed to identify WT (empty plasmid backbone) and PSIP1 KO clones. A protein quantification assay (BioRad DC assay) was used to quantify each protein sample prior to SDS-PAGE. Immunoblotting was performed using antibodies specific for PSIP1 or PCNA (housekeeping control protein). A total of 48 clones were analysed using western blotting with five samples (1 x WT and 4 x PSIP1 KO) being sent for Sanger sequencing to validate the desired frameshift mutation. One WT cell line and one PSIP1 KO HCT116 cell line were selected (Figure 5.5) for further experiments. Densitometry analysis was carried out on the selected WT and PSIP1 KO cell lines using ImageJ Fiji (Schindelin *et al.*, 2012); it was calculated that the PSIP1 KO cell line had a 98.3 % reduction in PSIP1 expression compared to WT control. Therefore, a PSIP1 knock-out HCT116 cell line was successfully generated.

Together siRNA mediated depletion and CRISPR-Cas9 PSIP1 KO cell lines will be used to explore the role of PSIP1 in CRC, whether it influences the progression of the disease, and investigate the response of PSIP1 to chemotherapeutic drugs.
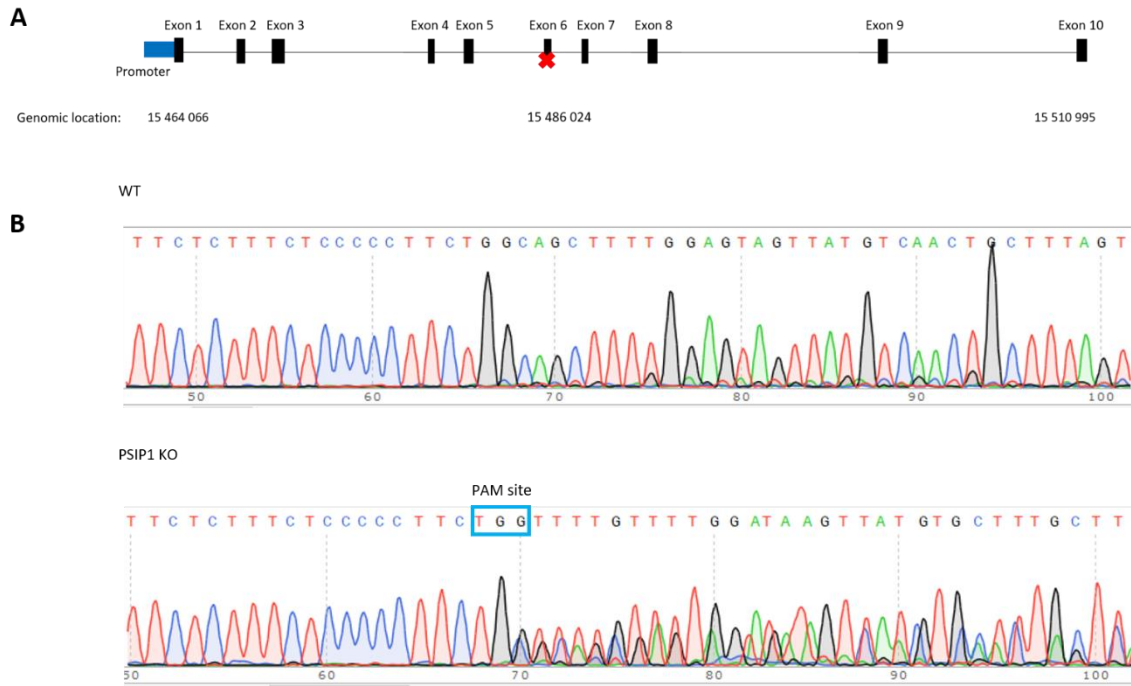
Figure 5.4 Guide RNA targeting of PSIP1 protein in humans and Sanger sequencing validation

(A) Schematic of the human PSIP1 protein located on chr6.22.3. The red cross marks the location of the gRNA used to target PSIP1 and create a frameshift mutation at exon 6 (21 958 bp from TSS) resulting in prevention of a functional PSIP1 protein being synthesized. (B) Genomic DNA from WT and positive PSIP1 KO HCT116 clones were extracted and subsequently sent for Sanger sequencing. Representative chromatograms (Snapgene) where the frameshift can be identified after the PAM site (blue box) indicating a change in KO DNA sequence from WT.

184
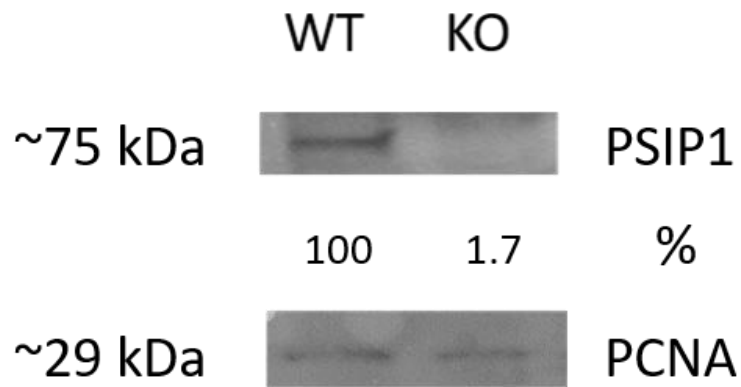
Figure 5.5 CRISPR-Cas9 mediated PSIP1 knockout validation via Western blot analysis

Protein lysate was extracted from CRISPR-Cas9 mediated PSIP1 KO and WT clones confirmed through Sanger sequencing. Protein expression levels of PSIP1 KO and WT control HCT116 cells were analysed via western blot. WT control mock transfected with empty CRISPR plasmid backbone (PX459) was treated as 100% protein expression when calculating densitometry values. Protein expression was normalised to that of PCNA (29kDa) and all analysis was carried out using ImageJ Fiji.

5.4 Movement and migration of cancer cells is reduced when PSIP1 expression is depleted in HCT116.

Cancer cell movement and migration is key to the progression of the disease (Leong, Chambers and Lewis, 2012). To investigate whether PSIP1 influences progressive cancer drivers such as these, a variety of assays were carried out to test the hypothesis that movement and migration of cancer cells is reduced when PSIP1 expression is depleted in CRC.

5.4.1 The effect of PSIP depletion on cell motility in colorectal cancer.

Single cell tracking analysis was used to analyse average cell speeds of PSIP1 depleted and control HCT116 cells. This will provide an indication as to whether PSIP1 is involved in CRC cell motility.

For this work, CYTO-ID dye (Enzo life sciences) was used to label cells, allowing fluorescence detection. Dyed cells were seeded sparsely in 96-well plates to enable individual analysis of a single cell to be possible. A Nikon Widefield microscope was used to capture images of cells every 20 minutes over a 24 h period. Cells were placed in a humidified CO_2 chamber to retain their optimum culturing conditions during this time. These images were stitched together and average cell speeds calculated using the Trackmate plugin on Image J Fiji (Tinevez *et al.*, 2017).

Firstly, the average speed of siRNA mediated PSIP1 depleted and NTC HCT116 cells were tested. An increase in average cell speed for cells transfected with siRNA PSIP KD 1 was observed, whereas the opposite was seen for cells transfected with siRNA

PSIP KD 2, with a decrease in average cell speed compared to control (Figure 5.6). This was not found to be significant in either case. CRISPR-Cas9 mediated stable PSIP1 KO cells exhibited reduced average cell speed compared to WT (Figure 5.7). Again, this was not found to be significant. This demonstrates that PSIP1 does not contribute to cell motility in HCT116 cells.
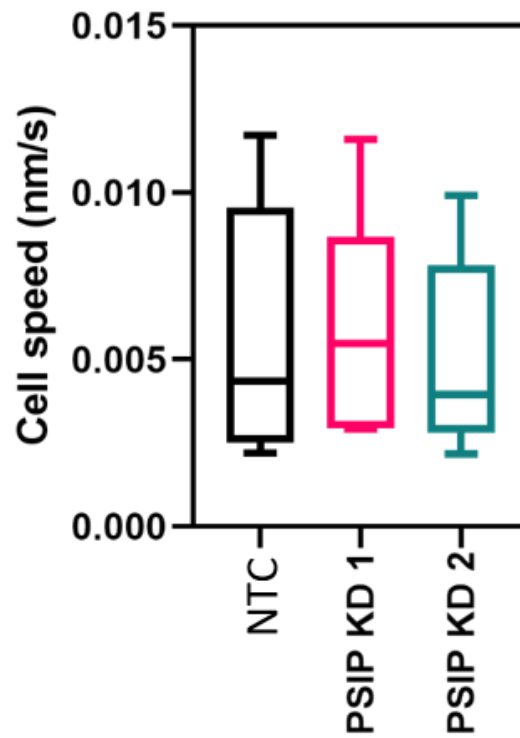
Figure 5.6 Single cell tracking analysis of siRNA mediated PSIP1 depleted HCT116 cells

Single cell tracking was used to measure the average speed of siRNA mediated PSIP1 depleted and NTC HCT116 cells. After sparsely being seeded in 96-well plates, cells were placed in a humidified CO_2 chamber attached to a Widefield microscope. Images were taken every 20 min for 24h and average speeds were calculated using ImageJ Fiji. Data are mean (± S.E.M) of 3 biological replicates (N=3). Kruskal-Wallis test with Dunn's post-hoc test was used to quantify the statistical significance (PSIP KD 1 P>0.9, PSIP KD 2 P>0.9).
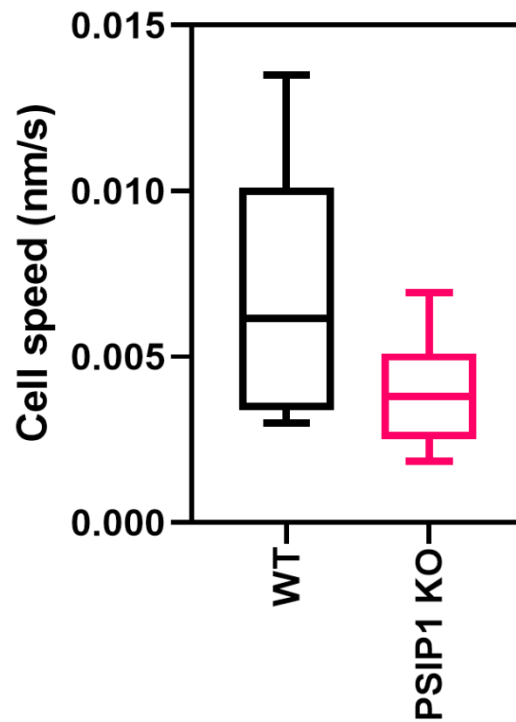
Figure 5.7 Single cell tracking of CRISPR-Cas9 PSIP1 KO cells reduces average cell speed

Single cell tracking was used to measure the average speed of PSIP1 KO and WT HCT116 cells. After sparsely being seeded in 96-well plates cells were placed in a humidified CO_2 chamber attached to a Widefield microscope. Images were taken every 20 min for 24h and average speeds were calculated using ImageJ Fiji. Data are mean (± S.E.M) of 3 biological replicates (N=3). Mann Whitney test was used to test statistical significance (P=0.16).

5.4.2 PSIP1 depletion has no significant effect on migration rate of HCT116 cells.

Wound assays were implemented to measure the migration rates of PSIP1 depleted and control CRC cells. To do this, cells were seeded in 6-well plates so they reached 100 % confluency within 24 h. A 'wound' was created in each well by scratching a gap in the confluent cells with a P20 pipette tip. A Nikon Widefield microscope was used to take pictures of each well every 20 minutes over a 24 h period. Cells were placed in a humidified CO_2 chamber to retain their optimum culturing conditions during this time. The percentage of cell coverage at each time point was analysed using ImageJ (Schindelin *et al.*, 2012).

A reduction in cell migration was observed for PSIP1 depleted cells compared to NTC, however this was not a significant difference (Figure 5.8). Similarly, CRISPR-Cas9 mediated stable PSIP1 KO cells also exhibited a slower migration rate compared to WT cells, but this was not significant (Figure 5.9). These findings show that PSIP1 has no significant effect on the migration rate of CRC.
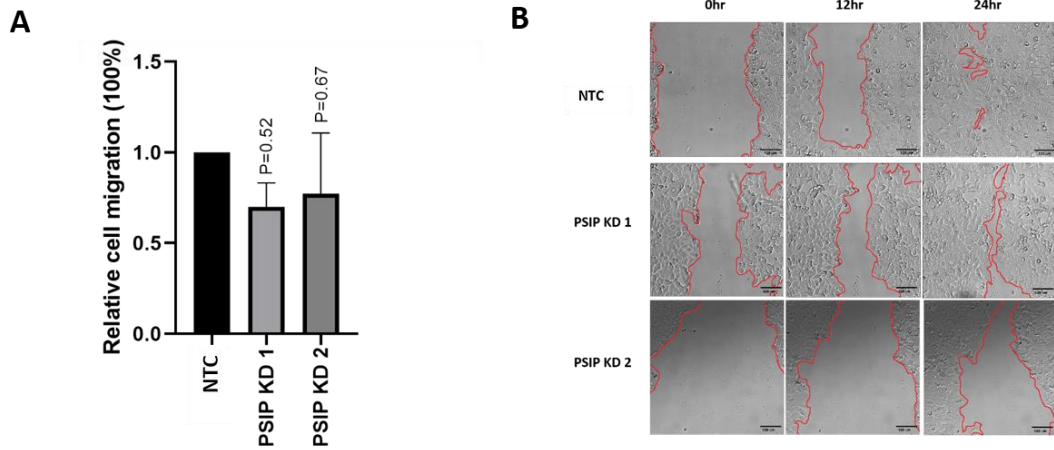
Figure 5.8 siRNA mediated PSIP1 depletion reduces migration rate of CRC cells

Wound healing assays were carried out to measure the migration rates of siRNA mediated PSIP1 depletion and NTC HCT116 cells. (A) 'Wounds' were tracked over 24 h and PSIP1 depleted cell migration was calculated relative to NTC. Data are mean (± S.E.M) of 3 biological replicates (N=3). One-way ANOVA with Dunnett's multiple comparison was used to test statistical significance, (PSIP KD 1 P=0.53, PSIP KD 2 P=0.67). (B) Representative images of PSIP1 KD and NTC 'wounds' at 0 h, 12 h, and 22 h after initial scratching of confluent cells taken using a Nikon Widefield microscope and analysed with Image J Fiji.
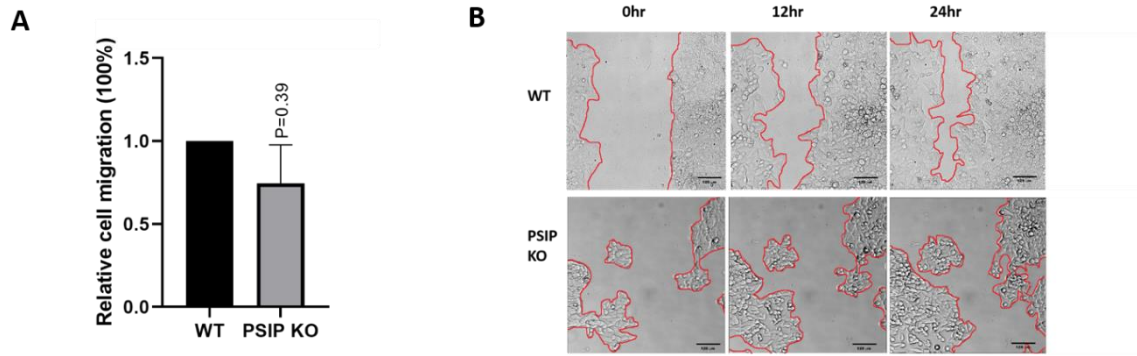
Figure 5.9 CRISPR-Cas9 mediated PSIP1 knock out reduces migration rate of CRC cells

Wound healing assays were carried out to measure the migration rates of PSIP1 KO and WT HCT116 cells. (A) 'Wounds' were tracked over 24h and PSIP1 KO cell migration was calculated relative to WT. Data are mean (± S.E.M) of 3 biological replicates (N=3). Unpaired t-test with Welch's correction was used to quantify statistical significance, P=0.39. (B) Representative images of WT and PSIP KO 'wounds' at 0h, 12h, and 22h after initial scratching of confluent cells taken using a Nikon Widefield microscope and analysed using ImageJ FIji.

5.4.3   PSIP1 KO significantly slows colony growth in HCT116 cells.

Colony formation assays were used to further investigate the effect of PSIP1 on HCT116 cell growth; this is a measurement of cell viability and the ability of cells in a population to continually divide (Puck and Marcus, 1956; Rafehi *et al.*, 2011) . PSIP1 KO and WT cells were seeded sparsely into 12-well plates and grown for ~10 days to allow single cells to form colonies. Plates were fixed and stained with crystal violet for analysis. The number of colonies formed was quantified using ImageJ FIji software (Schindelin *et al.*, 2012). PSIP1 KO results in highly significant loss of colony formation ability compared to WT, P<0.001 (Figure 5.10), suggesting that PSIP1 has roles in maintaining HCT116 cell viability and proliferation.

5.4.4   PSIP1 depletion has no significant effect on the growth rate of HCT116 cells

After PSIP1 KO cells exhibited a significant reduction in the ability of HCT116 cells to form colonies, the effect of PSIP1 deletion on growth rates was tested. Cells were seeded in 96-well plates and grown over a time series of up to 8 days. After each time point, cells were fixed and stained with crystal violet prior to colorimetric measurement (OD 490 nm), growth rates were calculated relative to day 0 (no growth). Lines of best fit to measure growth rates for both CRISPR-Cas9 mediated stable PSIP1 KO and WT HCT116 cells showed no significant difference in growth rate (Figure 5.11). Thus, it can be concluded that PSIP1 does not have a role in promoting HCT116 cell growth.
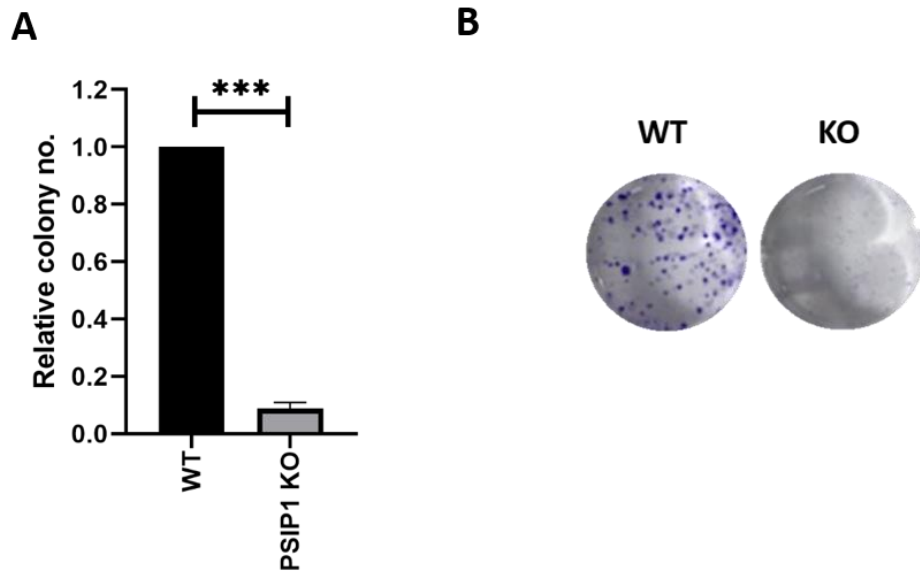
Figure 5.10 Significant loss of colony formation ability in CRISPR-Cas9 mediated PSIP1 KO cells

(A) Relative colony number of CRISPR-Cas9 mediated PSIP1 KO compared to WT HCT116 cells. Data are mean (± S.E.M) of 3 biological replicates (N=3) relative to control WT cells. Unpaired t-test with Welch's correction was used to quantify the statistical significance (*** P<0.001). (B) Representative wells of colonies stained with crystal violet after fixation with 4% PFA.
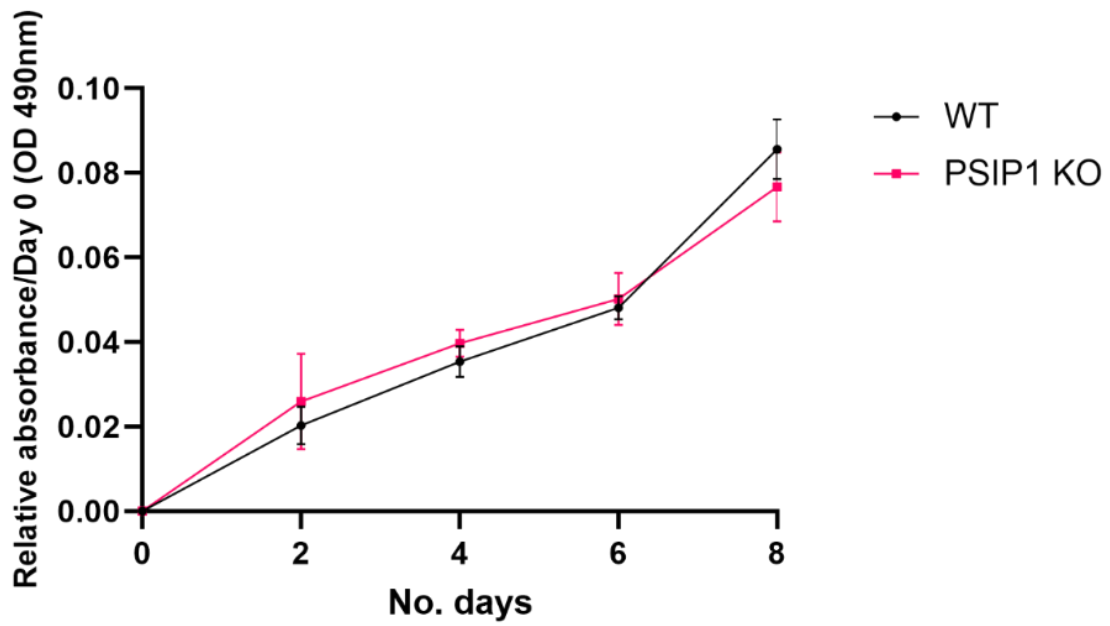
Figure 5.11 CRISPR-Cas9 mediated PSIP1 knockout cell growth assay

PSIP1 KO and WT HCT116 cells were seeded in 96-well plates and growth rates were measured over an 8-day time series. After each time point, cells were fixed and stained prior to colorimetric analysis (OD 490 nm). Growth rates are relative to day 0 (no growth). Data are mean (± S.E.M) of 3 biological replicates (N=3). Two-way ANOVA with Sidak's multiple comparisons test was used to quantify statistical significance (P>0.8).

5.4.5 PSIP1 depletion has no significant effect on apoptosis in HCT116 cells.

Flow cytometry was used to assess whether PSIP1 depletion leads to an increase in apoptosis of HCT116 cells, again siRNAs were used to knockdown PSIP1 expression. 72 h after transfection, all cells and media were collected and pelleted. Pelleted cells were re-suspended in Nicoletti buffer (Riccardi and Nicoletti, 2006) containing propidium iodide (PI) that is used to stain apoptotic cells. During the process of apoptosis DNA becomes fragmented. As a result, rates of apoptosis can be measured by the identification of hypodiploid cells using a DNA stain such as PI. Cellular PI intensity was quantified using flow cytometry and rates of apoptosis were compared to NTC siRNA controls.

An increase in the percentage of cells undergoing apoptosis was observed for HCT116 cells transfected with PSIP KD 1 compared to NTC, however this was non-significant. No change in percentage apoptosis was observed for HCT116 cells transfected with PSIP KD 2. Overall, PSIP1 depletion does not result in increased apoptosis in HCT116 cells (Figure 5.12).
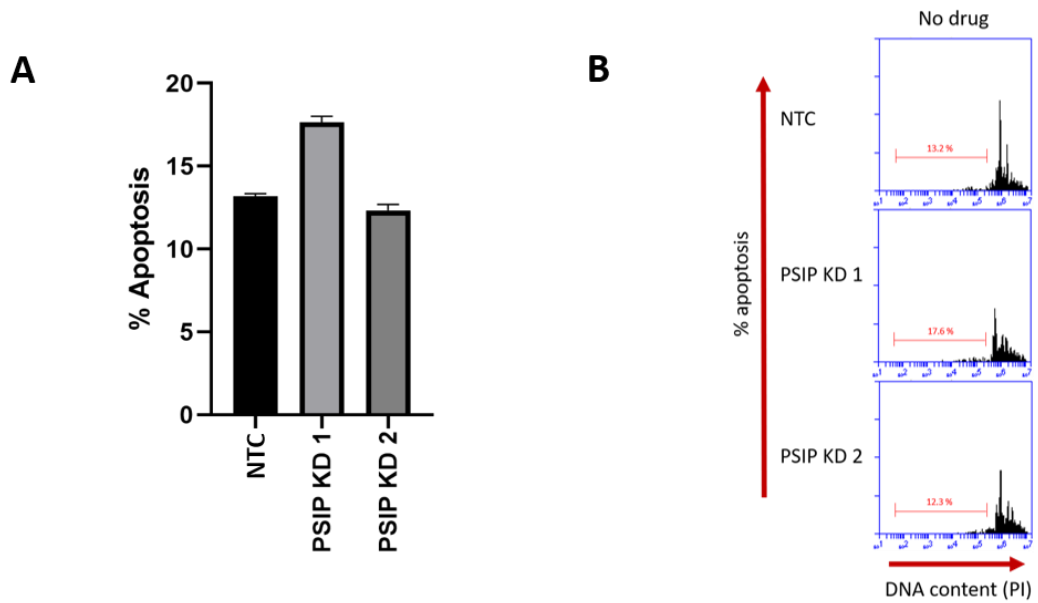
Figure 5.12 Apoptosis of siRNA mediated PSIP1 depletion in HCT116 cells

After transfection for 72 h with siRNA targeting PSIP1 or NTC, all cells and media were collected and pelleted. Pellets were re-suspended in Nicoletti buffer for DNA hypodiploidy analysis using a flow cytometer. Data are mean (± S.E.M) of 3 biological replicates (N=3). Two-way ANOVA with Dunnett's multiple comparisons test was used to quantify statistical significance (P>0.2). (A) Percentage apoptosis of siRNA mediated PSIP1 and NTC HCT116 cells. (B) Representative flow cytometry plots of HCT116 cells transfected with PSIP1 targeted and NTC siRNA, average Sub-G1 percentages are highlighted in red.

5.4.6 PSIP1 does not drive cell cycle progression in HCT116 cells.

PSIP1 has been described as having roles in the cell cycle, particularly in S and G2 phase (Daugaard *et al.*, 2012). Flow cytometry was used to investigate if this is also seen in CRC. Cells were transfected with PSIP1 KD or NTC siRNA for 72 h, after which flow cytometry was used to measure the percentage of cells in each stage of the cell cycle (G1 vs S vs G2/M). The percentage of cells in each phase of the cell cycle was analysed and PSIP1 depleted cells were compared to NTC.

PSIP1 depletion resulted in an increase in the percentage of cells in both S phase and G1 phase compared to NTC; a decrease in G2/M phase was also observed (Figure 5.13). This replicates what has been seen in other studies (Daugaard *et al.*, 2012), however the shifts in percentage of cells to any cell cycle stage were not significant for this experiment.
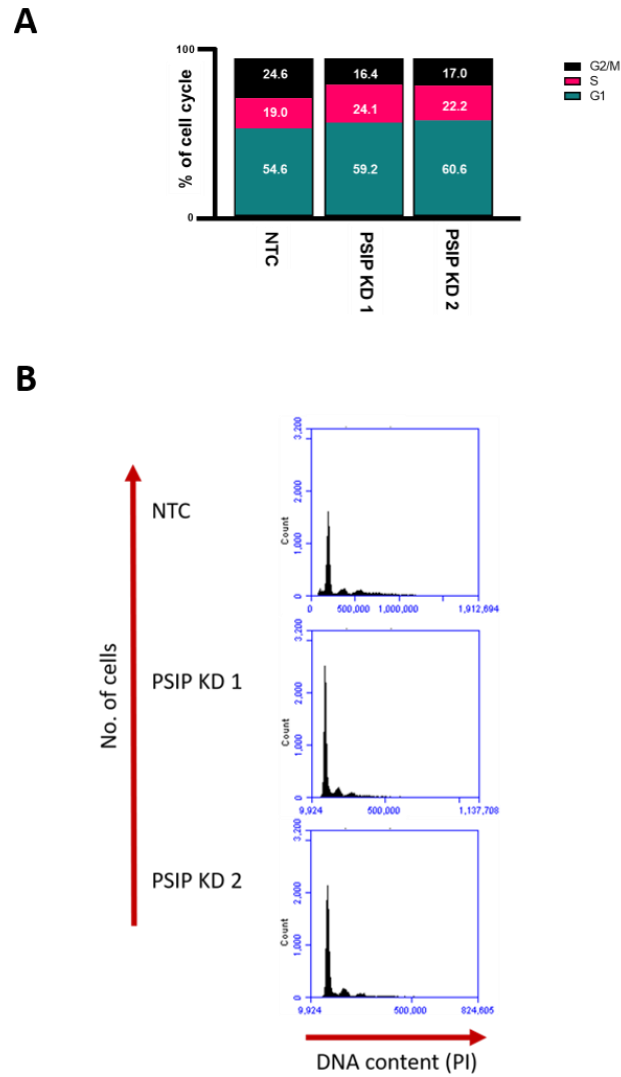
Figure 5.13 Cell cycle analysis of siRNA mediated PSIP1 depletion in HCT116 cells

(A) Cell cycle analysis of siRNA mediated PSIP1 depleted and NTC HCT116 cells. Data are mean (± S.E.M) of 3 biological replicates (N=3). Two-way ANOVA with Dunnett's multiple comparisons test was used to quantify statistical significance (P>0.98). (B) Representative flow cytometry plots of PSIP1 depleted and NTC HCT116 cells.

5.5 PSIP1 expression protects colorectal cancer cells against chemotherapeutic drugs.

As described previously, studies have suggested that the presence of PSIP1 can promote cancer cell survival, particularly in response to cell stress, such as treatment with chemotherapy (Basu et al. 2012). Two commonly used colorectal cancer chemotherapeutic drugs 5-Fluorouracil (5FU) (Carethers *et al.*, 2004) and Oxaliplatin (OX) (Comella *et al.*, 2009), were selected to investigate whether PSIP1 expression protects CRC cells against chemotherapy toxicity.

5.5.1 Reduction of PSIP1 expression results in sensitivity of cells towards chemotherapeutic drugs in HCT116.

Initially, the dose response of PSIP1 depleted HCT116 cells to chemotherapeutic drugs was tested in order to investigate whether PSIP1 depletion increases sensitivity of the cells to chemotherapy, indicating chemoresistant properties of PSIP1. Cells were seeded in 96-well plates and treated with a dose range of 5FU and OX for 72 h prior to being fixed and stained with crystal violet for colorimetric measurement (OD 490 nm). The optical density was calculated relative to no drug treatment (0 µM). At each maximum dose (100 µM of 5FU and 1000 µM of OX, Figure 5.13 A and B), all manipulations (siRNA NTC and KD) had equal optical density readings indicating the concentration of drug is lethal to all cells regardless of PSIP1 expression level. When transfected with siRNA KD 1, cells treated with 1 µM 5FU exhibited significantly more sensitivity to 5FU treatment. Cells transfected with siRNA KD 2 and treated with 5FU also exhibited increased sensitivity, however this was not significant (Figure 5.13A).

When treated with 10 µM OX, siRNA PSIP KD 1 transfected cells exhibited a significant increase in sensitivity to the drug. SiRNA PSIP KD 2 transfected cells exhibited sensitivity to OX at the10 µM and 100 µM doses (Figure 5.14B), however this was not found to be significant in either case. The increased sensitivity of cells transfected with PSIP KD 1 to both 5FU and OX reflects the PSIP1 expression levels witnessed in Figure 5.2, where siRNA PSIP KD 1 cells had a greater percentage of depletion than siRNA PSIP KD 2 cells.

siRNA knockdown demonstrated that PSIP1 plays a role in chemosensitivity in CRC. Therefore, the experiment was repeated with the CRISPR-Cas9 mediated stable PSIP1 KO and WT HCT116 cell lines. When treated with 5FU, PSIP1 KO cells exhibited more sensitivity to the drug compared to WT; this was significant when cells were treated with 1 µM 5FU (Figure 5.15A). When treated with 10 µM OX (Figure 5.15B), a significant increase in cell death was also observed. An increase in cell death was observed for PSIP1 KO cells treated with 100 µM OX, however this was not a significant effect. PSIP1 KO cells are more sensitive to treatment with 5FU out of the two drugs tested.

Overall, HCT116 cells with depleted levels of PSIP1 are more sensitive to chemotherapy treatment than control cells. This indicates PSIP1 may have a role in protecting CRC cells against chemotherapy as when PSIP1 expression is reduced, cell survival is also reduced. This is in agreement with what has been described in other cancer types including prostate (Ríos-Colón *et al.*, 2017) and ovarian (French *et al.*, 2016).
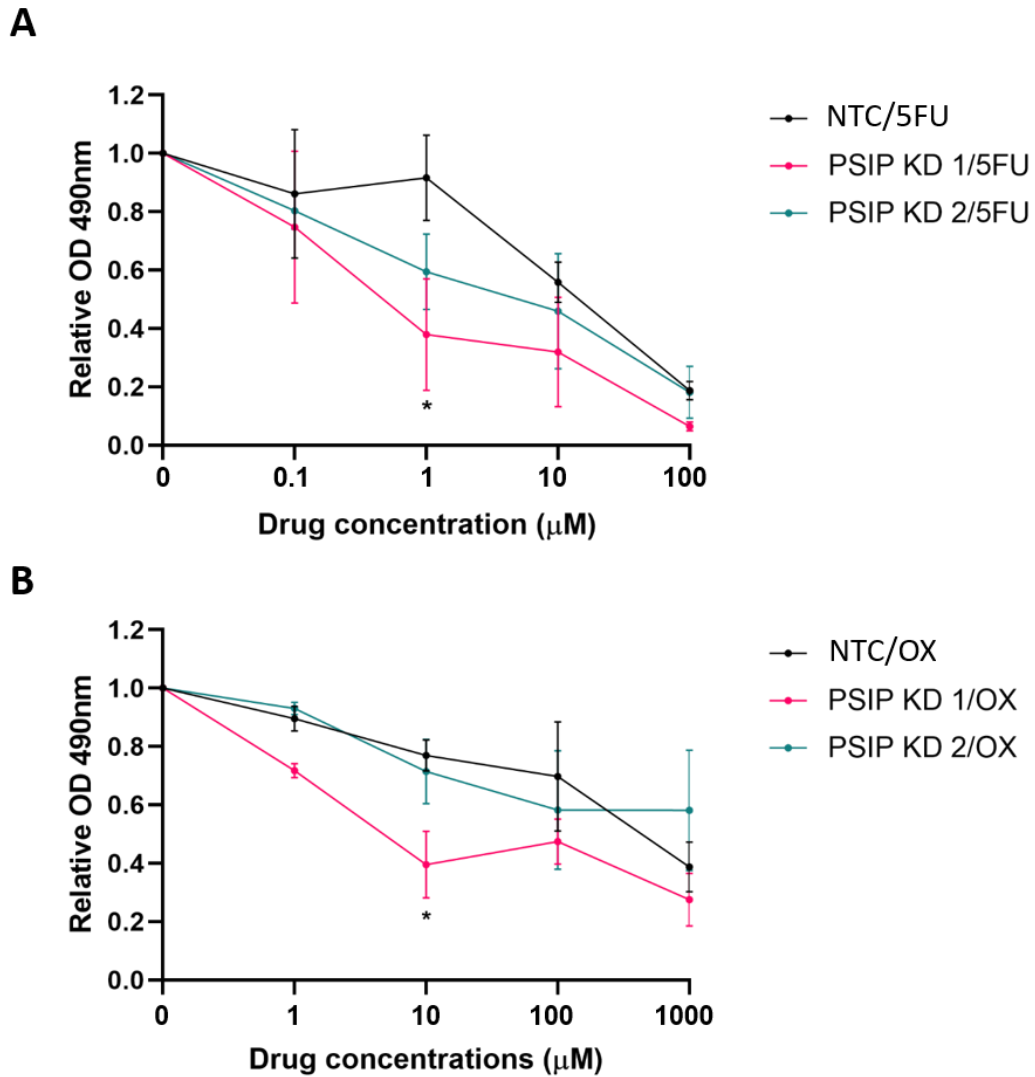
Figure 5.14 Dose response of siRNA mediated PSIP1 depleted HCT116 cells to chemotherapeutic drugs

72 h after transfection with PSIP1 targeting or NTC siRNA for 72 h, HCT116 cells were subsequently treated with a dose response of (A) 5FU (0, 0.1, 1, 10, 100 µM) or (B) OX (0, 1, 10, 100, 1000 µM) for a further 72 h. The dose response of siRNA mediated PSIP1 depleted HCT116 cells to chemotherapeutic drugs was examined and compared to NTC. All data are mean (± S.E.M) of 3 biological replicates (N=3). Two-way ANOVA with Dunnett's multiple comparisons test was used to quantify statistical significance (*$P < 0.05$).
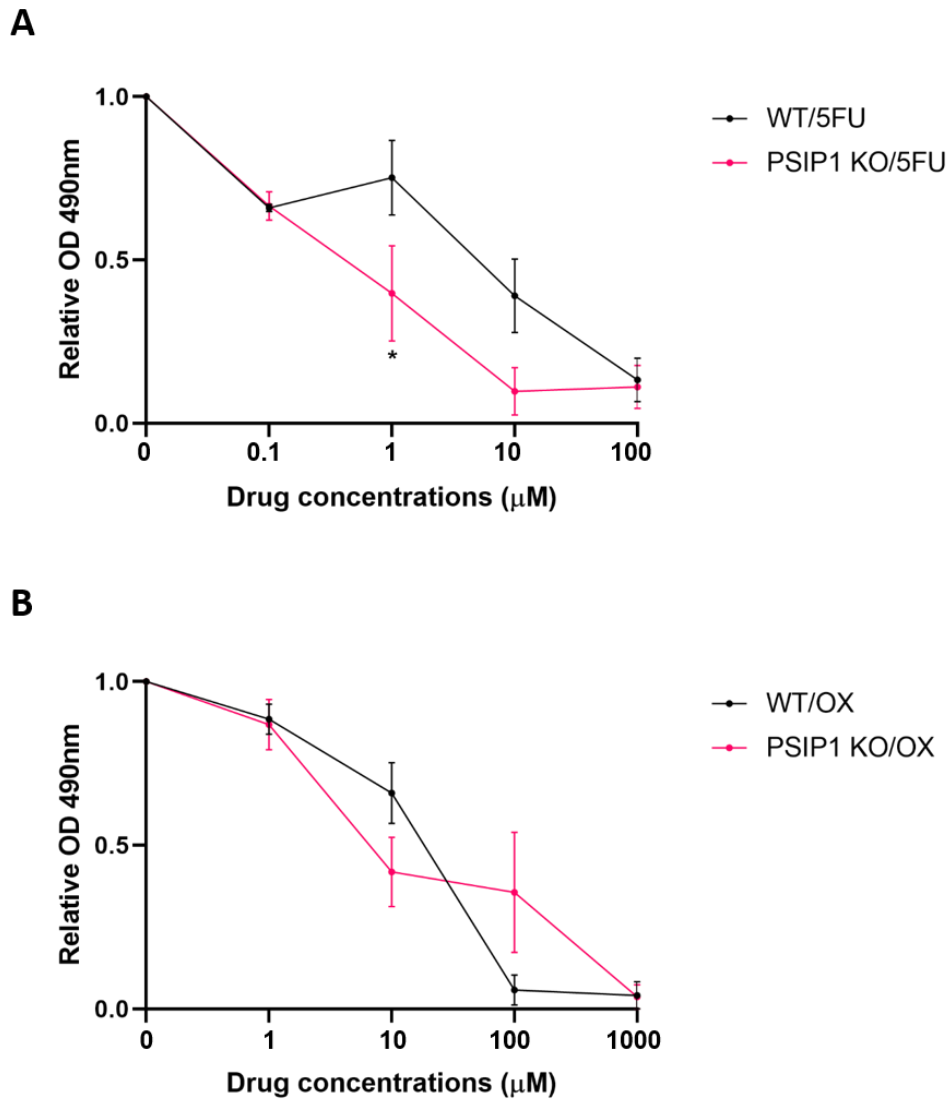
Figure 5.15 Dose response of CRISPR-Cas9 mediated PSIP1 KO and WT HCT116 cells to chemotherapeutic drugs

Stable PSIP1 CRISPR-Cas9 KO and WT HCT116 cells were seeded in 96-well plates and subsequently treated with a dose response of (A) 5FU (0, 0.1, 1, 10, 100 μM) or (B) OX (0, 1, 10, 100, 1000 μM) for a further 72 h. Data are mean (± S.E.M) of 3 biological replicates (N=3). Two-way ANOVA with Sidak's multiple comparisons test was used to quantify statistical significance (*P<0.05).

5.5.2 Reduction in PSIP1 expression leads to an increase in cell death when HCT116 cells are treated with chemotherapeutic drugs.

After increased sensitivity to chemotherapeutic drugs was observed in cells with reduced PSIP1 expression, rates of cell death (apoptosis) were analysed by flow cytometry (as described in 5.4.5) in these cells after exposure to 5FU and OX. After 72 h of incubation with siRNA to deplete PSIP1, cells were subsequently treated with 10 µM 5FU or 10 µM OX over a time series of 0 h, 24 h, 48 h and 72 h. A no drug comparison was also included.

An increase in apoptosis was observed in PSIP1-depleted HCT116 cells prior to drug treatment (no drug control) (Figure 5.16). The percentage of cells undergoing apoptosis was higher for cells transfected with PSIP KD 1 than PSIP KD 2, reflecting the knockdown efficiency observed in Figure 5.2. However, the increased apoptosis as a result of PSIP1 knock-down was not significant. PSIP KD 1 depleted cells treated with 5FU resulted in a highly significant increase in the percentage apoptosis of cells across all time points. PSIP KD 2 depleted cells were also found to significantly increase cell death at 72 h treatment with 5FU (Figure 5.16A). A significant increase in percentage apoptosis was observed when PSIP1 depleted cells were treated with OX (Figure 5.16C), however this was only significant for PSIP KD 1 transfected cells at the 72 h time point.

Overall, PSIP1 depleted HCT116 cells were found to be significantly more sensitive to 5FU. Sensitivity to OX was also observed after 72 h treatment, however this was only applicable for cells transfected with PSIP KD 1 KD siRNA.
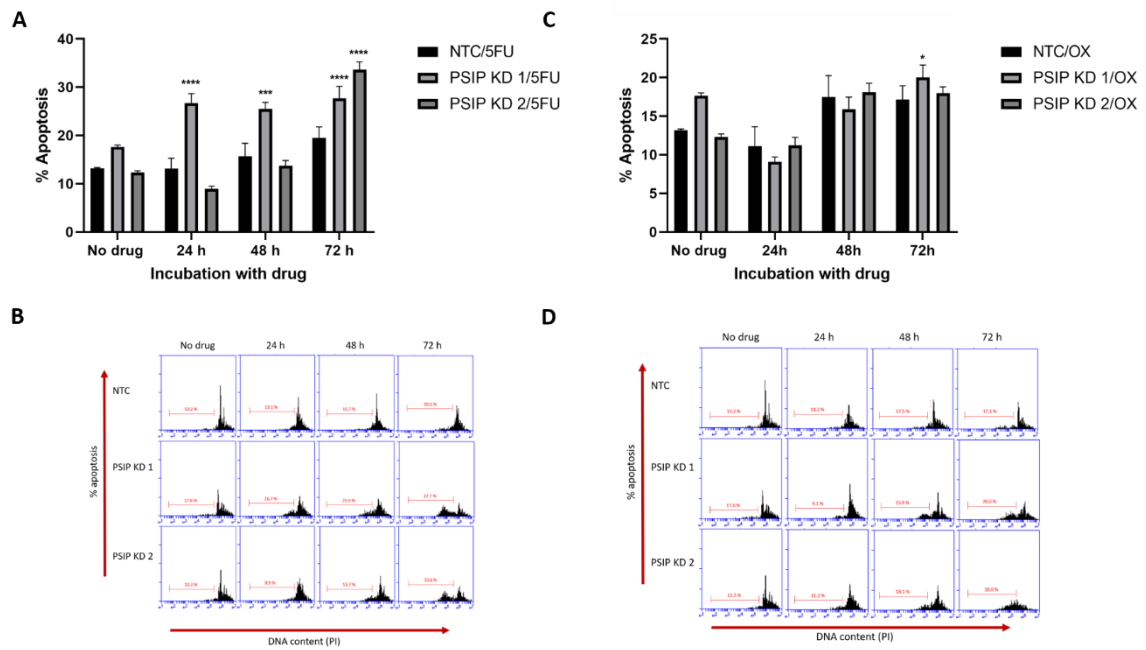
Figure 5.16 PSIP1 depleted HCT116 cells are more sensitive to chemotherapy

HCT116 cells were transfected with PSIP1 targeting or NTC siRNA for 72 h and subsequently treated with (A) 10 μM 5FU or (B) 10 μM OX for up to 72 h for DNA hypodiploidy analysis via apoptosis assay using a flow cytometer. No drug controls were also included. Data are mean (± S.E.M) of 3 biological replicates (N=3). Two-way ANOVA via Dunnett's comparison test was used to quantify the statistical significance (*P<0.05, ***P<0.001. ****P<0.0001). Representative flow cytometry plots of PSIP1 KD and NTC cells treated with (B) 5FU or (D) OX, average Sub-G1 percentages highlighted in red.

5.5.3 PSIP1 deletion results in reduced colony formation ability of HCT116 cells.

Colony formation assays were used to further investigate the effect of PSIP deletion on CRC cell survival when exposed to chemotherapeutic drugs. CRISPR-Cas9 PSIP1 KO and WT stable cells were seeded sparsely in 12-well plates. After 3-4 days, cells were treated with 10 µM 5FU or 10 µM OX. A no drug control was also included to measure the colony growth without the addition of chemotherapy treatment.

PSIP1 KO cells have a highly significant reduction in colony formation ability compared to WT prior to the addition of any chemotherapeutic drugs (fold change = 12.5) (Figure 5.17). When treated with 5FU and OX, colony formation ability of PSIP1 KO cells was also highly significantly reduced compared to WT (5FU fold change = 20, OX fold change = 25). Despite the increased fold change with the addition of chemotherapy, it cannot be confirmed that reduced colony formation ability is a direct result of treatment with 5FU or OX as similar colony numbers were observed to that of the no treatment control.
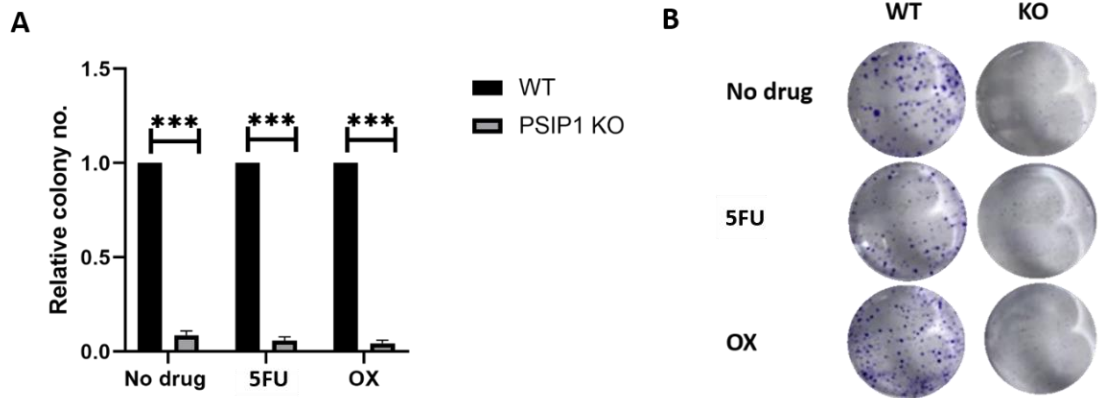
Figure 5.17 CRISPR-Cas9 mediated PSIP1 knockout cells exhibit significant loss of colony formation ability in HCT116 cells

(A) Relative colony number of PSIP1 KO and WT HCT116 cells were compared with no drug, treatment with 10 μM 5FU or 10 μM OX. Data are mean (± S.E.M) of 3 biological replicates (N=3) relative to control WT cells. Two-way ANOVA with Sidak's multiple comparisons test was used to quantify statistical significance (*** P<0.001). (B) Representative wells of colonies formed and stained with crystal violet after treatment with 5FU or OX.

5.5.4 Treatment with chemotherapeutic drugs results in restricted growth when PSIP1 is deleted in HCT116.

The proliferation rate of PSIP1 deleted HCT116 cells when treated with chemotherapeutic drugs was investigated. Cells were seeded in 96-well plates, treated with 10 µM 5FU or 10 µM OX and grown over a time series for 6 days. After each time point, cells were fixed and stained with crystal violet prior to colorimetric measurement (OD 490 nm). Growth rates were calculated relative to day 0.

Prior to the addition of chemotherapy treatment, no significant difference in proliferation was observed between PSIP1 KO and WT HCT116 cells (Figure 5.18A). When treated with 5FU (Figure 5.18B), a reduction in proliferation compared to WT was observed for PSIP1 KO cells at day 2 and 4. When treated with OX (Figure 5,18C), a reduction in proliferation was observed for PSIP1 KO cells at days 4 and 6. However, in both cases, this result was not found to be significant.
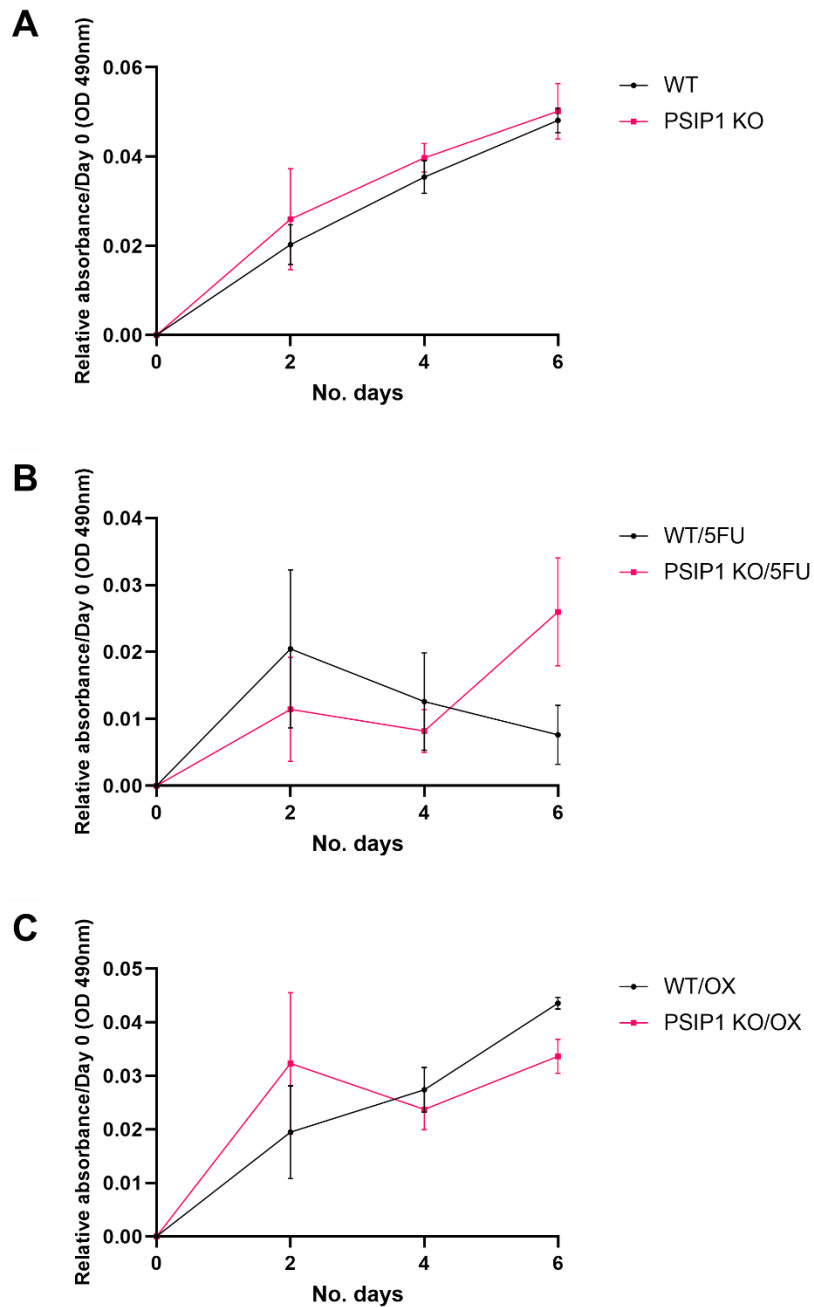
Figure 5.18 Growth assay of CRISPR-Cas9 mediated PSIP1 KO and WT HCT116 cells when treated with chemotherapeutic drugs

CRISPR-Cas9 mediated PSIP1 knockout and WT HCT116 cells were grown over a 6-day time course in the presence of (A) no drug, (B) 10 µM 5FU and (B) 10 µM OX. Cells were fixed with 4% PFA and stained with crystal violet prior to colorimetric assay measurement (OD 490 nm). Growth rates were calculated relative to day 0 (no growth or drug treatment). Data are mean (± S.E.M) of 3 biological replicates (N=3). Two-way ANOVA with Sidak's multiple comparison test was used to quantify statistical significance.

5.5.5 5FU and Oxaliplatin do not induce arrest in cell cycle phases when PSIP1 is depleted in HCT116.

After sensitivity to chemotherapy treatment was observed in PSIP1 depleted cells, it was decided to investigate whether 5FU or OX treatment influences changes in the cell cycle when PSIP1 is depleted. Cells were transfected with PSIP1 KD or NTC siRNA for 72 h and then treated with either 10 µM 5FU or 10 µM OX for a further 72 h; no drug controls were also included. A flow cytometer was used to measure the percentage of cells in each stage of the cell cycle (G1 vs S vs G2/M).

PSIP1 depletion resulted in a decrease in G2/M phase compared to NTC prior to the addition of chemotherapeutic drugs. Conversely, an increase in S and G1 phase was also observed for PSIP1 depleted, non-drug treated cells (Figure 5.19 Cell **cycle analysis of siRNA mediated PSIP1 depletion in HCT116 cells**

Cell cycle analysis of (A) siRNA mediated PSIP1 depletion and NTC HCT116 cells treated with (B) 10 µM 5FU or (C) 10 µM OX for 72 h. A no drug control was also included. Data are mean (± S.E.M) of 3 biological replicates (N=3). Two-way ANOVA with Dunnett's multiple comparisons test was used to quantify statistical significance. (D) Representative flow cytometry plots of PSIP1 depleted and NTC cells with and without drug treatment.

An increase in G1 phase and a decrease in G2/M and S phase was observed for PSIP1 depleted cells treated with 5FU (Figure 5.19B). A reduction in G2/M and S phase was also observed when PSIP depleted cells were treated with OX, however the percentage of cells in G1 phase fluctuated depending on the siRNA used to target PSIP1, with PSIP1 KD 1 resulting in decreased in G1, and PSIP KD 2 resulting in increased G2 (Figure 5.19 Cell **cycle analysis of siRNA mediated PSIP1 depletion in HCT116 cells**

Cell cycle analysis of (A) siRNA mediated PSIP1 depletion and NTC HCT116 cells treated with (B) 10 µM 5FU or (C) 10 µM OX for 72 h. A no drug control was also included. Data are mean (± S.E.M) of 3 biological replicates (N=3). Two-way ANOVA with Dunnett's multiple comparisons test was used to quantify statistical significance. (D) Representative flow cytometry plots of PSIP1 depleted and NTC cells with and without drug treatment.

None of these data were found to be statistically significant, therefore, the introduction of chemotherapeutic drug treatment to PSIP1 depleted HCT116 cells could not be confirmed to cause a shift in the cell cycle.
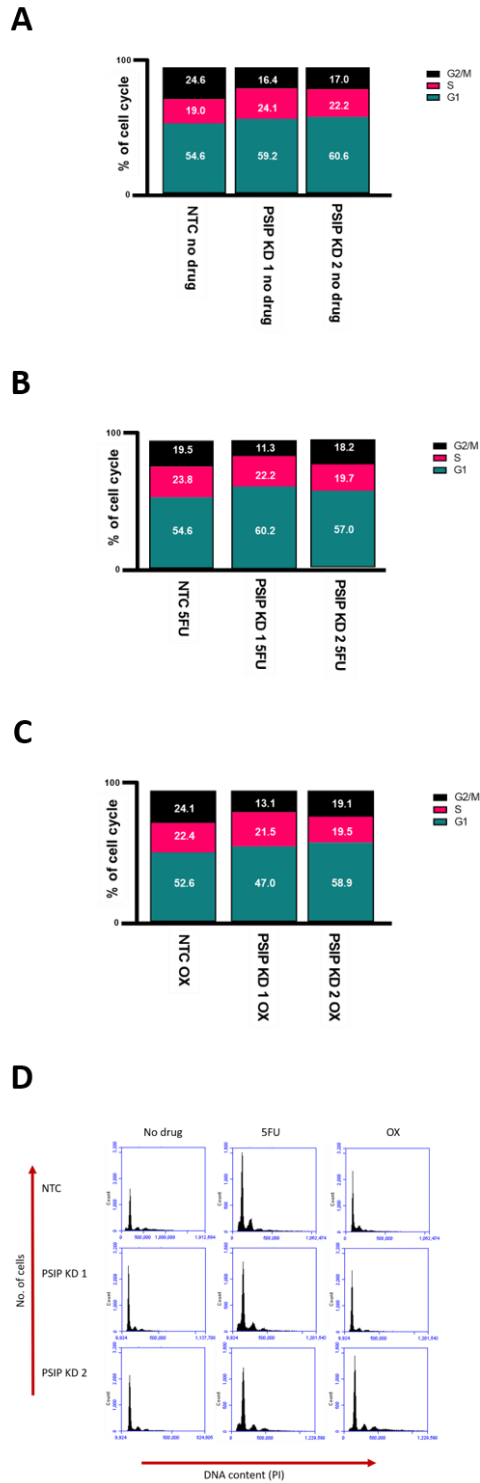
Figure 5.19 Cell cycle analysis of siRNA mediated PSIP1 depletion in HCT116 cells

Cell cycle analysis of (A) siRNA mediated PSIP1 depletion and NTC HCT116 cells treated with (B) 10 µM 5FU or (C) 10 µM OX for 72 h. A no drug control was also included. Data are mean (± S.E.M) of 3 biological replicates (N=3). Two-way ANOVA with Dunnett's multiple comparisons test was used to quantify statistical significance. (D) Representative flow cytometry plots of PSIP1 depleted and NTC cells with and without drug treatment.

5.6 Discussion

PSIP1 has previously been implicated in several cancers, including leukaemia (Yokoyama and Cleary, 2008) prostate (Basu, et al. 2012), breast (Singh *et al.*, 2017) and ovarian cancer (French *et al.*, 2016), however knowledge on its role in CRC is limited. K-M survival plots indicated that high expression of PSIP1 is associated with poorer survival rate in CRC, suggesting that PSIP1 may play an important role in the carcinogenesis of this disease.

5.6.1 PSIP1 regulates *HOXA13* expression in CRC.

Upon siRNA mediated PSIP1 depletion, *HOXA13* expression was found to be significantly downregulated, strongly suggesting that PSIP1 regulates *HOXA13* in CRC. *HOTTIP*, a lncRNA located in close proximity to *HOXA13* on the *HOXA* cluster was also non-significantly downregulated with PSIP1 depletion. PSIP1 has previously been described as regulating the expression of *HOXA* genes through the lncRNA *Hottip* in mouse models (Pradeepa *et al.*, 2017) which has now been replicated in this CRC model. This is the first time that a direct role of PSIP1 regulating *HOXA13* has been described in CRC.

5.6.2 PSIP1 depletion results in loss of colony formation ability in HCT116 cells, however it is not a key driver of cell proliferation and migration in CRC.

PSIP1 has been implicated in promoting cell-cycle progression, metastasis, migration and invasion in breast cancer (Singh *et al.*, 2017). However, this was not replicated here in CRC, as no significant difference in motility, migration or

proliferation was observed for either siRNA mediated PSIP1 knockdown or stable PSIP1 KO cells compared to controls. Similarly, previous studies have observed PSIP1 promoting the expression of cell cycle genes in breast cancer (Singh *et al.*, 2017); these effects were not confirmed in this study. Together, these data suggest that PSIP1 is not a key growth driver and does not influence CRC progression through promoting key cell cycle genes to drive cell growth.

On the other hand, the colony formation ability of cells was highly significantly reduced in PSIP1 KO HCT116 cells. The formation of colonies is particularly important to the progression of CRC as at early stages, cells first form precursor adenomatous polyps before turning cancerous into invasive adenocarcinomas, metastasising and migrating to other areas of the body (Aarons, Shanmugan and Bleier, 2014; Delavari *et al.*, 2014). Therefore, this reduction in colony formation ability for PSIP1 KO cells suggests a key role for PSIP1 in this process. As of yet, there have been no studies investigating the role of PSIP1 in promoting cell growth or movement in CRC so further work needs to be done to confirm this observation.

5.6.3   PSIP1 protects HCT116 cells from cell death when exposed to 5FU.

PSIP1 is a stress survival protein (Basu, et al. 2012) and has been observed having roles in preventing apoptosis when cells are exposed to stress, for example, in patients with inflammatory conditions such as dermatitis (Ganapathy, Daniels and Casiano, 2003; Sutherland *et al.*, 2006). This could be the same in CRC when cells are under stress from chemotherapy exposure (Basu et al. 2012). To date, no previous studies have described PSIP1 as having a protective role against chemotherapy in CRC. This has

however, been described in other cancers including prostate (Ríos-Colón *et al.*, 2017) and ovarian (French *et al.*, 2016) cancer.

Here, chemosensitivity to 5FU (1 µM) and OX (10 µM) was observed in siRNA mediated PSIP1 depletion HCT116 cells. It should be noted, however, that PSIP KD 1 exhibited a higher sensitivity to both 5FU and OX treatment than NTC - this is due to the increased knockdown efficiency for this siRNA. This result was confirmed with the stable CRISPR lines, where PSIP1 KO also resulted in sensitivity to 5FU. Conversely, no sensitivity to OX treatment was observed in stable PSIP1 KO HCT116 cells. A similar pattern was seen when investigating apoptosis rates of PSIP1 depleted cells. 5FU treated PSIP1 KD cells showed an increase in percentage apoptosis at each time point that was examined (24 h, 48 h, 72 h). Whereas, PSIP1 depleted cells treated with OX showed an increase in percentage apoptosis only at the 72 h time point. Overall, these data suggest that PSIP1 KD/KO cells exhibit sensitivity to 5FU treatment; further work would need to be carried out to confirm any OX sensitivity. It is possible that PSIP1 depleted cells exhibit OX sensitivity when incubated for longer than 72 h. Therefore, testing both the dose response and apoptosis rates of PSIP1 KD cells over a longer time series would have been useful to draw more conclusions.

PSIP1 has previously been reported to have roles in the cell cycle, particularly in S and G2 phase (Daugaard *et al.*, 2012). Arrest in S phase was observed in PSIP1 depleted HCT116 cells, and this arrest increased with the addition of 5FU. This may suggest some sensitivity to 5FU, but the result was not significant so this cannot be concluded without further experimentation. OX has been shown to induce arrest in G2/M and S phase (William-Faltaos *et al.*, 2007; Todd and Lippard, 2009; T. Alcindor

215

and Beauger, 2011), however this was not replicated in this study. No arrest in G2/M was observed for OX-treated NTC HCT116, although there was an increase in S phase. This experiment could have been optimisied further to ensure the drugs were working correctly in control samples; this would have enabled better conlclusions to be drawn from this data.

Overall, cells with PSIP1 depletion or stable PSIP1 KO were observed to exhibit more sensitivity to chemotherapeutic drug treatment than control cells, particularly towards 5FU. These findings may be useful when applying this in a clinical setting as CRC tumour cells with lower PSIP1 expression may respond better to 5FU treatment than CRC tumour cells with a higher PSIP1 expression. Testing patients for levels of PSIP1 expression may decipher how well a treatment course may work for a patient.

5.7   Summary

In summary, PSIP1 exhibits some chemosensitive properties in HCT116 cells when exposed to chemotherapeutic drugs, particularly towards 5FU. This was observed both in siRNA mediated PSIP1 depletion and in stable PSIP1 KO cell lines, although the stable cell lines provided more significant and therefore conclusive results. PSIP1 has not previously been implicated in CRC, therefore, more study into its chemosensitive properties is needed to confirm what has been observed here. Overall, this work shows potential for testing PSIP1 expression in CRC tumours to identify patients who may become resistance to chemotherapy. This could prevent administration of ineffective drugs and avoid patients suffering the side effects associated with chemotherapy.

Limitations of this work include discrepancies between siRNAs targeting PSIP1, with PSIP KD 1 having a stronger KD effect than PSIP KD 2. Including a larger panel of siRNAs would improve the quality of the data and ensure conclusions can be drawn confidently. Knock-down success was checked regularly but was not performed for every experiment; therefore, providing confirmation of siRNA knockdown (via qPCR/Sanger sequencing) for each of the cell assays would also add confidence to this data. Further optimisation of the chemotherapeutic drug assays (time points, concentrations, controls) would improve the significance of the data observed in this chapter, adding confidence to the suggestion of a potential chemosensitive role of PSIP1 in CRC.

6 General Discussion

Treatments for both colorectal cancer (CRC) and prostate cancer (PCa) have greatly improved over the last 10-20 years (Saltz, 2016; Litwin and Tan, 2017). However, there is still a high mortality rate for both cancers worldwide, with an estimated 880 792 deaths from CRC and 358 989 deaths from PCa in 2018 (Bray *et al.*, 2018). There is therefore a great need to better understand the factors that drive disease development and progression, and therapy resistance.

6.1 Key findings of the roles of *HOTTIP, HOXA13* and PSIP1 in CRC and PCa.

The main aim of this thesis was to investigate the role of *HOTTIP, HOXA13* and PSIP1 in CRC and PCa. Through loss of function studies, a combination of transient siRNA knockdown and CRISPR-Cas9 stable knockout cell lines were used to explore the role of each gene in CRC and PCa.

6.1.1 *HOTTIP*

Long non-coding RNAs (lncRNAs) have gained attention in recent years as potential targets for therapies, including cancer. They have key regulatory roles in many cellular processes and can influence the progression of cancer (Hajjari and Salavaty, 2015). Some lncRNAs are detectable in bodily fluids such as blood serum and the urine (Qi, Zhou and Du, 2016). This highlights huge potential for this group of ncRNAs as attractive biomarkers to provide non-invasive detection methods that are reasonably cheap and easy to perform. *HOTTIP* is one such lncRNA that is gaining

traction as a potential therapeutic drug or biomarker target due to its implications in cancer progression.

HOTTIP is located on the 5' end of the *HOXA* cluster and influences the regulation of nearby *HOX* genes, including *HOXA13*, through interacting with chromatin modifying complexes (Wang *et al.*, 2011). *HOTTIP* is in turn regulated by the chromatin adapter protein PSIP1, with the shorter PSIP1/p52 isoform regulating *HOTTIP* through binding to the regulatory MLL/WDR5 complex (Pradeepa *et al.*, 2017).

Previous studies have reported upregulation of *HOTTIP* in both CRC and PCa (Ren *et al.*, 2015; C. Liu *et al.*, 2018; Lee *et al.*, 2019). *HOTTIP* has roles in promoting both of these cancers through regulation of cell proliferation, migration, invasion and metastasis (Lian, Y; Cai, Z; Gong, 2016; Malek *et al.*, 2017; Yang *et al.*, 2018; Oehme *et al.*, 2019; Rui *et al.*, 2019). Some of these properties were replicated throughout this thesis. For example, the role of *HOTTIP* in cell migration, proliferation and apoptosis were confirmed in CRC and PCa.

The key finding of Chapter 3 is the identification of a potential role of *HOTTIP* in regulating chemoresistance in both CRC and PCa. Chemoresistant properties of *HOTTIP* have been described only once before in PCa (Jiang *et al.*, 2019) and this is the first time *HOTTIP* has been implicated in CRC chemoresistance. Cells were observed to be more sensitive to chemotherapy when *HOTTIP* expression was either depleted or stably removed through apoptosis, colony proliferation and proliferation assays.

HOX genes are key regulatory genes, heavily involved in development as well as other regulatory cellular processes (Shah and Sukumar, 2010; Wang *et al.*, 2016). As a result, any alterations in the expression levels of *HOX* genes has the potential to progress into cancer (Wang *et al.*, 2016). Aberrant expression of *HOXA13*, the most distally located of the *HOXA* genes, located ~330 bp from *HOTTIP* (Wang *et al.*, 2011) has been associated with the progression of several cancers, including prostate (Dong *et al.*, 2017b; Luo *et al.*, 2017). It is upregulated in PCa and has been found to promote cell proliferation, migration, invasion and inhibit tumour cell apoptosis (Zhang *et al.*, 2016; Dong *et al.*, 2017b). This has also been observed in Chapter 4, where reduced cell migration and an increase in apoptosis were reported upon *HOXA13* depletion in DU145 PCa cells.

The data produced in Chapter 4 has also reported a link between *HOXA13* and CRC. This is the first time a relationship between *HOXA13* and CRC has been suggested. Reduced cell migration and increased apoptosis were observed when *HOXA13* expression was depleted in HCT116 cells. However, it must be noted that some opposing results were documented in RKO1 cells, where *HOXA13* depletion resulted in increased proliferation and reduced apoptosis. Including a larger panel of CRC cell lines would allow better conclusions on the role of *HOXA13* in CRC to be drawn.

One finding in Chapter 4 across all cell lines (HCT116, RKO1 and DU145) is the suggestion of *HOXA13* contributing to chemoresistance in both CRC and PCa. This is

the first time this has been reported in both cancers. *HOXA13* has previously been described as contributing to 5FU resistance in gastric cancer, where affects the stomach and therefore is in close proximity to the colon (Han *et al.*, 2018). This may provide some evidence that further study into whether *HOXA13* exhibits chemoresistant properties in other cancers, including the ones described in this study.

6.1.3   PSIP1

PSIP1 is a chromatin-adapter protein (Singh *et al.*, 2017) that interacts with chromatin in order to regulate gene expression (Sutherland *et al.*, 2006b). PSIP1 has been implicated in several diseases, including in HIV replication (Baid *et al.*, 2013), leukaemia (El Ashkar *et al.*, 2017) and other cancers including breast, ovarian and prostate (Basu, *et al.*, 2012; French *et al.*, 2016; *et al.*, 2017; Woods-Burnham *et al.*, 2018). This thesis has contributed to this research by reporting a role for PSIP1 in CRC. Here I have identified a role of PSIP1 in promoting colony formation ability. The formation of colonies plays a critical part in the pathogenesis of CRC aiding in promoting polyp development (Aarons, Shanmugan and Bleier, 2014; Delavari *et al.*, 2014). This is the first time a relationship between PSIP1 and CRC has been described.

Consistently with *HOTTIP* and *HOXA13*, Chapter 5 also reported a possible role of PSIP1 in CRC chemosensitivity. Again, this is a novel description for the role of PSIP1 in CRC, and PSIP1 has only been documented in contributing to chemoresistance once before, in prostate cancer (Ríos-Colón *et al.*, 2017).

6.2 Exploring gene regulatory roles of *HOTTIP, HOXA13* and PSIP1 in CRC and PCa.

Previous reports have reported *HOTTIP* regulates *HOXA13* expression in mouse models (Pradeepa *et al.*, 2017). This has been replicated in this thesis in both CRC and PCa, confirming that this regulation model is also observed in human cells, and in disease states. All gene regulation observed in this thesis has been summarised in Figure 6.1. Both siRNA mediated *HOTTIP* depletion or CRISPR-Cas9 stable *HOTTIP* KO resulted in *HOXA13* depletion in HCT116, RKO1 and DU145 cells. *HOTTIP* was also observed to regulate the expression of *HOXA11* in HCT116. This is consistent for what has been described in mouse models where *Hottip* activates 5' *Hoxa* genes, including *Hoxa13* and *Hoxa11* (Wang *et al.*, 2011; Pradeepa *et al.*, 2017)*.*

When investigating the global effects of stable *HOTTIP* KO in HCT116 cells, *HOXD8* expression was downregulated in *HOTTIP* KO compared to WT, as well as *HOTTIP* and *HOXA13*. Interestingly, the 3' *HOXA3* gene, and several *HOXB* genes (*HOXB3, HOXB4, HOXB6, HOXB8*) were upregulated in *HOTTIP* KO cells. This altered expression could be an indirect result of *HOXA13* depletion, as *HOX* transcription factors (TFs) are known to regulate expression of each other (Pradeepa *et al.*, 2017). This would also explain what was observed in Chapter 4 where upon *HOXA13* depletion, both *HOTTIP* and other nearby *HOXA* genes were downregulated. Alternatively, *HOXA3* upregulation could also be a result of *HOXA-AS2* upregulation, a lncRNA that was also found to be upregulated in *HOTTIP* KO HCT116 cells. *HOXA-AS2* is located between *HOXA3* and *HOXA4* in the *HOXA* cluster (Ding *et al.*, 2017)

and has previously been described as regulating *HOXA3* in leukaemia (Zhao *et al.*, 2019) and thyroid cancer (Jiang *et al.*, 2019).

As well as altered *HOX* gene expression, two gene clusters: *PADI* and *PCDHA* were also found to be differentially expressed in *HOTTIP* KO HCT116 cells. These enzymes involved in citrullination, a post-translational modification that can promote cancer progression through modifying methylation patterns (Yuzhalin, 2019), were found to be upregulated in HCT116 upon *HOTTIP* deletion. Both genes have previously been reported in CRC in tumour suppressive roles (Cantarino *et al.*, 2016; Chai *et al.*, 2019; Chang *et al.*, 2019), which fits with what has been observed in this data. This suggests that *HOTTIP* may act as a tumour suppressor via regulation of *PADI2* and *PADI3*, as upon loss of *HOTTIP*, these genes are upregulated in HCT116.

The *PCDHA* cluster on the other hand were found to be upregulated in WT HCT116 cells compared to *HOTTIP* KO. Protocadherins have important roles in specific cell-cell connections and in promoting tumour development (Berx and van Roy, 2009). *PCDHA* genes are also involved in development, as regulators of the neural circuit formation (Peek, Mah and Weiner, 2017). As *HOX* expression was shown to be mysregulated with *HOTTIP* deletion, these TFs could be regulating the expression of *PCDHA*'s in CRC rather than *HOTTIP* having a direct effect on their expression.

PSIP1 depletion resulted in a reduction of *HOTTIP* and *HOXA13* in HCT116 cells. This is consistent for what has been described previously in mouse models, of the shorter PSIP1/p52 isoform regulating *HOTTIP* which in turn effects 5' *HOXA* gene

expression (Pradeepa *et al.*, 2017). However, this is the first time this has been

replicated in CRC.
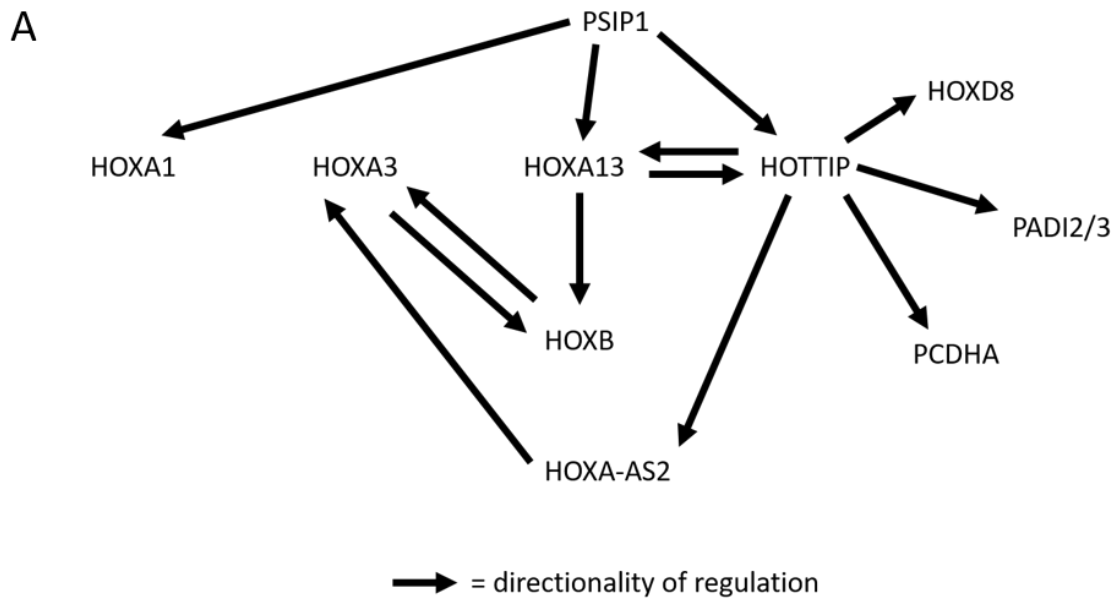
Figure 6.1 Summary of gene regulation observed.

A summary of the key gene regulation patterns observed in this thesis. (A) Directionality of gene regulation is outlined. The black arrow points away from the regulatory gene and towards the gene where expression was found to be up or downregulated as a result of loss of function studies (e.g., PSIP1 depletion also resulted in loss of HOTTIP and HOXA gene expression). (B) These interactions are summarised in a table. Green arrows represent upregulation and red arrows represent downregulation.

6.3 Limitations of this work

Using a combination of transient siRNA mediated knockdown and stable CRISPR-Cas9 KO techniques to carry out loss of function studies has provided strong, comparative data throughout this thesis. It has allowed validation of results through a cross-comparison of gene editing methods. However, it was observed that the stable CRISPR-Cas9 *HOTTIP* or PSIP1 knockout cell lines that were created generally provided more statistically significant data compared to their transient gene knockdown counterparts. This is possibly due to three main factors. Firstly, the stability of CRISPR-Cas9 gene knockdown is consistent for each cell and across each experiment replicate, providing reproducibility, whereas transient knockdown efficiency may vary between experiment. Secondly, total deletion of the genes may have provided a stronger indication of the functional role of *HOTTIP* and PSIP1 in CRC compared to the siRNA mediated knockdown approach, where some functional transcript remains in the cell. Thirdly, when studying lncRNAs such as *HOTTIP* other RNAi approaches may provide a more efficient knockdown. For example, shRNA are able to be incorporated directly into the nucleus via viral vector transduction compared to cytoplasmic disruption that is usually associated with siRNA knockdown (Zong *et al.*, 2015). Although expressed in the cytoplasm, *HOTTIP* is mainly located in the nucleus (Fu *et al.*, 2017); therefore, an alternative method may provide a more efficient knockdown. Overall, in combination, use of both techniques provides a good indication of the role of *HOTTIP* and PSIP1 in CRC. The creation of a stable *HOXA13* cell line may have provided further validation of any conclusions drawn from Chapter 4.

In each chapter, a non-cancerous control cell line would have further provided evidence to support the findings in this thesis. Additional CRC and PCa cell lines would have given a better representation of each disease as in some experiments different results were obtained from the different cell lines (e.g. discrepancies between HCT116 and RKO1 cell lines were observed). To increase specificity of these data, comparisons of this work to patient CRC and PCa tumour samples would also have further validated my conclusions. However, being granted access to patient samples can be difficult and is accompanied by ethical and data protection concerns. These concerns are easily overcome through the use of cell lines.

The significance of the data could have been improved by including more biological repeats of each experiment. This would allow any anomalies in the data to be identified and excluded with more confidence. Including a larger panel of siRNAs would also improve significance and therefore the quality of the data. Knock-down success was checked regularly but was not performed for every experiment; therefore, providing confirmation of siRNA knockdown (via qPCR/Sanger sequencing) for each of the cell assays would also add confidence to this data. Further optimisation of the chemotherapeutic drug assays (time points, concentrations, controls) would improve the significance of the data observed in this thesis, adding confidence to the suggestion of a potential chemosensitive role of *HOTTIP, HOXA13* and P*SIP1* in CRC and PCa.

As one of the key findings of this thesis was the association of *HOTTIP, HOXA13* and PSIP1 with chemoresistance, introducing more chemotherapeutic

drugs to test would decipher if this relationship is drug specific or may be in response to any chemical cancer cell stressor. Often, chemotherapy is administered by a combination of more than one drug; this again would have been interesting to test in response to the chemoresistant capacity of each gene.

6.4   Future implications

The role of *HOTTIP, HOXA13* and PSIP1 in contributing to chemoresistance in both CRC and PCa is the key finding of this thesis. It has highlighted the importance of understanding chemoresistance pathways to provide patients with the most promising treatment options.

As outlined in Chapter 1 (1.2.2.4), therapy resistance is a major concern when treating PCa. After failure of androgen deprivation therapy (ADT) as a result of tumour cells becoming castrate resistant (CRPC) (Brooke *et al.*, 2015), chemotherapy is often the treatment of choice (Wang *et al.*, 2016). However, chemoresistance of docetaxel (DOC)-mediated chemotherapy can still occur (Yuan Wang *et al.*, 2016). Therefore, identifying genes such as *HOTTIP* and *HOXA13* that can promote PCa chemoresistance will help with overcoming failed therapies.

Chemoresistance is also an issue when treating CRC, with most patients eventually developing chemoresistance, which ultimately results in poor prognosis (Huang *et al.*, 2018; Wei *et al.*, 2019). 5FU-mediated chemotherapy is commonly used as a first response therapy, and is followed by secondary treatment with OX (Arango *et al.*, 2004) or in combination with OX when CRC cells develop 5FU resistance (Gonçalves-Ribeiro *et al.*, 2016; McQuade *et al.*, 2017; García-Alfonso *et*

228

al., 2019). The results outlined in this thesis has suggested a role in CRC for *HOTTIP,*

HOXA13 and PSIP1 in both 5FU and OX sensitivity. If CRC tumour cells could be

tested for expression of these genes, this could potentially identify patients who

may be at risk of developing chemoresistance. This could prevent the administration

of ineffective drugs and avoid patients suffering the side effects associated with

chemotherapy.

More studies could be carried out to see if *HOTTIP, HOXA13* and PSIP1

expression is correlated with therapy response. If other studies are found to also

observe what has been reported in this thesis, further characterisation of what

regulates these genes could identify methods to enhance therapy response or re-

sensitise tumours to chemotherapy. This has been suggested in the literature for

Taurine Up-Regulated 1 (TUG1) and Cancer Susceptibility Candidate 15 (CASC15),

two other lncRNAs that have previously been implicated in CRC (C. Li *et al.*, 2017;

Gao *et al.*, 2019; Wang *et al.*, 2019). In line with this, *PCDHA*s were observed to be

downregulated as a result of *HOTTIP* deletion in CRC in this study. Male

protocadherin-PC (PCDHA-PC) has previously been implicated in chemoresistance in

PCa through Androgen Receptor (AR) regulation (Terry *et al.*, 2013). Further study

into the implications of *HOTTIP* and *PCDHA* together in PCa chemoresistance may

present a new target pathway for PCa therapy.

LncRNAs have gained attention as potential biomarkers for cancer. The

lncRNA Prostate Cancer Antigen 3 (PCA3) has been proven to have biomarker

properties in PCa. It is overexpressed in 95 % of PCa sites and is the first urine-based

diagnostic test that has been approved for use by the Food and Drug Administration

(FDA) in the U.S. (Qi, Zhou and Du, 2016). Due to the increasing evidence of a role for *HOTTIP* in promoting cancer and its ability to be detected in blood plasma, a biomarker role has been suggested for this lncRNA (Ali Akbar-Esfahani *et al.*, 2019). The findings described in this thesis support this evidence and also suggest a prognostic biomarker role for *HOTTIP* in both CRC and PCa.

6.5 Concluding remarks

The work presented in this thesis has uncovered a potential new relationship between both *HOXA13* and PSIP1 in the progression of CRC, whilst also contributing further to the current understanding of the role of *HOTTIP* in CRC. A novel suggestion for a chemosensitive role has been reported for *HOTTIP, HOXA13* and PSIP1 in CRC, and for *HOXA13* in PCa. These data also support current literature of chemoresistant behaviour exhibited by *HOTTIP* in PCa. In summary, these conclusions highlight the importance of understanding factors that drive disease development and progression, and identifying genes involved in chemoresistance to help overcome therapy resistance in CRC and PCa.

7 References

Aarons, C. B., Shanmugan, S. and Bleier, J. I. S. (2014) 'Management of malignant colon polyps: Current status and controversies', *World Journal of Gastroenterology*, pp. 16178–16183. doi: 10.3748/wjg.v20.i43.16178.

Adam, V. *et al.* (2012) 'Synergistic and selective cancer cell killing mediated by the oncolytic adenoviral mutant adδδ and dietary phytochemicals in prostate cancer models', *Human Gene Therapy*, 23(9), pp. 1003–1015. doi: 10.1089/hum.2012.046.

Alcindor, T. and Beauger, N. (2011) 'Oxaliplatin: A review in the era of molecularly targeted therapy', *Current Oncology*, 18(1), pp. 18–25. doi: 10.3747/co.v18i1.708.

Alexander, R. P. *et al.* (2010) 'Annotating non-coding regions of the genome', *Nature Reviews Genetics*, 11(8), pp. 559–571. doi: 10.1038/nrg2814.

Ali Akbar-Esfahani, S. *et al.* (2019) Diagnostic Value of Plasma Long Non-coding RNA HOTTIP as a Non-invasive Biomarker for Colorectal Cancer (A Case-Control Study*)*, *International Journal of Molecular and Cellular Medicine (IJMCM)*, 8(4), pp.240-246. doi: 10.22088/IJMCM.BUMS.8.4.240.

Almeida, G. M. *et al.* (2006) 'Detection of oxaliplatin-induced DNA crosslinks in vitro and in cancer patients using the alkaline comet assay', *DNA Repair*, 5(2), pp. 219–225. doi: 10.1016/j.dnarep.2005.09.010.

Altwaijry, N., Somani, S. and Dufès, C. (2018) 'Targeted nonviral gene therapy in prostate cancer', *International Journal of Nanomedicine*. Dove Medical Press Ltd., pp. 5753–5767. doi: 10.2147/IJN.S139080.

Arango, D. *et al.* (2004) 'Molecular mechanisms of action and prediction of response to oxaliplatin in colorectal cancer cells', *British Journal of Cancer*, 91(11), pp. 1931–1946. doi: 10.1038/sj.bjc.6602215.

El Ashkar, S. *et al.* (2018) 'LEDGF/p75 is dispensable for hematopoiesis but essential for MLL-rearranged leukemogenesis', *Blood*, 131(1), pp. 95–107. doi: 10.1182/blood-2017-05-786962.

Baid, R. *et al.* (2013) 'Biosynthesis, Characterization, and Efficacy in Retinal Degenerative Diseases of Lens Epithelium-derived Growth Factor Fragment (LEDGF 1-326), a Novel Therapeutic Protein *' *The Journal of Biological Chemistry,* 288(24), pp. 17372-17383. doi: 10.1074/jbc.M112.441618.

Baker, A. T. *et al.* (2018) 'Designer oncolytic adenovirus: Coming of age', *Cancer,* 10(6), pp. 201. doi: 10.3390/cancers10060201.

Basu, A., Rojas, H., Banerjee, H., Cabrera, I. B., Perez, K. Y., De Leó N, M., *et al.* (2012) 'Expression of the stress response oncoprotein LEDGF/p75 in human cancer: a study of 21 tumor types.', *PLoS One,* 7(1), p. e30132. doi: 10.1371/journal.pone.0030132.

Basu, A., Drame, A., *et al.* (2012) 'Pathway Specific Gene Expression Profiling Reveals Oxidative Stress Genes Potentially Regulated by Transcription Co- Activator LEDGF/p75 in Prostate Cancer Cells NIH Public Access', *Prostate. May*, 1(726), pp.

597–611. doi: 10.1002/pros.21463.

Berx, G. and van Roy, F. (2009) 'Involvement of members of the cadherin superfamily in cancer.', *Cold Spring Harbor perspectives in biology*, 1(6), pp. a003129. doi: 10.1101/cshperspect.a003129.

Bhatlekar, S., Fields, J. Z. and Boman, B. M. (2018) 'Role of HOX Genes in Stem Cell Differentiation and Cancer', *Stem Cells International,* 2018, 3569493. doi: 10.1155/2018/3569493.

Bolha, L., Ravnik-Glavač, M. and Glavač, D. (2017) 'Long Noncoding RNAs as Biomarkers in Cancer', *Disease Markers*, 2017, pp. 1–14. doi: 10.1155/2017/7243968.

Boyd, D. *et al.* (1988) 'Determination of the Levels of Urokinase and Its Receptor in Human Colon Carcinoma Cell Lines', *Cancer Research,* 48(11), pp.3112-3116. .

Brattain, M. G. *et al.* (1981) 'Heterogeneity of Malignant Cells from a Human Colonic Carcinoma', *Cancer Research*, 41(5), pp. 1751–1756.

Brattain, M. G. *et al.* (1984) 'Heterogeneity of human colon carcinoma', *Cancer and metastasis review*, 3(3), pp. 177–191. doi: 10.1007/BF00048384.

Bray, F. *et al.* (2018) 'Global cancer statistics 2018: GLOBOCAN estimates of incidence and mortality worldwide for 36 cancers in 185 countries', *CA: A Cancer Journal for Clinicians*, 68(6), pp. 394–424. doi: 10.3322/caac.21492.

Brenner, H., Kloor, M. and Pox, C. P. (2014) 'Colorectal cancer', *The Lancet*, 383(9927), pp. 1490–1502. doi: 10.1016/S0140-6736(13)61649-9.

Bridges, C. B. and Morgan, T. H. (1923) 'The third-chromosome group of mutant characters of Drosophila melanogaster', *Carnegie Institution of Washington*, 327, pp. 1–251.

Brooke, G. N. *et al.* (2015) 'Antiandrogens act as selective androgen receptor modulators at the proteome level in prostate cancer cells', *Molecular and Cellular Proteomics*, 14(5), pp. 1201–1216. doi: 10.1074/mcp.M113.036764.

Caffo, O. *et al.* (1996) 'Assessment of quality of life after radical radiotherapy for prostate cancer', *British Journal of Urology*, 78(4), pp. 557–563. doi: 10.1046/j.1464-410x.1996.14812.x.

Cantarino, N. *et al.* (2016) 'Downregulation of the deiminase PADI2 is an early event in colorectal carcinogenesis and indicates poor prognosis', *Molecular Cancer Research*, 14(9), pp. 841–848. doi: 10.1158/1541-7786.MCR-16-0034.

Carethers, J. M. *et al.* (2004) 'Use of 5-Fluorouracil and Survival in Patients with Microsatellite-Unstable Colorectal Cancer', *Gastroenterology*, 126(2), pp. 394–401. doi: 10.1053/j.gastro.2003.12.023.

Cermakova, K. *et al.* (2016) 'Lessons Learned: HIV Points the Way Towards Precision Treatment of Mixed-Lineage Leukemia', *Trends in Pharmacological Sciences*, 37(8), pp. 660–671. doi: 10.1016/J.TIPS.2016.05.005.

Chai, Z. *et al.* (2019) 'PADI3 plays an antitumor role via the Hsp90/CKS1 pathway in colon cancer', *Cancer Cell International*, 19(1), pp. 729-742. doi: 10.1186/s12935-019-0999-3.

Chang, S. *et al.* (2016) 'HOTTIP and HOXA13 are oncogenes associated with gastric cancer progression', *Oncology Reports*, 35(6), pp. 3577–3585. doi: 10.3892/or.2016.4743.

Chang, X. *et al.* (2019) 'PADI3 induces cell cycle arrest via the Sirt2/AKT/p21 pathway and acts as a tumor suppressor gene in colon cancer', *Cancer Biology and Medicine*, 16(4), pp. 729–742. doi: 10.20892/j.issn.2095-3941.2019.0065.

Chen, D. *et al.* (2017) 'The lncRNA HOXA11-AS functions as a competing endogenous RNA to regulate PADI2 expression by sponging miR-125a-5p in liver metastasis of colorectal cancer', *Oncotarget*, 8(41), pp. 70642–70652. doi: 10.18632/oncotarget.19956.

Cheng, Y. *et al.* (2015) 'The long non-coding RNA HOTTIP enhances pancreatic cancer cell proliferation, survival and migration.', *Oncotarget*, 6(13), pp. 10840-10852. doi: 10.18632/oncotarget.3450.

Chu, E. and Allegra, C. J. (1996) 'The role of thymidylate synthase in cellular regulation', *Advances in Enzyme Regulation*, 36, pp. 143–163. doi: 10.1016/0065-2571(95)00004-6.

Cockle, J. V. and Scott, K. J. (2018) 'What is oncolytic virotherapy?', *Archives of Disease in Childhood: Education and Practice Edition*, 103(1), pp. 43–45. doi: 10.1136/archdischild-2016-311922.

Comella, P. *et al.* (2009) 'Role of oxaliplatin in the treatment of colorectal cancer', *Therapeutics and Clinical Risk Management*, 5(1), pp. 229–238. doi: 10.2147/tcrm.s3583.

Daugaard, M. *et al.* (2012) 'LEDGF (p75) promotes DNA-end resection and homologous recombination', *Nature Structural & Molecular Biology*, 19(8), pp. 803-810. doi: 10.1038/nsmb.2314.

Delavari, A. *et al.* (2014) 'Characteristics of colorectal polyps and cancer; a retrospective review of colonoscopy data in iran.', *Middle East journal of digestive diseases*, 6(3), pp. 144–50. doi: 10.15171/middleeastjdi.v6i3.1349.

Dempsey, J. L. and Cui, J. Y. (2016) 'Long Non-Coding RNAs: A Novel Paradigm for Toxicology', 155(1), pp. 1–19. doi: 10.1093/toxsci/kfw203.

Ding, J. *et al.* (2017) 'Long noncoding RNA HOXA-AS2 represses P21 and KLF2 expression transcription by binding with EZH2, LSD1 in colorectal cancer', *Oncogenesis*, 6(1), pp. e288. doi: 10.1038/oncsis.2016.84.

Dong, Y. *et al.* (2017) 'HOXA13 is associated with unfavorable survival and acts as a novel oncogene in prostate carcinoma', *Future Oncology*, 13(17), pp. 1505–1516. doi: 10.2217/fon-2016-0522.

Dowty, J. G. *et al.* (2013) 'Cancer risks for MLH1 and MSH2 mutation carriers',

Human Mutation, 34(3). pp. 490-497. doi: 10.1002/humu.22262.

Duan, R. *et al.* (2015) 'HOXA13 is a potential GBM diagnostic marker and promotes glioma invasion by activating the Wnt and TGF-β pathways', *Oncotarget*, 6(29), pp. 27778–27793. doi: 10.18632/oncotarget.4813.

Engreitz, J. M., Ollikainen, N. and Guttman, M. (2016) 'Long non-coding RNAs: spatial amplifiers that control nuclear structure and gene expression', *Nature Reviews Molecular Cell Biology*, 17(12), pp. 756–770. doi: 10.1038/nrm.2016.126.

Epstein, J. I. (2018) 'Prostate cancer grading: a decade after the 2005 modified system', *Modern Pathology*, 31(1), pp. 47–63. doi: 10.1038/modpathol.2017.133.

Evans, A. J. (2018) 'Treatment effects in prostate cancer', *Modern Pathology*, 31(1), pp. 110–121. doi: 10.1038/modpathol.2017.158.

Falaschi, A., Abdurashidova, G. and Biamonti, G. (2010) 'DNA replication, development and cancer: A homeotic connection?', *Critical Reviews in Biochemistry and Molecular Biology*, 45(1) pp. 14–22. doi: 10.3109/10409230903365608.

Fearon, E. R. and Vogelstein, B. (1990) 'A genetic model for colorectal tumorigenesis', *Cell*, 61(5), pp. 759–767. doi: 10.1016/0092-8674(90)90186-I.

Flynn, R. A. and Chang, H. Y. (2014) 'Cell Stem Cell Long Noncoding RNAs in Cell-Fate Programming and Reprogramming', *Stem Cell*, 14, pp. 752–761. doi: 10.1016/j.stem.2014.05.014.

Focaccetti, C. *et al.* (2015) 'Effects of 5-Fluorouracil on Morphology, Cell Cycle, Proliferation, Apoptosis, Autophagy and ROS Production in Endothelial Cells and Cardiomyocytes', *Cell Cycle*, 10(2), p. 115686. doi: 10.1371/journal.pone.0115686.

French, J. D. *et al.* (2016) 'Germline polymorphisms in an enhancer of PSIP1 are associated with progression-free survival in epithelial ovarian cancer.', *Oncotarget*, 7(6), pp. 6353–68. doi: 10.18632/oncotarget.7047.

Fu, Z. *et al.* (2017) 'LncRNA HOTTIP modulates cancer stem cell properties in human pancreatic cancer by regulating HOXA9', *Cancer Letters,* 410, pp.68-81. doi: 10.1016/j.canlet.2017.09.019.

Funayama, R. *et al.* (2017) 'Protein-arginine deiminase 2 suppresses proliferation of colon cancer cells through protein citrullination', *Cancer Science*, 108(4), pp. 713–718. doi: 10.1111/cas.13179.

Gamat, M. and McNeel, D. G. (2017) 'Androgen deprivation and immunotherapy for the treatment of prostate cancer', *Endocrine-Related Cancer*, 24(1), pp. T297–T310. doi: 10.1530/ERC-17-0145.

Ganapathy, V., Daniels, T. and Casiano, C. A. (2003) 'LEDGF/p75: A novel nuclear autoantigen at the crossroads of cell survival and apoptosis', *Autoimmunity Reviews*, 2(5), pp. 290–297. doi: 10.1016/S1568-9972(03)00063-6.

Gandomani, H. S. *et al.* (2017) 'Colorectal cancer in the world: incidence, mortality and risk factors', *Biomedical Research and Therapy*, 4(10), p. 1656. doi:

10.15419/bmrat.v4i10.372.

Gao, R. *et al.* (2019) 'LncRNA CACS15 contributes to oxaliplatin resistance in colorectal cancer by positively regulating ABCC1 through sponging miR-145', *Archives of Biochemistry and Biophysics*, 663, pp. 183–191. doi: 10.1016/j.abb.2019.01.005.

García-Alfonso, P. *et al.* (2019) 'FOLFOXIRI plus biologics in advanced colorectal cancer', *Expert Opinion on Biological Therapy*, 19(5) pp. 411–422. doi: 10.1080/14712598.2019.1595580.

Garrett, W. S. (2019) 'The gut microbiota and colon cancer', *Science*, 364(6446), pp. 1133–1135. doi: 10.1126/science.aaw2367.

Ge, H., Si, Y. and Roeder, R. G. (1998) 'Isolation of cDNAs encoding novel transcription coactivators p52 and p75 reveals an alternate regulatory mechanism of transcriptional activation', *The EMBO Journal*, 17(22), pp. 6723–6729. doi: 10.1093/emboj/17.22.6723

Ge, H., Si, Y. and Wolffe, A. P. (1998) 'A Novel Transcriptional Coactivator, p52, Functionally Interacts with the Essential Splicing Factor ASF/SF2 a complex interplay of protein–DNA and protein–protein interactions. Once synthesis of pre-messenger RNA (pre-mRNA) is initiated in the eukaryotic nucleus, the introns must be accurately removed through splicing from pre-mRNA', *Molecular Cell*, 2, pp. 751–759. doi: 10.1016/S1097-2765(00)80290-7

Giri, V. N. and Beebe-Dimmer, J. L. (2016) 'Familial prostate cancer', *Seminars in Oncology*, 43(5), pp. 560–565. doi: 10.1053/j.seminoncol.2016.08.001.

Gonçalves-Ribeiro, S. *et al.* (2016) 'Carcinoma-associated fibroblasts affect sensitivity to oxaliplatin and 5FU in colorectal cancer cells', *Oncotarget*, 7(37), pp. 59766–59780. doi: 10.18632/oncotarget.11121.

Gordetsky, J. and Epstein, J. (2016) 'Grading of prostatic adenocarcinoma: Current state and prognostic implications', *Diagnostic Pathology*, 11(1), pp. 25. doi: 10.1186/s13000-016-0478-2.

Grozescu, T. and Popa, F. (2017) 'Prostate cancer between prognosis and adequate/proper therapy.', *Journal of medicine and life*, 10(1), pp. 5–12.

Guo, X. *et al.* (2008) 'Cell cycle perturbation and acquired 5-fluorouracil chemoresistance', *Anticancer Research*, 28(1 A), pp. 9–14.

Győrffy, B. *et al.* (2010) 'An online survival analysis tool to rapidly assess the effect of 22,277 genes on breast cancer prognosis using microarray data of 1,809 patients', *Breast Cancer Research and Treatment*, 123(3), pp. 725–731. doi: 10.1007/s10549-009-0674-9.

Hadjipetrou, A. *et al.* (2017) 'Colorectal cancer, screening and primary care: A mini literature review', *World Journal of Gastroenterology*, 23(33) pp. 6049–6058. doi: 10.3748/wjg.v23.i33.6049.

Hajjari, M. and Salavaty, A. (2015) 'HOTAIR: an oncogenic long non-coding RNA in

different cancers.', *Cancer biology & medicine*, 12(1), pp. 1–9. doi: 10.7497/j.issn.2095-3941.2015.0006.

Han, Y. *et al.* (2018) 'HOXA13 contributes to gastric carcinogenesis through DHRS2 interacting with MDM2 and confers 5-FU resistance by a p53-dependent pathway', *Molecular Carcinogenesis*, 57(6), pp. 722–734. doi: 10.1002/mc.22793.

He, Y. X. *et al.* (2017) 'HOXA13 upregulation in gastric cancer is associated with enhanced cancer cell invasion and epithelial-to-mesenchymal transition', *European review for medical and pharmacological sciences*, 21(2), pp. 258–265.

Holland, P. W. H. (2013) 'Evolution of homeobox genes', *Wiley Interdisciplinary Reviews: Developmental Biology*, 2(1), pp. 31–45. doi: 10.1002/wdev.78.

Hoover, P. and Naz, R. K. (2012) 'Do men with prostate abnormalities (prostatitis/benign prostatic hyperplasia/prostate cancer) develop immunity to spermatozoa or seminal plasma?', *International Journal of Andrology*, 35(4), pp. 608–615. doi: 10.1111/j.1365-2605.2011.01246.x.

Huang, C. Y. *et al.* (2018) 'HMGB1 promotes ERK-mediated mitochondrial Drp1 phosphorylation for chemoresistance through RAGE in colorectal cancer', *Cell Death and Disease*, 9(10), pp. 1004. doi: 10.1038/s41419-018-1019-6.

Huang, J. Z. *et al.* (2017) 'A Peptide Encoded by a Putative lncRNA HOXB-AS3 Suppresses Colon Cancer Growth', *Molecular Cell*, 68(1), pp. 171-184.e6. doi: 10.1016/j.molcel.2017.09.015.

Ignarski, M. *et al.* (2019) 'Long Non-Coding RNAs in Kidney Disease', *International Journal of Molecular Sciences*, 20(13), p. 3276. doi: 10.3390/ijms20133276.

Ilic, D. *et al.* (2018) 'Prostate cancer screening with prostate-specific antigen (PSA) test: A systematic review and meta-analysis', *BMJ (Online)*, 362. doi: 10.1136/bmj.k3519.

Iman, M. *et al.* (2016) 'HOXB7 and Hsa-miR-222 as the Potential Therapeutic Candidates for Metastatic Colorectal Cancer', *Recent Patents on Anti-Cancer Drug Discovery*, 11(4), pp. 434–443. doi: 10.2174/1574892811999160628114857.

Ito, K. *et al.* (2018) 'Does docetaxel prolong survival of patients with non-metastatic castration-resistant prostate cancer?', *Prostate*, 78(7), pp. 498–505. doi: 10.1002/pros.23493.

Jasperson, K. and Burt, R. W. (2015) 'The Genetics of Colorectal Cancer', *Surgical Oncology Clinics of North America*, 24(4), pp. 683–703. doi: 10.1016/j.soc.2015.06.006.

Jiang, H. *et al.* (2019) 'Knockdown of the long noncoding RNA HOTTIP inhibits cell proliferation and enhances cell sensitivity to cisplatin by suppressing the Wnt/β-catenin pathway in prostate cancer', *Journal of Cellular Biochemistry*, 120(6), pp. 8965–8974. doi: 10.1002/jcb.27851.

Jiang, L. *et al.* (2019) 'LncRNA HOXA-AS2 Facilitates Tumorigenesis and Progression of Papillary Thyroid Cancer by Modulating the miR-15a-5p/HOXA3 Axis', *Human*

Gene Therapy, 30(5), pp. 618–631. doi: 10.1089/hum.2018.109.

Joo, M. K., Park, J. J. and Chun, H. J. (2016) 'Impact of homeobox genes in gastrointestinal cancer', *World Journal of Gastroenterology*, 22(37), pp. 8247–8256. doi: 10.3748/wjg.v22.i37.8247.

Khalil, A. M. *et al.* (2009) 'Many human large intergenic noncoding RNAs associate with chromatin-modifying complexes and affect gene expression.', *Proceedings of the National Academy of Sciences of the United States of America*, 106(28), pp. 11667–11672. doi: 10.1073/pnas.0904715106.

Kim, K. H. and Sederstrom, J. M. (2015) 'Assaying cell cycle status using flow cytometry', *Current Protocols in Molecular Biology*, 2015, pp. 28.6.1-28.6.11. doi: 10.1002/0471142727.mb2806s111.

Kim, T. K. and Shiekhattar, R. (2016) 'Diverse regulatory interactions of long noncoding RNAs', *Current Opinion in Genetics and Development*, 36, pp. 73–82. doi: 10.1016/j.gde.2016.03.014.

Kimura, T. and Egawa, S. (2018) 'Epidemiology of prostate cancer in Asian countries', *International Journal of Urology*, 25(6), pp. 524–531. doi: 10.1111/iju.13593.

Kingston, R. E. and Tamkun, J. W. (2014) 'Transcriptional regulation by trithorax-group proteins', *Cold Spring Harbor Perspectives in Biology*, 6(10), pp. a019349. doi: 10.1101/cshperspect.a019349.

Knudsen, B. S. and Vasioukhin, V. (2010) 'Mechanisms of Prostate Cancer Initiation and Progression', in *Advances in Cancer Research*, 109(C), pp. 1–50. doi: 10.1016/B978-0-12-380890-5.00001-6.

Koh, C. M. *et al.* (2010) 'MYC and prostate cancer', *Genes and Cancer*, 1(6), pp. 617–628. doi: 10.1177/1947601910379132.

Kolligs, F. T. (2016) 'Diagnostics and Epidemiology of Colorectal Cancer', *Visceral Medicine*, 32(3), pp. 158–164. doi: 10.1159/000446488.

Koo, S. *et al.* (2017) 'The NHS Bowel Cancer Screening Program: current perspectives on strategies for improvement.', *Risk management and healthcare policy*, 10, pp. 177–187. doi: 10.2147/RMHP.S109116.

Kuipers, E. J. *et al.* (2015) 'Colorectal cancer.', *Nature reviews. Disease primers*, 1, p. 15065. doi: 10.1038/nrdp.2015.65.

De Kumar, B. and Krumlauf, R. (2016) 'HOXs and lincRNAs: Two sides of the same coin.', *Science advances*, 2(1), p. e1501402. doi: 10.1126/sciadv.1501402.

Lappin, T. R. J. *et al.* (2006) 'HOX genes: seductive science, mysterious mechanisms.', *The Ulster medical journal*, 75(1), pp. 23–31.

Lee, Y. J. *et al.* (2019) 'Long noncoding RNA HOTTIP overexpression: A potential prognostic biomarker in prostate cancer', *Pathology Research and Practice*, 215(11), p. 152649. doi: 10.1016/j.prp.2019.152649.

Leong, H. S., Chambers, A. F. and Lewis, J. D. (2012) 'Assessing cancer cell migration

and metastatic growth in vivo in the chick embryo using fluorescence intravital imaging', *Methods in Molecular Biology*, 872, pp. 1–14. doi: 10.1007/978-1-61779-797-2_1.

Li, C. *et al.* (2017) 'TUG1 mediates methotrexate resistance in colorectal cancer via miR-186/CPEB2 axis', *Biochemical and Biophysical Research Communications*, 491(2), pp. 552–557. doi: 10.1016/j.bbrc.2017.03.042.

Li, Q. *et al.* (2018) 'Over-expressed lncRNA HOTAIRM1 promotes tumor growth and invasion through up-regulating HOXA1 and sequestering G9a/EZH2/Dnmts away from the HOXA1 gene in glioblastoma multiforme', *Journal of Experimental & Clinical Cancer Research*, 37(1), p. 265. doi: 10.1186/s13046-018-0941-x.

Li, Z. *et al.* (2015) 'The long non-coding RNA HOTTIP promotes progression and gemcitabine resistance by regulating HOXA13 in pancreatic cancer', *Journal of Translational Medicine*, 13(1), p. 84. doi: 10.1186/s12967-015-0442-z.

Li, Z. *et al.* (2017) 'Integrated Analysis of Long Non-coding RNAs (LncRNAs) and mRNA Expression Profiles Reveals the Potential Role of LncRNAs in Skeletal Muscle Development of the Chicken', *Frontiers in Physiology*, 7, p. 687. doi: 10.3389/fphys.2016.00687.

Li, Z., Zhao, L. and Wang, Q. (2016) 'Overexpression of long non-coding RNA HOTTIP increases chemoresistance of osteosarcoma cell by activating the Wnt/β-catenin pathway', *American Journal of Translational Research*, 8(5), p. 2385.

Lian, Y; Cai, Z; Gong, H. (2016) 'HOTTIP: a critical oncogenic long non-coding RNA in human cancers', *Mol. BioSyst*, 12, pp. 3247–3253. doi: 10.1039/c6mb00475j

Lin, Y. *et al.* (2007) 'Up-regulation of Bcl-2 is required for the progression of prostate cancer cells from an androgen-dependent to an androgen-independent growth stage', *Cell Research*, 17(6), pp. 531–536. doi: 10.1038/cr.2007.12.

Litwin, M. S. and Tan, H. J. (2017) 'The diagnosis and treatment of prostate cancer: A review', *Journal of the American Medical Association,* 317(24), pp. 2532–2542. doi: 10.1001/jama.2017.7248.

Liu, C. *et al.* (2018) 'Long Non-coding RNA DLEU1 Promotes Proliferation and Invasion by Interacting With miR-381 and Enhancing HOXA13 Expression in Cervical Cancer', *Frontiers in Genetics*, 9, pp. 629. doi: 10.3389/fgene.2018.00629.

Liu, T. *et al.* (2018) 'Knockdown of the long non-coding RNA HOTTIP inhibits colorectal cancer cell proliferation and migration and induces apoptosis by targeting SGK1', *Biomedicine and Pharmacotherapy*, 98, pp. 286–296. doi: 10.1016/j.biopha.2017.12.064.

Longley, D. B., Harkin, D. P. and Johnston, P. G. (2003) '5-Fluorouracil: Mechanisms of action and clinical strategies', *Nature Reviews Cancer,* 3(5), pp. 330–338. doi: 10.1038/nrc1074.

Luo, Z. *et al.* (2017) 'A Prostate Cancer Risk Element Functions as a Repressive Loop that Regulates HOXA13', *Cell Reports*, 21(6), pp. 1411–1417. doi: 10.1016/j.celrep.2017.10.048.

Malek, R. *et al.* (2017) 'TWIST1-WDR5-Hottip regulates Hoxa9 chromatin to facilitate prostate cancer metastasis', *Cancer Research*, 77(12), pp. 3181-3193. doi: 10.1158/0008-5472.CAN-16-2797.

Mansour, M. A. and Senga, T. (2017) 'HOXD8 exerts a tumor-suppressing role in colorectal cancer as an apoptotic inducer', *International Journal of Biochemistry and Cell Biology*, 88, pp. 1–13. doi: 10.1016/j.biocel.2017.04.011.

Marley, A. R. and Nan, H. (2016) 'Epidemiology of colorectal cancer', *Int J Mol Epidemiol Genet*, 7(3), pp. 105–114. doi: 10.2169/naika.96.200.

Mármol, I. *et al.* (2017) 'Colorectal carcinoma: A general overview and future perspectives in colorectal cancer', *International Journal of Molecular Sciences*, 18(1), pp.197. doi: 10.3390/ijms18010197.

Marshall, H. M. *et al.* (2007) 'Role of PSIP 1/LEDGF/p75 in lentiviral infectivity and integration targeting', *PLoS ONE*, 2(12), pp. e1340. doi: 10.1371/journal.pone.0001340.

Masoodi, K. Z. *et al.* (2017) 'Inhibition of Androgen Receptor Nuclear Localization and Castration Resistant Prostate Tumor Growth by Pyrroloimidazole-Based Small Molecules HHS Public Access', *Molecular Cancer Ther*apy 16(10), pp. 2120–2129. doi: 10.1158/1535-7163.MCT-17-0176.

McQuade, R. M. *et al.* (2017) 'Colorectal Cancer Chemotherapy: The Evolution of Treatment and New Approaches', *Current Medicinal Chemistry*, 24(15), pp. 1537-1557. doi: 10.2174/0929867324666170111152436.

Mercader, M. *et al.* (2001) 'T cell infiltration of the prostate induced by androgen withdrawal in patients with prostate cancer', *Proceedings of the National Academy of Sciences of the United States of America*, 98(25), pp. 14565–14570. doi: 10.1073/pnas.251140998.

Metcalfe, M. J. *et al.* (2017) 'Role of radical prostatectomy in metastatic prostate cancer: A review', *Urologic Oncology: Seminars and Original Investigations*, 35(4), pp. 125–134. doi: 10.1016/j.urolonc.2017.01.001.

Mike, M. and Kano, N. (2015) 'Laparoscopic surgery for colon cancer: a review of the fascial composition of the abdominal cavity', *Surgery Today*, 45(2), pp. 129–139. doi: 10.1007/s00595-014-0857-9.

Milne, T. A. *et al.* (2002) 'MLL targets SET domain methyltransferase activity to Hox gene promoters', *Molecular Cell*, 10(5), pp. 1107–1117. doi: 10.1016/S1097-2765(02)00741-4.

Misawa, A., Takayama, K.-I. and Inoue, S. (2017) 'Long non-coding RNAs and prostate cancer.', *Cancer science*, 108(11), pp. 2107–2114. doi: 10.1111/cas.13352.

Misawa, A., Takayama, K. I. and Inoue, S. (2017) 'Long non-coding RNAs and prostate cancer', *Cancer Science*, 108(11), pp. 2107–2114. doi: 10.1111/cas.13352.

Mohr, A. *et al.* (2019) 'Msc.Strail has better eficacy than msc.fl-trail and in combination with akti blocks pro-metastatic cytokine production in prostate cancer

cells', *Cancers*, 11(4), pp. 568. doi: 10.3390/cancers11040568.

Motrich, R. D. *et al.* (2018) 'Implications of prostate inflammation on male fertility', *Andrologia*, 50(11), p. e13093. doi: 10.1111/and.13093.

Nader, R., El Amm, J. and Aragon-Ching, J. (2018) 'Role of chemotherapy in prostate cancer', *Asian Journal of Andrology*, 20(3), pp. 221–229. doi: 10.4103/aja.aja_40_17.

Nguyen, H. T. and Duong, H.-Q. (2018) 'The molecular characteristics of colorectal cancer: Implications for diagnosis and therapy', *Oncology Letters*, 16(1), p. 9. doi: 10.3892/OL.2018.8679.

Oehme, F. *et al.* (2019) 'Low level of exosomal long non-coding RNA HOTTIP is a prognostic biomarker in colorectal cancer', *RNA Biology*, 16(10), pp. 1339–1345. doi: 10.1080/15476286.2019.1637697.

Oppelt, K. A. *et al.* (2019) 'Incidence of advanced colorectal cancer in Germany: comparing claims data and cancer registry data', *BMC Medical Research Methodology*, 19(1), p. 142. doi: 10.1186/s12874-019-0784-y.

Pal, R. P. and Koupparis, A. J. (2018) 'Expanding the indications of robotic surgery in urology: A systematic review of the literature', *Arab Journal of Urology*. Arab Association of Urology, 16(3), pp. 270–284. doi: 10.1016/j.aju.2018.05.005.

Peek, S. L., Mah, K. M. and Weiner, J. A. (2017) 'Regulation of neural circuit formation by protocadherins', *Cellular and Molecular Life Sciences*, 74(22), pp. 4133–4157. doi: 10.1007/s00018-017-2572-3.

Pentyala, Srinivas *et al.* (2016) 'Prostate cancer markers: An update (Review)', *Biomedical Reports*, 4(3), pp. 263–268. doi: 10.3892/br.2016.586.

Pernar, C. H. *et al.* (2018) 'The Epidemiology of Prostate Cancer', *Cold Spring Harbor perspectives in medicine*, 8(12), p. a030361. doi: 10.1101/cshperspect.a030361.

Peters, G. J. *et al.* (2002) 'Induction of thymidylate synthase as a 5-fluorouracil resistance mechanism', *Molecular Basis of Disease*, 1587(2-3), pp. 194–205. doi: 10.1016/S0925-4439(02)00082-0.

Placzek, W. J. *et al.* (2010) 'A survey of the anti-apoptotic Bcl-2 subfamily expression in cancer types provides a platform to predict the efficacy of Bcl-2 antagonists in cancer therapy', *Cell Death and Disease*, 1(5), p. 1. doi: 10.1038/cddis.2010.18.

Pontes, J. E., Huben, R. and Wolf, R. (1986) 'Sexual function after radical prostatectomy', *The Prostate*, 8(2), pp. 123–126. doi: 10.1002/pros.2990080203.

Pradeepa, M. M. *et al.* (2012) 'Psip1/Ledgf p52 Binds Methylated Histone H3K36 and Splicing Factors and Contributes to the Regulation of Alternative Splicing', *PLoS Genetics*, 8(5), p. e1002717. doi: 10.1371/journal.pgen.1002717.

Pradeepa, M. M. *et al.* (2014) 'Psip1/Ledgf p75 restrains Hox gene expression by recruiting both trithorax and polycomb group proteins', *Nucleic Acids Research*, 42(14), pp. 9021–9032. doi: 10.1093/nar/gku647.

Pradeepa, M. M. *et al.* (2017) 'Psip1/p52 regulates posterior Hoxa genes through

activation of lncRNA Hottip', *PLOS Genetics*, 13(4), p. e1006677. doi: 10.1371/journal.pgen.1006677.

Puck, T. T. and Marcu, P. I. (1956) 'Action of x-rays on mammalian cells', *The Journal of experimental medicine*, 103(5), pp. 653–666. doi: 10.1084/jem.103.5.653.

Qi, P., Zhou, X.-Y. and Du, X. (2016) 'Circulating long non-coding RNAs in cancer: current status and future perspectives.', *Molecular cancer*, 15(1), p. 39. doi: 10.1186/s12943-016-0524-4.

Qin, Z. *et al.* (2019) 'Elevated HOXA13 expression promotes the proliferation and metastasis of gastric cancer partly via activating Erk1/2', *OncoTargets and Therapy*, 12, pp. 1803–1813. doi: 10.2147/OTT.S196986.

Quagliata, L. *et al.* (2015) 'lncRNA HOTTIP / HOXA13 expression is associated with disease progression and predicts outcome in hepatocellular carcinoma patients*', Heptatology*, 59(3), pp. 911–923. doi: 10.1002/hep.26740.lncRNA.

Quagliata, L. *et al.* (2018) 'High expression of HOXA13 correlates with poorly differentiated hepatocellular carcinomas and modulates sorafenib response in in vitro models', *Laboratory Investigation*, 98(1), pp. 95–105. doi: 10.1038/labinvest.2017.107.

Quinn, J. J. and Chang, H. Y. (2016) 'Unique features of long non-coding RNA biogenesis and function', *Nature Publishing Group*, 17, pp. 47-62. doi: 10.1038/nrg.2015.10.

Rafehi, H. *et al.* (2011) 'Clonogenic assay: Adherent cells', *Journal of Visualized Experiments*, (49), pp. 2573. doi: 10.3791/2573.

Rawla, P. (2019) 'Epidemiology of Prostate Cancer', *World Journal of Oncology,* 10(2), pp. 63–89. doi: 10.14740/wjon1191.

Rebbeck, T. R. (2017) 'Prostate Cancer Genetics: Variation by Race, Ethnicity, and Geography', *Seminars in Radiation Oncology*, 27(1), pp. 3–10. doi: 10.1016/j.semradonc.2016.08.002.

Ren, Y.-K. *et al.* (2015) 'Association of long non-coding RNA HOTTIP with progression and prognosis in colorectal cancer.', *International journal of clinical and experimental pathology*, 8(9), pp. 11458–63.

Riccardi, C. and Nicoletti, I. (2006) 'Analysis of apoptosis by propidium iodide staining and flow cytometry', *Nature Protocols*, 1(3), pp. 1458–1461. doi: 10.1038/nprot.2006.238.

Rinn, J. L. *et al.* (2007) 'Functional Demarcation of Active and Silent Chromatin Domains in Human HOX Loci by Noncoding RNAs', *Cell*, 129(7), pp. 1311–1323. doi: 10.1016/j.cell.2007.05.022.

Rinn, J. L. and Chang, H. Y. (2012) 'Genome regulation by long noncoding RNAs.', *Annual review of biochemistry*, 81, pp. 145–66. doi: 10.1146/annurev-biochem-051410-092902.

Ríos-Colón, L. *et al.* (2017) 'Targeting the stress oncoprotein LEDGF/p75 to sensitize chemoresistant prostate cancer cells to taxanes', *Oncotarget,* 8(15), pp. 24915–24931. doi: 10.18632/oncotarget.15323.

Romero-Otero, J. *et al.* (2016) 'Active surveillance for prostate cancer', *International Journal of Urology*, 23(3), pp. 211–218. doi: 10.1111/iju.13016.

Rose, M. G., Farrell, M. P. and Schmitz, J. C. (2002) 'Thymidylate synthase: A critical target for cancer chemotherapy', *Clinical Colorectal Cancer*, 1(4), pp. 220–229. doi: 10.3816/CCC.2002.n.003.

Rui, Y. *et al.* (2019) 'LncRNA HOTTIP mediated DKK1 downregulation confers metastasis and invasion in colorectal cancer cells', *Histology and Histopathology*, 34(6), pp. 619–630. doi: 10.14670/HH-18-043.

Saltz, L. B. (2016) 'Value in colorectal cancer treatment: Where it is lacking, and why', *Cancer Journal (United States)*, 22(3), pp. 232–235. doi: 10.1097/PPO.0000000000000194.

Schatoff, E. M., Leach, B. I. and Dow, L. E. (2017) 'WNT Signaling and Colorectal Cancer', *Current Colorectal Cancer Reports*, 13(2), pp. 101–110. doi: 10.1007/s11888-017-0354-9.

Schindelin, J. *et al.* (2012) 'Fiji: An open-source platform for biological-image analysis', *Nature Methods*, 9(7), pp. 676–682. doi: 10.1038/nmeth.2019.

Schroder, K. *et al.* (2004) 'Interferon-γ: an overview of signals, mechanisms and functions', *Journal of Leukocyte Biology*, 75(2), pp. 163–189. doi: 10.1189/jlb.0603252.

Shah, N. and Sukumar, S. (2010) 'The Hox genes and their roles in oncogenesis', *Nature Reviews Cancer*, 10(5), pp. 361–371. doi: 10.1038/nrc2826.

Sharifi, N. *et al.* (2016) 'HER2 gene amplification in patients with prostate cancer: Evaluating a CISH-based method', *Oncology Letters*, 12(6), pp. 4643–4650. doi: 10.3892/ol.2016.5235.

Shen, L. Y. and Chen, K. N. (2011) 'Exploration of target genes of HOXA13 in esophageal squamous cell carcinoma cell line', *Cancer Letters*, 312(1), pp. 18–23. doi: 10.1016/j.canlet.2011.07.020.

Shen, M., Li, M. and Liu, J. (2019) 'Long noncoding RNA HOTTIP promotes nasopharyngeal cancer cell proliferation, migration, and invasion by inhibiting miR-4301', *Medical Science Monitor*, 25, pp. 778–785. doi: 10.12659/MSM.912728.

Shi, Q. *et al.* (2018) 'Downregulation of HOXA13 sensitizes human esophageal squamous cell carcinoma to chemotherapy', *Thoracic Cancer*, 9(7), pp. 836–846. doi: 10.1111/1759-7714.12758.

Singh, Deepak K. *et al.* (2017) 'PSIP1/p75 promotes tumorigenicity in breast cancer cells by promoting the transcription of cell cycle genes', *Carcinogenesis*, 38(10), pp. 966–975. doi: 10.1093/carcin/bgx062.

Singh, Deepak K *et al.* (2017) 'PSIP1/p75 promotes tumorigenicity in breast cancer cells by promoting the transcription of cell cycle genes', *Carcinogenesis*, 38(10), pp. 966–975. doi: 10.1093/carcin/bgx062.

Smith, J., Zyoud, A. and Allegrucci, C. (2019) 'A case of identity: Hox genes in normal and cancer stem cells', *Cancers*, 11(4). doi: 10.3390/cancers11040512.

Stone, K. R. *et al.* (1978) 'Isolation of a human prostate carcinoma cell line (DU 145)', *International Journal of Cancer*, 21(3), pp. 274–281. doi: 10.1002/ijc.2910210305.

Sulaiman, S. and Marciani, L. (2019) 'MRI of the Colon in the Pharmaceutical Field: The Future before us', *Pharmaceutics,* 11(4), pp. 146. doi: 10.3390/pharmaceutics11040146.

Sun, Y., Zeng, C., *et al.* (2018) 'LncRNA HOTTIP-Mediated HOXA11 Expression Promotes Cell Growth, Migration and Inhibits Cell Apoptosis in Breast Cancer.', *International journal of molecular sciences*, 19(2), pp. 472. doi: 10.3390/ijms19020472.

Sun, Y., Hu, B., *et al.* (2018) 'Long non-coding RNA HOTTIP promotes BCL-2 expression and induces chemoresistance in small cell lung cancer by sponging miR-216a', *Cell Death and Disease*, 9(2), pp. 85. doi: 10.1038/s41419-017-0113-5.

Sutherland, H. G. *et al.* (2006) 'Disruption of Ledgf/Psip1 Results in Perinatal Mortality and Homeotic Skeletal Transformations', *Molecular and Cellular Biology* 26(19), pp. 7201–7210. doi: 10.1128/MCB.00459-06.

Tabaczar, S. *et al.* (2010) '[Molecular mechanisms of antitumor activity of taxanes. I. Interaction of docetaxel with microtubules].', *Postepy higieny i medycyny doswiadczalnej (Online)*, 64, pp. 568–81.

Taitt, H. E. (2018) 'Global Trends and Prostate Cancer: A Review of Incidence, Detection, and Mortality as Influenced by Race, Ethnicity, and Geographic Location', *American Journal of Men's Health*, 12(6), pp. 1807–1823. doi: 10.1177/1557988318798279.

Tamura, R. E. *et al.* (2018) 'Improving adenoviral vectors and strategies for prostate cancer gene therapy', *Clinics*, 73, pp. e476s. doi: 10.6061/clinics/2018/e476s.

Tao, L. *et al.* (2019) 'ARHGAP25: A negative regulator of colorectal cancer (CRC) metastasis via the Wnt/β-catenin pathway', *European Journal of Pharmacology*, 858, p. 172476. doi: 10.1016/J.EJPHAR.2019.172476.

Tatangelo, F. *et al.* (2018) 'Posterior HOX genes and HOTAIR expression in the proximal and distal colon cancer pathogenesis', *Journal of Translational Medicine*, 16(1), p. 350. doi: 10.1186/s12967-018-1725-y.

Teo, M. Y., Rathkopf, D. E. and Kantoff, P. (2019) 'Treatment of Advanced Prostate Cancer', *Annual Review of Medicine*, 70(1), pp. 479–499. doi: 10.1146/annurev-med-051517-011947.

Terry, S. *et al.* (2013) 'Cross modulation between the androgen receptor axis and protocadherin-PC in mediating neuroendocrine transdifferentiation and therapeutic

resistance of prostate cancer', *Neoplasia (United States)*, 15(7), pp. 761–772. doi: 10.1593/neo.122070.

Testa, U., Pelosi, E. and Castelli, G. (2018) 'Colorectal Cancer: Genetic Abnormalities, Tumor Progression, Tumor Heterogeneity, Clonal Evolution and Tumor-Initiating Cells', *Medical Sciences*, 6(2), p. 31. doi: 10.3390/medsci6020031.

Thrymurthy, S. G. *et al.* (2016) 'Colorectal adenocarcinoma: risks, prevention and diagnosis', *The British Journal of Medicine*, 354, pp. i3590. doi: 10.1136/bmj.i3590

Tinevez, J. Y. *et al.* (2017) 'TrackMate: An open and extensible platform for single-particle tracking', *Methods*, 115, pp. 80–90. doi: 10.1016/j.ymeth.2016.09.016.

Todd, R. C. and Lippard, S. J. (2009) 'Inhibition of transcription by platinum antitumor compounds', *Metallomics*, 1(4), pp. 280–291. doi: 10.1039/b907567d.

Triantafillidis, J. K., Nasioulas, G. and Kosmidid, P. A. (2009) 'Colorectal Cancer and Inflammatory Bowel Disease: Epidemiology, Risk Factors, Mechanisms of Carcinogenesis and Prevention Strategies', *Anticancer Research*, 29(7), pp. 2727–2737.

Van Triest, B. *et al.* (1999) 'Thymidylate Synthase Level as the Main Predictive Parameter for Sensitivity to 5-Fluorouracil, but not for Folate-based Thymidylate Synthase Inhibitors, in 13 Nonselected Colon Cancer Cell Lines', *Clinical Cancer Research,* 5(3), pp.643-654.

 Valderrama-Treviño, A. I. *et al.* (2017) 'Hepatic Metastasis from Colorectal Cancer.', *Euroasian journal of hepato-gastroenterology*, 7(2), pp. 166–175. doi: 10.5005/jp-journals-10018-1241.

Verze, P., Cai, T. and Lorenzetti, S. (2016) 'The role of the prostate in male fertility, health and disease', *Nature Reviews Urology*, 13(7), pp. 379–386. doi: 10.1038/nrurol.2016.89.

Wang, G. *et al.* (2018) 'Genetics and biology of prostate cancer', *Genes and Development*, 32(17-18), pp. 1105–1140. doi: 10.1101/gad.315739.118.

Wang, K. C. *et al.* (2011) 'A long noncoding RNA maintains active chromatin to coordinate homeotic gene expression.', *Nature*, 472(7341), pp. 120–4. doi: 10.1038/nature09819.

Wang, K. C. and Chang, H. Y. (2011) 'Molecular mechanisms of long noncoding RNAs.', *Molecular cell*, 43(6), pp. 904–14. doi: 10.1016/j.molcel.2011.08.018.

Wang, M. *et al.* (2019) 'Long non-coding RNA TUG1 mediates 5-Fluorouracil resistance by acting as a ceRNA of mir-197-3p in colorectal cancer', *Journal of Cancer*, 10(19), pp. 4603–4613. doi: 10.7150/jca.32065.

Wang, Yuan *et al.* (2016) 'miR-375 induces docetaxel resistance in prostate cancer by targeting SEC23A and YAP1', *Molecular Cancer*, 15(1). doi: 10.1186/s12943-016-0556-9.

Wang, Yingchao *et al.* (2016) 'The function of ho meobox genes and lncRNAs in

cancer (Review)', *Oncology Letters*, 12(3), pp. 1635–1641. doi: 10.3892/ol.2016.4901.

Watanabe, Y. *et al.* (2018) 'Upregulated HOXA9 expression is associated with lymph node metastasis in colorectal cancer', *Oncology Letters*, 15(3), pp. 2756–2762. doi: 10.3892/ol.2017.7650.

Wei, L. *et al.* (2019) 'The emerging role of noncoding RNAs in colorectal cancer chemoresistance', *Cellular Oncology*, 42(6), pp. 757–768. doi: 10.1007/s13402-019-00466-8.

Wen, Y. *et al.* (2018) 'The prognostic value of HOXA13 in solid tumors: A meta-analysis', *Clinica Chimica Acta*, 483, pp. 64–68. doi: 10.1016/j.cca.2018.04.024.

William-Faltaos, S. *et al.* (2007) 'Cell cycle arrest by oxaliplatin on cancer cells', *Fundamental and Clinical Pharmacology*, 21(2), pp. 165–172. doi: 10.1111/j.1472-8206.2007.00462.x.

Wlodarska, M., Kostic, A. D. and Xavier, R. J. (2015) 'An integrative view of microbiome-host interactions in inflammatory bowel diseases.', *Cell host & microbe*, 17(5), pp. 577–91. doi: 10.1016/j.chom.2015.04.008.

Woenckhaus, J. and Fenic, I. (2008) 'Proliferative inflammatory atrophy: a background lesion of prostate cancer?', *Andrologia*, 40(2), pp. 134–137. doi: 10.1111/j.1439-0272.2007.00831.x.

Wolpin, B. M. and Mayer, R. J. (2008) 'Systemic Treatment of Colorectal Cancer', *Gastroenterology*, 134(5), pp. 1296. doi: 10.1053/j.gastro.2008.02.098.

Woods-Burnham, L. *et al.* (2018) 'Glucocorticoids Induce Stress Oncoproteins Associated with Therapy-Resistance in African American and European American Prostate Cancer Cells', *Scientific Reports*, 8(1), pp. 1–15. doi: 10.1038/s41598-018-33150-2.

Wyatt, M. D. and Wilson, D. M. (2009) 'Participation of DNA repair in the response to 5-fluorouracil', *Cellular and Molecular Life Sciences*, 66(5), pp. 788–799. doi: 10.1007/s00018-008-8557-5.

Xie, B. *et al.* (2019) 'Tumor-suppressive function and mechanism of HOXB13 in right-sided colon cancer', *Signal Transduction and Targeted Therapy*, 4(1), pp. 51. doi: 10.1038/s41392-019-0086-1.

Yamamoto, S. *et al.* (2019) 'Hoxa13 regulates expression of common Hox target genes involved in cartilage development to coordinate the expansion of the autopodal anlage', *Development Growth and Differentiation*, 61(3), pp. 228–251. doi: 10.1111/dgd.12601.

Yang, B. *et al.* (2018) 'Long non-coding RNA HOTTIP promotes prostate cancer cells proliferation and migration by sponging miR-216a-5p.', *Bioscience reports*, 38(5). doi: 10.1042/BSR20180566.

Yang, Y. *et al.* (2017) 'The prognostic value of long noncoding RNA HOTTIP on clinical outcomes in breast cancer.', *Oncotarget*, 8(4), pp. 6833–6844. doi:

10.18632/oncotarget.14304.

Yeh, Y. *et al.* (2019) 'Wnt/Beta-Catenin Signaling and Prostate Cancer Therapy Resistance', in *Advances in Experimental Medicine and Biology*, 1210, pp. 351–378. doi: 10.1007/978-3-030-32656-2_16.

Ying, Y. *et al.* (2020) 'Oncogenic HOXB8 is driven by MYC-regulated super-enhancer and potentiates colorectal cancer invasiveness via BACH1', *Oncogene*, 39(5), pp. 1004–1017. doi: 10.1038/s41388-019-1013-1.

Yokoyama, A. and Cleary, M. L. (2008) 'Menin Critically Links MLL Proteins with LEDGF on Cancer-Associated Target Genes', *Cancer Cell*, 14(1), pp. 36–46. doi: 10.1016/j.ccr.2008.05.003.

Young, S. M. *et al.* (2015) 'Systematic review of clinical features of suspected prostate cancer in primary care', *Canadian Family Physician*, 61(1), pp. e26–e35.

Yuan, Q. *et al.* (2018) 'LncRNA HOTTIP promotes papillary thyroid carcinoma cell proliferation, invasion and migration by regulating miR-637', *International Journal of Biochemistry and Cell Biology*, 98, pp. 1–9. doi: 10.1016/j.biocel.2018.02.013.

Yuzhalin, A. E. (2019) 'Citrullination in cancer', *Cancer Research*, 79(7), pp. 1274–1284. doi: 10.1158/0008-5472.CAN-18-2797.

Zarour, L. R. *et al.* (2017) 'Colorectal Cancer Liver Metastasis: Evolving Paradigms and Future Directions.', *Cellular and molecular gastroenterology and hepatology*, 3(2), pp. 163–173. doi: 10.1016/j.jcmgh.2017.01.006.

Zellweger, M. *et al.* (2018) 'Surgical treatment of pulmonary metastasis in colorectal cancer patients: Current practice and results', *Critical Reviews in Oncology/Hematology*, 127, pp. 105–116. doi: 10.1016/j.critrevonc.2018.05.001.

Zhang, N. *et al.* (2008) '5-Fluorouracil: Mechanisms of resistance and reversal strategies', *Molecules*, 13(8), pp. 1551–1569. doi: 10.3390/molecules13081551.

Zhang, S.-R. *et al.* (2016) 'Long noncoding RNA HOTTIP contributes to the progression of prostate cancer by regulating HOXA13.', *Cellular and molecular biology*, 62(3), pp. 84–8. doi: 10.14715/cmb/2016.62.3.14.

Zhang, Y. *et al.* (2018) 'Seasonal expression of 5α-reductases and androgen receptor in the prostate gland of the wild ground squirrel (Spermophilus dauricus)', *Comparative Biochemistry and Physiology -Part A : Molecular and Integrative Physiology*, 226, pp. 11–16. doi: 10.1016/j.cbpa.2018.06.023.

Zhao, Q. *et al.* (2019) 'TCF7L2 activated HOXA-AS2 decreased the glucocorticoid sensitivity in acute lymphoblastic leukemia through regulating HOXA3/EGFR/Ras/Raf/MEK/ERK pathway', *Biomedicine and Pharmacotherapy*, 109, pp. 1640–1649. doi: 10.1016/j.biopha.2018.10.046.

Zhou, P. *et al.* (2016) 'Roles of Non-Coding RNAs in Acute Kidney Injury', *Kidney Blood Pressure Res*earch, 41, pp. 757–769. doi: 10.1159/000450566.

Zhu, J. J. *et al.* (2013) 'Function of lncRNAs and approaches to lncRNA-protein

interactions', *Science China Life Sciences*, 56(10), pp. 876–885. doi: 10.1007/s11427-013-4553-6.

Zhuang, M. F., Li, L. J. and Ma, J. B. (2019) 'LncRNA HOTTIP promotes proliferation and cell cycle progression of acute myeloid leukemia cells', *European Review for Medical and Pharmacological Sciences*, 23(7), pp. 2908–2915. doi: 10.26355/eurrev_201904_17569.

Zong, X. *et al.* (2015) 'Knockdown of nuclear-retained long noncoding RNAs using modified DNA antisense oligonucleotides', *Methods in Molecular Biology*, 1262, pp. 321–331. doi: 10.1007/978-1-4939-2253-6_20.

8 Supplementary information

Table 8.1 RNA-Seq upregulated genes

Probe	Chromosome	ID	P-value	FDR	Log2Fold	WT RPKM			HOTTIP KO RPKM		
HSD3B7	16	ENSG00000099377	4.65E-04	7.65E-03	-0.62	161	139	196	226	207	265
MOK	14	ENSG00000080823	4.04E-06	1.28E-04	-0.62	278	297	343	409	424	449
HIST1H2BD	6	ENSG00000158373	1.65E-04	3.19E-03	-0.62	158	161	189	234	203	282
AC090607.4	15	ENSG00000272418	2.38E-04	4.34E-03	-0.62	136	171	174	225	183	272
CILP2	19	ENSG00000160161	4.39E-08	2.15E-06	-0.63	937	772	1122	1271	1217	1521
ZNF703	8	ENSG00000183779	6.42E-06	1.91E-04	-0.63	318	304	453	467	497	541
FKBP11	12	ENSG00000134285	3.24E-08	1.65E-06	-0.63	543	698	739	945	688	1183
NKX1-2	10	ENSG00000229544	2.68E-06	8.97E-05	-0.63	309	393	339	471	479	519
DNAJB5	9	ENSG00000137094	3.47E-07	1.43E-05	-0.63	294	328	346	422	412	542
AP003419.1	11	ENSG00000256514	3.10E-05	7.61E-04	-0.63	163	227	235	284	247	353
FOXA3	19	ENSG00000170608	3.31E-06	1.08E-04	-0.63	241	283	290	387	352	411
PROS1	3	ENSG00000184500	5.39E-09	3.03E-07	-0.63	517	710	695	832	908	958
OR51B4	11	ENSG00000183251	2.94E-07	1.24E-05	-0.63	289	426	394	509	462	596
AP000924.1	11	ENSG00000254416	4.98E-04	8.08E-03	-0.64	137	136	144	185	175	238
PTRH1	9	ENSG00000187024	1.86E-05	4.89E-04	-0.64	199	227	328	338	318	407
CACNB1	17	ENSG00000067191	2.57E-08	1.34E-06	-0.64	364	440	527	633	576	666
IGFBP6	12	ENSG00000167779	1.94E-07	8.54E-06	-0.64	510	450	595	683	722	812
AC013394.1	15	ENSG00000279765	4.75E-09	2.69E-07	-0.64	469	678	614	790	697	1032
SCML1	X	ENSG00000047634	1.81E-09	1.09E-07	-0.64	432	616	576	746	666	902
SLC38A5	X	ENSG00000017483	2.93E-12	2.35E-10	-0.64	905	899	1087	1280	1301	1553
ROMO1	20	ENSG00000125995	9.79E-07	3.66E-05	-0.65	753	648	1011	1111	1166	1131
RRAD	16	ENSG00000166592	5.27E-04	8.49E-03	-0.65	138	148	216	269	181	265

DNLZ	9	ENSG00000213221	6.57E-05	1.46E-03	-0.65	239	202	298	362	334	358
AL353689.2	1	ENSG00000233706	7.93E-05	1.72E-03	-0.65	141	209	211	231	233	342
HIST3H2A	1	ENSG00000181218	1.78E-06	6.16E-05	-0.65	267	287	322	394	419	440
PDLIM3	4	ENSG00000154553	4.25E-06	1.34E-04	-0.66	209	224	270	304	301	411
AC000123.3	7	ENSG00000280347	1.66E-04	3.20E-03	-0.66	128	203	178	245	198	290
PLEKHO1	1	ENSG00000023902	1.54E-09	9.33E-08	-0.66	368	482	541	611	634	752
PEX11A	15	ENSG00000166821	3.18E-05	7.82E-04	-0.67	140	209	236	260	258	322
AC018665.1	17	ENSG00000279382	1.92E-05	5.02E-04	-0.67	190	234	226	317	239	398
AL355916.3	14	ENSG00000258989	1.12E-04	2.29E-03	-0.67	151	191	232	318	226	281
KREMEN2	16	ENSG00000131650	7.93E-07	3.03E-05	-0.67	445	441	704	731	769	780
ARL4D	17	ENSG00000175906	3.18E-06	1.04E-04	-0.67	395	355	546	621	631	613
OPLAH	8	ENSG00000178814	4.41E-05	1.03E-03	-0.67	247	222	396	437	344	472
TAF3	10	ENSG00000165632	8.12E-12	6.16E-10	-0.68	625	768	936	1053	1102	1208
MRVI1	11	ENSG00000072952	9.48E-14	8.89E-12	-0.68	708	908	934	1214	1163	1323
ACAD11	3	ENSG00000240303	1.20E-11	8.95E-10	-0.68	599	827	786	1032	880	1341
CYTOR	2	ENSG00000222041	1.82E-06	6.29E-05	-0.68	334	348	385	511	544	495
SSC4D	7	ENSG00000146700	2.96E-04	5.22E-03	-0.68	99	139	179	205	175	224
AL451085.2	1	ENSG00000271380	1.95E-09	1.16E-07	-0.69	327	391	416	541	473	656
SYDE1	19	ENSG00000105137	2.50E-05	6.34E-04	-0.69	196	210	293	265	338	423
WTIP	19	ENSG00000142279	1.11E-08	6.09E-07	-0.69	328	338	410	505	452	634
EEF1AKMT3	12	ENSG00000123427	2.66E-06	8.89E-05	-0.69	205	222	274	291	321	423
GPR162	12	ENSG00000250510	1.04E-05	2.92E-04	-0.69	195	208	259	356	258	360
KIAA1614	1	ENSG00000135835	8.39E-06	2.41E-04	-0.69	155	188	211	265	233	318
SCUBE1	22	ENSG00000159307	4.94E-04	8.03E-03	-0.69	92	166	194	187	212	257
TBC1D3P1-DHX40P1	17	ENSG00000267104	5.54E-05	1.26E-03	-0.69	199	196	192	270	300	298
ZBED6CL	7	ENSG00000188707	4.50E-08	2.19E-06	-0.70	525	465	535	781	706	787

TM2D3	15	ENSG00000184277	1.20E-15	1.35E-13	-0.70	668	781	820	1041	1019	1322
B3GNT7	2	ENSG00000156966	3.84E-06	1.23E-04	-0.70	230	229	339	334	393	453
ARSG	17	ENSG00000141337	5.61E-13	4.91E-11	-0.70	510	582	647	775	790	1029
AC022150.4	19	ENSG00000269825	1.35E-06	4.78E-05	-0.71	187	266	245	334	288	422
KCNC3	19	ENSG00000131398	3.97E-06	1.26E-04	-0.71	217	258	234	308	297	469
RHOD	11	ENSG00000173156	7.98E-09	4.39E-07	-0.71	929	795	1161	1463	1390	1420
RELB	19	ENSG00000104856	3.54E-08	1.77E-06	-0.71	310	303	342	454	435	545
ITPKA	15	ENSG00000137825	3.95E-08	1.95E-06	-0.71	313	344	424	580	467	558
ELOA-AS1	1	ENSG00000236810	2.76E-09	1.62E-07	-0.71	289	423	423	536	517	634
WIPI1	17	ENSG00000070540	4.53E-13	4.01E-11	-0.72	457	583	634	830	722	952
SLC45A1	1	ENSG00000162426	3.57E-06	1.15E-04	-0.72	185	200	291	296	309	406
AL445237.1	10	ENSG00000271434	4.33E-04	7.22E-03	-0.72	101	121	116	147	178	181
VCAN-AS1	5	ENSG00000249835	5.07E-05	1.16E-03	-0.72	128	222	220	266	219	372
AL627171.2	14	ENSG00000282885	7.44E-06	2.17E-04	-0.72	205	285	276	384	400	351
TFR2	7	ENSG00000106327	1.16E-10	7.78E-09	-0.73	332	434	492	564	587	741
ZNF710	15	ENSG00000140548	7.21E-12	5.53E-10	-0.73	472	492	614	785	731	867
SMAD6	15	ENSG00000137834	3.55E-09	2.06E-07	-0.73	279	320	407	481	479	558
L1CAM	X	ENSG00000198910	5.80E-11	4.06E-09	-0.73	555	578	802	864	832	1261
CCN3	8	ENSG00000136999	6.07E-11	4.22E-09	-0.74	390	444	464	637	627	707
DZIP1L	3	ENSG00000158163	6.70E-07	2.60E-05	-0.74	182	215	269	291	325	394
SRPK3	X	ENSG00000184343	1.02E-04	2.12E-03	-0.74	111	145	199	191	193	312
GLIS3	9	ENSG00000107249	2.22E-05	5.75E-04	-0.74	116	194	218	236	251	310
RASSF2	20	ENSG00000101265	2.71E-17	3.60E-15	-0.75	641	827	856	1068	1088	1415
RIOX1	14	ENSG00000170468	1.50E-07	6.71E-06	-0.75	222	311	375	464	443	463
MLLT11	1	ENSG00000213190	7.60E-06	2.21E-04	-0.75	135	183	164	238	209	298
PCSK6	15	ENSG00000140479	7.32E-12	5.60E-10	-0.76	351	415	495	585	578	782
ZNF587B	19	ENSG00000269343	8.91E-15	9.18E-13	-0.76	490	635	635	820	843	1056

FXYD6	11	ENSG00000137726	9.57E-05	2.01E-03	-0.76	100	119	168	212	163	218
PAX2	10	ENSG00000075891	2.80E-06	9.30E-05	-0.76	173	189	296	333	280	399
ADAT3	19	ENSG00000213638	4.37E-10	2.79E-08	-0.76	315	330	449	539	506	643
LYSMD4	15	ENSG00000183060	9.58E-10	5.89E-08	-0.76	312	344	362	537	478	560
AC129492.2	17	ENSG00000214999	1.25E-04	2.52E-03	-0.76	146	108	180	231	190	254
AL133410.1	9	ENSG00000227388	2.16E-04	4.00E-03	-0.77	83	109	117	159	122	201
NEURL1B	5	ENSG00000214357	6.62E-18	9.54E-16	-0.77	718	851	1023	1182	1227	1614
PTCHD4	6	ENSG00000244694	1.14E-06	4.14E-05	-0.77	145	218	241	316	274	338
BEGAIN	14	ENSG00000183092	1.37E-06	4.85E-05	-0.77	153	174	202	265	260	293
TARSL2	15	ENSG00000185418	4.54E-13	4.01E-11	-0.77	399	453	559	670	678	842
RCCD1	15	ENSG00000166965	3.03E-17	3.99E-15	-0.77	728	838	1051	1373	1132	1578
SELENOM	22	ENSG00000198832	4.63E-14	4.42E-12	-0.78	607	707	902	1083	1132	1211
AC132217.2	11	ENSG00000284779	8.98E-12	6.73E-10	-0.78	404	429	536	698	574	893
CEL	9	ENSG00000170835	1.42E-04	2.81E-03	-0.78	88	109	113	141	135	216
TESC	12	ENSG00000088992	1.05E-06	3.91E-05	-0.78	156	202	275	306	323	351
ULK2	17	ENSG00000083290	2.66E-08	1.37E-06	-0.78	215	229	317	395	348	449
CEMIP2	9	ENSG00000135048	1.53E-19	2.57E-17	-0.79	647	874	886	1196	1125	1465
ZNF710-AS1	15	ENSG00000259291	5.86E-05	1.33E-03	-0.79	129	111	150	223	177	215
FOS	14	ENSG00000170345	1.11E-05	3.12E-04	-0.79	107	178	180	230	236	258
PDE8A	15	ENSG00000073417	3.57E-16	4.24E-14	-0.80	603	797	711	1037	1016	1309
IGF2	11	ENSG00000167244	1.29E-12	1.09E-10	-0.80	433	442	565	744	622	935
DPYSL4	10	ENSG00000151640	4.04E-05	9.63E-04	-0.80	87	123	164	185	171	233
PXDN	2	ENSG00000130508	3.58E-16	4.24E-14	-0.80	546	679	808	929	1007	1296
EFR3B	2	ENSG00000084710	4.71E-05	1.09E-03	-0.80	88	104	131	153	160	200
AC008914.1	5	ENSG00000262211	3.29E-05	8.04E-04	-0.81	105	105	126	169	172	196
ARC	8	ENSG00000198576	3.54E-08	1.77E-06	-0.82	210	217	273	401	326	394
LINC01578	15	ENSG00000272888	2.27E-22	4.66E-20	-0.82	717	885	940	1310	1262	1511

TRPV3	17	ENSG00000167723	1.81E-04	3.43E-03	-0.82	112	115	118	168	129	275
SLC16A6	17	ENSG00000108932	5.13E-10	3.25E-08	-0.83	215	263	288	393	390	451
EFL1	15	ENSG00000140598	5.81E-18	8.56E-16	-0.83	551	604	725	991	933	1115
SDSL	12	ENSG00000139410	2.12E-09	1.26E-07	-0.83	527	413	584	731	847	908
AC091167.6	15	ENSG00000275674	1.73E-07	7.69E-06	-0.83	146	159	210	264	248	325
HAPLN3	15	ENSG00000140511	1.00E-06	3.72E-05	-0.83	123	143	168	208	211	290
LINC01271	20	ENSG00000233077	1.36E-07	6.12E-06	-0.84	150	206	198	258	295	348
OLFML2A	9	ENSG00000185585	2.80E-12	2.26E-10	-0.84	337	471	595	674	682	917
MEIS2	15	ENSG00000134138	1.16E-16	1.45E-14	-0.84	579	642	711	1007	1032	1106
SERTAD1	19	ENSG00000197019	5.18E-11	3.65E-09	-0.85	611	600	751	1089	1106	988
AL356652.1	20	ENSG00000278367	4.07E-08	1.99E-06	-0.85	247	200	313	385	382	489
SEMA3F	3	ENSG00000001617	2.82E-16	3.37E-14	-0.85	757	701	895	1299	1181	1398
ARPIN-AP3S2	15	ENSG00000250021	4.11E-19	6.64E-17	-0.85	629	662	858	1092	1095	1345
LINC01270	20	ENSG00000203999	6.17E-12	4.81E-10	-0.86	295	361	365	472	521	707
ASB7	15	ENSG00000183475	1.14E-17	1.59E-15	-0.86	516	651	691	982	992	1077
KRT15	17	ENSG00000171346	5.10E-12	4.02E-10	-0.86	314	322	412	533	482	737
KLK10	19	ENSG00000129451	1.52E-10	1.01E-08	-0.86	208	265	306	428	397	457
PAPSS2	10	ENSG00000198682	4.38E-16	5.15E-14	-0.87	414	597	597	859	734	1086
AL137129.1	14	ENSG00000258964	3.22E-15	3.46E-13	-0.87	428	598	575	893	834	921
OPTN	10	ENSG00000123240	2.58E-10	1.69E-08	-0.87	229	371	317	455	468	605
ADGRB1	8	ENSG00000181790	1.51E-04	2.97E-03	-0.88	68	76	122	127	122	200
AC138904.1	16	ENSG00000246465	3.27E-04	5.70E-03	-0.88	58	83	73	98	127	134
HOXB8	17	ENSG00000120068	5.80E-06	1.74E-04	-0.89	113	123	200	267	192	269
FAH	15	ENSG00000103876	6.90E-13	6.02E-11	-0.89	247	287	347	482	432	572
SELENOS	15	ENSG00000131871	1.43E-24	3.37E-22	-0.89	639	795	944	1253	1211	1536
LYPLAL1	1	ENSG00000143353	7.47E-23	1.56E-20	-0.89	523	648	693	1006	920	1231
TP53I3	2	ENSG00000115129	9.64E-20	1.65E-17	-0.89	549	584	684	977	974	1124

GDPGP1	15	ENSG00000183208	5.33E-08	2.54E-06	-0.90	186	180	256	355	350	341
EBF4	20	ENSG00000088881	3.16E-11	2.29E-09	-0.90	214	306	361	429	451	617
AOPEP	9	ENSG00000148120	7.77E-17	9.96E-15	-0.91	454	523	722	936	891	1058
ARL14EPL	5	ENSG00000268223	1.44E-04	2.83E-03	-0.91	55	75	83	123	93	150
TINCR	19	ENSG00000223573	1.50E-08	8.02E-07	-0.91	172	174	244	277	328	408
FES	15	ENSG00000182511	2.82E-09	1.65E-07	-0.91	295	227	313	472	455	517
AC132938.4	17	ENSG00000278964	1.53E-04	2.99E-03	-0.92	60	73	98	99	135	162
HOXB4	17	ENSG00000182742	1.37E-13	1.28E-11	-0.92	306	293	377	537	500	654
TRIM46	1	ENSG00000163462	1.51E-07	6.74E-06	-0.92	132	152	158	229	203	344
ARPIN	15	ENSG00000242498	4.74E-18	7.14E-16	-0.92	443	504	678	931	803	1066
NDRG4	16	ENSG00000103034	4.99E-21	9.44E-19	-0.92	520	551	681	926	947	1161
SCARF1	17	ENSG00000074660	5.66E-04	8.96E-03	-0.93	56	51	82	129	84	114
CTSH	15	ENSG00000103811	6.10E-14	5.80E-12	-0.93	293	364	400	610	594	618
MSLNL	16	ENSG00000162006	1.29E-06	4.60E-05	-0.94	87	105	115	165	155	221
CEBPD	8	ENSG00000221869	1.08E-06	3.98E-05	-0.95	228	163	348	463	399	422
GHRLOS	3	ENSG00000240288	4.66E-04	7.66E-03	-0.95	39	62	96	102	93	150
IFITM2	11	ENSG00000185201	1.04E-20	1.94E-18	-0.95	551	543	707	996	993	1195
CAPS	19	ENSG00000105519	4.95E-06	1.53E-04	-0.96	111	85	113	167	163	227
LRRK1	15	ENSG00000154237	7.74E-20	1.35E-17	-0.96	693	629	812	1197	1078	1566
C15orf40	15	ENSG00000169609	7.93E-19	1.26E-16	-0.97	386	526	481	777	704	1019
WHAMM	15	ENSG00000156232	8.20E-15	8.53E-13	-0.97	289	318	344	572	529	593
GAL3ST4	7	ENSG00000197093	2.56E-12	2.10E-10	-0.97	277	353	389	602	433	805
AC022558.3	15	ENSG00000273747	1.57E-08	8.34E-07	-0.97	116	144	143	231	202	293
MIR22HG	17	ENSG00000186594	1.90E-04	3.56E-03	-0.98	60	86	86	141	81	202
TEX19	17	ENSG00000182459	3.87E-10	2.49E-08	-0.98	143	159	205	282	277	350
AC118344.2	19	ENSG00000279759	5.19E-08	2.49E-06	-0.98	171	259	196	355	267	527
AC004805.1	17	ENSG00000266076	2.92E-22	5.92E-20	-0.98	515	648	706	1093	1084	1157

AC048382.5	15	ENSG00000275120	2.60E-04	4.67E-03	-0.98	51	51	65	95	105	98
TTC23	15	ENSG00000103852	2.13E-15	2.34E-13	-0.98	224	309	329	488	473	589
RNF157-AS1	17	ENSG00000267128	8.06E-05	1.74E-03	-0.99	55	62	65	92	100	141
AC078816.1	3	ENSG00000286273	3.02E-05	7.47E-04	-0.99	52	72	77	119	111	132
VPS33B	15	ENSG00000184056	1.84E-21	3.55E-19	-0.99	452	478	562	823	874	1014
CST6	11	ENSG00000175315	2.24E-12	1.85E-10	-0.99	295	264	347	559	529	554
SNCA	4	ENSG00000145335	1.07E-04	2.21E-03	-1.00	51	87	73	93	118	176
SMAD7	18	ENSG00000101665	7.46E-05	1.63E-03	-1.00	77	58	76	108	109	178
NANOS1	10	ENSG00000188613	2.50E-04	4.52E-03	-1.01	44	75	49	94	98	116
CDIP1	16	ENSG00000089486	2.90E-20	5.24E-18	-1.01	348	388	470	673	696	838
AC016074.2	8	ENSG00000286122	8.58E-16	9.80E-14	-1.01	422	672	567	934	803	1340
KALRN	3	ENSG00000160145	8.64E-10	5.35E-08	-1.01	123	216	220	307	299	414
AC048382.6	15	ENSG00000276278	5.13E-09	2.89E-07	-1.01	109	143	152	211	234	299
MESP1	15	ENSG00000166823	4.14E-05	9.81E-04	-1.01	92	65	137	184	185	164
SUSD3	9	ENSG00000157303	1.09E-04	2.23E-03	-1.02	44	74	80	116	130	110
AC068831.1	15	ENSG00000258384	2.78E-08	1.43E-06	-1.02	171	142	149	263	282	318
FNDC4	2	ENSG00000115226	2.65E-04	4.75E-03	-1.02	35	91	111	155	109	163
AP003392.1	11	ENSG00000254428	1.46E-04	2.87E-03	-1.02	48	72	51	98	85	138
DET1	15	ENSG00000140543	4.47E-06	1.40E-04	-1.03	55	89	96	145	134	162
IFIT1	10	ENSG00000185745	3.61E-08	1.80E-06	-1.03	153	147	175	332	201	365
ZCCHC12	X	ENSG00000174460	4.90E-09	2.76E-07	-1.04	122	150	207	323	264	295
MRPL46	15	ENSG00000259494	6.35E-26	1.62E-23	-1.04	463	655	656	1047	1033	1219
GASK1A	3	ENSG00000144649	3.67E-05	8.88E-04	-1.04	59	52	74	122	100	125
CACNA1G	17	ENSG00000006283	7.00E-09	3.87E-07	-1.04	114	119	171	246	202	313
COL9A2	1	ENSG00000049089	2.02E-05	5.27E-04	-1.04	49	64	91	107	120	154
SERPINA5	14	ENSG00000188488	5.70E-07	2.25E-05	-1.05	87	88	143	168	203	223
RNF128	X	ENSG00000133135	5.09E-15	5.41E-13	-1.05	226	247	281	432	470	517

MYL9	20	ENSG00000101335	2.97E-28	8.82E-26	-1.05	646	667	895	1296	1288	1580
GPR87	3	ENSG00000138271	2.48E-07	1.07E-05	-1.05	73	93	105	155	163	192
ESRRB	14	ENSG00000119715	2.28E-05	5.89E-04	-1.06	58	61	60	109	110	122
AL022318.4	22	ENSG00000284554	2.47E-07	1.07E-05	-1.06	92	116	143	196	160	322
LUCAT1	5	ENSG00000248323	7.89E-05	1.71E-03	-1.07	72	107	66	120	115	250
DSC3	18	ENSG00000134762	1.76E-20	3.23E-18	-1.08	423	588	582	823	1027	1208
APOBEC3D	22	ENSG00000243811	2.07E-07	9.08E-06	-1.08	90	131	148	213	163	345
TMEM200A	6	ENSG00000164484	6.76E-24	1.55E-21	-1.08	517	672	613	1160	1114	1195
SLC7A8	14	ENSG00000092068	1.31E-17	1.81E-15	-1.09	207	268	300	450	446	612
RAMAC	15	ENSG00000169612	2.30E-07	1.00E-05	-1.10	79	120	93	190	186	189
SYNJ2	6	ENSG00000078269	1.09E-35	4.80E-33	-1.10	634	800	802	1313	1285	1791
AC013489.1	15	ENSG00000173867	5.37E-23	1.17E-20	-1.10	345	489	519	828	850	936
ZSCAN2	15	ENSG00000176371	6.42E-28	1.85E-25	-1.10	383	452	520	810	828	1017
MEGF11	15	ENSG00000157890	8.37E-05	1.80E-03	-1.11	33	53	57	101	81	96
ST20-MTHFS	15	ENSG00000259332	2.13E-15	2.34E-13	-1.12	261	307	424	650	653	627
AC011483.2	19	ENSG00000269495	1.09E-27	3.04E-25	-1.12	420	451	532	894	873	1015
MEX3B	15	ENSG00000183496	1.16E-27	3.20E-25	-1.13	390	510	531	960	860	1016
MIA	19	ENSG00000261857	2.11E-04	3.92E-03	-1.13	25	56	60	75	81	123
EFCC1	3	ENSG00000114654	2.60E-07	1.11E-05	-1.14	85	80	80	163	161	170
NRP1	10	ENSG00000099250	7.46E-10	4.68E-08	-1.14	98	115	110	216	194	242
CACNA1D	3	ENSG00000157388	2.05E-12	1.71E-10	-1.14	137	159	146	282	266	349
SPHK1	17	ENSG00000176170	1.51E-12	1.27E-10	-1.15	166	161	273	391	351	463
CORO1A	16	ENSG00000102879	9.97E-15	1.02E-12	-1.15	157	210	264	390	417	453
CEACAM1	19	ENSG00000079385	3.52E-07	1.44E-05	-1.17	52	69	86	143	116	165
LAMC3	9	ENSG00000050555	1.00E-33	4.16E-31	-1.18	563	555	720	1184	1136	1485
CSRNP1	3	ENSG00000144655	3.28E-20	5.87E-18	-1.18	262	374	478	754	706	804
AC013489.3	15	ENSG00000279945	1.18E-15	1.33E-13	-1.18	180	192	215	401	391	417

F5	1	ENSG00000198734	2.75E-04	4.92E-03	-1.19	23	43	40	66	56	99
SOCS1	16	ENSG00000185338	2.75E-12	2.23E-10	-1.19	157	144	253	345	362	436
CCNJL	5	ENSG00000135083	8.44E-22	1.69E-19	-1.19	292	358	461	704	775	805
ISM1	20	ENSG00000101230	1.55E-11	1.15E-09	-1.20	123	162	161	303	326	291
CORO2B	15	ENSG00000103647	8.87E-07	3.36E-05	-1.20	45	83	82	128	115	199
PADI2	1	ENSG00000117115	4.46E-09	2.53E-07	-1.20	67	84	114	175	163	215
BVES	6	ENSG00000112276	6.82E-11	4.71E-09	-1.20	122	235	156	318	324	438
HIF1A-AS1	14	ENSG00000258777	7.05E-23	1.49E-20	-1.22	363	385	560	916	882	941
CORO6	17	ENSG00000167549	9.85E-17	1.25E-14	-1.22	264	344	448	768	513	974
MTHFS	15	ENSG00000136371	6.72E-18	9.60E-16	-1.22	263	308	447	714	714	695
TFAP2E	1	ENSG00000116819	3.25E-10	2.11E-08	-1.23	86	92	115	223	174	228
NOVA2	19	ENSG00000104967	3.31E-18	5.05E-16	-1.24	185	182	215	387	378	493
UNC5B-AS1	10	ENSG00000237512	3.82E-04	6.55E-03	-1.24	30	29	26	55	51	81
PLXNB3	X	ENSG00000198753	1.35E-16	1.67E-14	-1.25	248	221	364	552	482	788
RAMACL	6	ENSG00000235272	9.04E-20	1.56E-17	-1.25	199	215	270	499	463	513
SRPX2	X	ENSG00000102359	1.00E-23	2.23E-21	-1.25	236	269	268	539	516	630
RAB15	14	ENSG00000139998	5.28E-29	1.64E-26	-1.27	338	341	443	735	774	955
LINS1	15	ENSG00000140471	4.36E-29	1.38E-26	-1.27	312	314	372	705	651	849
AC092306.1	19	ENSG00000285128	1.22E-09	7.44E-08	-1.28	64	94	110	194	147	253
SERPINF2	17	ENSG00000167711	1.39E-14	1.39E-12	-1.29	139	149	143	332	294	335
BCL11A	2	ENSG00000119866	7.06E-07	2.74E-05	-1.29	56	55	52	100	107	164
AC025419.1	12	ENSG00000250748	4.76E-15	5.09E-13	-1.32	121	230	180	403	347	452
GOLGA6L9	15	ENSG00000197978	1.90E-17	2.55E-15	-1.32	206	280	268	524	409	817
GAS6-DT	13	ENSG00000272695	4.62E-05	1.08E-03	-1.34	21	62	37	90	78	106
NAALAD2	11	ENSG00000077616	2.52E-04	4.55E-03	-1.34	15	49	38	57	65	113
PLEKHA4	19	ENSG00000105559	2.03E-38	1.06E-35	-1.34	397	405	521	1006	891	1170
KLHL25	15	ENSG00000183655	5.83E-23	1.26E-20	-1.35	256	235	293	605	592	627

AC103718.1	8	ENSG00000285108	8.01E-09	4.40E-07	-1.36	108	122	73	213	181	343
ALPK3	15	ENSG00000136383	8.22E-11	5.62E-09	-1.36	67	76	101	203	150	219
SPRED3	19	ENSG00000188766	2.14E-14	2.09E-12	-1.37	90	132	188	305	276	374
SNHG21	15	ENSG00000250988	4.39E-06	1.38E-04	-1.37	33	38	39	73	73	118
AC243919.2	15	ENSG00000278202	2.34E-07	1.01E-05	-1.38	49	67	52	128	90	189
AL121906.2	20	ENSG00000275223	4.18E-04	7.04E-03	-1.38	21	17	24	51	42	55
PON3	7	ENSG00000105852	6.45E-04	9.93E-03	-1.38	10	26	46	71	54	62
NECTIN4	1	ENSG00000143217	7.94E-12	6.04E-10	-1.40	85	85	112	197	176	317
IFIT2	10	ENSG00000119922	1.32E-07	5.96E-06	-1.40	32	66	58	126	98	151
GPR15	3	ENSG00000154165	5.07E-05	1.16E-03	-1.41	26	32	22	66	54	77
MAMDC2	9	ENSG00000165072	6.36E-09	3.53E-07	-1.43	52	59	67	143	102	198
LOXL4	10	ENSG00000138131	3.90E-11	2.79E-09	-1.43	54	87	77	175	148	213
FAT2	5	ENSG00000086570	2.13E-10	1.40E-08	-1.44	52	75	77	149	133	226
SKAP1	17	ENSG00000141293	3.01E-06	9.96E-05	-1.45	22	48	61	113	106	95
EPB41L4A-DT	5	ENSG00000278921	7.40E-07	2.86E-05	-1.45	34	36	85	130	102	148
DNAH12	3	ENSG00000174844	4.07E-04	6.87E-03	-1.46	20	32	14	68	44	54
CNTNAP1	17	ENSG00000108797	2.32E-25	5.75E-23	-1.46	208	222	239	597	429	671
B3GALT5	21	ENSG00000183778	2.93E-05	7.27E-04	-1.47	15	29	52	77	64	97
AC106875.1	2	ENSG00000228496	4.55E-04	7.50E-03	-1.48	13	15	34	55	35	66
CDKN2B	9	ENSG00000147883	5.43E-32	1.89E-29	-1.49	177	238	284	556	544	686
EDAR	2	ENSG00000135960	2.32E-30	7.82E-28	-1.52	185	216	224	483	532	619
AC004231.1	17	ENSG00000234477	1.65E-15	1.83E-13	-1.54	80	86	87	206	208	259
GLT8D2	12	ENSG00000120820	1.03E-12	8.89E-11	-1.54	58	60	91	173	168	211
CNTNAP2	7	ENSG00000174469	1.83E-16	2.22E-14	-1.54	77	146	122	309	277	320
GRIN2C	17	ENSG00000161509	2.12E-36	9.60E-34	-1.55	308	333	381	970	687	1086
ACTL8	1	ENSG00000117148	8.13E-05	1.75E-03	-1.55	9	29	42	69	70	66
TNNC1	3	ENSG00000114854	3.18E-12	2.53E-10	-1.56	49	67	72	172	133	201

NFASC	1	ENSG00000163531	4.09E-05	9.72E-04	-1.56	26	24	16	53	52	78
OASL	12	ENSG00000135114	1.39E-14	1.39E-12	-1.56	70	71	82	186	189	228
AC090023.1	12	ENSG00000255866	3.50E-07	1.44E-05	-1.57	25	48	31	97	81	103
MYOM3	1	ENSG00000142661	1.86E-37	9.04E-35	-1.57	194	255	273	613	545	806
LGALS9	17	ENSG00000168961	2.93E-04	5.19E-03	-1.58	9	14	35	50	45	59
LINC01405	12	ENSG00000185847	0.00E+00	1.50E-44	-1.59	262	356	404	862	793	1145
SLC6A20	3	ENSG00000163817	7.59E-08	3.58E-06	-1.59	29	50	35	85	91	140
TNXB	6	ENSG00000168477	1.71E-19	2.81E-17	-1.59	139	105	163	365	361	395
DAPK1	9	ENSG00000196730	1.26E-24	3.02E-22	-1.60	111	135	166	339	327	476
IQGAP2	5	ENSG00000145703	1.68E-36	7.75E-34	-1.60	173	236	246	584	565	658
FLNC-AS1	7	ENSG00000242902	5.93E-04	9.29E-03	-1.62	11	15	12	31	34	42
NR2F2-AS1	15	ENSG00000247809	4.90E-05	1.13E-03	-1.63	8	43	28	73	59	87
MUC19	12	ENSG00000205592	1.66E-06	5.80E-05	-1.63	24	38	32	83	52	138
KISS1R	19	ENSG00000116014	4.31E-34	1.82E-31	-1.64	199	188	280	602	576	712
SUSD2	22	ENSG00000099994	4.12E-33	1.57E-30	-1.64	163	224	302	577	597	774
NTF4	19	ENSG00000225950	1.48E-05	3.98E-04	-1.65	24	20	18	47	62	72
PLEKHA6	1	ENSG00000143850	9.61E-42	5.79E-39	-1.67	205	254	309	656	636	950
AC100793.3	17	ENSG00000267765	8.04E-05	1.74E-03	-1.68	26	12	16	59	46	56
FHAD1	1	ENSG00000142621	1.44E-14	1.43E-12	-1.68	54	117	87	207	223	325
LTBP2	14	ENSG00000119681	4.69E-33	1.76E-30	-1.69	191	174	231	572	470	729
RNF227	17	ENSG00000179859	1.92E-04	3.60E-03	-1.69	12	27	12	65	33	52
PRSS33	16	ENSG00000103355	8.31E-06	2.39E-04	-1.69	12	21	31	60	61	63
PGBD5	1	ENSG00000177614	3.76E-05	9.07E-04	-1.69	12	19	23	37	48	75
NTNG2	9	ENSG00000196358	3.69E-06	1.19E-04	-1.70	20	15	37	73	64	73
SECTM1	17	ENSG00000141574	5.83E-07	2.30E-05	-1.70	26	21	28	71	76	75
AC080038.1	17	ENSG00000011028	0.00E+00	0.00E+00	-1.71	315	323	395	936	946	1218
HOMER2	15	ENSG00000103942	8.70E-08	4.08E-06	-1.72	18	60	44	106	89	171

EGR3	8	ENSG00000179388	7.64E-13	6.63E-11	-1.73	48	89	75	231	216	178
ASGR1	17	ENSG00000141505	9.11E-08	4.24E-06	-1.74	34	19	46	83	86	136
SPNS3	17	ENSG00000182557	7.40E-05	1.62E-03	-1.74	13	12	21	44	52	41
IL11	19	ENSG00000095752	9.97E-07	3.72E-05	-1.74	30	16	44	100	92	77
TSPOAP1	17	ENSG00000005379	1.28E-09	7.83E-08	-1.75	48	33	56	117	100	215
SEMA3A	7	ENSG00000075213	0.00E+00	0.00E+00	-1.75	411	515	514	1396	1331	1686
KIF7	15	ENSG00000166813	1.36E-16	1.67E-14	-1.76	87	59	122	249	240	348
KRTAP2-3	17	ENSG00000212724	1.50E-14	1.49E-12	-1.78	40	66	72	172	142	245
CHD5	1	ENSG00000116254	0.00E+00	2.06E-43	-1.79	279	277	396	973	986	1019
AP000779.1	11	ENSG00000285921	2.04E-05	5.31E-04	-1.80	14	18	15	35	50	66
ABCA1	9	ENSG00000165029	6.25E-07	2.45E-05	-1.81	35	18	25	85	56	118
IFI35	17	ENSG00000068079	3.92E-06	1.25E-04	-1.81	18	26	14	64	64	57
AC090907.2	15	ENSG00000259755	3.68E-06	1.18E-04	-1.81	20	12	24	57	60	62
COL16A1	1	ENSG00000084636	1.69E-19	2.80E-17	-1.82	60	69	108	225	219	319
ALPL	1	ENSG00000162551	2.77E-06	9.23E-05	-1.83	13	19	19	54	50	61
HAS2	8	ENSG00000170961	8.86E-12	6.67E-10	-1.86	25	47	42	111	117	147
AC010261.2	5	ENSG00000251187	5.07E-08	2.44E-06	-1.86	13	30	36	73	71	117
OR51M1	11	ENSG00000184698	5.20E-04	8.39E-03	-1.87	4	18	10	33	24	50
FAM184A	6	ENSG00000111879	1.11E-07	5.11E-06	-1.88	13	25	28	65	74	79
ALOX5	10	ENSG00000012779	2.06E-13	1.87E-11	-1.90	44	42	47	142	164	144
ARMC4	10	ENSG00000169126	3.91E-38	1.94E-35	-1.90	111	127	157	426	386	540
MAML2	11	ENSG00000184384	0.00E+00	0.00E+00	-1.91	152	232	234	635	675	801
AC015712.7	15	ENSG00000278456	4.41E-04	7.33E-03	-1.92	9	7	9	28	25	34
ZC3H11B	1	ENSG00000215817	0.00E+00	0.00E+00	-1.92	209	331	321	881	933	1154
ID2	2	ENSG00000115738	0.00E+00	0.00E+00	-1.93	369	375	367	1284	1257	1314
IGFL4	19	ENSG00000204869	2.29E-04	4.20E-03	-1.95	8	19	8	42	19	67
AC080038.4	17	ENSG00000279713	8.15E-10	5.08E-08	-1.96	20	27	27	91	79	92

GGT5	22	ENSG00000099998	1.01E-10	6.89E-09	-1.98	25	31	25	95	84	114
TRIM22	11	ENSG00000132274	6.52E-12	5.06E-10	-1.98	23	37	40	115	87	160
DHRS2	14	ENSG00000100867	2.08E-23	4.59E-21	-1.99	67	80	68	272	233	273
ISG20	15	ENSG00000172183	8.71E-14	8.21E-12	-1.99	23	56	48	134	136	187
AC008957.1	5	ENSG00000250155	1.14E-05	3.17E-04	-2.00	14	14	10	38	36	69
AC002351.1	12	ENSG00000258240	4.48E-19	7.18E-17	-2.02	47	45	57	180	161	211
ANKRD2	10	ENSG00000165887	6.26E-04	9.68E-03	-2.07	9	8	6	28	13	52
AC015712.5	15	ENSG00000272639	1.40E-33	5.67E-31	-2.07	80	82	121	339	327	413
CPA4	7	ENSG00000128510	9.41E-35	4.07E-32	-2.09	119	99	104	393	375	505
CREB3L1	11	ENSG00000157613	3.38E-04	5.89E-03	-2.11	5	9	6	25	24	30
TNFSF18	1	ENSG00000120337	7.70E-28	2.19E-25	-2.14	86	71	72	314	273	342
MSX2	5	ENSG00000120149	0.00E+00	0.00E+00	-2.14	286	378	401	1398	1321	1534
CEND1	11	ENSG00000184524	5.81E-06	1.74E-04	-2.14	6	13	14	37	47	46
NRG1	8	ENSG00000157168	1.25E-12	1.06E-10	-2.16	33	37	25	118	90	193
CSMD3	8	ENSG00000164796	1.01E-04	2.12E-03	-2.18	16	4	6	33	35	44
QPRT	16	ENSG00000103485	1.68E-05	4.47E-04	-2.20	5	6	23	36	44	59
FOXJ1	17	ENSG00000129654	5.91E-05	1.34E-03	-2.23	6	7	9	29	23	43
CSF1R	5	ENSG00000182578	2.13E-04	3.95E-03	-2.24	3	9	7	29	21	31
REEP2	5	ENSG00000132563	3.66E-33	1.45E-30	-2.26	71	79	91	388	322	335
C3	19	ENSG00000125730	3.03E-04	5.33E-03	-2.27	11	2	6	23	24	41
DUOX1	15	ENSG00000137857	9.06E-24	2.05E-21	-2.28	62	54	46	227	194	314
SLC2A3	12	ENSG00000059804	0.00E+00	4.30E-44	-2.32	129	200	188	672	580	1152
EVA1A	2	ENSG00000115363	1.22E-21	2.40E-19	-2.38	24	52	66	203	232	223
MKX	10	ENSG00000150051	0.00E+00	0.00E+00	-2.42	248	299	272	1321	1230	1464
ALPP	2	ENSG00000163283	4.54E-06	1.42E-04	-2.47	8	5	9	46	31	34
STRA6	15	ENSG00000137868	5.28E-27	1.42E-24	-2.48	34	76	54	225	238	379
HEPH	X	ENSG00000089472	0.00E+00	0.00E+00	-2.50	239	299	301	1293	1393	1627

MAB21L4	2	ENSG00000172478	4.92E-04	8.01E-03	-2.52	4	0	11	20	30	26
SPOCK3	4	ENSG00000196104	3.90E-13	3.48E-11	-2.58	20	17	16	68	105	120
SYT8	11	ENSG00000149043	6.32E-08	3.00E-06	-2.60	8	6	13	40	40	71
HOXA-AS2	7	ENSG00000253552	1.06E-14	1.08E-12	-2.60	13	22	18	85	88	122
PRF1	10	ENSG00000180644	0.00E+00	0.00E+00	-2.65	198	186	207	977	1125	1313
APOBEC3G	22	ENSG00000239713	0.00E+00	9.80E-45	-2.66	68	87	67	357	377	568
ORM2	9	ENSG00000228278	5.04E-05	1.16E-03	-2.69	7	1	6	25	21	39
ALPG	2	ENSG00000163286	8.29E-05	1.78E-03	-2.70	3	8	2	29	26	21
KRT39	17	ENSG00000196859	2.34E-05	6.02E-04	-2.71	7	7	1	26	26	41
MYL2	12	ENSG00000111245	8.52E-06	2.45E-04	-2.72	11	1	6	42	35	33
LINC00518	6	ENSG00000183674	5.39E-05	1.23E-03	-2.74	1	4	8	24	25	28
PPP1R1A	12	ENSG00000135447	1.44E-04	2.83E-03	-2.75	1	4	6	23	19	24
AC008957.3	5	ENSG00000279400	1.19E-32	4.31E-30	-2.77	33	49	45	243	189	369
PLEKHS1	10	ENSG00000148735	8.88E-05	1.89E-03	-2.77	0	11	3	26	24	36
HLA-DRA	6	ENSG00000204287	1.48E-17	2.01E-15	-2.77	15	15	34	102	142	149
ZNF850	19	ENSG00000267041	1.66E-10	1.09E-08	-2.78	19	4	13	76	75	78
FAM92B	16	ENSG00000153789	3.56E-07	1.46E-05	-2.80	1	13	8	47	31	61
FER1L5	2	ENSG00000249715	4.81E-20	8.46E-18	-2.84	18	20	21	129	95	166
AL121748.1	10	ENSG00000238258	1.34E-04	2.67E-03	-2.89	1	2	7	23	17	26
SPTSSB	3	ENSG00000196542	0.00E+00	0.00E+00	-2.89	63	86	97	513	492	661
HRNR	1	ENSG00000197915	1.20E-10	8.03E-09	-2.90	6	14	7	54	56	75
PTPN7	1	ENSG00000143851	2.60E-04	4.67E-03	-2.94	2	3	3	23	12	21
FLG-AS1	1	ENSG00000237975	4.68E-11	3.31E-09	-2.96	5	18	7	53	74	86
KCNJ4	22	ENSG00000168135	9.26E-05	1.96E-03	-3.03	3	7	0	36	16	23
HOXA3	7	ENSG00000105997	0.00E+00	0.00E+00	-3.10	42	52	62	335	373	518
AC018398.1	8	ENSG00000288076	1.05E-04	2.17E-03	-3.12	1	6	1	21	20	22
CAPN6	X	ENSG00000077274	0.00E+00	0.00E+00	-3.14	59	67	114	557	658	689

TNFSF4	1	ENSG00000117586	0.00E+00	0.00E+00	-3.16	94	153	109	835	857	1248
ZNF804A	2	ENSG00000170396	6.68E-24	1.54E-21	-3.20	11	26	15	129	143	162
POF1B	X	ENSG00000124429	2.37E-05	6.06E-04	-3.25	0	7	2	22	20	36
HOTAIR	12	ENSG00000228630	4.87E-05	1.13E-03	-3.28	3	3	1	16	19	29
RASGRF1	15	ENSG00000058335	3.76E-28	1.10E-25	-3.32	13	16	22	138	146	180
AC003112.1	19	ENSG00000105696	0.00E+00	0.00E+00	-3.44	68	99	114	883	834	1049
MYBPH	1	ENSG00000133055	3.47E-04	6.02E-03	-3.44	1	4	0	19	16	14
KLK5	19	ENSG00000167754	1.13E-41	6.62E-39	-3.48	21	20	28	240	217	243
SLCO3A1	15	ENSG00000176463	4.52E-05	1.06E-03	-3.55	0	3	3	20	25	16
NMB	15	ENSG00000197696	3.62E-42	2.25E-39	-3.55	16	31	22	226	247	258
OLFML3	1	ENSG00000116774	1.23E-06	4.42E-05	-3.61	0	3	5	30	29	27
AL355916.1	14	ENSG00000232774	4.14E-07	1.67E-05	-3.64	5	46	20	236	220	334
TPO	2	ENSG00000115705	1.02E-04	2.13E-03	-3.72	0	0	5	20	15	23
AC007342.5	16	ENSG00000262714	1.47E-05	3.97E-04	-3.83	1	1	3	17	19	29
AC015712.6	15	ENSG00000272808	4.25E-18	6.45E-16	-3.85	5	6	9	72	78	114
AP000851.1	11	ENSG00000256916	4.79E-05	1.11E-03	-4.00	1	0	3	25	12	21
ELF5	11	ENSG00000135374	3.40E-37	1.61E-34	-4.07	12	11	14	172	153	250
FLG	1	ENSG00000143631	4.50E-25	1.09E-22	-4.09	3	16	7	140	124	134
ICAM1	19	ENSG00000090339	4.46E-20	7.92E-18	-4.12	19	40	83	701	637	827
RIMS2	8	ENSG00000176406	5.03E-18	7.49E-16	-4.15	28	115	107	1295	1198	1379
ANKRD1	10	ENSG00000148677	5.17E-12	4.06E-10	-4.20	1	2	7	50	45	71
MMP20	11	ENSG00000137674	7.42E-07	2.86E-05	-4.23	2	0	3	38	19	28
LINC01907	2	ENSG00000226125	4.80E-17	6.28E-15	-4.26	0	5	10	72	71	117
AC011511.5	19	ENSG00000267607	3.74E-32	1.33E-29	-4.28	2	15	12	175	136	197
SLC30A10	1	ENSG00000196660	0.00E+00	0.00E+00	-4.35	10	34	28	424	409	498
SALL4	20	ENSG00000101115	6.39E-29	1.95E-26	-4.41	5	5	15	156	105	228
AL049830.3	14	ENSG00000258525	2.17E-17	2.89E-15	-4.45	3	5	4	82	69	87

AC113410.5	5	ENSG00000287054	1.19E-06	4.30E-05	-4.46	0	1	3	29	21	29
SPOCK1	5	ENSG00000152377	0.00E+00	0.00E+00	-4.50	9	11	19	242	260	299
IGFBP3	7	ENSG00000146674	1.80E-05	4.74E-04	-4.52	0	1	2	17	15	31
COCH	14	ENSG00000100473	9.04E-33	3.33E-30	-4.58	6	8	8	166	133	180
AMIGO1	1	ENSG00000181754	4.30E-04	7.18E-03	-4.59	1	0	1	20	17	5
AC011944.1	15	ENSG00000177699	5.56E-06	1.69E-04	-4.69	0	3	0	20	21	30
LINC01411	5	ENSG00000249306	7.40E-06	2.16E-04	-4.70	0	3	0	33	17	20
LYPLAL1-AS1	1	ENSG00000228536	0.00E+00	0.00E+00	-4.71	5	19	12	273	272	310
TGFB2	1	ENSG00000092969	7.46E-05	1.63E-03	-4.74	15	0	5	151	177	200
ZNF280A	22	ENSG00000169548	3.35E-11	2.41E-09	-4.79	5	0	1	40	52	64
AC015712.1	15	ENSG00000232386	7.19E-05	1.58E-03	-4.87	2	0	0	14	12	31
RUNX2	6	ENSG00000124813	0.00E+00	0.00E+00	-4.89	23	43	68	1131	1051	1430
ANXA10	4	ENSG00000109511	1.63E-19	2.72E-17	-4.94	5	1	4	96	86	99
AC096667.1	2	ENSG00000283839	4.92E-04	8.01E-03	-5.12	1	0	0	10	16	7
SH3GL3	15	ENSG00000140600	5.46E-10	3.43E-08	-5.22	1	3	0	39	41	57
MKX-AS1	10	ENSG00000230500	1.10E-04	2.25E-03	-5.47	1	0	0	15	7	23
KCNQ5	6	ENSG00000185760	6.31E-04	9.76E-03	-5.47	0	0	0	7	9	6
TGFB2-OT1	1	ENSG00000281453	2.91E-09	1.70E-07	-5.63	1	0	2	38	55	40
AL450345.2	6	ENSG00000287550	2.50E-04	4.52E-03	-5.71	0	0	0	5	13	8
JAKMIP2	5	ENSG00000176049	1.68E-04	3.22E-03	-5.76	0	0	0	9	10	8
EHF	11	ENSG00000135373	0.00E+00	0.00E+00	-5.87	9	21	28	928	987	1154
IGFL2-AS1	19	ENSG00000268621	2.50E-05	6.34E-04	-6.18	0	0	0	17	6	14
ADGRL2	1	ENSG00000117114	2.69E-05	6.75E-04	-6.20	0	0	0	19	11	6
KLHDC9	1	ENSG00000162755	2.22E-06	7.58E-05	-6.24	0	0	1	19	20	37
AC092604.1	2	ENSG00000286260	2.91E-06	9.66E-05	-6.54	0	0	0	14	11	23
LGALS7B	19	ENSG00000178934	3.18E-06	1.04E-04	-6.59	0	0	0	22	17	8
AL096865.1	6	ENSG00000271857	3.42E-07	1.41E-05	-7.05	0	0	0	6	25	38

TGFBI	5	ENSG00000120708	2.55E-08	1.33E-06	-7.30	0	0	0	22	22	37
KCNB2	8	ENSG00000182674	1.88E-08	9.91E-07	-7.35	0	0	0	22	30	30
KRTAP3-1	17	ENSG00000212901	2.17E-10	1.42E-08	-7.80	0	1	0	79	65	74
TACSTD2	1	ENSG00000184292	1.51E-38	8.13E-36	-7.96	1	5	0	349	419	611
LINC00698	3	ENSG00000244342	1.35E-26	3.54E-24	-12.63	0	0	0	976	886	1384

Table 8.2 RNA-Seq down regulated genes

Probe	Chromosome	ID	P-value	FDR	Log2Fold	WT RPKM			HOTTIP KO RPKM		
SOHLH2	13	ENSG00000120669	5.34E-21	1.00E-18	11.17	402	510	484	0	0	0
AC105460.1	4	ENSG00000250920	2.54E-20	4.62E-18	10.98	323	433	480	0	0	0
CCDC169-SOHLH2	13	ENSG00000250709	1.91E-19	3.11E-17	10.74	297	378	361	0	0	0
PODXL2	3	ENSG00000114631	0.00E+00	0.00E+00	7.10	1095	1131	1359	8	9	7
AC105460.2	4	ENSG00000251577	5.32E-05	1.21E-03	5.93	10	15	12	0	0	0
LYL1	19	ENSG00000104903	1.23E-07	5.62E-06	5.90	36	45	51	2	0	0
RAD51AP2	2	ENSG00000214842	1.64E-04	3.17E-03	5.33	9	13	27	0	0	1
CD96	3	ENSG00000153283	4.48E-24	1.05E-21	5.14	128	156	144	3	7	1
LDB2	4	ENSG00000169744	4.57E-04	7.52E-03	5.06	11	9	20	0	0	1
AC079949.4	12	ENSG00000286016	3.67E-04	6.32E-03	4.54	11	20	19	0	0	2
NCAM1	11	ENSG00000149294	2.91E-13	2.61E-11	4.39	49	69	111	3	0	7
CU633904.1	21	ENSG00000276077	1.75E-09	1.05E-07	4.23	44	108	27	2	1	6
CU634019.1	21	ENSG00000277067	2.29E-15	2.50E-13	4.13	76	149	72	3	2	11
RAB3C	5	ENSG00000152932	1.52E-06	5.36E-05	4.05	24	27	39	1	1	3
FBLIM1	1	ENSG00000162458	4.84E-41	2.75E-38	3.67	264	279	255	23	15	20
GRM1	6	ENSG00000152822	2.95E-04	5.20E-03	3.65	13	21	20	0	1	3
LINC00944	12	ENSG00000256128	5.14E-05	1.18E-03	3.44	19	28	24	4	0	2
SEMA3D	7	ENSG00000153993	8.46E-16	9.71E-14	3.37	63	130	115	6	8	13
LRP1B	2	ENSG00000168702	1.19E-27	3.25E-25	3.37	180	215	245	15	7	36
KLRC4	12	ENSG00000183542	3.93E-33	1.53E-30	3.32	176	226	231	15	20	23
EVX1	7	ENSG00000106038	1.16E-04	2.36E-03	3.27	10	37	36	0	1	7
LINC00846	21	ENSG00000186842	3.11E-04	5.45E-03	3.21	20	22	20	0	5	1
AL033397.1	6	ENSG00000231683	1.90E-04	3.56E-03	3.18	33	14	21	5	1	1
AC016717.2	2	ENSG00000273301	2.64E-06	8.87E-05	3.07	30	27	44	3	3	5
IRX6	16	ENSG00000159387	4.18E-04	7.04E-03	3.04	21	14	28	5	0	2

MAP2K6	17	ENSG00000108984	0.00E+00	2.00E-43	2.70	311	451	426	50	52	65
STXBP6	14	ENSG00000168952	2.46E-30	8.14E-28	2.68	186	259	324	33	35	40
HOTTIP	7	ENSG00000243766	1.56E-07	6.96E-06	2.62	48	46	53	5	8	9
KLRC4-KLRK1	12	ENSG00000255819	0.00E+00	0.00E+00	2.58	613	766	817	112	97	125
ZNF91	19	ENSG00000167232	0.00E+00	0.00E+00	2.58	658	1059	927	111	120	174
SLC26A4	7	ENSG00000091137	1.49E-07	6.70E-06	2.53	47	63	57	10	3	14
TNC	9	ENSG00000041982	5.40E-04	8.65E-03	2.49	18	26	25	5	4	2
LCT	2	ENSG00000115850	2.76E-05	6.89E-04	2.44	34	28	44	8	3	7
AL158071.5	9	ENSG00000273381	1.09E-07	5.02E-06	2.40	58	58	59	11	5	15
FGFBP1	4	ENSG00000137440	1.39E-13	1.29E-11	2.38	88	111	133	17	17	24
PRKAA2	1	ENSG00000162409	1.08E-17	1.52E-15	2.37	118	218	229	23	36	39
FAM129C	19	ENSG00000167483	2.51E-04	4.53E-03	2.35	16	52	27	4	5	8
KLRK1	12	ENSG00000213809	0.00E+00	0.00E+00	2.24	480	618	679	114	102	126
LNCAROD	10	ENSG00000231131	7.33E-06	2.14E-04	2.08	54	45	62	7	8	21
LPAR5	12	ENSG00000184574	4.91E-16	5.74E-14	2.07	139	162	212	30	32	50
AC022075.1	12	ENSG00000245648	0.00E+00	0.00E+00	2.04	598	770	822	145	142	199
TMEM74	8	ENSG00000164841	3.76E-10	2.43E-08	2.01	69	148	149	28	21	33
SPARC	5	ENSG00000113140	1.17E-25	2.95E-23	2.00	255	289	336	69	53	79
TCP10L	21	ENSG00000242220	3.24E-05	7.96E-04	2.00	57	37	56	14	13	7
GPR143	X	ENSG00000101850	3.85E-05	9.25E-04	1.99	46	50	63	3	15	19
SLAMF8	1	ENSG00000158714	9.97E-05	2.09E-03	1.88	50	35	52	7	9	19
ANKRD22	10	ENSG00000152766	1.26E-26	3.33E-24	1.88	352	450	467	76	91	151
KLHL32	6	ENSG00000186231	1.74E-11	1.28E-09	1.82	114	146	141	28	34	42
LINP1	10	ENSG00000223784	6.83E-06	2.01E-04	1.80	48	64	69	13	12	23
NRP2	2	ENSG00000118257	1.16E-06	4.20E-05	1.78	66	82	67	17	16	25
ATP8A1	4	ENSG00000124406	5.71E-15	6.04E-13	1.77	176	344	302	62	56	103
GLDN	15	ENSG00000186417	1.26E-08	6.78E-07	1.75	94	131	108	30	19	43

MANSC4	12	ENSG00000205693	1.27E-05	3.48E-04	1.73	61	86	55	15	13	29
IL20RA	6	ENSG00000016402	2.82E-04	5.03E-03	1.72	33	58	64	10	22	9
CPQ	8	ENSG00000104324	1.31E-04	2.60E-03	1.71	54	41	91	24	7	21
BAMBI	10	ENSG00000095739	0.00E+00	0.00E+00	1.71	844	1016	1175	261	271	314
CALB2	16	ENSG00000172137	6.02E-18	8.80E-16	1.64	285	283	369	88	97	88
ZNF772	19	ENSG00000197128	8.26E-07	3.14E-05	1.62	85	88	94	23	18	40
FOXP2	7	ENSG00000128573	9.63E-07	3.60E-05	1.62	73	119	102	27	17	45
LINC00886	3	ENSG00000240875	4.02E-09	2.31E-07	1.56	145	151	155	44	29	70
LHFPL6	13	ENSG00000183722	2.65E-06	8.89E-05	1.56	64	104	103	34	25	23
AC108047.1	2	ENSG00000233654	5.65E-04	8.95E-03	1.56	39	54	43	14	8	21
MRPS30-DT	5	ENSG00000251141	8.67E-12	6.56E-10	1.55	158	230	188	51	57	72
TENM3	4	ENSG00000218336	0.00E+00	0.00E+00	1.55	905	1162	1322	310	321	424
CYP39A1	6	ENSG00000146233	2.34E-06	7.94E-05	1.53	76	103	83	23	24	37
CXXC4	4	ENSG00000168772	2.36E-09	1.39E-07	1.51	121	164	153	47	34	61
EMP1	12	ENSG00000134531	8.72E-40	4.81E-37	1.49	916	1087	1238	293	297	469
SCN9A	2	ENSG00000169432	2.21E-04	4.07E-03	1.49	37	75	65	13	19	25
DUSP19	2	ENSG00000162999	1.56E-12	1.30E-10	1.48	206	293	261	60	92	96
RHOU	1	ENSG00000116574	1.41E-31	4.83E-29	1.48	578	781	782	201	205	300
LINC00896	22	ENSG00000236499	2.85E-05	7.09E-04	1.46	102	71	82	35	24	27
PDE11A	2	ENSG00000128655	4.32E-05	1.02E-03	1.46	70	73	104	18	19	47
PRSS3	9	ENSG00000010438	2.03E-14	2.00E-12	1.45	247	276	296	85	97	90
ADAM32	8	ENSG00000197140	1.02E-04	2.12E-03	1.45	65	132	81	24	17	55
TGFBR3	1	ENSG00000069702	1.90E-26	4.91E-24	1.44	456	575	580	161	174	206
B3GALT1	2	ENSG00000172318	1.32E-07	5.96E-06	1.42	96	156	146	33	46	56
SYK	9	ENSG00000165025	1.85E-22	3.84E-20	1.39	458	553	664	179	147	260
AK7	14	ENSG00000140057	4.37E-09	2.49E-07	1.39	138	147	197	50	46	73
FBXO32	8	ENSG00000156804	8.98E-18	1.27E-15	1.38	348	436	498	112	141	198

TNFRSF19	13	ENSG00000127863	6.81E-11	4.71E-09	1.37	159	250	234	66	73	87
LIPH	3	ENSG00000163898	3.23E-38	1.65E-35	1.37	915	1064	1066	326	322	437
MAATS1	3	ENSG00000183833	3.89E-05	9.32E-04	1.37	73	113	84	20	30	47
CRYZL2P-SEC16B	1	ENSG00000254154	3.08E-06	1.01E-04	1.36	89	113	125	32	27	59
SEC16B	1	ENSG00000120341	8.01E-05	1.73E-03	1.34	63	74	85	25	18	38
ZNF780B	19	ENSG00000128000	9.53E-16	1.08E-13	1.32	409	454	422	123	144	210
P3H2	3	ENSG00000090530	4.44E-04	7.37E-03	1.32	52	57	88	16	29	26
MSH4	1	ENSG00000057468	5.27E-06	1.61E-04	1.31	85	116	127	30	33	59
AL512785.2	1	ENSG00000254706	1.81E-07	8.00E-06	1.30	127	156	234	67	41	83
MAML3	4	ENSG00000196782	1.13E-12	9.61E-11	1.29	247	294	342	105	79	148
ADAMTS15	11	ENSG00000166106	1.83E-04	3.46E-03	1.29	54	74	97	20	24	40
VIM	10	ENSG00000026025	3.85E-06	1.23E-04	1.29	105	109	130	39	49	39
EDNRA	4	ENSG00000151617	2.98E-15	3.22E-13	1.28	372	411	380	146	138	156
EHHADH-AS1	3	ENSG00000223358	2.14E-05	5.54E-04	1.27	74	94	113	33	37	35
AL590560.1	1	ENSG00000256029	2.55E-05	6.44E-04	1.26	98	90	123	26	38	56
AC005699.1	4	ENSG00000249631	2.30E-05	5.91E-04	1.26	75	140	124	30	48	50
TXK	4	ENSG00000074966	6.45E-06	1.91E-04	1.25	91	109	127	32	44	49
PDK4	7	ENSG00000004799	1.88E-06	6.46E-05	1.25	109	135	121	50	38	53
UBA7	3	ENSG00000182179	8.77E-05	1.87E-03	1.25	82	119	93	51	25	37
IL1RAP	3	ENSG00000196083	3.93E-14	3.81E-12	1.24	285	399	362	116	125	163
PAQR8	6	ENSG00000170915	9.42E-19	1.49E-16	1.24	640	694	686	236	201	361
KLHL35	11	ENSG00000149243	2.28E-04	4.19E-03	1.24	75	90	67	23	31	37
CALCRL	2	ENSG00000064989	1.33E-06	4.74E-05	1.24	101	184	159	62	43	66
AP003119.3	11	ENSG00000261578	1.33E-05	3.64E-04	1.23	85	108	106	36	35	46
SERTAD4	1	ENSG00000082497	6.63E-17	8.61E-15	1.23	347	408	444	145	146	177
GPRIN3	4	ENSG00000185477	2.04E-06	7.00E-05	1.22	128	216	177	89	50	63
PBX1	1	ENSG00000185630	4.22E-14	4.07E-12	1.20	476	652	633	162	215	330

TM4SF19	3	ENSG00000145107	6.39E-04	9.84E-03	1.20	63	58	71	25	23	29
PXMP4	20	ENSG00000101417	1.27E-15	1.42E-13	1.19	464	450	557	158	189	245
KLRC3	12	ENSG00000205810	2.25E-07	9.81E-06	1.18	155	169	162	67	52	79
NFIA	1	ENSG00000162599	7.37E-29	2.22E-26	1.17	850	1231	1204	428	382	518
ENPP1	6	ENSG00000197594	2.94E-30	9.59E-28	1.17	930	1202	1248	400	451	517
C1orf226	1	ENSG00000239887	2.41E-21	4.61E-19	1.15	648	679	835	261	259	376
ZNF283	19	ENSG00000167637	5.51E-09	3.09E-07	1.14	227	315	254	124	94	111
AL161431.1	13	ENSG00000275216	2.68E-15	2.91E-13	1.12	519	645	627	235	184	345
KLRC2	12	ENSG00000205809	3.22E-10	2.09E-08	1.12	246	318	296	109	125	127
DRP2	X	ENSG00000102385	4.83E-04	7.90E-03	1.11	63	79	87	35	29	32
TMEM37	2	ENSG00000171227	3.44E-04	5.98E-03	1.11	116	72	158	56	36	55
THSD4	15	ENSG00000187720	1.13E-16	1.42E-14	1.10	517	667	701	263	270	260
ATP6V1FNB	7	ENSG00000272899	1.07E-04	2.21E-03	1.10	84	109	103	33	41	53
PLCB2	15	ENSG00000137841	4.20E-05	9.92E-04	1.10	121	158	140	67	64	45
SLC7A11-AS1	4	ENSG00000250033	1.94E-09	1.16E-07	1.09	231	295	314	93	106	164
ZNF44	19	ENSG00000197857	6.92E-07	2.69E-05	1.09	159	207	169	68	71	93
DPP4	2	ENSG00000197635	4.18E-04	7.04E-03	1.08	95	97	91	47	25	53
CLVS1	8	ENSG00000177182	2.57E-18	3.96E-16	1.08	759	1163	943	377	367	498
TNFRSF6B	20	ENSG00000243509	6.57E-14	6.21E-12	1.07	436	425	558	186	195	235
STYK1	12	ENSG00000060140	9.53E-19	1.49E-16	1.07	553	699	711	282	227	347
TMTC1	12	ENSG00000133687	3.90E-07	1.58E-05	1.06	167	231	296	91	72	141
DICER1-AS1	14	ENSG00000235706	7.17E-05	1.58E-03	1.06	93	140	159	67	36	68
SLC27A6	5	ENSG00000113396	8.32E-18	1.18E-15	1.06	557	788	889	336	268	369
CR2	1	ENSG00000117322	1.20E-21	2.38E-19	1.05	714	999	982	351	349	487
ANTXR2	4	ENSG00000163297	1.59E-29	5.09E-27	1.05	1184	1592	1552	607	596	694
LNCOC1	8	ENSG00000253741	7.00E-08	3.31E-06	1.05	204	215	221	93	85	106
AC025262.3	12	ENSG00000280320	1.27E-19	2.16E-17	1.05	950	1486	1224	518	469	630

C10orf91	10	ENSG00000180066	6.09E-04	9.49E-03	1.05	84	77	131	44	28	58
TBL1XR1-AS1	3	ENSG00000231310	2.55E-07	1.10E-05	1.04	170	220	209	75	80	113
CDKN1C	11	ENSG00000129757	1.65E-11	1.22E-09	1.03	454	422	636	215	221	233
FAM43A	3	ENSG00000185112	6.30E-15	6.63E-13	1.01	562	550	724	261	263	306
TDRD6	6	ENSG00000180113	2.74E-06	9.15E-05	1.01	161	290	221	91	80	135
AC068775.1	12	ENSG00000255641	7.89E-07	3.02E-05	1.01	189	187	201	81	83	99
CUBN	10	ENSG00000107611	2.76E-05	6.89E-04	1.00	138	166	139	71	51	83
ZNF585A	19	ENSG00000196967	1.46E-08	7.83E-07	0.99	232	294	298	131	95	154
EHHADH	3	ENSG00000113790	2.34E-25	5.75E-23	0.99	995	1166	1233	498	487	573
TM4SF18	3	ENSG00000163762	7.62E-17	9.84E-15	0.99	555	732	807	282	281	404
C10orf55	10	ENSG00000222047	2.94E-13	2.64E-11	0.98	577	541	760	291	260	318
PCDHAC1	5	ENSG00000248383	6.03E-11	4.21E-09	0.98	306	436	452	169	179	201
COL4A3	2	ENSG00000169031	1.62E-08	8.58E-07	0.98	303	435	364	129	163	224
SYNE3	14	ENSG00000176438	4.68E-08	2.26E-06	0.96	214	251	293	104	115	135
AKAP6	14	ENSG00000151320	4.51E-06	1.41E-04	0.96	164	198	185	93	72	92
ETS1	11	ENSG00000134954	1.80E-21	3.51E-19	0.96	748	941	1065	404	387	497
AC019080.1	2	ENSG00000213963	7.19E-07	2.78E-05	0.96	181	252	217	94	91	121
NOS1AP	1	ENSG00000198929	8.53E-07	3.24E-05	0.96	248	219	296	98	102	164
CP	3	ENSG00000047457	1.48E-05	3.98E-04	0.95	138	225	198	97	79	85
SLCO4A1-AS1	20	ENSG00000232803	1.22E-16	1.52E-14	0.95	656	715	910	342	299	439
P2RY1	3	ENSG00000169860	4.12E-05	9.77E-04	0.95	121	224	203	76	66	118
UPP1	7	ENSG00000183696	1.50E-18	2.33E-16	0.94	726	815	920	389	354	427
SKIL	3	ENSG00000136603	1.54E-13	1.41E-11	0.94	659	961	873	347	319	533
GUCA1B	6	ENSG00000112599	2.44E-08	1.28E-06	0.93	236	320	306	139	117	156
SAP30L-AS1	5	ENSG00000245275	1.71E-07	7.61E-06	0.93	269	339	315	117	123	209
SLC2A12	6	ENSG00000146411	1.92E-07	8.46E-06	0.93	210	288	266	116	100	152
ZNF616	19	ENSG00000204611	1.72E-17	2.32E-15	0.92	702	923	898	358	373	486

TMEM171	5	ENSG00000157111	8.40E-05	1.80E-03	0.92	180	148	218	81	61	127
TMEM150C	4	ENSG00000249242	2.12E-06	7.26E-05	0.91	196	346	300	107	130	170
HPS3	3	ENSG00000163755	6.47E-23	1.38E-20	0.91	1145	1489	1586	707	574	759
SPEF2	5	ENSG00000152582	5.46E-06	1.67E-04	0.91	244	368	303	108	121	224
ACOX2	3	ENSG00000168306	2.56E-07	1.10E-05	0.91	241	299	303	138	138	130
ZNF624	17	ENSG00000197566	8.53E-05	1.82E-03	0.91	111	172	176	75	72	73
FAT4	4	ENSG00000196159	3.91E-04	6.66E-03	0.90	126	193	154	84	45	106
ST8SIA6	10	ENSG00000148488	6.87E-05	1.53E-03	0.90	125	179	166	61	74	96
NGEF	2	ENSG00000066248	2.70E-07	1.15E-05	0.90	247	260	319	131	104	174
RNF144B	6	ENSG00000137393	1.73E-05	4.58E-04	0.90	141	193	228	74	90	110
ARMC2	6	ENSG00000118690	1.29E-04	2.59E-03	0.89	131	173	172	92	52	91
CADPS2	7	ENSG00000081803	4.40E-14	4.23E-12	0.89	676	843	946	389	409	404
SLIT2	4	ENSG00000145147	4.48E-10	2.85E-08	0.88	371	604	584	237	238	289
AQP3	9	ENSG00000165272	7.71E-10	4.82E-08	0.88	423	411	555	232	207	247
CCSER1	4	ENSG00000184305	9.12E-06	2.59E-04	0.88	151	197	211	84	86	106
IQCG	3	ENSG00000114473	1.69E-16	2.05E-14	0.88	643	767	861	361	321	445
PCDHA12	5	ENSG00000251664	2.84E-07	1.21E-05	0.88	215	332	316	128	132	166
TM4SF19-TCTEX1D2	3	ENSG00000273331	8.81E-06	2.52E-04	0.88	156	206	205	88	83	111
PCDHA1	5	ENSG00000204970	2.97E-07	1.24E-05	0.88	215	330	316	128	132	166
PCDHA13	5	ENSG00000239389	2.97E-07	1.24E-05	0.88	215	330	316	128	132	166
PCDHA3	5	ENSG00000255408	2.97E-07	1.24E-05	0.88	215	330	316	128	132	166
PCDHA5	5	ENSG00000204965	2.97E-07	1.24E-05	0.88	215	330	316	128	132	166
PCDHA6	5	ENSG00000081842	2.97E-07	1.24E-05	0.88	215	330	316	128	132	166
PCDHA7	5	ENSG00000204963	2.97E-07	1.24E-05	0.88	215	330	316	128	132	166
PCDHA8	5	ENSG00000204962	2.97E-07	1.24E-05	0.88	215	330	316	128	132	166
PCDHA9	5	ENSG00000204961	2.97E-07	1.24E-05	0.88	215	330	316	128	132	166

TCP11L2	12	ENSG00000166046	2.01E-05	5.26E-04	0.88	182	188	233	99	71	134
PCDHA11	5	ENSG00000249158	3.24E-07	1.34E-05	0.87	215	334	326	128	132	174
SNX33	15	ENSG00000173548	5.05E-18	7.49E-16	0.87	839	958	1029	453	394	571
MBD5	2	ENSG00000204406	3.08E-12	2.46E-10	0.87	566	804	776	293	326	456
PCDHA2	5	ENSG00000204969	3.78E-07	1.54E-05	0.87	215	330	316	128	134	166
CHSY3	5	ENSG00000198108	1.14E-06	4.14E-05	0.87	200	229	281	113	108	133
AL136982.7	10	ENSG00000273413	7.90E-16	9.13E-14	0.87	1191	1197	1573	606	665	700
PLCXD2	3	ENSG00000240891	5.44E-16	6.32E-14	0.86	902	1062	1194	523	406	673
AP001372.2	11	ENSG00000254837	5.06E-06	1.55E-04	0.86	184	241	251	118	107	113
ARSJ	4	ENSG00000180801	1.81E-06	6.27E-05	0.85	245	315	314	131	108	209
KLF4	9	ENSG00000136826	1.69E-13	1.54E-11	0.85	740	718	936	373	372	468
BCL2	18	ENSG00000171791	1.49E-09	9.08E-08	0.85	425	621	527	244	221	337
MAST4	5	ENSG00000069020	9.14E-07	3.44E-05	0.85	232	245	294	124	108	161
CCDC39	3	ENSG00000284862	1.15E-08	6.24E-07	0.85	410	608	506	225	212	343
C3orf67	3	ENSG00000163689	1.17E-04	2.38E-03	0.85	163	155	180	71	72	114
OLMALINC	10	ENSG00000235823	3.00E-14	2.92E-12	0.85	748	997	1087	422	393	630
HECA	6	ENSG00000112406	6.09E-18	8.83E-16	0.85	813	1097	1161	483	472	600
MDFIC	7	ENSG00000135272	4.55E-11	3.23E-09	0.85	547	663	619	311	296	321
LPAR1	9	ENSG00000198121	5.60E-13	4.91E-11	0.84	548	718	780	310	340	384
TENT5C	1	ENSG00000183508	8.57E-05	1.83E-03	0.84	149	192	202	86	65	129
DEPTOR	8	ENSG00000155792	6.50E-05	1.45E-03	0.84	192	183	223	98	72	141
PCDHA4	5	ENSG00000204967	8.79E-07	3.34E-05	0.84	215	330	316	132	136	170
PCDHA10	5	ENSG00000250120	1.14E-06	4.14E-05	0.83	221	344	324	132	140	184
HECW1	7	ENSG00000002746	2.12E-06	7.26E-05	0.82	270	326	308	176	136	153
FAM81A	15	ENSG00000157470	2.16E-13	1.95E-11	0.82	668	998	1046	461	403	527
MCF2L2	3	ENSG00000053524	1.48E-12	1.25E-10	0.82	904	1493	1308	642	554	705
SLC9A2	2	ENSG00000115616	2.65E-06	8.89E-05	0.82	228	389	409	145	173	206

TMEM170B	6	ENSG00000205269	1.36E-05	3.70E-04	0.82	232	319	260	144	100	181
NEK5	13	ENSG00000197168	1.58E-06	5.56E-05	0.82	366	439	394	197	143	295
DYNC2H1	11	ENSG00000187240	5.32E-05	1.21E-03	0.82	152	181	216	87	95	100
PLA2G7	6	ENSG00000146070	1.45E-08	7.79E-07	0.82	344	420	560	228	198	254
ZBTB18	1	ENSG00000179456	7.63E-15	7.98E-13	0.81	884	1317	1437	601	569	708
RUNDC3B	7	ENSG00000105784	5.17E-06	1.58E-04	0.81	220	320	314	115	149	181
REPS2	X	ENSG00000169891	1.71E-06	5.97E-05	0.80	256	420	379	190	170	185
ABLIM3	5	ENSG00000173210	3.82E-12	3.02E-10	0.80	536	704	698	319	295	405
SLC2A13	12	ENSG00000151229	7.45E-11	5.11E-09	0.80	677	1033	942	385	458	544
PRKCQ	10	ENSG00000065675	4.06E-09	2.33E-07	0.80	364	431	454	202	197	259
FBXO36	2	ENSG00000153832	1.37E-06	4.85E-05	0.80	251	300	317	125	146	187
ZC3H6	2	ENSG00000188177	8.80E-10	5.43E-08	0.79	391	506	537	228	236	290
RNF113A	X	ENSG00000125352	9.29E-07	3.49E-05	0.79	301	354	475	165	208	217
THRB	3	ENSG00000151090	4.47E-04	7.41E-03	0.79	114	181	227	82	75	117
FA2H	16	ENSG00000103089	4.71E-06	1.46E-04	0.79	210	260	273	131	110	153
BCL6	3	ENSG00000113916	2.60E-12	2.13E-10	0.79	730	1053	1098	486	401	641
CLDN3	7	ENSG00000165215	3.02E-11	2.20E-09	0.79	656	715	871	426	338	419
PELI2	14	ENSG00000139946	4.23E-04	7.08E-03	0.79	151	333	328	112	117	199
CCDC68	18	ENSG00000166510	5.69E-06	1.72E-04	0.78	253	420	350	169	141	235
ABCA3	16	ENSG00000167972	6.06E-08	2.89E-06	0.78	443	444	609	224	226	351
ZNF385B	2	ENSG00000144331	1.38E-13	1.28E-11	0.78	809	1036	998	444	491	577
CEP19	3	ENSG00000174007	5.97E-07	2.35E-05	0.78	280	368	453	165	193	224
MTSS1	8	ENSG00000170873	2.02E-16	2.43E-14	0.77	929	1252	1321	617	544	702
CEMIP	15	ENSG00000103888	6.83E-12	5.28E-10	0.77	1021	1051	1292	484	556	778
COL4A4	2	ENSG00000081052	2.25E-12	1.85E-10	0.77	613	873	893	401	371	498
TCTEX1D2	3	ENSG00000213123	1.07E-07	4.91E-06	0.77	330	469	440	229	186	248
SH3TC2	5	ENSG00000169247	1.05E-16	1.33E-14	0.77	979	1172	1253	546	548	742

TSPAN7	X	ENSG00000156298	3.52E-07	1.44E-05	0.77	289	394	397	165	187	227
ZNF502	3	ENSG00000196653	1.03E-04	2.14E-03	0.76	167	214	197	96	101	114
AC008014.1	12	ENSG00000257261	4.48E-04	7.41E-03	0.76	147	208	181	80	77	136
LYPD6	2	ENSG00000187123	6.04E-09	3.37E-07	0.76	512	719	644	282	301	435
GVQW3	11	ENSG00000179240	5.52E-06	1.68E-04	0.76	470	581	453	233	210	392
BACH2	6	ENSG00000112182	6.13E-04	9.52E-03	0.75	150	260	275	82	123	164
AC018629.1	17	ENSG00000279806	1.21E-04	2.46E-03	0.75	252	261	261	116	107	208
OTUD1	10	ENSG00000165312	4.59E-05	1.07E-03	0.75	184	285	324	122	144	159
SGK1	6	ENSG00000118515	1.61E-04	3.12E-03	0.75	204	203	215	100	92	153
AL158151.3	9	ENSG00000268050	4.28E-06	1.35E-04	0.74	298	309	399	150	188	209
MAT1A	10	ENSG00000151224	3.76E-04	6.45E-03	0.74	152	195	264	124	97	107
CD55	1	ENSG00000196352	8.75E-15	9.06E-13	0.74	1171	1470	1443	768	672	787
KIF9-AS1	3	ENSG00000227398	3.87E-05	9.29E-04	0.74	184	248	266	112	110	161
AL133355.1	10	ENSG00000260461	3.46E-06	1.12E-04	0.74	259	301	352	170	133	198
PCDHAC2	5	ENSG00000243232	6.22E-09	3.46E-07	0.74	406	575	604	278	254	333
XRCC4	5	ENSG00000152422	1.13E-10	7.64E-09	0.73	920	1424	1292	703	576	704
PRSS12	4	ENSG00000164099	1.47E-17	2.01E-15	0.73	1122	1337	1501	692	625	867
KLF7	2	ENSG00000118263	4.28E-10	2.74E-08	0.73	946	1241	1271	541	503	889
WDR53	3	ENSG00000185798	7.17E-12	5.53E-10	0.73	624	789	830	393	379	464
CARF	2	ENSG00000138380	3.87E-05	9.28E-04	0.72	255	436	353	155	183	241
SQOR	15	ENSG00000137767	3.12E-07	1.30E-05	0.72	404	583	624	263	311	308
AC005696.2	17	ENSG00000272770	3.87E-09	2.24E-07	0.72	520	687	814	322	366	426
AC010198.2	12	ENSG00000285517	2.99E-10	1.95E-08	0.72	624	856	796	397	355	520
PPP1R3E	14	ENSG00000235194	6.39E-04	9.84E-03	0.71	164	206	213	77	100	151
INSIG1	7	ENSG00000186480	1.05E-12	9.01E-11	0.71	941	1192	1216	584	615	660
C6orf141	6	ENSG00000197261	8.96E-06	2.56E-04	0.71	319	420	424	207	153	298
GAB1	4	ENSG00000109458	5.17E-07	2.06E-05	0.71	343	412	439	202	185	286

PDGFC	4	ENSG00000145431	5.78E-12	4.52E-10	0.70	865	1138	1188	618	537	621
RCAN2	6	ENSG00000172348	3.50E-05	8.50E-04	0.70	214	329	338	166	152	171
KMO	1	ENSG00000117009	4.74E-04	7.77E-03	0.70	158	221	217	115	110	106
SERPINI1	3	ENSG00000163536	4.47E-04	7.41E-03	0.70	177	294	219	112	121	156
HOXA13	7	ENSG00000106031	6.42E-06	1.91E-04	0.70	303	488	426	204	224	252
RBM43	2	ENSG00000184898	1.83E-04	3.46E-03	0.69	225	240	295	132	104	200
FRY	13	ENSG00000073910	1.69E-04	3.23E-03	0.69	184	252	224	119	115	139
ABCA5	17	ENSG00000154265	2.48E-05	6.32E-04	0.69	371	598	428	261	206	330
RNASE4	14	ENSG00000258818	8.23E-05	1.77E-03	0.69	216	382	337	156	156	216
PRKCQ-AS1	10	ENSG00000237943	3.22E-06	1.05E-04	0.69	287	336	379	180	161	229
LZTFL1	3	ENSG00000163818	3.11E-09	1.81E-07	0.69	899	1285	1049	537	547	764
WWOX	16	ENSG00000186153	1.20E-07	5.49E-06	0.69	676	667	905	378	444	445
CAMK2N2	3	ENSG00000163888	9.76E-05	2.05E-03	0.68	295	260	434	171	163	229
VAMP4	1	ENSG00000117533	1.24E-05	3.42E-04	0.68	354	641	547	258	287	327
SFR1	10	ENSG00000156384	1.71E-09	1.03E-07	0.67	999	1393	1130	609	598	824
MIGA1	1	ENSG00000180488	6.85E-11	4.71E-09	0.67	1129	1461	1288	741	606	895
RGS17	6	ENSG00000091844	4.71E-06	1.46E-04	0.67	326	462	407	233	200	251
BFSP1	20	ENSG00000125864	1.25E-08	6.76E-07	0.67	566	672	709	366	360	386
GLDC	9	ENSG00000178445	3.60E-05	8.72E-04	0.67	237	337	396	162	159	235
CRPPA	7	ENSG00000214960	3.35E-05	8.17E-04	0.67	231	295	325	142	154	193
AL138689.2	13	ENSG00000284966	9.45E-15	9.68E-13	0.67	1097	1394	1550	755	690	872
LEPR	1	ENSG00000116678	3.50E-08	1.76E-06	0.66	491	554	620	313	298	347
TMTC2	12	ENSG00000179104	1.25E-14	1.26E-12	0.66	1180	1499	1560	731	728	993
EPHA4	2	ENSG00000116106	2.42E-08	1.26E-06	0.66	467	589	630	293	306	372
WWC3	X	ENSG00000047644	2.98E-09	1.74E-07	0.66	845	862	1088	474	461	698
AKAP3	12	ENSG00000111254	2.97E-04	5.22E-03	0.66	214	280	249	121	150	159
EEPD1	7	ENSG00000122547	4.99E-07	1.99E-05	0.65	685	782	938	477	472	426

KHDRBS3	8	ENSG00000131773	1.84E-06	6.35E-05	0.65	381	429	487	226	210	325
TET1	10	ENSG00000138336	1.59E-05	4.24E-04	0.65	310	432	373	202	183	268
AL163636.2	14	ENSG00000259171	1.15E-04	2.34E-03	0.65	229	393	355	168	166	233
SATB2-AS1	2	ENSG00000225953	1.79E-04	3.39E-03	0.65	205	261	271	139	140	147
FAM172A	5	ENSG00000113391	5.48E-11	3.85E-09	0.65	1007	1372	1235	644	646	822
BEND7	10	ENSG00000165626	9.09E-08	4.24E-06	0.65	606	939	809	419	421	531
AGTPBP1	9	ENSG00000135049	2.93E-12	2.35E-10	0.65	1059	1273	1274	652	668	786
PLD1	3	ENSG00000075651	4.11E-05	9.77E-04	0.65	249	399	418	186	184	248
FAM241A	4	ENSG00000174749	5.21E-08	2.49E-06	0.64	807	1038	979	595	506	544
LINC00339	1	ENSG00000218510	3.58E-04	6.17E-03	0.63	252	294	363	189	118	232
ZNF845	19	ENSG00000213799	3.62E-07	1.47E-05	0.63	556	878	780	427	358	518
ANKRD44	2	ENSG00000065413	5.28E-04	8.49E-03	0.63	204	230	241	107	130	163
LANCL3	X	ENSG00000147036	1.07E-04	2.21E-03	0.63	277	389	398	191	153	289
MAP3K13	3	ENSG00000073803	3.35E-11	2.41E-09	0.63	1052	1453	1372	764	670	849
AKT3	1	ENSG00000117020	4.52E-08	2.20E-06	0.63	526	687	750	333	362	462
ARMH4	14	ENSG00000139971	2.76E-05	6.89E-04	0.63	291	350	346	197	165	223
ACBD7	10	ENSG00000176244	1.03E-04	2.14E-03	0.63	229	317	321	150	167	193
OVGP1	1	ENSG00000085465	1.29E-04	2.58E-03	0.63	248	340	302	161	173	191
LMLN	3	ENSG00000185621	1.69E-11	1.24E-09	0.63	1041	1344	1283	657	652	871
LACTB2	8	ENSG00000147592	1.43E-13	1.32E-11	0.63	1205	1436	1686	842	753	958
DNAJC19	3	ENSG00000205981	1.03E-10	6.96E-09	0.62	1013	1309	1286	742	612	783
C16orf46	16	ENSG00000166455	2.40E-05	6.14E-04	0.62	508	624	497	273	327	374
BDNF-AS	11	ENSG00000245573	3.95E-08	1.95E-06	0.62	522	637	674	339	313	440
PRSS23	11	ENSG00000150687	1.63E-09	9.82E-08	0.62	659	859	890	469	422	535
AC004797.1	17	ENSG00000177369	3.07E-05	7.57E-04	0.62	316	447	390	203	199	287
TMEM158	3	ENSG00000249992	4.83E-06	1.49E-04	0.62	589	538	644	296	345	421
TTC39B	9	ENSG00000155158	7.74E-07	2.97E-05	0.62	411	588	620	290	288	381

PAIP2B	2	ENSG00000124374	1.58E-08	8.41E-07	0.62	627	792	760	403	376	524
MGAT4A	2	ENSG00000071073	5.56E-07	2.21E-05	0.62	424	559	614	320	264	363
LINC00326	6	ENSG00000231023	8.06E-07	3.07E-05	0.61	506	759	747	360	396	432
STON2	14	ENSG00000140022	1.50E-04	2.95E-03	0.61	269	342	350	157	161	262
TRMT10A	4	ENSG00000145331	1.09E-06	4.02E-05	0.61	600	818	672	407	352	501
HOXD8	2	ENSG00000175879	4.42E-04	7.34E-03	0.61	196	248	274	148	129	150
SWAP70	11	ENSG00000133789	2.67E-12	2.17E-10	0.61	1274	1644	1569	850	822	1022
AL365181.2	1	ENSG00000272068	7.93E-05	1.72E-03	0.60	349	514	442	212	229	350
SULT1A1	16	ENSG00000196502	1.07E-07	4.91E-06	0.60	714	844	866	529	408	522
HTR1D	1	ENSG00000179546	7.42E-05	1.63E-03	0.60	256	372	394	194	171	249
OSBPL10	3	ENSG00000144645	1.00E-12	8.66E-11	0.60	1176	1495	1507	793	737	991
B4GALT6	18	ENSG00000118276	6.52E-08	3.09E-06	0.60	841	1331	1162	633	584	791
MAP6D1	3	ENSG00000180834	6.99E-06	2.05E-04	0.60	601	644	766	384	429	388
KCTD12	13	ENSG00000178695	9.27E-06	2.63E-04	0.60	376	494	494	251	225	354
THNSL1	10	ENSG00000185875	4.46E-11	3.18E-09	0.59	1087	1226	1303	703	622	877
SPATA1	1	ENSG00000122432	1.69E-04	3.24E-03	0.59	274	422	365	216	171	256
PIM1	6	ENSG00000137193	1.72E-08	9.09E-07	0.59	672	760	841	426	435	515
ACSM3	16	ENSG00000005187	8.62E-06	2.47E-04	0.59	455	744	646	348	319	450
AC093297.2	5	ENSG00000272335	7.36E-05	1.62E-03	0.59	383	501	423	218	261	319
KLF9	9	ENSG00000119138	4.02E-04	6.81E-03	0.59	441	670	504	236	334	418
PIGX	3	ENSG00000163964	1.73E-11	1.27E-09	0.59	1183	1551	1588	853	812	951
MELTF-AS1	3	ENSG00000228109	4.19E-04	7.04E-03	0.59	310	282	332	183	183	198
ULBP1	6	ENSG00000111981	1.76E-05	4.65E-04	0.58	341	416	461	232	203	310
AC015813.6	17	ENSG00000279207	5.60E-06	1.70E-04	0.58	860	1321	1115	618	503	913
SLC35F3	1	ENSG00000183780	2.45E-06	8.28E-05	0.58	434	488	609	291	283	357
ARL4C	2	ENSG00000188042	6.61E-09	3.66E-07	0.58	843	1071	1257	590	627	698
RPS6KA2	6	ENSG00000071242	4.65E-08	2.26E-06	0.58	711	913	1047	543	506	564

SAMD5	6	ENSG00000203727	6.51E-05	1.45E-03	0.58	322	341	403	212	178	265
SYT13	11	ENSG00000019505	1.30E-05	3.56E-04	0.58	341	426	471	228	224	305
ZNF302	19	ENSG00000089335	5.61E-06	1.70E-04	0.58	708	984	853	443	424	712
AC005747.1	17	ENSG00000007237	6.72E-06	1.98E-04	0.58	412	467	565	301	243	339
TICAM2	5	ENSG00000243414	1.00E-05	2.83E-04	0.58	375	489	503	256	235	350
CA2	8	ENSG00000104267	1.49E-10	9.93E-09	0.57	1134	1543	1689	817	842	1000
MB21D2	3	ENSG00000180611	7.61E-05	1.66E-03	0.57	294	396	379	197	195	266
NADK2	5	ENSG00000152620	1.49E-10	9.93E-09	0.57	1211	1548	1488	807	825	974
ENPP5	6	ENSG00000112796	4.03E-04	6.81E-03	0.57	316	471	390	191	218	321
TMEM221	19	ENSG00000188051	3.99E-04	6.77E-03	0.57	261	322	395	172	211	211
ZNF594	17	ENSG00000180626	3.05E-05	7.53E-04	0.57	367	576	545	308	264	336
UACA	15	ENSG00000137831	4.22E-09	2.41E-07	0.57	1217	1722	1552	843	883	1034
ANKRD33B	5	ENSG00000164236	2.97E-11	2.17E-09	0.57	1074	1307	1476	774	687	916
KIFAP3	1	ENSG00000075945	1.31E-07	5.95E-06	0.56	663	929	896	470	444	626
PLEKHM3	2	ENSG00000178385	6.40E-07	2.50E-05	0.56	637	788	788	399	392	591
B3GLCT	13	ENSG00000187676	6.92E-05	1.53E-03	0.56	299	434	464	233	225	278
ALDH6A1	14	ENSG00000119711	2.77E-07	1.18E-05	0.56	782	981	1013	577	555	574
ALG10B	12	ENSG00000175548	4.68E-05	1.09E-03	0.56	623	948	792	395	417	671
HRK	12	ENSG00000135116	6.20E-04	9.62E-03	0.56	268	268	305	166	147	215
CTBS	1	ENSG00000117151	1.10E-06	4.05E-05	0.56	852	1274	1036	614	570	789
ZNF572	8	ENSG00000180938	2.36E-04	4.32E-03	0.55	483	641	571	326	249	501
ZNF177	19	ENSG00000188629	6.07E-04	9.48E-03	0.55	239	310	284	166	152	203
ZNF607	19	ENSG00000198182	1.22E-06	4.40E-05	0.55	620	725	690	404	370	504
FBXL17	5	ENSG00000145743	3.43E-08	1.74E-06	0.55	806	929	983	537	478	697
C1D	2	ENSG00000197223	1.40E-05	3.78E-04	0.55	455	630	595	325	288	444
GCA	2	ENSG00000115271	3.79E-06	1.22E-04	0.55	461	606	626	316	330	412
FAM83B	6	ENSG00000168143	1.09E-06	4.02E-05	0.54	717	1045	929	508	535	640

MANEA	6	ENSG00000172469	4.61E-07	1.85E-05	0.54	1158	1725	1488	947	732	1068
FGD1	X	ENSG00000102302	1.35E-05	3.68E-04	0.54	526	532	673	338	352	394
IFIH1	2	ENSG00000115267	3.24E-04	5.66E-03	0.54	304	424	424	207	252	258
LPCAT2	16	ENSG00000087253	4.53E-07	1.82E-05	0.54	824	1264	1145	628	590	813
FNDC10	1	ENSG00000228594	1.77E-04	3.36E-03	0.53	320	349	432	208	202	287
ARHGEF28	5	ENSG00000214944	3.83E-05	9.23E-04	0.53	377	530	524	271	263	370
AC090527.2	15	ENSG00000260170	1.43E-04	2.83E-03	0.53	338	490	526	238	280	330
SEMA3C	7	ENSG00000075223	5.03E-07	2.00E-05	0.53	936	1328	1160	664	608	904
SATB2	2	ENSG00000119042	4.98E-10	3.16E-08	0.53	1257	1415	1654	824	796	1124
TMEM56	1	ENSG00000152078	1.12E-07	5.12E-06	0.53	940	1417	1346	717	722	886
JRK	8	ENSG00000234616	4.34E-05	1.02E-03	0.53	967	1093	1225	585	515	1022
DENND3	8	ENSG00000105339	1.37E-05	3.72E-04	0.53	467	611	601	331	292	446
XXYLT1	3	ENSG00000173950	3.39E-08	1.72E-06	0.53	1230	1212	1477	779	774	935
TRIM38	6	ENSG00000112343	5.25E-10	3.31E-08	0.53	1078	1248	1376	753	691	904
LGR4	11	ENSG00000205213	4.58E-06	1.43E-04	0.53	546	804	756	413	406	511
ZNF510	9	ENSG00000081386	2.86E-05	7.10E-04	0.52	476	639	565	357	310	401
C12orf66	12	ENSG00000174206	1.14E-08	6.23E-07	0.52	853	1114	1221	647	599	771
FOXO1	13	ENSG00000150907	9.22E-05	1.95E-03	0.52	482	674	775	317	406	497
PLCB1	20	ENSG00000182621	3.24E-06	1.05E-04	0.52	833	1221	1018	593	613	748
SAMD13	1	ENSG00000203943	4.54E-05	1.06E-03	0.52	409	468	537	258	285	358
NR3C1	5	ENSG00000113580	1.05E-04	2.18E-03	0.52	464	731	597	378	322	440
ATP6V1E2	2	ENSG00000250565	1.62E-06	5.68E-05	0.52	551	665	714	375	372	483
DHRS7B	17	ENSG00000109016	3.47E-06	1.13E-04	0.52	572	685	716	395	405	452
COL13A1	10	ENSG00000197467	1.08E-05	3.04E-04	0.52	583	706	757	385	448	461
ZNF525	19	ENSG00000203326	1.02E-05	2.88E-04	0.52	805	1226	1032	667	518	770
TMEM173	5	ENSG00000184584	2.43E-05	6.19E-04	0.52	753	743	862	408	458	658
STPG1	1	ENSG00000001460	4.68E-05	1.09E-03	0.52	390	459	553	277	281	332

CEP41	7	ENSG00000106477	1.27E-07	5.75E-06	0.52	901	992	1117	564	579	793
SPCS2	11	ENSG00000118363	1.14E-06	4.14E-05	0.51	869	1249	1075	650	611	782
RNF217	6	ENSG00000146373	4.11E-06	1.30E-04	0.51	1190	1841	1440	915	867	1077
AC008771.1	5	ENSG00000249042	8.77E-05	1.87E-03	0.51	408	578	538	312	263	405
STXBP5	6	ENSG00000164506	2.53E-07	1.09E-05	0.51	1128	1573	1359	825	801	972
TFPI	2	ENSG00000003436	6.96E-05	1.54E-03	0.51	449	630	634	391	321	375
NBEA	13	ENSG00000172915	1.76E-04	3.35E-03	0.51	461	567	569	267	354	403
MLLT3	9	ENSG00000171843	4.02E-04	6.81E-03	0.51	369	560	497	277	311	317
ZNF268	12	ENSG00000090612	1.44E-08	7.78E-07	0.51	885	1108	1181	655	587	794
COMMD8	4	ENSG00000169019	7.76E-07	2.98E-05	0.51	1061	1382	1205	800	672	876
DISP1	1	ENSG00000154309	8.78E-06	2.51E-04	0.51	508	661	690	351	377	465
ZNF16	8	ENSG00000170631	6.26E-04	9.68E-03	0.51	267	344	371	189	205	234
RNF170	8	ENSG00000120925	3.08E-04	5.40E-03	0.51	542	732	677	308	399	559
ERCC8	5	ENSG00000049167	2.57E-07	1.10E-05	0.51	789	938	973	530	550	657
STAMBPL1	10	ENSG00000138134	1.61E-04	3.12E-03	0.51	382	511	579	339	254	348
NKD1	16	ENSG00000140807	4.82E-08	2.33E-06	0.50	933	1113	1154	616	643	805
ZDHHC14	6	ENSG00000175048	4.74E-06	1.47E-04	0.50	585	638	752	390	396	486
CD44-AS1	11	ENSG00000255443	3.35E-04	5.85E-03	0.50	339	460	450	233	226	351
PKIA	8	ENSG00000171033	1.53E-04	2.99E-03	0.50	361	481	451	252	252	331
RRAGD	6	ENSG00000025039	2.19E-06	7.46E-05	0.50	923	1380	1255	701	744	830
CLCN5	X	ENSG00000171365	1.12E-06	4.10E-05	0.50	680	940	986	528	524	616
ZKSCAN4	6	ENSG00000187626	2.14E-04	3.97E-03	0.50	335	401	434	224	241	289
AC069257.3	3	ENSG00000272741	2.51E-06	8.48E-05	0.50	666	747	802	471	437	522
LINC01963	2	ENSG00000260804	1.09E-06	4.02E-05	-0.50	668	955	851	987	1022	1173
ADSSL1	14	ENSG00000185100	5.21E-04	8.41E-03	-0.50	245	293	410	358	345	524
NOL4L	20	ENSG00000197183	1.59E-04	3.08E-03	-0.50	266	367	411	449	350	554
AC008840.1	5	ENSG00000250240	2.74E-04	4.91E-03	-0.51	243	301	317	396	299	422

HOXB9	17	ENSG00000170689	1.75E-06	6.09E-05	-0.51	623	672	719	747	784	1114
XKR8	1	ENSG00000158156	1.35E-05	3.68E-04	-0.51	361	432	523	587	488	625
ATP8B3	19	ENSG00000130270	1.95E-07	8.56E-06	-0.51	519	612	683	727	680	966
MMP24OS	20	ENSG00000126005	3.83E-06	1.23E-04	-0.51	603	576	730	840	758	888
IL11RA	9	ENSG00000137070	2.81E-04	5.02E-03	-0.51	230	274	333	358	285	452
AC012459.1	2	ENSG00000287299	2.09E-08	1.10E-06	-0.52	691	766	950	1009	954	1169
ARID3B	15	ENSG00000179361	6.24E-05	1.40E-03	-0.52	341	374	410	478	484	499
CARD9	9	ENSG00000187796	3.41E-04	5.93E-03	-0.52	340	323	426	513	438	462
BMP7	20	ENSG00000101144	1.15E-05	3.20E-04	-0.52	408	481	514	581	611	630
CFAP157	9	ENSG00000160401	1.05E-04	2.17E-03	-0.52	291	301	418	385	408	531
RGS14	5	ENSG00000169220	1.96E-04	3.66E-03	-0.52	358	316	392	473	438	489
KIF5A	12	ENSG00000155980	5.55E-04	8.85E-03	-0.52	256	277	371	367	296	536
RAB43	3	ENSG00000172780	1.48E-05	3.98E-04	-0.52	471	451	585	603	655	716
ACER2	9	ENSG00000177076	2.37E-04	4.33E-03	-0.52	199	298	319	334	304	430
CHN1	2	ENSG00000128656	1.31E-05	3.58E-04	-0.53	295	348	424	444	416	541
RGMA	15	ENSG00000182175	3.58E-05	8.68E-04	-0.53	334	343	441	469	476	520
RASAL1	12	ENSG00000111344	3.96E-07	1.60E-05	-0.53	584	616	840	884	769	1033
SCAMP5	15	ENSG00000198794	1.21E-06	4.36E-05	-0.53	384	470	476	559	528	670
TRNP1	1	ENSG00000253368	2.17E-09	1.29E-07	-0.53	727	816	997	1096	993	1261
MFSD2A	1	ENSG00000168389	8.15E-06	2.36E-04	-0.53	448	470	655	651	674	736
CISH	3	ENSG00000114737	6.08E-04	9.48E-03	-0.54	232	269	329	399	347	338
NPIPB3	16	ENSG00000169246	2.52E-04	4.55E-03	-0.54	325	431	367	532	357	619
AGAP9	10	ENSG00000204172	5.62E-04	8.92E-03	-0.54	204	354	318	361	305	499
BIK	22	ENSG00000100290	9.00E-07	3.39E-05	-0.54	509	539	627	693	735	792
DPF1	19	ENSG00000011332	5.70E-06	1.72E-04	-0.54	406	462	635	657	615	705
DHRS3	1	ENSG00000162496	3.69E-08	1.83E-06	-0.54	908	880	1075	1123	1138	1586
GSTT2B	22	ENSG00000133433	1.65E-05	4.37E-04	-0.54	298	325	426	451	426	513

RHBDF1	16	ENSG00000007384	4.93E-05	1.14E-03	-0.55	350	317	435	495	442	531
LIMD2	17	ENSG00000136490	1.68E-04	3.22E-03	-0.55	322	274	396	415	425	482
ADAP1	7	ENSG00000105963	1.39E-05	3.76E-04	-0.55	784	763	1188	1322	1061	1219
TUBG2	17	ENSG00000037042	5.64E-07	2.23E-05	-0.55	595	614	623	728	756	992
BRSK1	19	ENSG00000160469	1.46E-10	9.75E-09	-0.55	950	987	1163	1276	1241	1653
MCTP2	15	ENSG00000140563	5.92E-05	1.34E-03	-0.56	229	366	344	411	378	462
PLEKHG2	19	ENSG00000090924	2.12E-07	9.27E-06	-0.56	724	729	1028	1112	899	1330
HOXB3	17	ENSG00000120093	2.37E-06	8.03E-05	-0.56	355	464	551	544	521	780
TMEM63C	14	ENSG00000165548	3.07E-08	1.57E-06	-0.56	489	570	609	738	635	879
SERPINA1	14	ENSG00000197249	8.25E-05	1.77E-03	-0.56	214	238	258	310	281	367
GAD1	2	ENSG00000128683	1.91E-04	3.57E-03	-0.56	228	292	237	324	305	398
SOBP	6	ENSG00000112320	2.23E-04	4.11E-03	-0.56	204	256	258	351	253	365
WNT3A	1	ENSG00000154342	4.94E-05	1.14E-03	-0.56	241	252	340	368	333	420
LY6G5B	6	ENSG00000240053	4.15E-08	2.03E-06	-0.57	659	678	875	897	851	1268
LONRF2	2	ENSG00000170500	5.84E-06	1.75E-04	-0.57	301	416	391	442	439	627
AL157871.1	14	ENSG00000258504	4.68E-06	1.46E-04	-0.57	305	333	353	439	394	517
CCDC189	16	ENSG00000196118	5.32E-05	1.21E-03	-0.57	203	241	257	308	283	361
DLG4	17	ENSG00000132535	3.87E-11	2.78E-09	-0.57	787	937	1127	1233	1090	1553
ARID3A	19	ENSG00000116017	1.08E-09	6.60E-08	-0.57	583	751	743	882	870	1068
SCG2	2	ENSG00000171951	2.65E-08	1.37E-06	-0.57	758	1060	894	1155	1040	1520
SLC43A2	17	ENSG00000167703	1.01E-06	3.76E-05	-0.58	467	470	588	620	701	753
POLD4	11	ENSG00000175482	2.16E-05	5.59E-04	-0.58	221	301	306	356	313	464
UBAP1L	15	ENSG00000246922	6.94E-05	1.54E-03	-0.58	231	308	339	435	298	467
RNFT1	17	ENSG00000189050	1.02E-07	4.70E-06	-0.58	515	750	644	797	810	1003
GSDME	7	ENSG00000105928	6.09E-06	1.82E-04	-0.59	317	355	427	538	395	574
FAM122C	X	ENSG00000156500	4.97E-06	1.53E-04	-0.59	282	294	353	412	390	473
AP000763.4	11	ENSG00000256928	2.53E-05	6.41E-04	-0.59	219	250	280	308	329	391

HOXB6	17	ENSG00000108511	7.28E-08	3.44E-06	-0.59	585	785	826	925	784	1345
AP000892.3	11	ENSG00000280143	3.88E-09	2.24E-07	-0.60	586	626	649	828	796	964
ABTB2	11	ENSG00000166016	3.52E-08	1.77E-06	-0.60	570	615	758	804	911	961
ZNF358	19	ENSG00000198816	2.63E-06	8.86E-05	-0.60	592	499	753	756	840	962
SESN2	1	ENSG00000130766	8.48E-10	5.26E-08	-0.60	870	875	1205	1311	1277	1486
AL158206.1	9	ENSG00000260912	4.84E-04	7.90E-03	-0.61	161	181	168	200	220	297
SEC14L2	22	ENSG00000100003	6.67E-07	2.60E-05	-0.61	589	546	753	885	844	880
PADI3	1	ENSG00000142619	1.28E-04	2.57E-03	-0.61	148	223	224	256	258	308
LRRC28	15	ENSG00000168904	3.27E-05	8.01E-04	-0.61	216	376	340	382	408	499
HDDC3	15	ENSG00000184508	6.63E-06	1.96E-04	-0.61	236	281	383	391	366	496
NPR2	9	ENSG00000159899	3.13E-08	1.60E-06	-0.62	404	558	636	745	607	876